Aalto University
School of Chemical
Technology

School of Chemical Technology
Degree Programme of Materials Science and Engineering

Maria Leikola

SOLID STATE REDUCTION OF CHROMITE WITH METHANE AND HYDROGEN

Master's thesis for the degree of Master of Science in Technology submitted for inspection, Espoo, August 28th, 2015.

Supervisor **Professor Pekka Taskinen**

Instructors **Professor Rauf Hürman Eriç**
MSc Petteri Halli

Aalto-yliopisto
Kemian tekniikan korkeakoulu

Aalto-yliopisto, PL 11000, 00076 AALTO
www.aalto.fi
Diplomityön tiivistelmä

Tekijä Maria Katariina Leikola

Työn nimi Kromiitin esipelkistys metaanilla ja vedyllä

Laitos Materiaalitekniikka

Professuuri Metallurgisten prosessien termodynamiikka ja mallinnus **Professuurikoodi** MT-37

Työn valvoja Professori Pekka Taskinen

Työn ohjaaja(t)/Työn tarkastaja(t) Professori Rauf Hürman Eriç ja DI Petteri Halli

Päivämäärä 28.8.2015 **Sivumäärä** 239 **Kieli** Englanti

Tiivistelmä

Energian kulutus ja sen säästötoimenpiteet ovat erittäin tärkeitä aiheita nykypäivänä. Tämä diplomityö tutkii kromiitin kiinteäfaasipelkistystä metaanin ja vedyn kaasuseoksilla, jotta ferrokromin, ruostumattoman teräksen raaka-aineen, valmistusprosessin energiankulutusta voitaisiin vähentää. Tätä samaista prosessia on tutkittu jo aikaisemmin, muttei tässä työssä käytetyn Kemin kromiittiesiintymän yhteydessä. Metaanin käyttö grafiitin sijaan on tutkittu mahdollistavan kromiitin pelkistämisen paljon alhaisemmissa lämpötiloissa, mikä johtaa energiasäästöihin ja mahdollisesti myös taloudellisiin hyötyihin.

Tämän työn kokeellinen osuus toteutettiin laboratoriomittakaavassa lämpötilan, metaanin pitoisuuden ja pelkistysajan vaihdellessa. Saadut tulokset olivat erittäin lupaavia. Niistä kävi ilmi, että rauta ja kromi pelkistyvät nopeasti ja perusteellisesti, mikä oli yhteensopivaa aikaisemman tutkimuksen kanssa koskien muita kromiittiesiintymiä. Pelkistysmekanismia ja metallisoitumista tarkasteltiin eniten, mikä johti siihen johtopäätökseen, että metaani on erittäin tehokas pelkistin Kemin kromiitin esikäsittelyssä. Jatkotutkimukset prosessin soveltamisesta teolliseen mittakaavaan ovat suositeltavia.

Avainsanat Kromiitti, Kiinteätila, Esipelkistys, Metaani, Vety

Aalto University
School of Chemical
Technology

Aalto University, P.O. BOX 11000, 00076 AALTO
www.aalto.fi

Abstract of master's thesis

Author Maria Katariina Leikola

Title of thesis Solid State Reduction of Chromite with Methane and Hydrogen

Department Materials Science and Engineering

Professorship Metallurgical Thermodynamics and Modelling **Code of professorship** MT-37

Thesis supervisor Professor Pekka Taskinen

Thesis advisor(s)/Thesis examiner(s) Professor Rauf Hürman Eriç and MSc Petteri Halli

Date 28.8.2015 **Number of pages** 239 **Language** English

Abstract

In today's World the issue of energy consumption and conservation is of high importance. This Master's Thesis studies the solid state reduction of ferrous chromite with a methane hydrogen gas mixture in order to reduce the energy needed to produce ferrochrome, a raw material for stainless steel. The process has been studied before, but not with the same exact raw material from the Kemi chromite deposit. Earlier studies have shown, that the use of methane instead of graphite enables the reduction of chromite in much lower temperatures, thus reducing energy usage and possibly resulting in economic savings.

The experiments conducted in this work were done in laboratory scale with varying temperature, methane concentration and reduction time. The results were very promising, showing rapid and thorough reduction of iron and chromium, which is consistent with earlier studies on other chromite ores. The reduction mechanism and metallization were examined most thoroughly, leading to the conclusion that methane as the reducing agent is an effective way for prereducing Kemi chromite. Continued investigations of the process for industrial scale applications is recommended.

Keywords Chromite, Solid-State, Prereduction, Methane, Hydrogen

Foreword

I thank my supervisor, Professor Pekka Taskinen, and my instructor, Professor Rauf Hürman Eriç, for their guidance and support during this project. The knowledge and insight they shared with me, was essential for this Master's Thesis.

My second instructor, Master of Science Petteri Halli, also deserves a thank you for his help. He instructed me throughout the experimental part, and gave me lots of advice. Also my colleague, Lassi Klemettinen, was very helpful in performing the SEM analyses.

I also thank the industrial partners of the FiDiPro (Finland Distinguished Professor Programme) Project, which this Master's Thesis is a part of. Special thanks go to Outokumpu for providing the raw material in question and Outotec for performing carbon analyses on the samples. Furthermore, I would like to thank the research group of Metallurgical Thermodynamics and Modelling and my co-workers for the time I got to spend with them.

Last, but certainly not least, I thank my family, friends and my partner, Henri Mäkelä, for their love and support during my studies. As the old saying goes; it takes a village to raise an engineer.

List of Symbols and Abbreviations

AOD	Argon oxygen decarburization
˚C	Degrees Celsius
CDR	Chrome direct reduction
Cr met	Metallic chromium
DSC	Differential scanning calorimetry
EDS	Energy-dispersive X-ray Spectroscopy
Fe met	Metallic iron
K	Kelvin
l/min	Liters per minute
p_{80}	80 % of particles are smaller than p_{80}
S/C analyzer	Sulphur/carbon analyzer
SAF	Submerged electric arc furnace
SEM	Scanning electron microscope
SRC	Solid state reduction with carbon
TG	Thermogravimetry
vol%	Volume percent
wt%	Weight percent
XRD	X-ray Diffraction

Contents

Foreword I

List of Symbols and Abbreviations II

Contents III

1 Introduction 1

2 Chromite Ore 2

2.1 Properties and Mineralogy 2

2.2 Chromite Deposits Worldwide 4

2.3 Kemi Chromite 5

3 Ferrochrome 7

3.1 Usage and Production 7

3.2 Submerged Electric Arc Furnace Process 10

3.2.1 Concentration and Pelletizing 11

3.2.2 Sintering 11

3.2.3 Smelting in SAF 12

4 Prereduction of Chromite 15

4.1 Prereduction with Carbon 15

4.1.1 Solid State Reduction with Carbon 15

4.1.2 Commercialized Prereduction Processes 23

4.2 Reduction of Chromite with Methane 25

4.2.1 Methane as a Source for Solid Carbon 25

4.2.2 Methane Adsorption 28

4.3 Hydrogen as a Reductant 34
5 Research Methods 36
5.1 Experimental Equipment and Methods 36
5.2 Conducted Experiments 38
5.3 Chemical Analysis 38
5.3.1 XRD 38
5.3.2 SEM-EDS 39
5.3.3 S/C analyzer 39
6 Results and Discussion 40
6.1 Reduction Mechanism 40
6.2 Metallization 52
6.2.1 Iron-Chromium Carbide Formation 58
6.2.2 Iron- and Chromium Based Alloys 60
6.3 Carbon Deposition 66
6.4 Mineralogy from XRD Measurements and Rietveld Calculations 73
7 Summary and Conclusions 76
7.1 Reduction Mechanism 76
7.2 Future Work 78
8 References 80
Appendices 87
Appendix I 87
Appendix II 88
Appendices III-XLIV - SEM micrographs 89
Appendices XLV-CXII - SEM micrographs and SEM-EDS analyses 132

Appendices CXIII-CL - XRD Patterns and Rietveld Analyses 200

Appendices CLI-CLII - S/C analysis results 238

1 Introduction

The world advances technologically creating new applications and increasing demand for a durable material like stainless steel, which can sustain corrosive environments. Stainless steel is and will continue to be a crucial material for the modern civilization, while more materials are consumed by the developing countries and the growing population of the World. Increasing concerns for the environment and the fluctuating economic stability are driving development for more efficient manufacturing processes, also for stainless steel.

One company in the metals industry is Outokumpu Oyj from northern Finland. They produce high quality stainless steel and have mined one of its key substances – chromite – since 1968. Ferrous chromite is an ore type that contains chromium and iron along with other elements. The chromium and iron are in oxide form and need to be reduced into ferrochrome, a metallic mixture of the two, before utilization in the process of manufacturing stainless steel.

Currently the reduction is done in submerged electric arc furnaces by using coke as the reductant. This requires extreme temperatures and therefore the furnace consumes a lot of electricity. Substantial benefits could come about, if an alternative production method requiring less energy could be generated. This thesis studies the possibility of lowering the production costs of ferrochrome by incorporating methane as a reductant in a prereduction step. If the ore could be significantly reduced before the smelting, this would lower the furnace's need for energy.

In the present work, the aim is to achieve knowledge of the characteristics of methane reduction for the specific chromite mined in Finland. This information could be used to develop the process of conventional ferrochrome production towards a more sustainable direction.

2 Chromite Ore

Chromite (ferrous chromite) ore is the starting point of producing metallic chromium and ferrochrome. This chapter will review chromite's essential properties as a mineral, deposits and the particularities of the chromite deposit in Kemi, Finland.

2.1 Properties and Mineralogy

Chromite is the only ore that contains enough chromium for it to be economically feasible for mining and chromium production. It is grey or black with a metallic luster and possible brown streaks of side rock. High specific gravity is characteristic of chromite and at times it can be slightly magnetic. (King, 2015) Figure 1 shows a specimen of Kemi chromite.

Figure 1 Piece of chromite ore; [Maria Leikola]

Chromite's most valuable mineral is chromium spinelide, which is part of the spinel group of minerals. Spinels have a simple cubic structure and they can be characterized with the general formula AB_2O_4, where metals A and B form the solid compound together with oxygen. There are exceptions to the general formula, for example Cr_3S_4 is a spinel although it is a sulfide, not an oxide. (Lyakishev & Gasik, 1998)

The cubic crystalline structure of spinels is represented in Figure 2. The first image in Figure 2 is that of a unit cell of the spinel structure, which is divided into eight separate octants. The second image incorporates two adjacent octants, where the white circles are O^{2-} -ions and the black circles represent metal ions. The third and fourth images clarify the configuration of metal ions in the tetrahedral and octahedral intersites respectively. In a normal spinel structure, bivalent metal cations, which are represented by A in the general formula, occupy the tetrahedral sites, whereas trivalent cations, the B ions in the formula, occupy octahedral sites. (Lyakishev & Gasik, 1998)

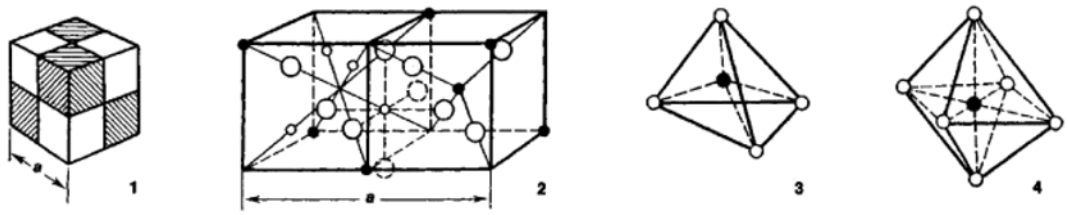

Figure 2 The cubic structure of spinel minerals (Lyakishev & Gasik, 1998)

In chromite ores, the metal cations are often Fe^{2+} and Cr^{3+}, which gives the general formula of $FeCr_2O_4$. Depending on the deposit, other cations such as Al^{3+} and Mg^{2+} ions can be found occupying some of the octahedral and tetrahedral sites. (Lyakishev & Gasik, 1998)

Additionally to the chromium spinel, chromite ore includes various types of side rock that encompass many different minerals. Some examples of these minerals are chrysolite; $3MgO_2SiO_2 \cdot 2H_2O$, actinolite; $2[Ca_2(Mg,Fe^{2+})_5Si_8O_{22}(OH,F)_8]$, magnetite; Fe_3O_4, and calcite; $CaCO_3$. The specific composition of chromite varies between deposits and influences the chemical and physical properties of the ore. (Lyakishev & Gasik, 1998)

2.2 Chromite Deposits Worldwide

The annual production amount of chromite in the World was approximately 29 million tons in 2014 (Papp, 2015). Exploitable deposits of chromite exist around the world, but mostly in Africa and Eurasia. The leading producer for chromite is the Republic of South Africa, which produced 43 % of the World's chromite in 2012. Other big producers were Kazakhstan and India, both producing around 15 %. Outokumpu Oyj is the only chromite producer in Finland and it alone accounted for 1.6 % of the world's production in the same year. (Papp, 2014)

The countries that produced chromite in the year 2012 are pointed on the World map in Figure 3. The light yellow pins represent production percentage of under 1 % of the annual total, the light green pins represent 1-5 %, the three darker green pins 5-40 % and the one blue pin in South Africa represents over 40 %. The detailed production amounts from 2008-2012 and list of countries can be found in Appendix I. (Papp, 2014)

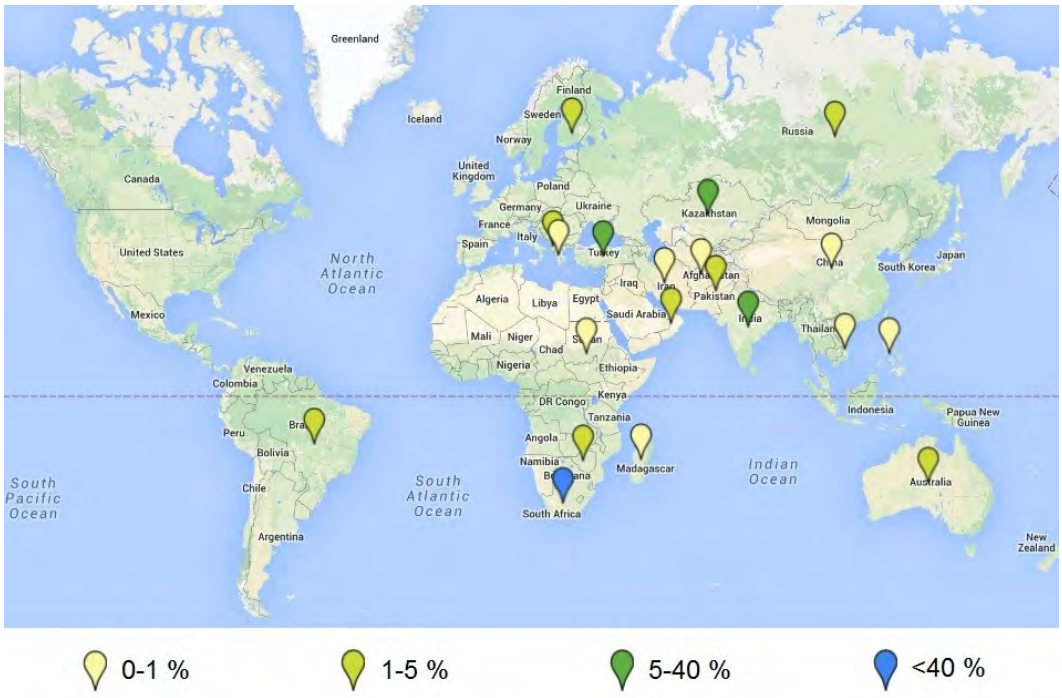

Figure 3 Chromite production by country in 2012 (Papp, 2014); [Maria Leikola]

2.3 Kemi Chromite

The chromite ore under investigation in this thesis has been mined in Kemi since 1968. The site is located in the northern part of Finland on the coast of the Gulf of Bothnia. The chromite ore in Kemi has a relatively low Cr/Fe ratio, but due to the mine's proximity to the Outokumpu Oyj's stainless steel factory, it is still a profitable deposit for mining (Huovinen, 2007). The deposit and its features have been studied by Alapieti et al. (1989). According to them, the entire length of the chromite layer is 15 km and the mineable part of this is 4.5 km long, which has an average Cr_2O_3 percentage of 26.6 %. (Alapieti, et al., 1989)

A chemical analysis of the chromite ore used for this thesis in in Table 1. The analysis was done by Outotec Research Center. The chemical composition of

the deposit varies within itself, therefore also an extensive chemical analysis of various samples from the Kemi mine is in Appendix II (Alapieti & Huhtelin, 2005).

Table 1 Chemical analysis of Kemi chromite ore; [Outotec Research Center]

Element	wt%
Mg	6.50
Al	6.60
Ca	0.41
Ti	0.28
Cr	29.90
Cr met	0.02
Fe	17.60
Fe met	0.21
SiO_2	3.40

Particle size distribution of the ore concentrate used is in Figure 4. The analysis was done using particle sizing instrument Mastersizer 2000 by Malvern Instruments. Five measurements were conducted using 4 bar dispersion pressure and Fraunhofer approximation for the calculations.

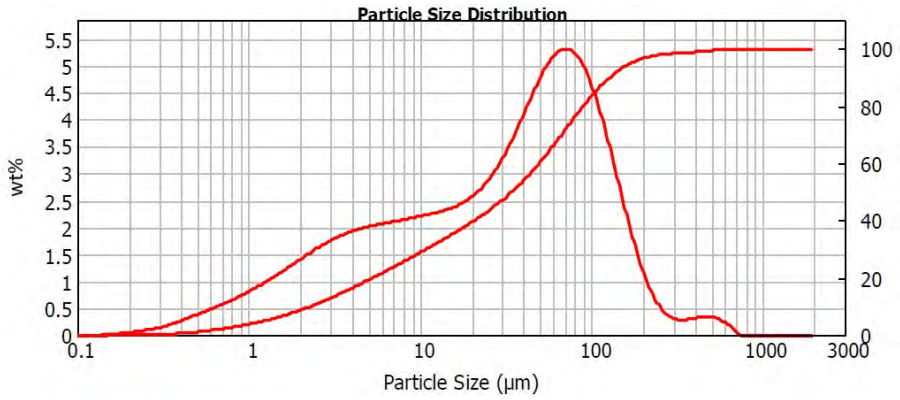

Figure 4 Typical particle size distribution of the chromite concentrate; [Maria Leikola]

3 Ferrochrome

There are three kinds of ferrochrome; high, medium and low carbon types, of which high carbon ferrochrome is the most commonly produced one (Kojo & Holappa, 1991). The following chapter will discuss the current state of ferrochrome usage and the most common production method for high carbon ferrochrome - the submerged electric arc furnace.

3.1 Usage and Production

Ferrochrome is generally used in the production of stainless steel as an alloying element. It is a mixture of iron and chromium in metallic form represented simply with FeCr. Chromium as an alloying element in steel gives it its corrosion resistant properties by forming an oxide layer on the surface of the material, thus resulting in stainless steel. The production amount of stainless steel is about 2 % of the total amount of steel produced worldwide (worldsteel association, 2014).

The evolution of stainless steel production in the 21st century is illustrated in Figure 5 (International Stainless Steel Forum, 2015). Apart from the economic recession in 2008-2009, the trend is clearly upward.

Figure 5 Stainless steel production amounts (International Stainless Steel Forum, 2015); [Maria Leikola]

Figure 5 clearly shows a significant rise in the production amount of stainless steel. It is expected that the overall growth fate for stainless steel manufacturing would be around 5 % per annum at least until 2040 (Taskinen, et al., 2014). Since ferrochrome is an essential raw material for stainless steel, its demand has increased worldwide. Ferrochrome production is illustrated in Figure 6 and there is a clear increasing trend.

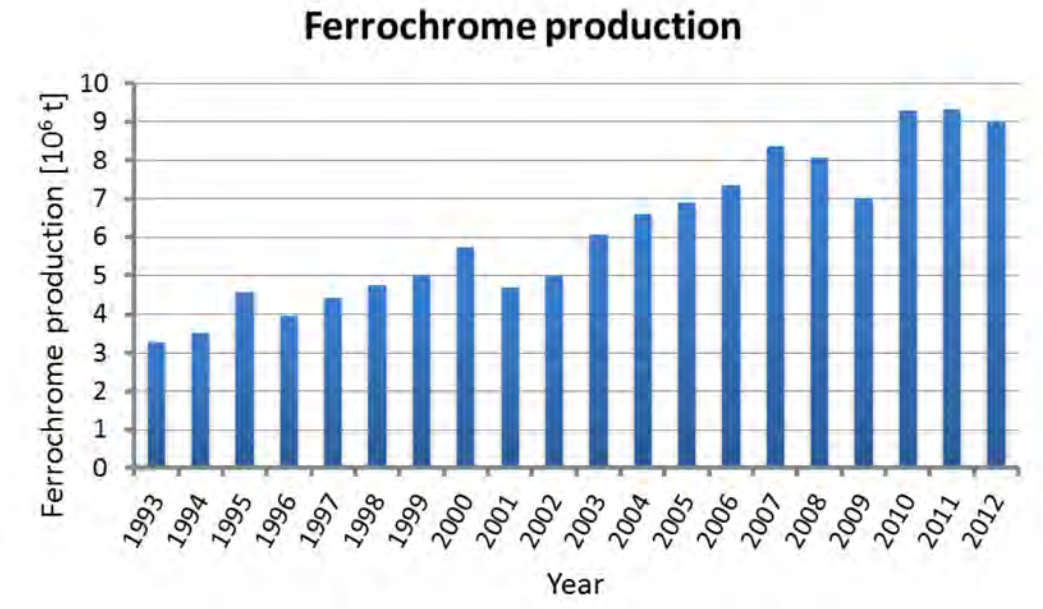

Figure 6 Ferrochrome production amounts (USGS, 2015); [Maria Leikola]

The trend lines in both of the Figures 5 and 6 are very similar as ferrochrome production is directly dependent on stainless steel production. While the demand for ferrochrome is increasing, it is a very energy intensive process, which consumes a lot of electricity and carbon per produced metric ton of ferrochrome. This increasing demand for ferrochrome, while it being a relatively expensive process, drives the search for more economic methods of production.

The next section explains the ferrochrome manufacturing method that is most widely used in the industry – the submerged electric arc furnace.

3.2 Submerged Electric Arc Furnace Process

High carbon ferrochrome can be produced with several different methods, but almost all commercial processes use either an open or closed submerged electric arc furnace (SAF) as the main reduction step (Basson & Daavittila, 2013). Outokumpu's stainless steel mill uses an integrated closed SAF (Outokumpu Oyj, 2013). Therefore, the closed SAF process is discussed further in this section. Figure 7 has a flow diagram of a ferrochrome process by Outotec (Basson & Daavittila, 2013). The individual sub processes of pelletizing, sintering, preheating and smelting are examined in the following sections.

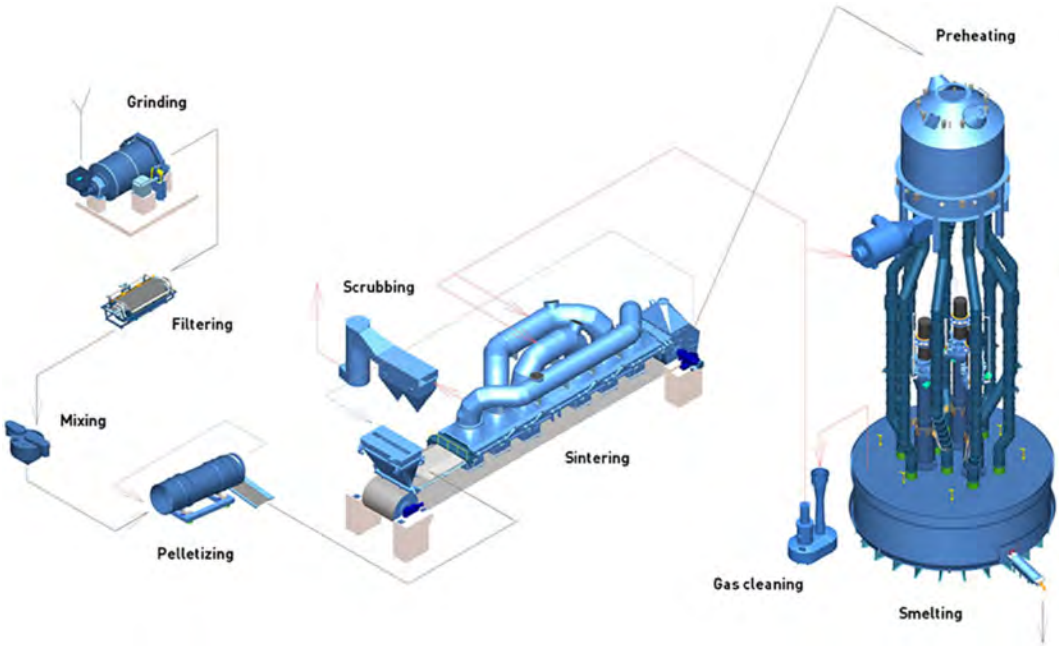

Figure 7 Basic flow chart of the submerged electric arc furnace process (Basson & Daavittila, 2013); Outotec

3.2.1 Concentration and Pelletizing

The chromite mineral is relatively dense and it is therefore most often beneficiated with different gravity concentration methods, such as a spiral concentrator (Murthy, et al., 2011). In the Outokumpu concentrator larger particles of rich ore, also known as lump ore, are first separated from the bulk and the rest is crushed and beneficiated further to create a fine concentrate (Outokumpu Oyj, 2013). The lump ore can be used directly in the SAF, but the fine ore needs further processing (Basson & Daavittila, 2013).

The proper function of the SAF requires for the feed to have a certain particle size and this is obtained by agglomerating fine ore particles and sintering them into pellets. Also, carbon is needed as a reductant in the process and therefore a carbonaceous material such as coke or char is combined into the chromite ore. The ore-carbon blend is first fed into a wet grinding mill to attain a favorable particle size for the pelletizing and sintering processes, p80 is 74 µm. After grinding the slurry is filtered to reach the suitable moisture content of under 9 %. The pelletizing step requires a binding material and for this purpose, fine bentonite powder is used. Additionally, dust from the pelletizing plant dust scrubber can be recycled into the concentrate. The final mixture of ore, carbon, bentonite and possible recycled dust is then pelletized in a pelletizing drum. The average pellet size of approximately 12 mm. As the agglomeration is complete, the pellets are ready for sintering. (Basson & Daavittila, 2013)

3.2.2 Sintering

The purpose of the sintering process is to transform the pellet into one solid particle as opposed to small particles that are simply agglomerated with bentonite. The pellets are fed onto a steel belt that carries the pellets through the furnace. The steel belt is protected by a layer of already sintered pellets

from the heat of the sintering process. The pellets are gradually heated by countercurrent flow of cooling gases from the end of the furnace where the gas burners operate at up to 1400˚ – 1500˚C. At this temperature, the pellets are converted into solid particles that can be fed into the SAF. (Basson & Daavittila, 2013)

3.2.3 Smelting in SAF

Smelting takes place in the SAF, but the raw materials are first preheated in a preheating shaft kiln by burning excess CO-gas from the smelting step. Coke is added as a reductant and quartzite for slag forming. Other slag forming materials, such as lime stone and dolomite, might also be added to adjust the slag chemistry. The ore pellets, lump ore, coke and quartzite are preheated to up to 700˚C before being charged into the SAF. Preheating the feed material lowers the electricity consumption of the furnace. (Basson & Daavittila, 2013)

After preheating, the hot feed advances down charging tubes into the furnace, which is sealed to prevent combustion of gas and leakages. In order to create the needed temperatures to reduce the chromium and iron into metal, graphite electrodes are submerged in the raw material and an electric arc is formed between the tip of the electrodes and the charge by applying electricity. The electric arc creates an extreme temperature in its immediate proximity; up to 2000˚ – 3000˚C. (Basson & Daavittila, 2013) A schematic illustration of the area around the electrode is in Figure 8.

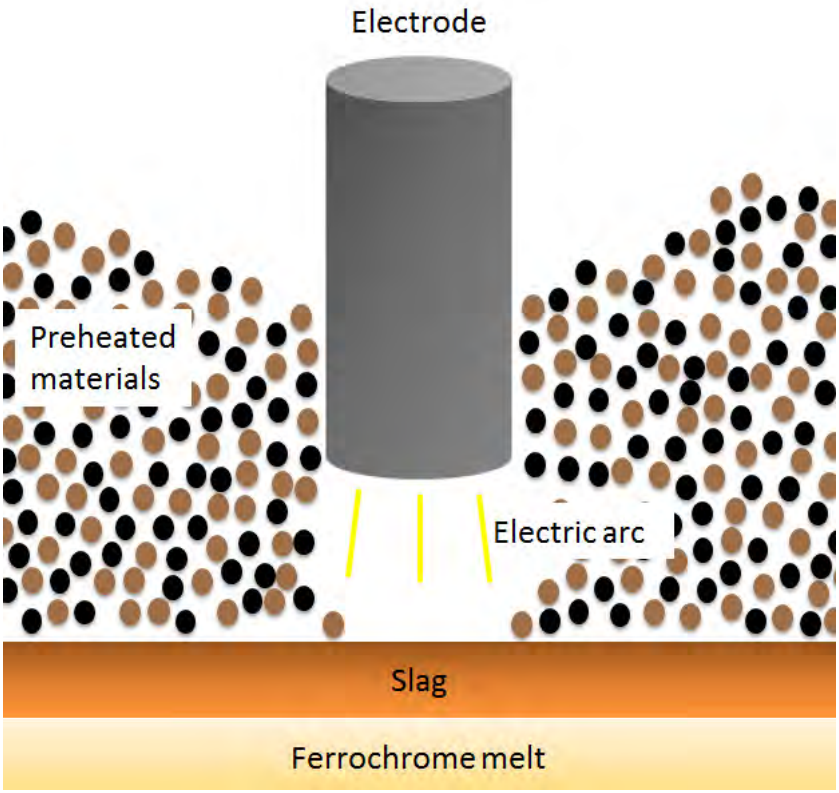

Figure 8 The basic principle of the SAF; [Maria Leikola]

The coke in the charge reduces the chromium and iron in the ore concentrate, forming excess CO that travels through the charge into the furnace's top half. The reduced chromium and iron then form a ferrochrome melt in the bottom of the furnace. On top of this molten ferrochrome layer, the slag layer is formed. Both molten layers are drained from the furnace at regular intervals. (Basson & Daavittila, 2013)

The final result is high carbon ferrochrome that has a chromium content of up to 60 - 70 wt% and carbon content of approximately 4 - 6 wt% (Basson & Daavittila, 2013). In the Outokumpu ferrochrome mill, the chromium content is close to 52 wt% and the carbon reaches 7 wt%. Outokumpu's ferrochrome plant is in close proximity of their stainless steel mill. Therefore, the molten ferrochrome can be utilized directly in the steel making process without the step

of solidifying it and reheating. This enables significant savings in energy use. After the alloying of steel with ferrochrome and other various alloying elements, the melt is refined in argon oxygen decarburization (AOD) converters. Then, the refined steel melt is cast into stainless steel and then manufactured further by means of different forming methods. (Outokumpu Oyj, 2013)

4 Prereduction of Chromite

In addition to the described method of producing ferrochrome, it is also possible to prereduce the pellets in solid form before charging them into the SAF. This procedure lowers the electricity consumption in the SAF. The next chapter discusses different methods of solid state prereduction of chromite that have been studied in this field.

4.1 Prereduction with Carbon

Carbon is the main reductant in the SAF process and already integrated into the chromite pellets. It has also been used to prereduce the ore in solid state before the SAF. First the chemical fundamentals are discussed and then the most successful commercialized processes are briefed.

4.1.1 Solid State Reduction with Carbon

When both chromium oxide and carbon are in solid form, the solid-solid reduction reaction between them happens through CO gas. (Niayesh & Dippenaar, 1992), (Kekkonen, et al., 1995), (Ramakrishna, et al., 2015). Carbon reacts with chromium oxide according to Equation [1]

$$Cr_2O_3 + 3C \rightarrow 2Cr + 3CO. \quad [1]$$

After this, the carbon monoxide proceeds to reduce the remaining oxides as in Equation [2]

$$Cr_2O_3 + CO \rightarrow 2Cr + 3CO_2. \quad [2]$$

When additional carbon is available, the carbon dioxide will transform back into carbon monoxide by the Boudouard reaction shown in Equation [3] as long as temperature remains above 1000˚C

$$CO_2 + C \rightarrow 2CO. \quad [3]$$

(Ramakrishna, et al., 2015)

The reduction of iron happens in the same manner, first by solid carbon after which the formed CO gas acts as the main reductant and is restored by the Boudouard reaction. (Ramakrishna, et al., 2015).

It was concluded by Niayesh & Dippenaar (1992) that the presence of fine particle carbon in the proximity of the chromite and thereafter the possibility of the Boudouard reaction are an essential part for the mechanism to work. It is therefore not feasible to use merely carbon monoxide as a reductant, but carbon is also needed to continuously restore the reducing potential of the gas mixture.

The solid state reduction mechanism of LG-6 chromite of the Bushweld complex was thoroughly established by Soykan et al. (1991a) at 1416˚C. Their study indicates that first the Fe^{3+} ions on the surface of the chromite particle are reduced by CO into Fe^{2+} ions. Then the Fe^{2+} ions are reduced into metallic form and simultaneously Cr^{3+} ions are reduced into Cr^{2+} ions. The Cr^{2+} ions diffuse inward to the chromite particle and reduce the Fe^{3+} ions underneath the surface into Fe^{2+} ions, which then diffuse towards the surface and reduce there into iron. After all the iron has been reduced, Cr ions are reduced into metal. The iron and chromium are in the form of carbides after the reduction has taken place. After the iron and chromium are reduced what is left is a Mg-Al spinel phase. (Soykan, et al., 1991a)

According to Soykan et al. (1991a) diffusion of the ions is driven by their concentration gradients which are illustrated in Figure 9 where the

concentration of ions is shown on the cross-section of a 44.96 % reduced chromite particle. It can be seen that the concentration of Fe ions is low on the surface, thus driving diffusion from the center. Cr^{3+} ions and Cr^{2+} ions have opposite concentration gradient trends and are therefore diffused in opposite directions. The middle of the particle's cross-section is the core that has not been effected by the reduction reactions and it has a composition near the original chromite ore.

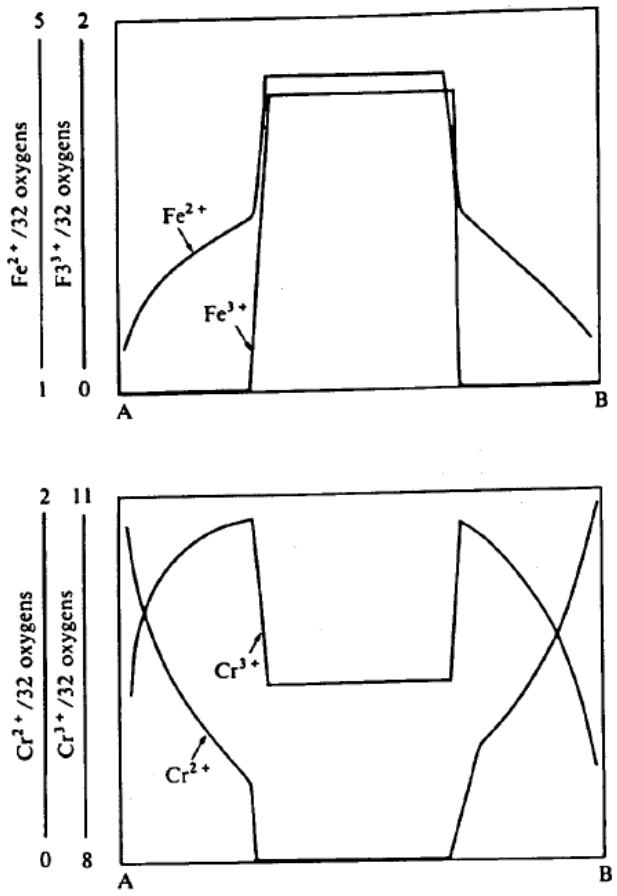

Figure 9 The concentration gradients of Fe and Cr ions on the cross-section of a chromite particle (Soykan, et al., 1991a).

The reduction mechanism of chromite ore depends on temperature. The reduction mechanism was studied by Perry et al. (1988) at lower temperatures than the experiments done by Soykan et al. (1991a). Perry et al. (1988) concluded that below a certain “cutoff” temperature, the reduction mechanism is different from the one discussed here earlier. Their basic principle is the same starting with iron reduction and ionic diffusion as the driving force for the mechanism. The difference is that the chromite does not remain as a spinel, but forms a Cr_2O_3 sesquioxide layer between the reductant and the chromite core. This sesquioxide layer can also crack apart from the spinel core enabling the reducing gas mixture to penetrate to the surface of the core. (Perry, et al., 1988)

Other aspects of the solid state reduction of the chromite mined specifically in Kemi has been studied in a CO atmosphere by Xiao et al. (2004). All together three types of ore products were examined by them; lab-made pellets, industrial pellets and lumpy ore. Their solid state reduction was examined in a CO atmosphere at the temperature range of 1450˚ - 1550˚C. Several findings were made about the process. Rising temperature increased the reduction rate and the reduction advanced from the outer region of the particle towards the center. (Xiao, et al., 2004) These phenomena have also been observed by other studies (Niayesh & Dippenaar, 1992), (Kekkonen, et al., 1995), (Syynimaa, 1996).

Both unsintered and sintered pellets reduced more rapidly compared to the lump ore due to their porous structure. Iron was reduced first forming metal beads of practically pure iron. As the reduction process continued, the chromium content in the metal phase elevated. This can be seen in Figure 10, where the iron percentage of the metal phase increases towards the center of the pellet. (Xiao, et al., 2004)

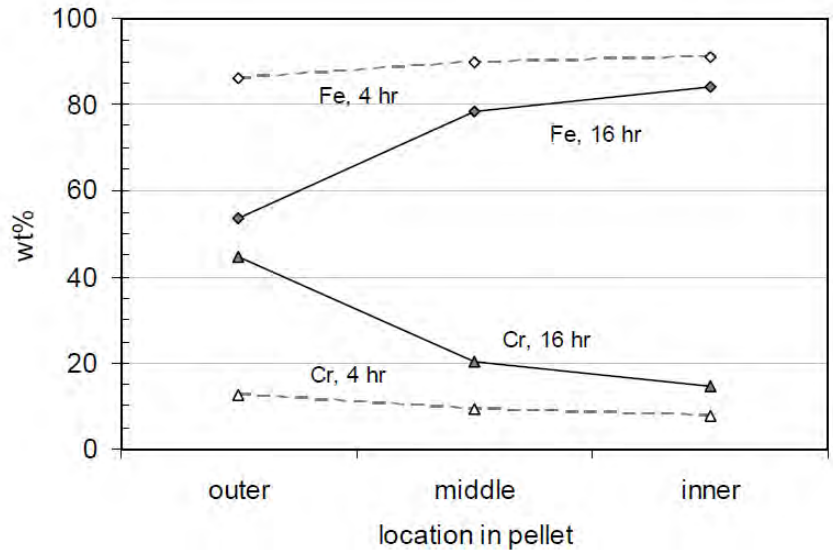

Figure 10 The Fe-Cr ratio from the surface of a sintered industrial pellet towards the middle. (Xiao, et al., 2004)

It was also discovered that in the highly reduced areas two separate FeCr alloys - an iron based and a chromium based - were observed. This is visible in Figure 11, where the surface of the pellet is completely reduced and the two alloys are visible. Also, the fact that the reduction advances from the surface of the pellet towards the center can be seen from Figure 11. (Xiao, et al., 2004)

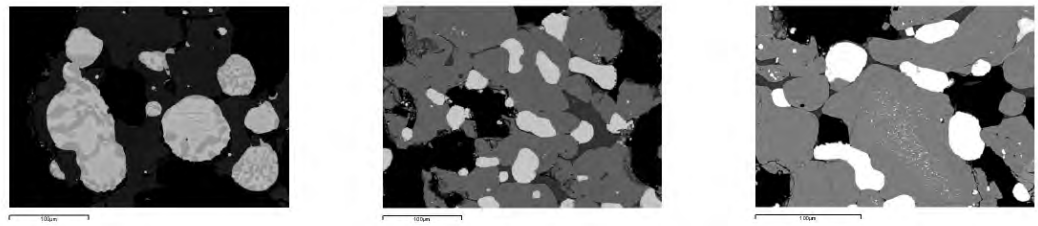

Figure 11 Microstructure of a sintered industrial pellet after 16 hours of reduction under CO atmosphere at 1500˚C (Xiao, et al., 2004)

Additionally, reducing the particle size of the fine ore that was used to make the pellets, or increasing the CO gas flow increased the reduction rate, whereas the increase of bentonite as binding material from 1.5 to 3 wt% lowered the rate. Finally, it was again observed, that using coke inside the pellets enables the Boudouard effect and increases the reduction rate significantly compared to merely using CO gas as a reducing agent. (Xiao, et al., 2004)

Additonally to the basic principle discussed above, some other factors of carbothermic reduction are briefly explored in the next two sections.

4.1.1.1 Carbothermic Reduction with Lime Catalyst

The use of lime as a catalyst for the reduction of chromite-carbon pellets was investigated by Ding & Warner (1997). The experiments performed were in the temperature range of 1270˚ - 1433˚C and employed chromite ore from South Africa. They discovered, that the addition of lime into the pellets with the carbon and chromite, increased the reduction rate significantly. The acquired results for reduction rate with increasing lime content, from 0.4 wt% to 13.52 wt% compared to chromite, for 1433˚C are presented in Figure 12. They discovered that the effect of lime addition increases as the temperature rises and the reduction continues. (Ding & Warner, 1997)

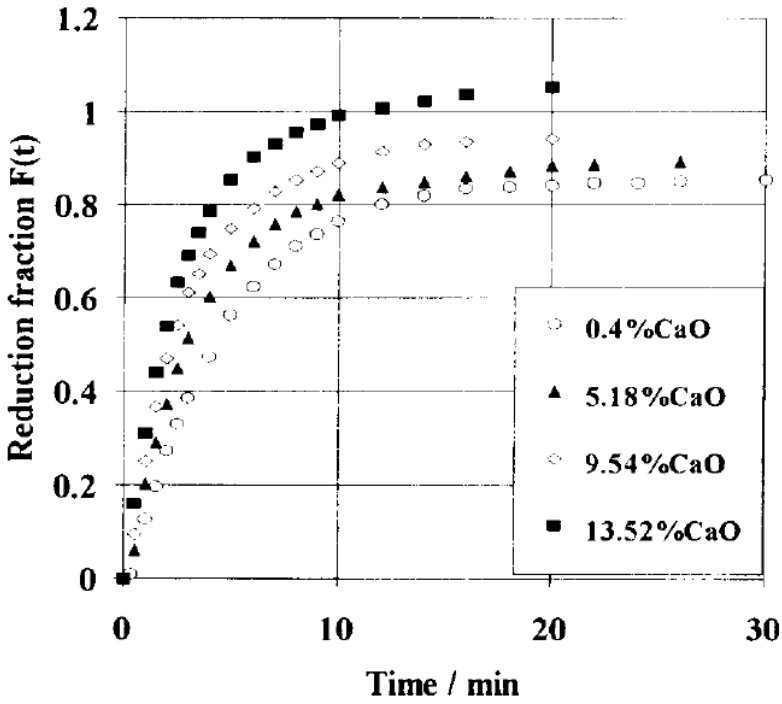

Figure 12 the effects of increased lime addition on the reduction rate of chromite at 1433 ˚C (Ding & Warner, 1997).

Ding & Warner (1996) proposed that the mechanism of the lime catalyst effect is that lime releases iron from chromite in the very first step of the reaction chain, after which the remaining iron and chromium are reduced.

4.1.1.2 Carbothermic Reduction in the Presence of Silica Flux

Using different flux materials in the process of chromite reduction can have an effect on the reaction mechanism itself. The use of silica flux was examined by Weber & Eric (2006) in the temperature range of 1300˚ - 1500˚C. They reduced natural chromite from the Bushweld complex in South Africa with graphite and in presence of silica powders. Notable differences in the reduction rate were observed at 1400˚C and the optimal benefits were achieved by adding 7.5 wt% of silica into the powder mix. The effects of silica addition at 1500˚C can be

seen in Figure 13, where the highest reduction rate is achieved with the 7.5 wt% silica addition. (Weber & Eric, 2006)

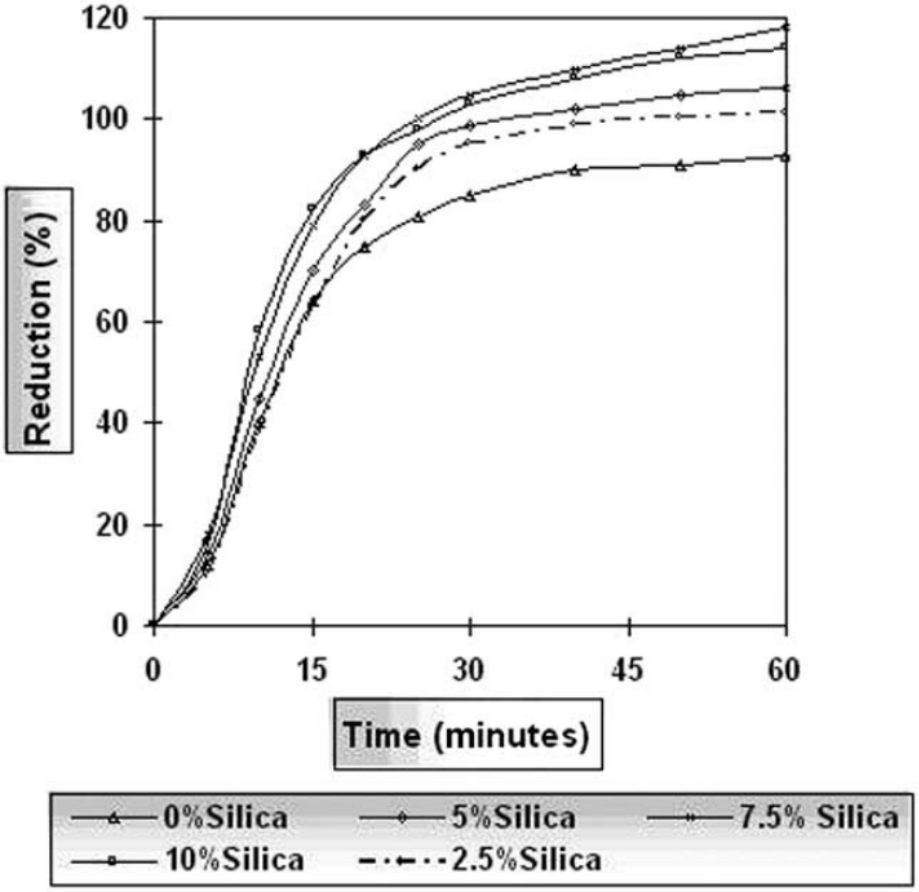

Figure 13 Effects of 0 - 10 wt% silica addition on the reduction of chromite at 1500˚C (Weber & Eric, 2006).

The reaction mechanism of chromite in the presence of silica flux has been established earlier by both Weber & Eric (1993) and Duong & Johnston (2000). They discovered that the reaction happens in two stages where the first part is mainly iron metallization, which forms an iron ring around the particles. After this, silicate slag forms in between the particles, which enables the further reduction of iron and the onset of chromium reduction. (Weber & Eric, 1993) (Duong & Johnston, 2000)

Solid-state reduction of chromite has been in commercial use as a way to prereduce chromite before charging it into the SAF. The next section discusses very briefly the two most successful processes.

4.1.2 Commercialized Prereduction Processes

There have been many attempts to produce a commercial process for prereducing chromite for the SAF. Among many other attempts was the Krupp Industrietechnik's chrome direct reduction (CDR) process, where nonagglomerated chromite is prereduced in a rotary kiln with carbon. CDR was commercialized by Middleburg Steel & Alloy, but the production through this method stopped in the 1990s. (Basson & Daavittila, 2013)

The most successful prereduction method has been using coke in the pellets to prereduce the metal oxides in a rotary kiln, which is called the solid state reduction with carbon (SRC) process. SRC was developed by Showa Denko and it is in use in South Africa by the company Xtrata. The process is slightly modified from Showa Denko's original, but it is the only large scale ferrochrome producing process that uses a prereduction step. Presently, the prereduction process at Xtrata also called the Premus process reaches a metallization degree of 50 % for chromium, before charging it into the SAF. Figure 14 shows that the process is very similar to the already described ferrochrome process, but it embodies a roasting step between preheating and SAF. In the roasting kiln, the coke in the pellets reduces the iron and chromium partly into metal. (Basson & Daavittila, 2013)

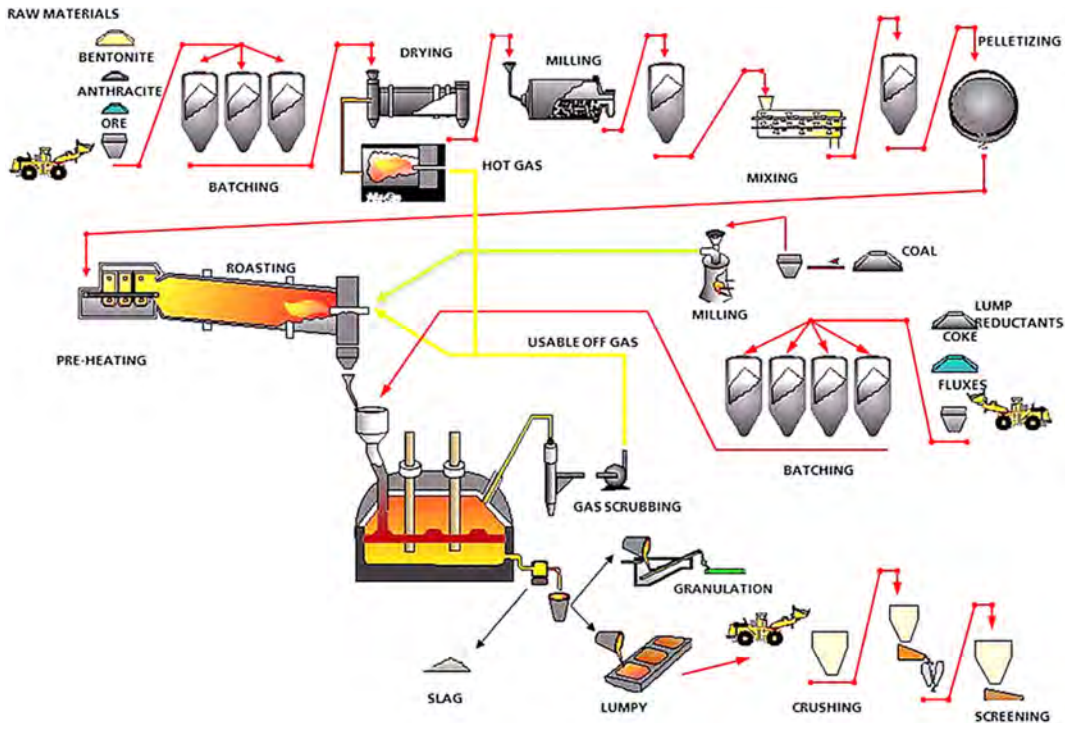

Figure 14 The Premus process of Xtrata with prereduction of chromite pellets (Basson & Daavittila, 2013) ;Xtrata

Both the discussed CDR and SRC processes use carbon as a reductant. However, according to several studies it is possible to reduce chromite also with methane (Read, et al., 1974), (Qayyum & Reeve, 1976), (Anacleto & Ostrovski, 2004), (Ostrovski & Zhang, 2006), (Khoshandam, et al., 2006), (Ebrahimi-Kahrizsangi, et al., 2010). This is a potential way for reducing production costs of the ferrochrome manufacturing process. The following section will go over methane reduction from the point of view of manufacturing prereduced chromite for the production of ferrochrome.

4.2 Reduction of Chromite with Methane

The scientific understanding of the reduction mechanism of chromium oxide has undergone an evolution through the recent decades. The next two sections discuss how the general opinion has evolved.

4.2.1 Methane as a Source for Solid Carbon

The prospect of reducing chromium oxide Cr_2O_3 with methane and hydrogen was examined by Read et al. (1974). The industrially most interesting aspect of this procedure was that the effluent could consist of mainly CO and H_2 and not CO_2 or H_2O. This would make the off-gas a feasible reducing agent for the following reduction step as the gas is still combustible. In other words, the calorific value of the off-gas could remain high while still producing reduced metal as the result. (Read, et al., 1974)

The research method included reducing experiments with Cr_2O_3 either mixed with solid carbon or not. The effluent was analyzed for H_2O and CO in order to determine its calorific value. The chemical reaction mechanism could be speculated on by performing several experiments in various temperatures and using different solid and gas combinations. (Read, et al., 1974)

It was discovered that with excess carbon available, carbides are formed, but with less carbon available, even pure chromium metal could be achieved. Also, the availability of carbon eliminated H_2O and CO_2 from the off-gas. If the experiment was conducted in an H_2 atmosphere, it would occur in approximately 100˚ - 150˚C lower temperature, as opposed to a CO or N_2 atmosphere. Therefore, hydrogen acts as a catalyst for the reaction. The reaction mechanism that was proposed by Read et al. (1974) is presented

here. First, the methane cracks and releases carbon and hydrogen according to Equation [4].

$$CH_4 \rightarrow C + 2H_2 \quad [4]$$

Then the chromium oxide reacts with the formed hydrogen as in Equation [5]

$$Cr_2O_3 + 3H_2 \rightarrow 2Cr + 9H_2O. \quad [5]$$

(Read, et al., 1974)

However, it should be noted that this reaction is thermodynamically questionable as the standard free enrgy of water formation is higher than that of chromium oxide formation

The carbon from Equation [4] and the chromium from Equation [5] now react into chromium carbide via Equation [6]

$$3Cr + 2C \rightarrow Cr_3C_2. \quad [6]$$

Then finally the off-gas is formed from the water and carbon as in Equation [7]

$$H_2O + C \rightarrow H_2 + CO. \quad [7]$$

If hydrogen is replaced with nitrogen gas, the reaction mechanism changes into a straight forward reaction in Equation [8] instead of Equations [5], [6] and [7]

$$3Cr_2O_3 + 13C \rightarrow 2Cr_3C_2 + 9CO. \quad [8]$$

Even though the former mechanism does not stoichiometrically need additional hydrogen, the supply of excess hydrogen is needed to enable a more rapid reaction. (Read, et al., 1974)

Methane can also be utilized as a reductant without feeding it into the system with the inward gas flow. It is also possible to heat chromite-carbon composite pellets in a hydrogen atmosphere as was done by Qayyum & Reeve (1976). In this method, the used carbon reacts with the hydrogen producing methane.

This enables the reduction mechanism to start already at 800˚C and become very rapid at 1000˚C. If the amount of carbon is stoichiometrically accurate, the process will result in sponge ferrochromium with very small carbon content. Additionally, the off-gas consists of H_2, CO and CH_4, thus maintaining a high calorific value. (Qayyum & Reeve, 1976)

Qayyum & Reeve (1976) conducted the experiments for two natural chromite concentrates as opposed to the pure Cr_2O_3 that was used by Read et al. (1974). One was from Canadian Bird River chromite and the other one from South Africa called the Transvaal chromite. Isothermal reduction curves for both chromites are presented in Figure 15. Both are reduced in a relatively short period of time; under 60 minutes. However, the Bird River chromite reduction is marginally slower than the Transval chromite's. Most importantly this reveals the fact that although chromite incorporates other materials and compounds besides chromium oxide, methane reduction is still a promising method for reducing it. (Qayyum & Reeve, 1976)

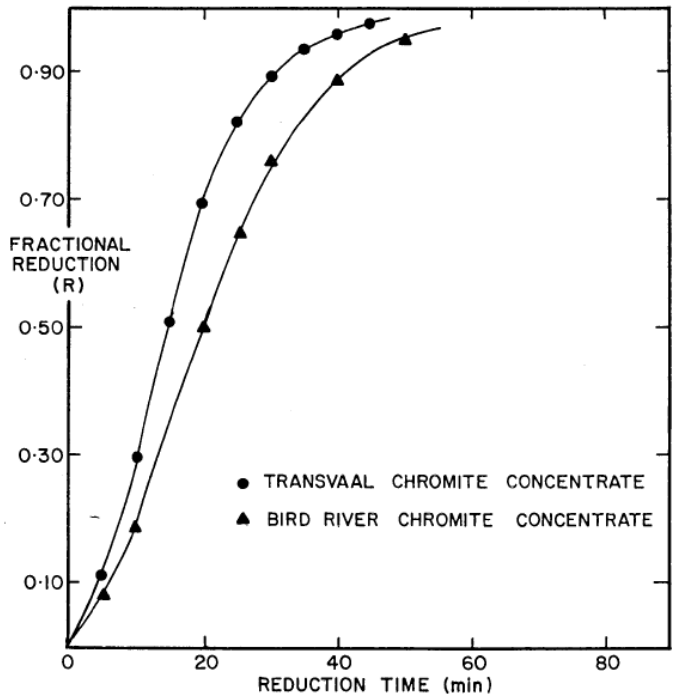

Figure 15 The isothermal reduction rate of natural chromite-carbon pellets at 1000˚C (Qayyum & Reeve, 1976).

4.2.2 Methane Adsorption

Decades after the research by Read et al. (1974) and Qayyum & Reeve (1976) the topic of methane reduction of Cr_2O_3 was examined further by Anacleto & Ostrovski (2004). They stated, that the chemical mechanism proposed by earlier research was not in line with the current knowledge of the kinetics of carbothermal reduction of Cr_2O_3. This was based on the fact that the reduction of Cr_2O_3 with CH_4 appears at temperatures above 841˚C whereas with solid graphite as the reductant, the necessary temperature is 1113˚C. This then indicated that the role of methane would be something else than providing solid carbon into the reaction. (Anacleto & Ostrovski, 2004)

Anacleto & Ostrovski (2004) performed numerous experiments to uncover the effects of increasing and uniform temperature, gas flow rate, CH_4 and H_2 ratios and also adding CO into gas flow. This led to defining the optimal conditions for Cr_2O_3 reduction into Cr_3C_2 as being 1100-1200˚C with gas ratios 10-15 vol% for CH_4 and above 20 vol% for H_2. (Anacleto & Ostrovski, 2004)

Finally, data from other researches was combined with the acquired results and compiled into Figure 16. It can be seen from this graph that the reduction of Cr_2O_3 with methane containing gas is more effective than with carbon at higher temperatures. This indicates that the reaction mechanism is indeed different from the previously suggested one where methane acts as a provider of solid carbon. It was deducted by Ancleto & Ostrovski (2004) that the activity of carbon in the methane containing gas is 15 to 50 times higher than the activity of graphite. (Anacleto & Ostrovski, 2004)

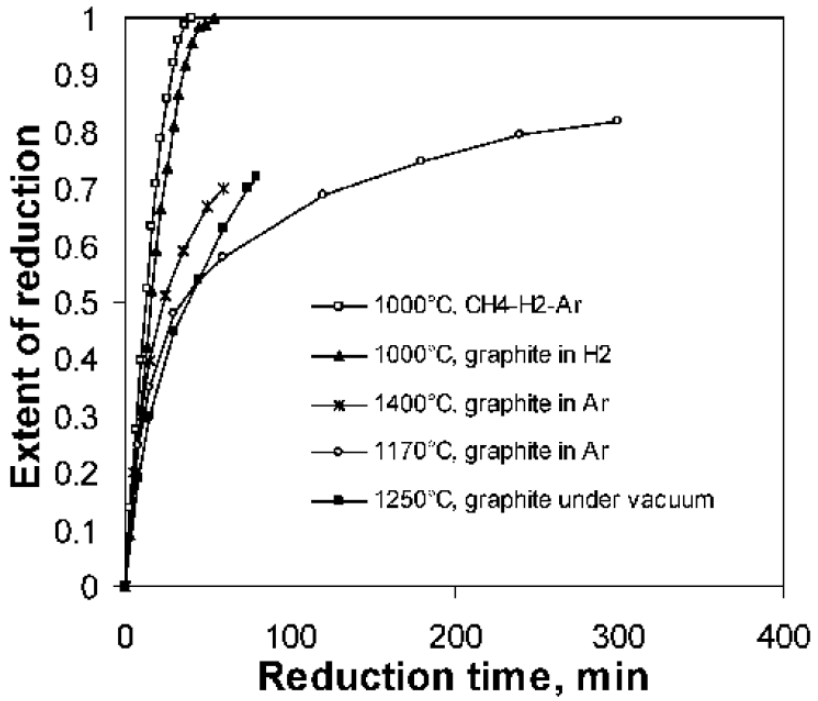

Figure 16 Methane reduction compared to graphite reduction at the same and higher temperatures, methane reduction being the more rapid (Anacleto & Ostrovski, 2004).

From these conclusions, Anacleto & Ostrovski (2004) proceeded to their proposal for the reduction mechanism. It was put forward that the mechanism starts with the adsorption of methane onto the active oxide surface, not its spontaneous cracking into carbon and hydrogen. After this, the methane decomposes producing hydrogen gas as described in Equations [9]-[14]

$$CH_4(g) \rightarrow CH_4(ad) \quad [9]$$

$$CH_4(ad) \rightarrow CH_3(ad) + H(ad) \quad [10]$$

$$CH_3(ad) \rightarrow CH_2(ad) + H(ad) \quad [11]$$

$$CH_2(ad) \rightarrow CH(ad) + H(ad) \quad [12]$$

$$CH(ad) \rightarrow C(ad) + H(ad) \quad [13]$$

$$2H(ad) \rightarrow H_2(g) \quad [14]$$

Leading to the resulting reaction of methane adsorption on the oxide's active surface in Equation [15]

$$CH_4(g) \rightarrow C(ad) + 2H_2. \quad [15]$$

The overall reaction for methane reduction of chromium oxide remains the same as in Equation [16], but the underlying mechanism is fundamentally different due to the adsorption of methane instead of it cracking independently

$$3Cr_2O_3(s) + 13CH_4(g) \rightarrow 2Cr_3C_2(s) + 9CO + 26H_2. \quad [16]$$

(Anacleto & Ostrovski, 2004)

Methane can also be used for treatment of other metal oxides. This same reaction mechanism has been concluded to apply also for iron and manganese oxides, producing cementite and manganese carbide respectively. The optimal conditions for reduction of iron into cementite are 750˚C with 40 - 55 vol% H_2 and 35 vol% CH_4. Reduction of manganese oxide intensifies still at temperature of 1200˚C and has the best reduction rate with the gas mixture of 10 - 15 vol% CH_4 and above 20 vol% H_2. (Ostrovski & Zhang, 2006)

The methane adsorption mechanism for reduction was studied further by de Campos & Eric (2006) by using chromite instead of pure Cr_2O_3. They used chromite from the LG-6 layer of the Bushweld complex found in South Africa. In the study, a loose chromite bed of fine particles was reduced in a vertical tube furnace in the temperature range of 1050˚ – 1250˚C. The methane was fed into the furnace with argon or hydrogen, while its own concentration, the temperature and reduction time were varied. After this, analyses were performed on the phase changes, metallization degrees and concentration structures of the samples. (de Campos & Eric, 2006)

Most importantly, de Campos & Eric (2006) demonstrated in their study, that the reduction mechanism is the same for chromite as it is for pure Cr_2O_3. They concluded that methane cracks into H_2 and solid C, thus enabling the reduction of chromium and iron oxides into metals and further on into carbides. The reaction happened on the surfaces of the particle, but also deeper in the cracks and pores. This is apparent in Figure 17 that shows Scanning Electron Microscopy (SEM) images of the samples reduced at 1100˚ – 1200˚C, from 30 to 120 minutes and in 10 vol% CH_4 in a H_2 atmosphere. (de Campos & Eric, 2006)

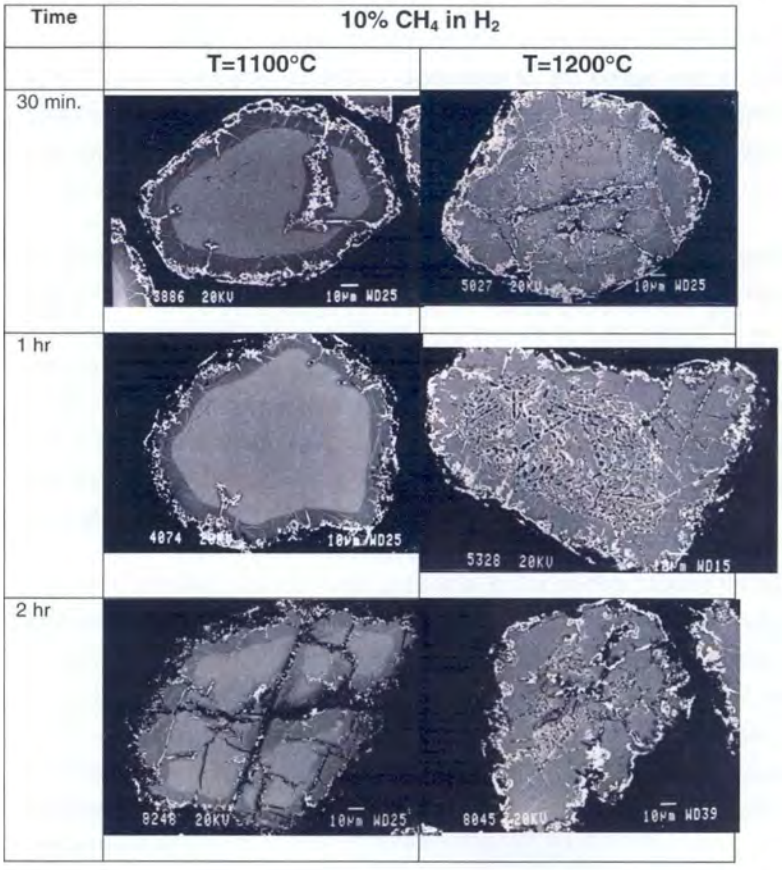

Figure 17 Images of the samples reduced at 1100˚ – 1200˚C, from 30 to 120 minutes and in 10 vol% CH_4 in a H_2 atmosphere (de Campos & Eric, 2006)

The use of methane has also been studied from the point of view of producing chromium carbide as an end product instead of a prereduced raw material for stainless steel production. For example, Khoshandam et al. (2006) conducted experiments with Cr_2O_3 reduction with a methane-hydrogen gas mixture. They were able to produce solid chromium carbide at 870˚C, which is approximately 140˚C lower than with the already discussed reduction with carbon or carbon monoxide as a reductant. In the same study, the product layer around the Cr_2O_3 grains was examined and the diffusion coefficient of methane in the product layer was calculated. The results of Khoshandam et al. (2006) diffusion coefficient calculations are in Table 2 for CH_4 mole fraction in the gas being 0.5. As is often the case, the diffusion coefficient and therefore the rate of diffusion increases as temperature rises. (Khoshandam, et al., 2006)

Table 2 Calculated diffusion coefficients for methane in the product layer (Khoshandam, et al., 2006).

T(˚ C)	$D_{CH_4,P}$
870	1.24
900	2.45
925	5.81

This topic was also studied by Ebrahimi-Kahrizsangi et al. (2010). They used 30 vol% methane gas and achieved a reduction temperature as low as 850˚C. This was lower than the temperature presented by Khoshandam et al. (2006) because of the lower methane concentration in the reducing gas. The excess of methane used by Khoshandam et al. (2006) would form a layer of solid carbon on the surface of the particle and thus hinder the penetration of the reducing gas onto the reaction site. Ebrahimi-Kahrizsangi et al. (2010) also reported that the fastest reduction time was achieved at 1000˚C, which was

only 20 minutes. They concluded that only Cr_3C_2 was produced and none of the other forms of chromium carbide (Cr_7C_3 or $Cr_{23}C_6$). Therefore considering all their findings, methane was seen as a superior reducing agent compared to other methods of chromium carbide production. (Ebrahimi-Kahrizsangi, et al., 2010)

Overall it can be stated that the scientific research presented earlier in this section has proven the reduction of chromite with methane to be potentially energy efficient compared to the conventional method of carbon reduction since the reduction takes place in a lower temperature. The principal of methane-hydrogen reduction is basically the same as with graphite, but the difference lies in the activity of carbon as was stated by Ancleto & Ostrovski (2004). In temperatures above 600˚C, the activity of molecular carbon starts to rise exponentially, as demonstrated by Taskinen et al. (2014). A graph is presented in Figure 18, where the activity rises exponentially as temperature and methane percentage increase. This phenomenon is at the heart of this Master's Thesis and is accountable for the potential benefits of the studied process. (Taskinen, et al., 2014)

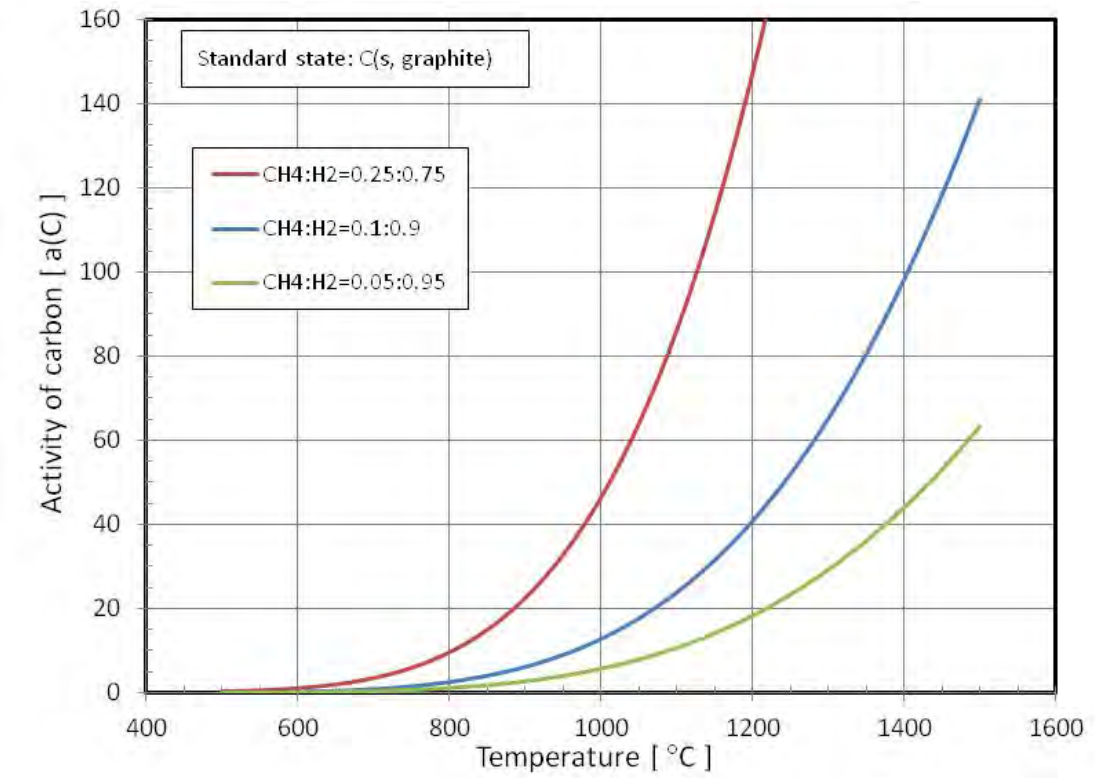

Figure 18 The development of carbon activity in methane-hydrogen atmosphere with respect to temperature (Taskinen, et al., 2014)

The reduction methods of chromite discussed in the previous sections are not, however, the only possibilities. One other method of chromite reduction, which is with hydrogen, is briefly discussed in the next section.

4.3 Hydrogen as a Reductant

The use of hydrogen as the sole reducing gas for chromite was studied by Arvanitidis et al. (1996). They used a synthetic $FeCr_2O_4$ powder and performed the experiments in the temperature range of 900˚ – 1150˚C. They discovered that the reduction was possible and that there was a change in the reducing

order of iron and chromium depending on the temperature. It turned out that below 1100˚C iron oxide was first reduced and then the remaining chromium oxide. This mechanism is presented in Equations [17] and [18].

$$FeCr_2O_4(s) + H_2(g) \rightarrow Fe(s) + Cr_2O_3(s) + H_2O(g) \quad [17]$$

$$Cr_2O_3(s) + 3H_2(g) \rightarrow 2Cr(s) + 3H_2O(g) \quad [18]$$

However, above 1100˚C the order was reversed and chromium was reduced before complete iron recovery. (Arvanitidis, et al., 1996). Equation [18] is again thermodynamically questionable as was Equation [5].

As discussed so far in the present work, the current knowledge of chromite reduction with methane is based on the mechanism of methane cracking and carbon adsorption onto the surface of the ore already at temperatures below 900˚C. This reaction temperature is considerably lower than that with reduction by solid carbon, which requires higher temperatures. This makes the process of prereducing chromite with methane a financially appealing method that could be incorporated in the production chain of ferrochrome.

In the experimental part of this study he methane reduction process was executed on laboratory scale electrical furnace for Kemi chromite. The next chapter describes the experimental setup and analyzing methods.

5 Research Methods

The experimental methods used were similar to the ones employed in an earlier Master's Thesis study performed in Aalto University (Halli, 2015). The methods are therefore only briefly discussed here.

5.1 Experimental Equipment and Methods

The experiments were conducted on a loose bed of chromite concentrate powder. Approximately 1 g of concentrate was reduced for various time intervals in controlled atmospheres of varying CH_4-H_2 contents. Argon was used for a reference test and as an inert gas for purging the furnace. A closed electrical horizontal tube furnace was used in order to reach the required temperatures and atmospheres. The detailed structure of the furnace and its gas train are described by Halli (2015). The gas components used were instrumental argon (Ar 99.999 %), industrial hydrogen (H_2 99.99 %) and industrial methane (CH_4 99.5 %); all supplied by AGA – member of the Linde Group. Other equipment used were alumina crucibles as sample holders and a calibrated Semi-Micro Balance made by Mettler Toledo with an error margin of ±0.00005 g.

After the reduction in the furnace, the sample was ground and divided into two parts. Approximately 0.2 g of the sample stayed at Aalto University and the rest was sent to the Outotec Research Center for analysis. The 0.2 g was first analyzed with X-ray Diffraction (XRD), a common analyzing method, using an X-ray diffractogram X'pert PRO for powders by PANalytical. XRD was used to determine the phases that were present in the samples. After this, quantitative phase analysis was used to determine the ratios of different phases in the

samples. This was done by using the Rietveld method, where the X-ray patterns of each phase are calculated and the cumulative theoretical X-ray diffractogram is compared to the observed one, minimizing the difference by adjusting the alleged sample composition (Hem, et al., 2009). Several commercial software packages are available to perform the Rietveld analysis and one of these is PANalytical's X'Pert HighScore Plus program, which was used for analyzing the samples in the present work (PANalytical, 2015).

The 0.2 g samples were then cast into epoxy and the surface of the samples was ground with silicon carbide sandpaper and polished with 3 µm and 1 µm monocrystalline diamonds supplied by Struers. After this the samples were coated with carbon using a cool sputtering device Leica EM SCD050 in order to enhance the conductivity of the sample surface for the SEM analysis. The equipment used for the SEM were LEO model 1450 VP and Oxford Instruments INCA Software. Also, higher resolution SEM micrographs were taken with MIRA^3 TESCAN XL.

Whereas the 0.2 g of each sample was analyzed with XRD and SEM at Aalto University, the remaining part of the sample was analyzed by Outotec Research Center in Pori, Finland with a Sulphur/Carbon Analyzer. This was done to determine the amount of carbon in the samples. The S/C analyzer used was Eltra CS-2000.

The isothermal sections and liquidus contour diagrams of the C-Cr-Fe system were calculated by MTDATA software (Davies, et al., 2002) using the iron-base alloy database TCFe (National Physical Laboratory, 2015). The calculation included 21 possible condensed phases and gas phase was excluded because it has minor importance in the calculations and phase equilibria of the system.

5.2 Conducted Experiments

Two reference tests were conducted in order to establish reference points for the actual experiments with the CH_4-H_2 atmosphere. One reference test was performed with synthetic graphite (C_{gr} 99.9995 %) by Alfa Aesar mixed with the ore concentrate with mass ratio of 1.5:1. The graphite-concentrate mixture was reduced in an argon atmosphere. Another reference test was done with plain chromite concentrate in hydrogen atmosphere. Both reference tests were performed at 1300˚C for two hours.

After the reference tests, the actual experiments with CH_4-H_2 atmosphere were performed with three variables, forming a matrix of 72 samples altogether. Four temperatures were used; 1100˚C, 1200˚C, 1300˚C and 1350˚C in order to achieve an extensive range while still staying under 1400˚C. Three different gas mixtures were used by varying the CH_4 volume fraction through 10, 20 and 30 vol%, whereas the gas flow was kept continually at 1 l/min. The reduction times used were 10, 20, 30, 60, 90 and 120 minutes.

5.3 Chemical Analysis

The specific details of the analyses performed by Aalto University are discussed in this section.

5.3.1 XRD

The XRD was performed to define the phases present in the samples and was used as a basis for the Rietveld analysis. The radiation used was Cu K-α, generator voltage was 40 kV and the current was 45 mA. In order to detect all

the necessary peaks, a 2θ range of 10˚-90˚ was used. All the XRD diffractograms and quantitative phase analyses obtained are shown in appendices CXIII-CL.

5.3.2 SEM-EDS

To acquire more information about the particles' microstructure and reaction mechanism, SEM with Energy Dispersive X-ray Spectroscopy (EDS) was used. This provided a detailed visual illustration of the ore particles' cross-section and how the reaction had progressed within them. All the micrographs taken with SEM are in appendices III-XLIV and the SEM-EDS analyses of the present phases in different samples are in appendices XLV-CXII.

5.3.3 S/C analyzer

During the reduction, the carbon from the methane that reduces the chromite, also accumulates in the sample as solid carbon. The amount of this deposited carbon was analyzed with an S/C analyzer. As well as acting as the reductant in the reaction, the solid carbon that forms around and in between the chromite particles can also hinder the reaction rate as was observed by Ostrovski & Zhang (2006). The results obtained from the carbon analysis are in appendices CLI-CLII.

6 Results and Discussion

The results acquired from the different analysis methods are discussed in this chapter. Firstly, what the results reveal about the reduction mechanism and secondly, the metallization of iron and chromium are examined. Finally, carbon deposition is briefly overviewed and the mineralogy is considered in the light of the XRD results.

6.1 Reduction Mechanism

As was seen in Figure 17, De Campos & Eric (2006) observed a shrinking core mechanism at 1100˚C with 30 and 60 min reduction times, but a collapsed core when the reduction time was 2 hours. When they increased the temperature to 1200˚C, the experiments produced a collapsed core already in 30 min reduction time.

During the SEM analyses of the present work, it was clearly seen that an outer layer of metal carbides formed, with inner layers of partly reduced chromite. Under the partly reduced regions, there was an unreacted core that had the same composition as the raw material. The shrinking core is observed throughout the experiment series and it appears to have two different stages. One where the iron is completely reduced along with part of the chromium and a second one, where the rest of the chromium is reduced completely.

The first stage can be seen in Figure 19, where the outer layer is almost white, the partly reduced area is a darker gray and the unreacted core is a lighter gray. The experiment was done at 1100˚C, with 10 vol% CH_4, for 20 min. EDS analysis was taken from the points indicated in the image. The composition trends of different elements are shown in Figure 20. Also an EDS analysis of

the raw material is illustrated using dashed lines in order to demonstrate that the core is, in fact, unreacted chromite ore. Silica and titanium were also detected in some of the points in very small concentrations, but are excluded from the image for clarity reasons.

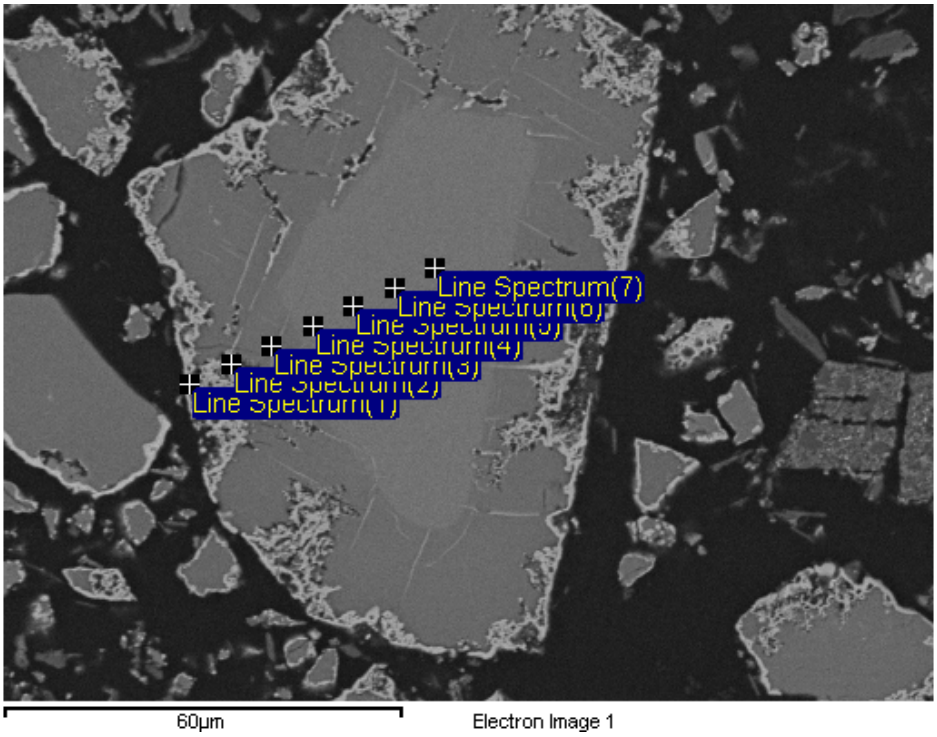

Figure 19 SEM micrograph of a sample reduced in conditions: 1100˚C, 10 vol% CH_4, 20 min

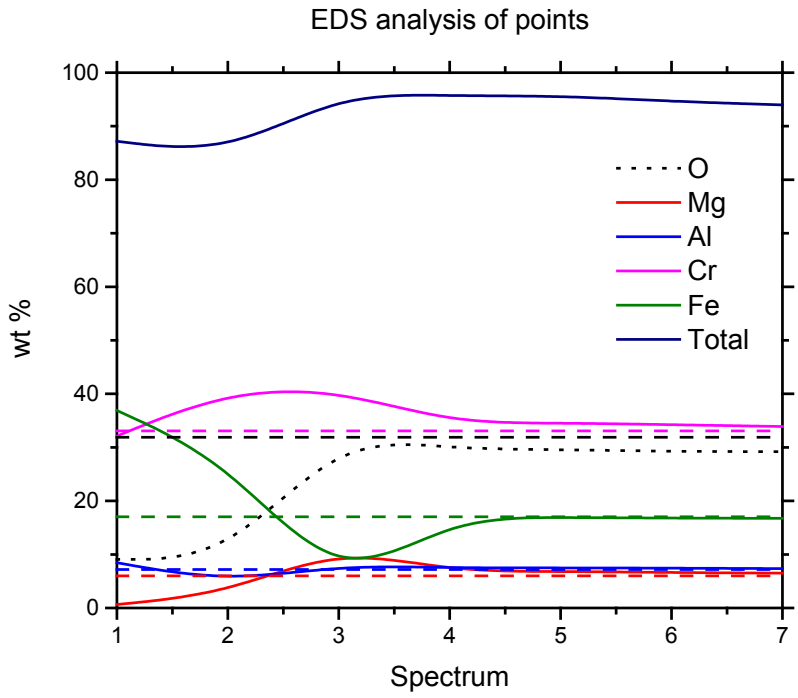

Figure 20 EDS analysis of the particle presented in Figure 19

As can be seen from the EDS analysis, the amount of oxygen, represented by black dots, is highest in the center and lower towards the edge of the particle. This indicates the reduction of the material proceeds from outside in. The outer rim is practically reduced iron and chromium, represented by green and magenta lines respectively. The second layer is partly reduced as it is evident that the amount of iron is lower in this region. The relative amount of chromium and magnesium represented by red, are higher in the middle layer because most of the iron has been removed from this area, see Figure 20.

Figure 21 and Table 3 show the SEM micrograph and EDS analysis for a particle in the second stage of the shrinking core mechanism, where iron has been almost completely reduced and chromium reduction is advancing. Table 3 shows the average EDS analysis results of the white areas, dark grey rims around the white beads and central areas respectively. The experiment was

done at 1300˚C, with 30 vol% CH_4, for 120 min. The small amounts of calcium and titanium were again excluded in the image for clarity reasons.

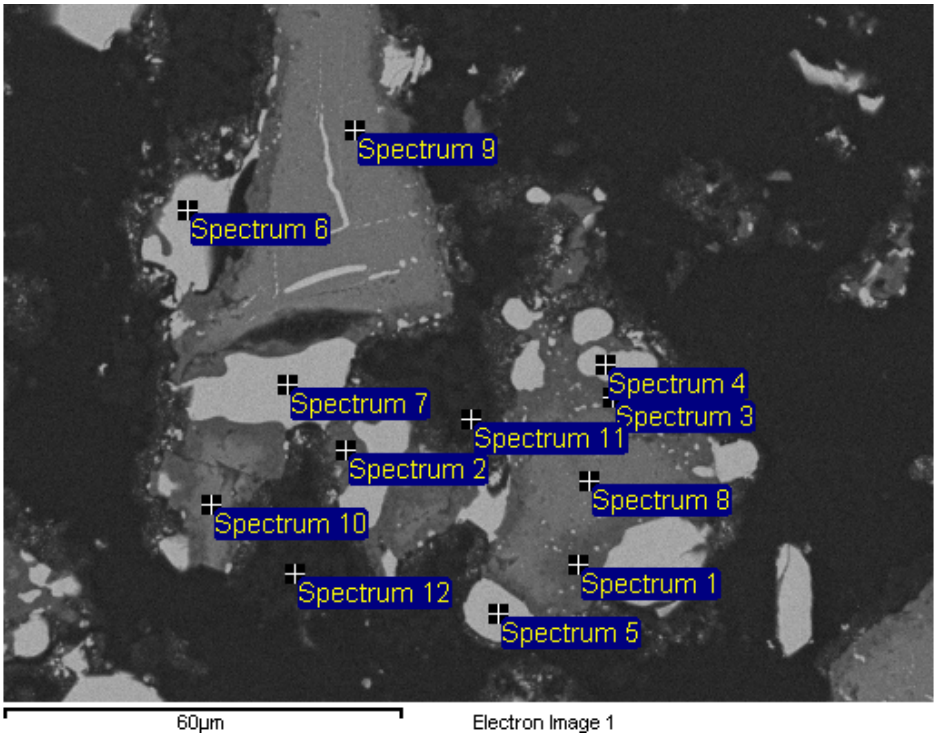

Figure 21 SEM micrograph of a sample reduced in conditions: 1300˚C, 30 vol% CH_4, 120 min

Table 3 EDS analyses of different phases in Figure 2, [wt%]

Element\Phase	White	Dark grey	Center
O	0.43	35.55	30.50
Mg	0.00	19.94	12.50
Al	0.00	18.62	9.45
Si	0.00	5.92	0.06
Ca	0.00	0.65	0.00
Ti	0.00	0.22	0.86
Cr	44.62	6.11	36.34
Fe	38.48	0.86	0.76
Total	**83.52**	**87.86**	**90.32**

The amount of iron is very low (< 1 wt%) outside the white areas. Then again, chromium concentration acts here more like iron did in Figure 20, by decreasing first, but increasing towards the center. This means that iron has been reduced and is gathered in the white areas as carbides and that chromium reduction is advancing towards the core of the particle.

It is seen in Figures 19 – 21 and Table 3 that the bright areas consist mostly of iron and chromium. However, the SEM samples were coated with carbon and therefore the EDS analysis excludes all carbon from the analyses. The total mass of the material is lower in the lighter areas and therefore it can be concluded that there is also carbon in the light areas on the edges of the particles. This indicates that iron and chromium form carbides as they are reduced, which was also observed by Soykan et al. (1991a) with solid carbon as the reductant.

Both Figures 19 and 21 show that the reduction also advances within the particle along cracks that form along the crystalline structure of the chromite spinel. This also was observed in other studes (Perry, et al., 1988) (Soykan, et al., 1991a) (de Campos & Eric, 2006).

To determine the onset of carbothermic reduction, thermogravimetry (TG) and differential scanning calorimetry (DSC) analyses were performed on the chromite at Aalto University. TG determines the changes of mass while DSC scans the energy needed to achieve an increase in temperature. The experiments were conducted with pure ore and also with solid carbon mixed into it as a reducing agent. Both experiments were done in argon atmosphere. The results are visible in Figure 22, where the green lines indicate the results for ore and the red lines are for the ore-carbon mixture. Solid lines tell the change in mass with respect to rising temperature and the dashed lines describe the amount of energy needed to increase the temperature.

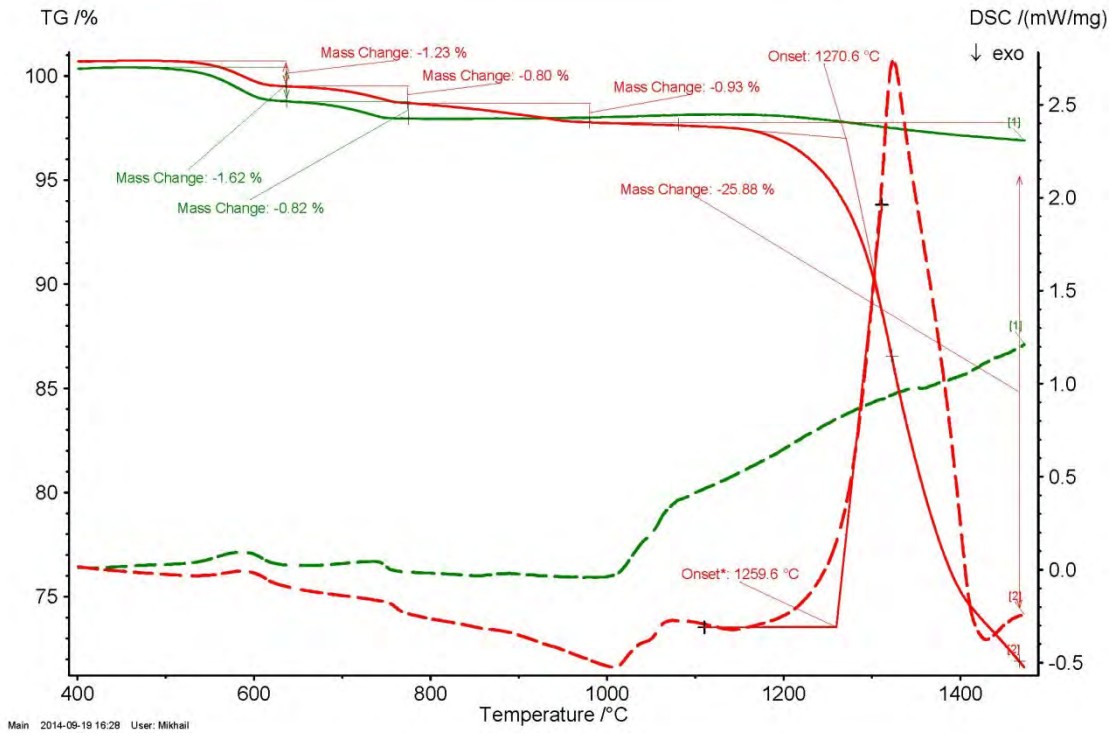

Figure 22 TG and DSC analyses of the chromite ore with solid lines indicating TG and dashed lines DSC – red lines indicating experiment with elemental carbon and green lines pure ore

It can be seen that the mass of the ore doesn't change significantly, but the mass of the sample with added carbon plummets as temperature rises high enough. This is a sign of carbon reducing the ore and decreasing the total mass of the sample by removing oxygen into gaseous phase. The red DSC curve spikes while the change in mass is occurring, because the reduction of the ore is an endothermic process, thus requiring more energy to heat up the sample as part of the energy is consumed by the reaction. The decrease in mass starts when the temperature is approximately 1170˚C. It is therefore concluded that the carbothermic reduction of Kemi chromite starts at this temperature.

As discussed earlier, Perry et al. (1988) concluded there is a cutoff temperature which determines if the reaction mechanism happens through a Cr_2O_3 sesquioxide or if the chromite depleted of iron remains a spinel. Whether the

reduction mechanism of Kemi chromite occurs through the sesquioxide or the spinel structure, depends on its specific “cutoff” temperature. The sesquioxide observed by Perry et al. (1988) slows the reduction rate significantly, but this was not observed in the present work. It is therefore suggested that the reduction mechanism of the Kemi chromite samples occurred through an intermediate phase, that had a spinel structure.

Though the shrinking core mechanism was easier to detect and analyze, also collapsed particles were present in all the samples. Most of the SEM analyses are from particles that remained intact simply because the larger phase areas were more suitable for EDS analysis. The amount of collapsed particles varied throughout the samples and the next sections discuss the reduction mechanism with respect to different experiment variables.

Shrinking core was observed to being dominant in the beginning of the reduction. As an example, there are three micrographs of the 10 minute experiments at different temperatures and with different methane concentrations in Figure 23. The temperatures are 1100˚, 1200˚ and 1300˚C and the methane concentrations 10, 20 and 30 vol%, respectively.

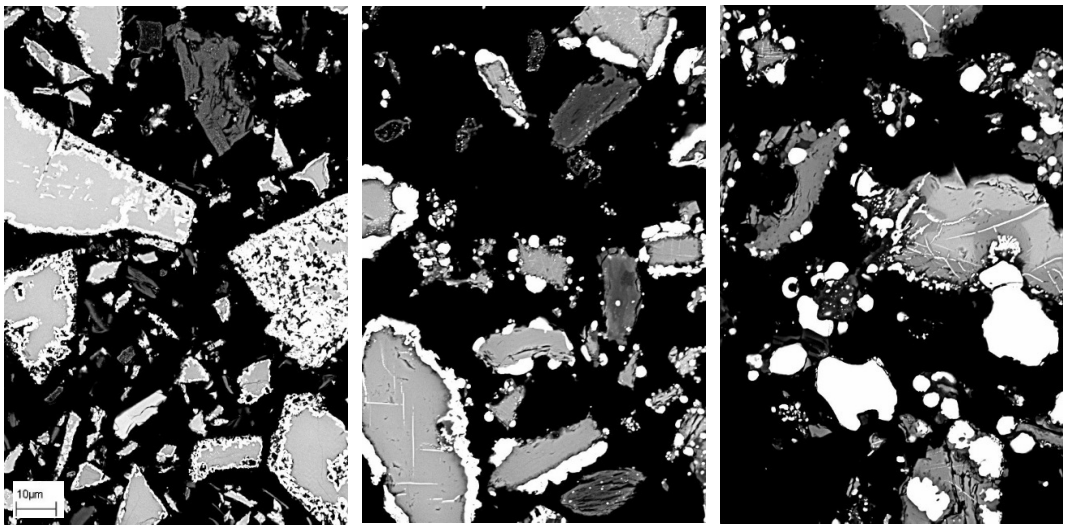

Figure 23 SEM micrographs of samples reduced for 10 min at 1100, 1200 and 1300˚C and with 10, 20 and 30 vol% CH_4, respectively

As the reduction progresses, many of the particles collapse, resulting in reduction also inside the particle and not just on the outer surface and in small cracks inside the particle. This is evident for example in Figure 24, where the particle structure at 1300˚C with varying methane concentration is compared between 10 min and 90 min reduction time. The upper row is with 10 min reduction time and the lower is with 90 min reduction. Methane compositions are 10, 20 and 30 vol%, respectively.

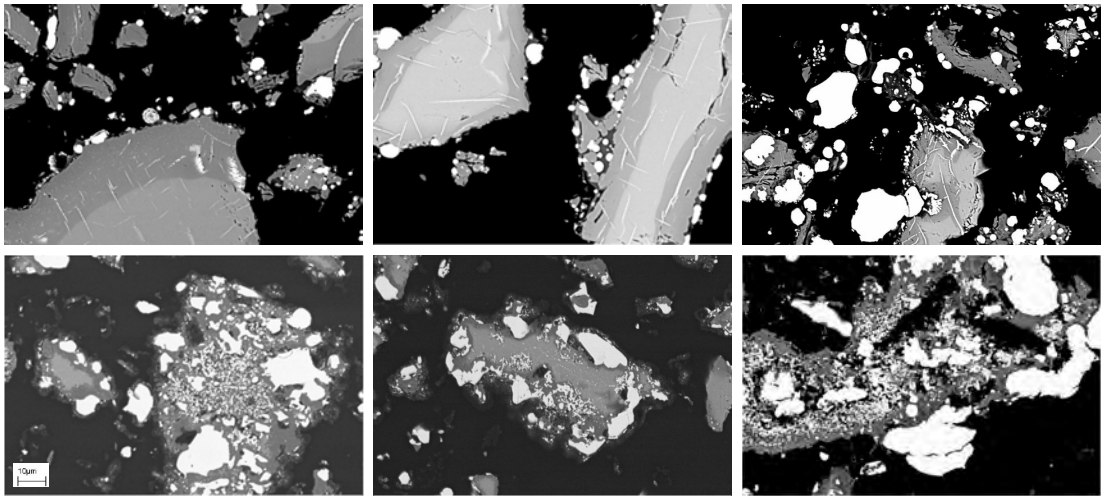

Figure 24 SEM micrographs of samples reduced for 10 min in upper row and 90 min in lower row. The reduction was done at 1300˚C and with 10, 20 and 30 vol% CH_4, respectively

Also, Figure 25 illustrates the reduction mechanism's change over reduction time. The samples were treated at 1100˚C, with 20 vol% CH_4, for 10, 60 and 120 min, respectively.

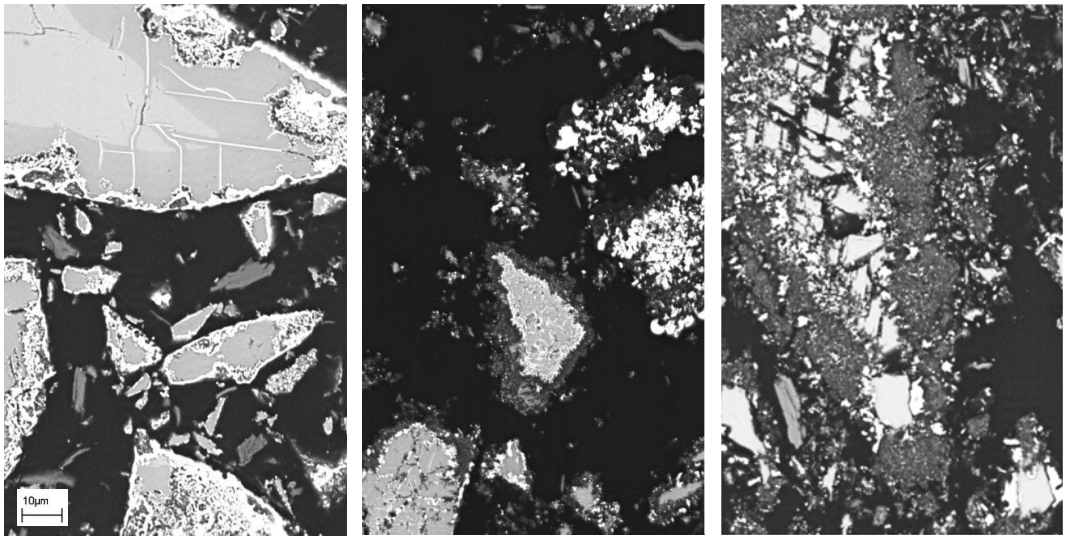

Figure 25 SEM micrographs of samples reduced at 1100˚C with 20 vol% CH_4 for 10, 60 and 120 min, respectively

Temperature was seen as the most affective variable on the reduction mechanism. This was clearly due to the rate of reduction, which increased rapidly with temperature. The particle started to crack and the reducing agent could penetrate into the particle core. Figure 26 shows six micrographs where the temperatures are 1100, 1300 and 1350˚C from left to right, the upper row was reduced with 30 vol% CH_4 for 20 min and the lower row with 20 vol% CH_4 for 30 min.

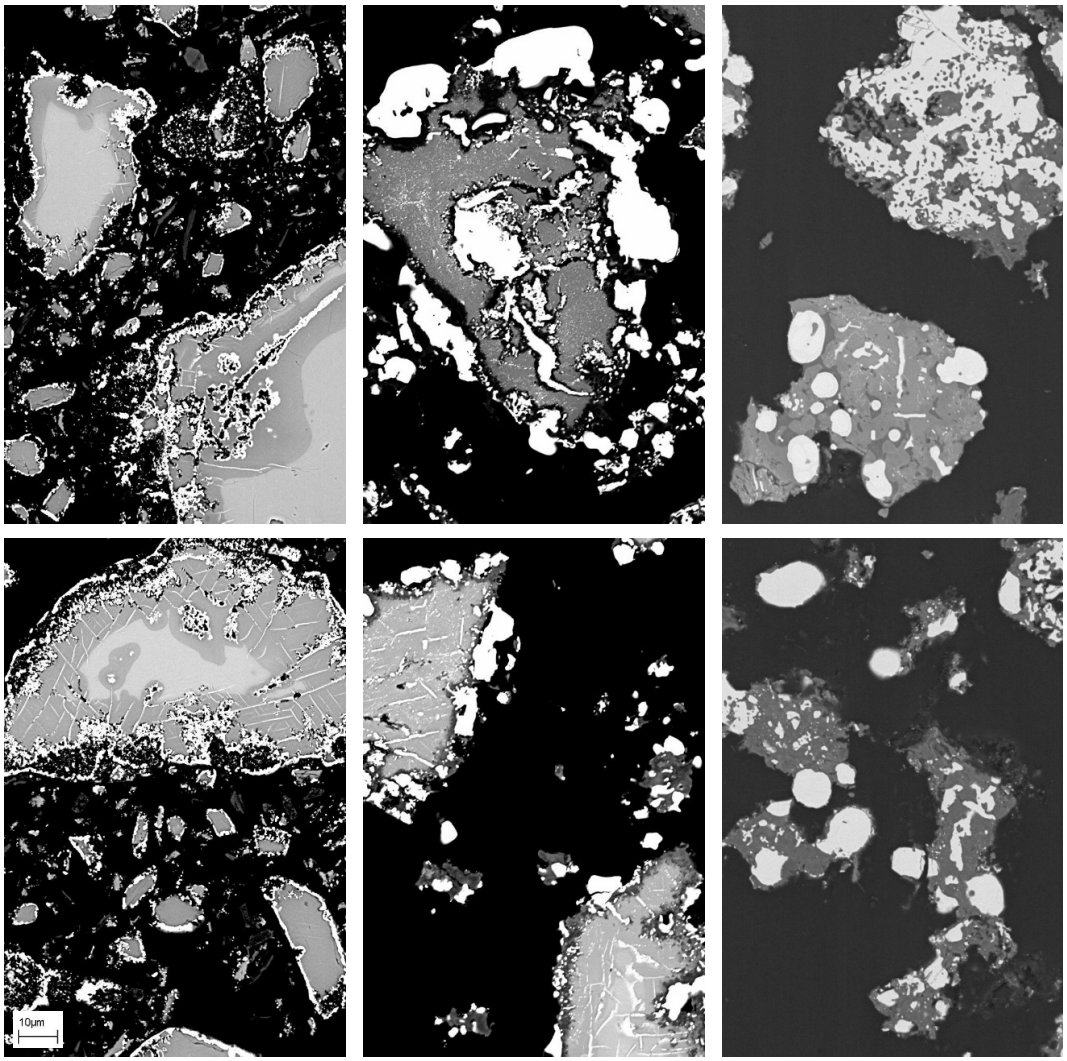

Figure 26 SEM micrographs of samples: upper row conditions were 30 vol% CH_4 and 20 min, lower row conditions were 20 vol% CH_4 and 30 min, temperatures were 1100, 1300 and 1350˚C from left to right

Metallization degree and metallization also within the particles increased together with temperature. The same phenomenon was observed throughout the experiments, where the collapsing of the cores correlated with the fraction of the white, reduced phase. Therefore, it was concluded that the underlying reason for the collapsing of particles was due to increased extent of metallization. It is probable that in the beginning chemical reaction acts as the rate controlling factor, but diffusion starts being the controlling factor after metallization has advanced for some time. The fact that diffusion becomes the

rate controlling factor induces the collapsing of the cores, because collapsing makes the chemical reaction again the rate controlling factor and increases the reduction rate.

In order to understand the reduction mechanism, it was important to examine the structure of the partly reduced phases. For this purpose, micrographs with greater magnification were taken of the intermediate phases. This was done to detect any pores or cracks that may occur in these areas. Figure 27 shows one of these micrographs, 20,000x magnified image of a sample reduced at 1350˚C, with 10 vol% CH_4 for 10 min. The light area is iron and chromium carbide, around it the darker area is depleted of iron and chromium and the lighter grey in the top and left is depleted of iron. There are no visible cracks or pores in the partly reduced area, which was seen to indicate that the material retains its dense structure, also while the shrinking core advances.

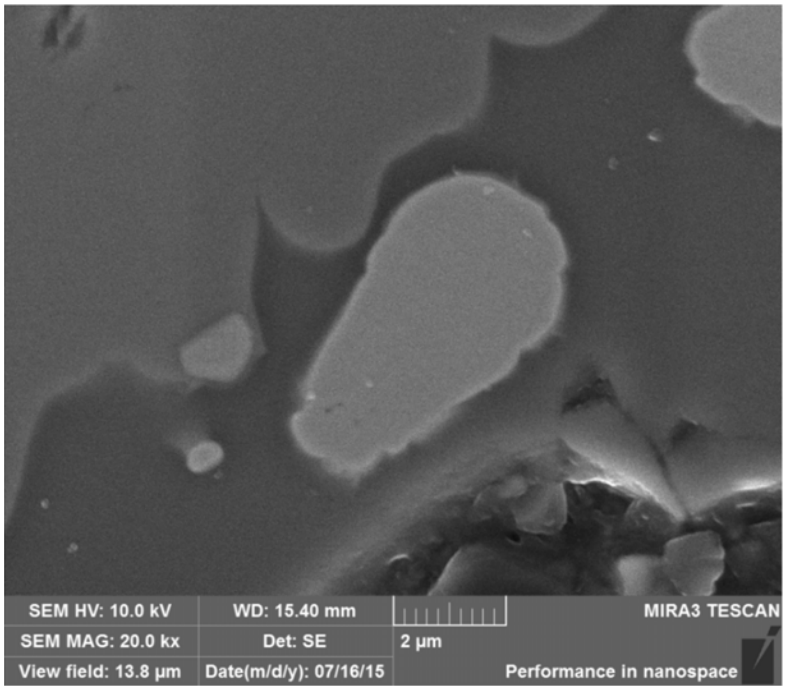

Figure 27 SEM micrograph of a sample reduced in conditions: 1350˚C, 10 vol% CH_4, 10 min

Also, the fact that the partly reduced areas are not porous is confirmed by the fact that the EDS analysis of these areas show a total value as high as the unreduced areas. If the material was simply depleted of iron and chromium without counter diffusion and densification, the total value of the EDS analyses would be lower than for plain chromite. As an example, Figure 28 shows two SEM micrographs of samples reduced at 1100˚C, for 30 min, with 10 and 20 vol% CH_4, respectively. The average total of the partly reduced areas, which are spectrums 6 - 8 and 4 - 7 is 96.27 and the average total for the unreacted core areas is 96.08.

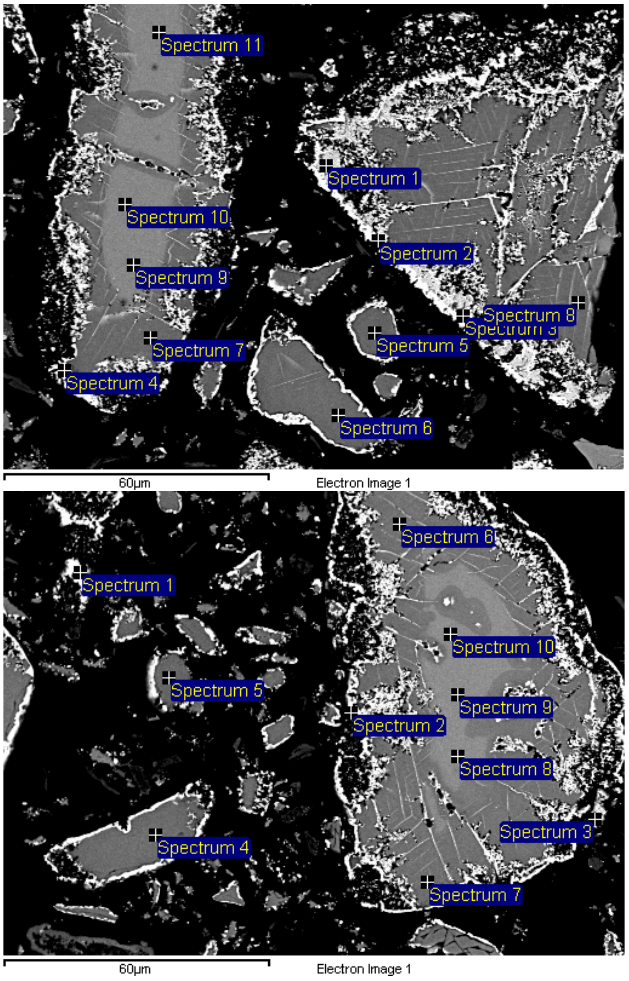

Figure 28 SEM micrographs of samples reduced at 1100˚C, for 30 min, with 10 and 20 vol% CH_4, respectively.

Therefore it was concluded that the reduction mechanism advances through a shrinking core, through two dense cores; i.e. outer and inner, in two stages. The partly reacted phases remain a spinel phase, as was also concluded by Soykan et al. (1991a)

6.2 Metallization

Since no quantitative chemical analysis method was used, the metallization degree is harder to define, because no accurate phase ratios could be derived from micrographs alone. However, the emergence and disappearance of the different phases can be monitored and their phase composition and its possible development over the test series can be traced.

The first stage of the reduction starts already within 10 min at all temperatures and with all different gas mixtures of CH_4 and H_2. Micrograph and EDS analysis of the reduced areas of the 10 minute sample treated with 10 vol% CH_4, at 1100˚C is available in Figure 29.

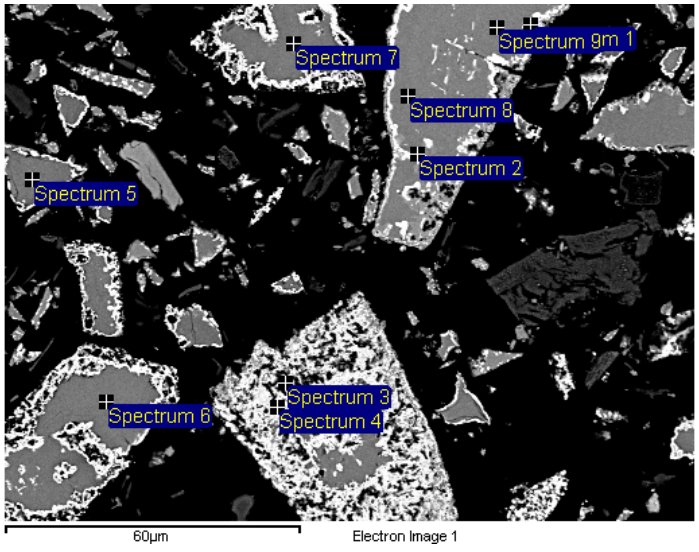

Figure 29 SEM micrograph of a sample reduced in conditions: 1100˚C, 10 vol% CH_4, 10 min

Table 4 shows the EDS analysis of the white areas, spectrums 1-4, which clearly shows that iron, and also chromium, have started to reduce in the lowest temperature, with the lowest CH_4 percentage and shortest reduction time used in this study. This finding is in line with previous studies by Ancleto & Ostrovski (2004) and Taskinen et al. (2014), where the activity of carbon was determined to be higher than that of graphite, when using methane. This leads to good reduction results at lower temperatures than the 1170˚C determined for carbothermmic reduction for this Thesis, see Figure 22.

Table 4 EDS analysis of spectrums 1-4 of a sample reduced in conditions: 1100˚C, 10 vol% CH_4, 10 min, [wt%]

Spectrum	O	Mg	Al	Ti	Cr	Fe	Total
Spectrum 1	2.74		0.95		13.84	78.87	**96.40**
Spectrum 2	2.88	0.16	0.70		16.73	77.78	**98.24**
Spectrum 3	7.76		8.11	0.37	27.79	49.79	**93.82**
Spectrum 4	6.28	0.27	6.49	0.19	38.69	38.89	**90.81**

At higher temperatures the reduction rate intensifies and at 1300˚C a stage was achieved, where practically all iron had reduced and diffused onto the white phase areas. Figure 30 compares two micrographs of samples reduced at 1300˚C, with 10 vol% CH_4 for 20 and 30 min, respectively. Table 5 shows the EDS analyses of the grey areas in the center of the particles.

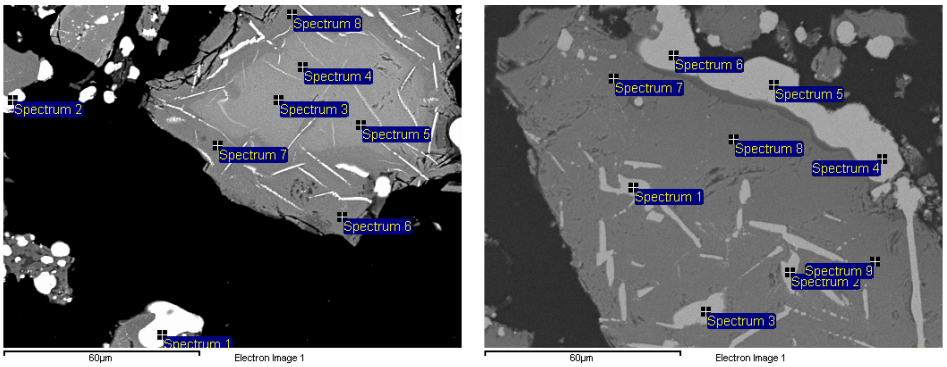

Figure 30 SEM micrographs of samples reduced in conditions: 1300˚C, 10 vol% CH_4, 20 and 30 min, respectively

Table 5 EDS analyses of samples reduced in conditions: 1300˚C, 10 vol% CH_4, [wt%]

Spectrum	O	Mg	Al	Ti	Cr	Fe	Total
20 min							
Spectrum 3	29.79	6.84	7.87	0.22	33.78	15.86	94.36
Spectrum 4	29.44	6.73	7.68	0.28	33.57	15.73	93.43
Spectrum 5	29.15	6.86	7.61	0.29	33.79	15.39	93.09
Spectrum 6	32.79	12.50	8.36	0.39	40.15	0.79	94.98
Spectrum 7	33.88	12.51	8.88	0.31	39.50	2.24	97.33
Spectrum 8	31.52	12.17	8.44	0.31	40.16	1.00	93.60
30 min							
Spectrum 7	30.68	10.14	11.93	0.45	36.11	1.34	90.65
Spectrum 8	31.37	9.96	11.93	0.50	35.68	0.91	90.35
Spectrum 9	30.62	9.45	12.15	0.35	35.38	1.06	89.02

After 20 min, the center of the particle still contains unreduced material in Spectrums 3-5, where the iron content is around 15 wt%, which is very close to the 17 wt% of the raw material. However after 30 min reduction time, such phase is no longer detectable and the iron content throughout the particle's grey center is around 1 wt%. The same phenomenon occurs at 1300˚C regardless of the methane content used. When temperature still increases to 1350˚C, the unreacted phase is barely detectable after 20 min reduction time.

The amount of time, in which the whole particle is reduced of iron is of course directly related to the size of the particle. The larger the particle, the longer it takes for the reduction to reach the center. Smaller particles were completely reduced already at lower temperatures and with shorter reduction times. However, larger particles in the size class of over 60 microns were considered here to make the results more comparable.

The second stage of the reduction was not detected at 1100˚C, but it appeared at 1200˚C. It was first observed after 30 min of reduction and the micrograph and EDS analysis are presented in Figure 31 and Table 6.

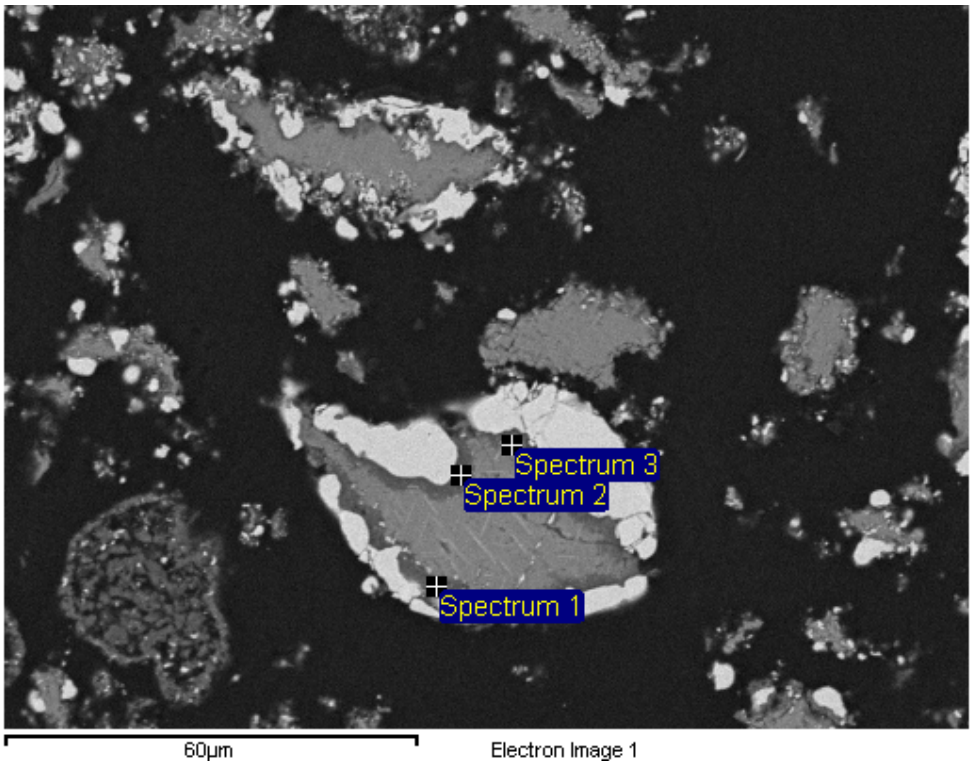

Figure 31 SEM micrograph of a sample reduced in conditions: 1200˚C, 10 vol% CH_4, 30 min

Table 6 EDS analysis for a sample reduced in conditions: 1200˚C, 10 vol% CH_4, 30 min, [wt%]

Spectrum	O	Mg	Al	Si	Ca	Ti	Cr	Fe	Total
Spectrum 1	39.67	17.46	25.69	3.27	0.91	0.30	9.81	0.56	**97.66**
Spectrum 2	39.29	15.90	20.46	9.37	2.27	0.26	7.48	0.48	**95.51**
Spectrum 3	36.18	14.23	21.18	2.66	0.50	0.42	16.08	0.49	**91.74**

Between the iron depleted center of the particle and the white reduced area, the phase depleted of chromium is starting to emerge. At the same temperature, 1200˚C, when the CH_4 content was raised to 20 vol%, the phase occurred after 20 min reduction and with CH_4 content of 30 vol%, the phase was visible already within 10 min reduction. At 1300 and 1350˚C, the phase depleted of chromium is visible with all gas compositions after 10 min reduction.

For example in Figure 32, the sample has been reduced at 1350˚C, with 20 vol% CH_4, for 10 min. The center of the particle is still unreacted chromite, the largest area is the spinel depleted of iron and the darker areas between the white beads is the Mg-Al spinel, depleted of both iron and chromium.

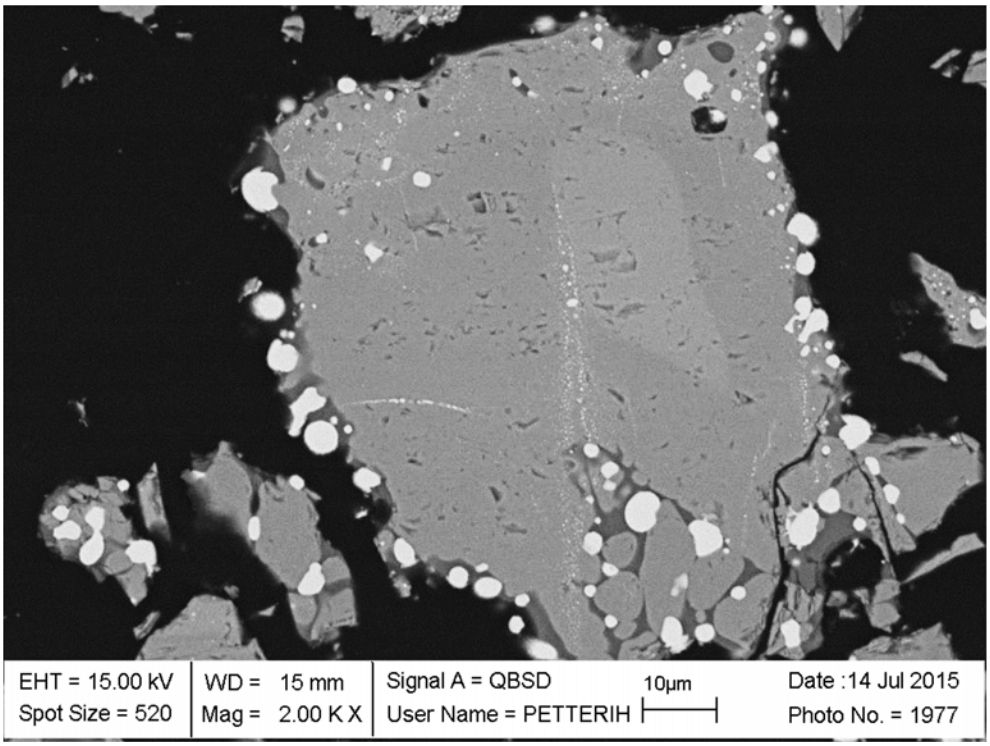

Figure 32 SEM micrograph of a sample reduced in conditions: 1350˚C, 20 vol% CH_4, 10 min

Generally, the phase that was depleted of iron, but rich in chromium disappeared at 1350˚C, when the reduction time was 60 min or over and the CH_4 content 10 and 20 vol%. With 30 vol% CH_4 the reduction time of only 30 min resulted in the disappearance of the phase. However, the 60 min, 30 vol% CH_4 sample deviated greatly from the general trend. Almost all of the chromium rich phase was still intact and even some unreacted chromite remained even though it was barely detected in the 20 min sample. It was therefore concluded, that the 1350˚C, 30 vol% CH_4, 60 min experiment had somehow failed.

A typical micrograph and EDS analysis of the samples reduced at 1350˚C for 60 min or more are shown in Figure 33 and Table 7. Only two phases remain in the particle; the light grey areas of iron-chromium carbide and grey areas consisting of Mg-Al spinel with some Si, Ca and traces of iron and chromium.

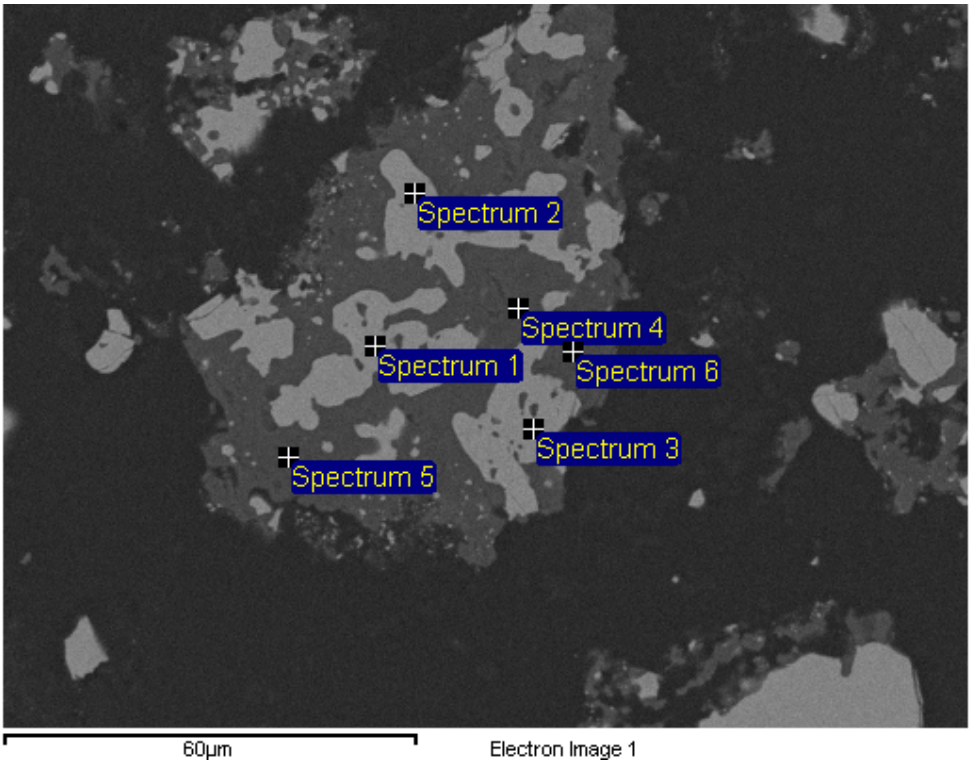

Figure 33 SEM micrograph of a sample reduced in conditions: 1350˚C, 20 vol% CH_4, 90 min

Table 7 EDS analysis of a sample reduced in conditions: 1350˚C, 20 vol% CH_4, 90 min, [wt%]

Spectrum	O	Mg	Al	Si	Ca	Ti	Cr	Fe	Total
Spectrum 1							57.15	26.10	**83.25**
Spectrum 2							56.28	25.26	**81.55**
Spectrum 3							56.72	26.03	**82.75**
Spectrum 4	40.94	28.77	6.30	15.56	2.33		0.81		**94.71**
Spectrum 5	43.92	24.16	20.59	7.69	1.56	0.41	2.28	0.55	**101.16**
Spectrum 6	39.36	30.97	3.02	14.87	2.45		0.51		**91.18**

The next two sections look at the way the reduced material behaves in different conditions.

6.2.1 Iron-Chromium Carbide Formation

When the micrographs from 1100˚C and 1350˚C are compared, it is apparent that the white carbide areas are formed very differently. At 1100˚C the reduced areas are more continuous and as temperature rises, the reduced phase becomes more segmented. It appears so that the reduced phase clusters more into beads when at higher temperatures. This is illustrated in Figure 34, where two micrographs are compared from 1100 and 1350˚C respectively. Both samples have been reduced with 10 vol% CH_4 for 30 min.

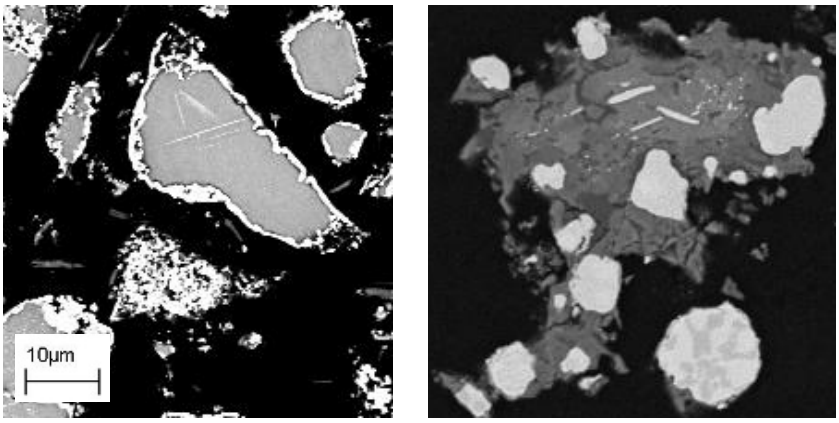

Figure 34 SEM micrographs of samples reduced with 10 vol% CH_4 for 30 min at 1100 and 1350˚C, respectively

This phenomenon is due to two factors. First, at higher temperatures the reduced phase becomes partly molten. If it was pure iron-chromium binary alloy this would not happen, but carbon lowers the liquidus temperature. This is shown in Figure 35, where the liquidus contours of Cr-Fe-C system is presented. The liquidus area emerges in the corner where iron content is very high and grows towards the chromium rich corner. Most importantly, small amounts of carbon result that equilibria lies within or closer to the liquidus area.

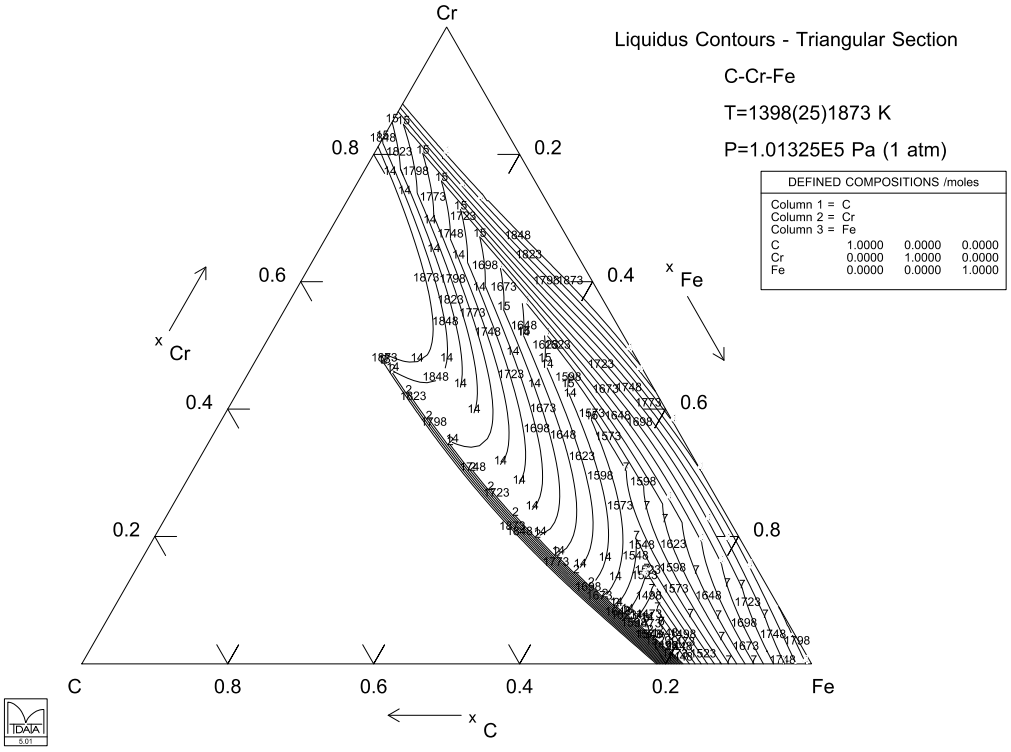

Figure 35 Liquidus contours of Cr-Fe-C ternary plot at 1125˚ - 1600˚C, temperatures in [K]

Because the reduced phase is partly molten, the surface energies between it and the solid spinel can drive it into the bead like shape. The driving force of this is that the partly molten phase tries to minimize its contact surface with the spinel phase, thus minimizing the surface energy between them. This particular phenomenon has been previously studied in Kemi chromite with the direct aim of maximizing the size of the reduced areas (Kytö, 1971) (Härkki, 1972).

6.2.2 Iron- and Chromium Based Alloys

During the first shrinking core stage, iron and some chromium are reduced into carbides. After roughly all iron is reduced, the second stage of the process continues to reduce chromium. As a result, the fraction of chromium in the reduced phase increases as the process advances. More chromium is reduced, until the solution becomes saturated with it. This is when a chromium based phase starts to form within the reduced phase. The two phases are visible in several samples and were analyzed where the surface areas were large enough for EDS analysis. Figure 36 shows the SEM micrograph and EDS analysis results for the two different phases. The sample was reduced at 1100˚C, with 10 vol% CH_4 for 120 min.

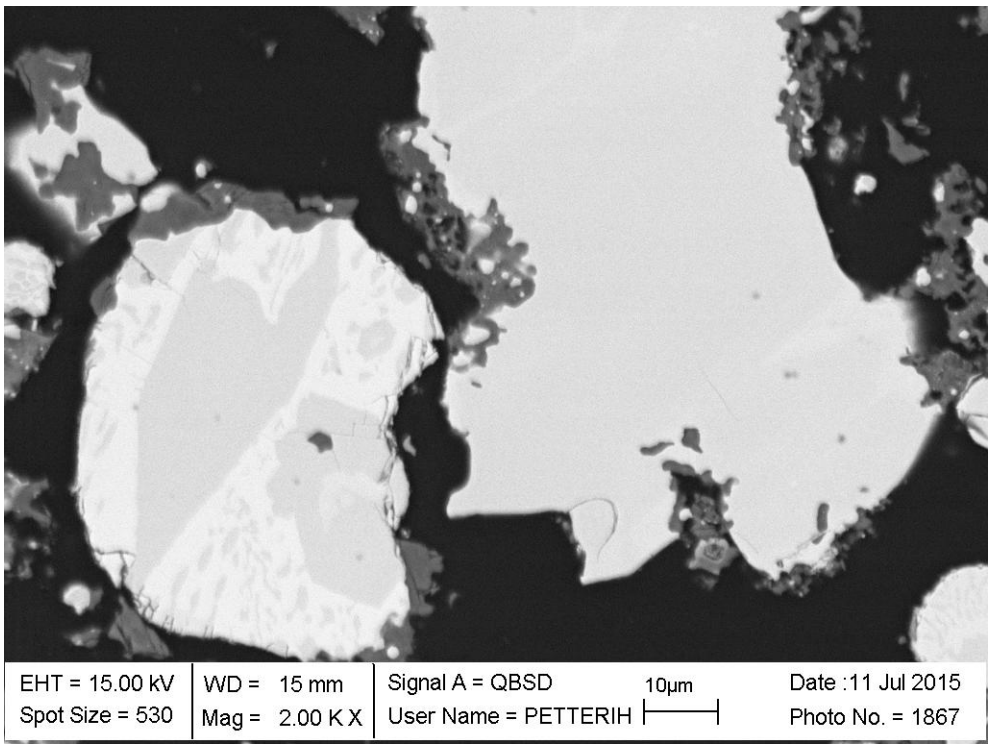

Figure 36 SEM micrograph for a sample reduced in conditions: 1100˚C, 10 vol% CH_4 120 min

Two separate phases can be seen in the left hand side particle, whereas the reduced area on the right hand side remains as a single phase. The EDS analyses from the left hand side area are presented in Table 8. The first three rows are the analyses from the brighter phase and the four following rows are from the darker areas. The composition is in weight percentages and the lower part of the table shows the average compositions of the two phases.

Table 8 EDS analyses of two reduced phases in Figure 36, [wt%]

Phase	O	Si	Cr	Fe	Total
Bright phase 1	0.59	4.15	39.98	49.76	94.47
Bright phase 2	0.53	4.28	40.28	49.55	94.65
Bright phase 3	0.56	3.82	40.82	50.94	96.13
Dark phase 1			70.17	14.11	84.29
Dark phase 2			74.02	9.98	84.01
Dark phase 3			71.61	12.94	84.55
Dark phase 4			74.68	9.98	84.66
Average					
Light phase	0.56	4.08	40.36	50.08	95.08
Dark phase			72.62	11.75	84.38

When reduction rate was fast enough, the segregation of the chromium based phase started very quickly. At 1350˚C, with 30 vol% CH_4, the two separate phases were detected already after 20 minutes of reduction. Figure 37 shows the SEM micrograph for this sample and the two phases are clear in the right hand side of the image. In the left hand side, the phases have begun to separate, but the surface of the particle was not suitable for EDS analysis. This picture shows how the separation of the two phases progresses through growth of smaller formations towards larger phase areas as diffusion progresses. The EDS analysis for the right hand side particle's two phases are collected in Table 9.

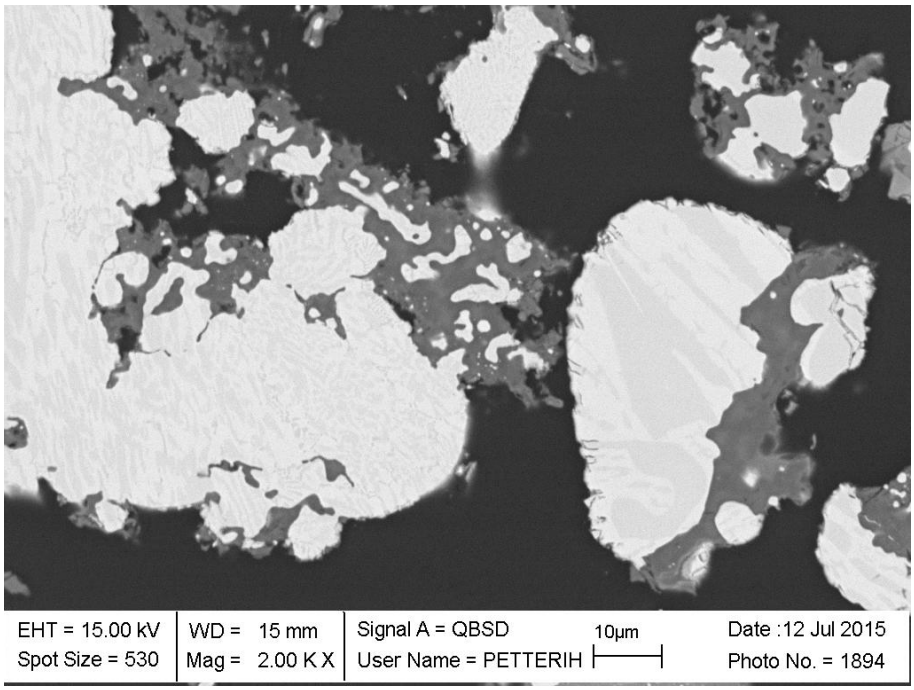

Figure 37 SEM micrograph of a sample reduced in conditions: 1350˚C, 30 vol% CH_4, 20 min

Table 9 EDS analyses of the two reduced phases in Figure 37, [wt%]

Phase	**O**	**Si**	**Cr**	**Fe**	**Total**
Bright phase 1		3.13	35.35	50.50	88.99
Bright phase 2		3.39	35.78	50.24	89.40
Dark phase 1	0.52		70.22	10.33	80.55
Dark phase 2			65.80	15.16	81.48
Average					
Bright phase		3.26	35.57	50.37	89.20
Dark phase	0.26		68.01	12.75	81.02

It is observed from both these examples, that the darker grey phase is mostly chromium and the brighter grey phase contains mostly iron. Therefore, the darker phase is the new, chromium based alloy. In both examples, the brighter phase has a higher total, which indicates that the darker phase contains more

carbon than the bright phase. A rough evaluation of the Cr-Fe-C ternary plot at 1300˚C, presented in Figure 38, would indicate that the iron based phase is partly molten, but the chromium based phase is completely solid. The sharp corners of the areas of chromium based alloy in Figures 36 and 37 also confirm that the phase is formed as a solid. The iron based phase is depicted with green lines and the composition of the chromium based phase with red lines in Figure 38.

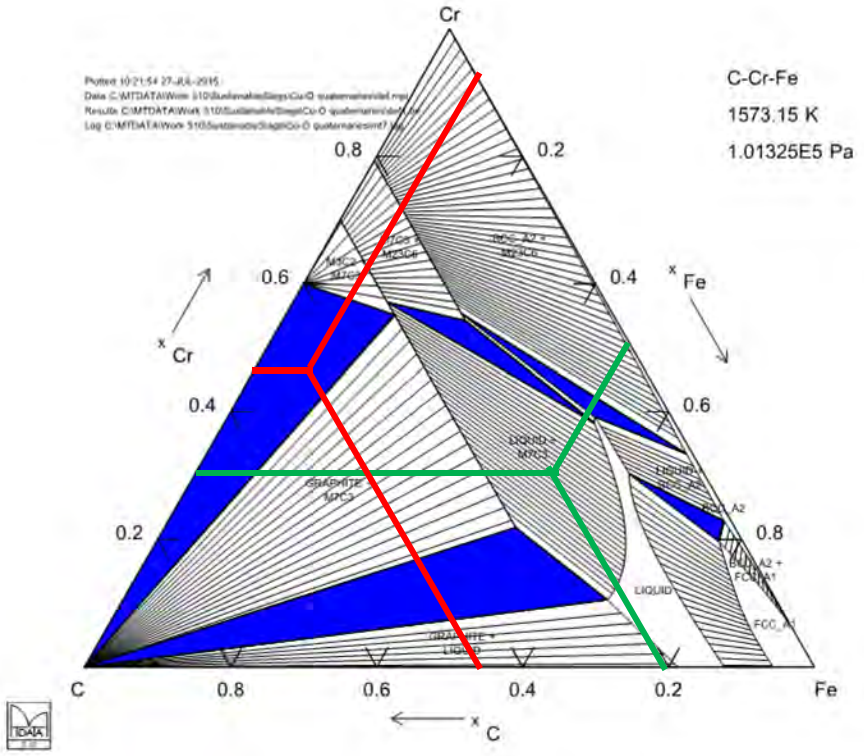

Figure 38 Fe-Cr-C ternary plot at 1300˚C [mol fraction], composition of the iron based, bright phase, in green and of the chromium based, dark phase, in red

The compositions of the phases in Figure 38 were calculated as an average from all the two phase analyses and presented in Table 10. Carbon was then assumed to balance the numbers to a hundred, but it should be noted that some amount of silica remains in the iron based phase, and a very small

amount of oxygen is present in some of the analysis points. Also, the ternary plot represents a system in equilibrium, but all the obtained results are from systems that most probably are not in equilibria, but are still transforming. The illustration is therefore just an approximation of a more complex system.

Table 10 Average EDS analyses of iron and chromium based alloys

Phase	x_{Cr}	x_{Fe}	x_C
Bright phase	0.31	0.47	0.22
Dark phase	0.46	0.08	0.46

In addition to the iron and chromium based alloys, a third reduced phase was observed in the sample that was treated at 1350˚C, with 30 vol% CH_4, for 120 min. Figure 39 shows a SEM micrograph of the sample and Table 11 has the EDS analysis from the analysis points indicated on the micrograph.

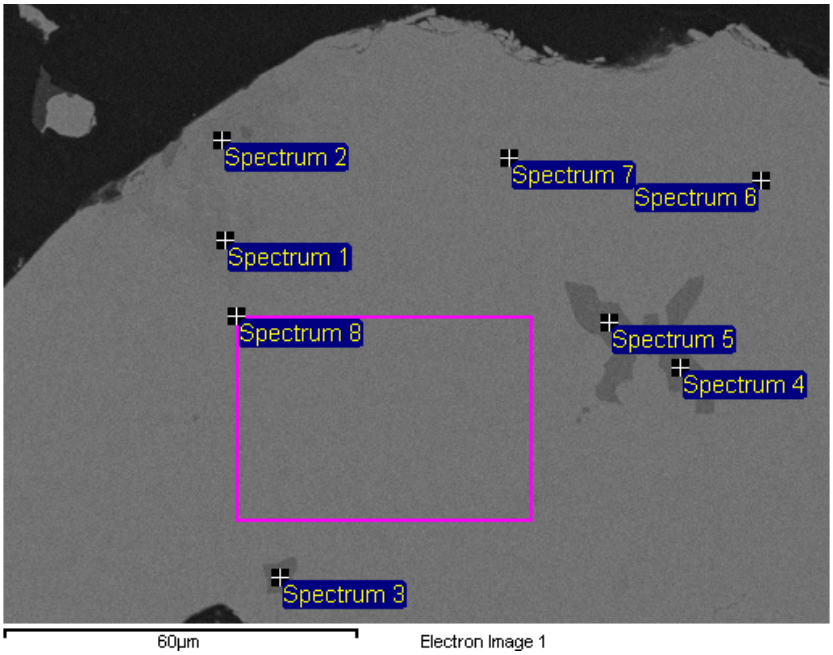

Figure 39 SEM micrograph of a sample reduced in conditions: 1350˚C, 30 vol% CH_4, 120 min

Table 11 EDS analysis of a sample reduced in conditions: 1350˚C, 30 vol% CH_4, 120 min, [wt%]

Spectrum	O	Al	Si	Ti	Cr	Fe	Total
Spectrum 1			14.46	0.98	37.48	25.78	**78.69**
Spectrum 2			14.39	0.85	37.62	25.57	**78.43**
Spectrum 3				32.18	33.57	1.25	**66.99**
Spectrum 4				33.56	30.76	0.97	**65.28**
Spectrum 5				31.09	33.95	1.05	**66.10**
Spectrum 6			8.53	0.38	30.48	37.39	**76.78**
Spectrum 7		0.43	9.81		22.05	47.53	**79.82**
Spectrum 8	0.67	0.33	7.27	0.32	29.82	39.98	**78.39**

The main phase from Spectra 6 - 8 is iron chromium carbide as was seen in other samples as well. However, in Spectra 3 - 5, it is seen that the dark grey phase within the main phase is a titanium-chromium carbide. Many of the analyzed samples contained titanium as a minor element, but in this case; the highest temperature and methane content together with the longest reduction time, titanium has started to reduce and form a new phase with chromium and carbon. This is also in accord with the findings of Halli (2015) about Mustavaara's titanium magnetite ore, where titanium reduced significantly.

6.3 Carbon Deposition

As the methane in the reducing gas provides carbon for the reduction of iron and chromium, part of the carbon accumulates on the sample as graphite, as illustrated by the XRD analyses. The graphite forms either separate particles or clusters on the surfaces of the ore particles. Even carbon formations that could be seen with the naked eye were observed during the experiments, but these were so fragile, that removal from the crucible crushed them.

The results obtained from the carbon analysis showed that the deposition of carbon increases as the reduction time increases. Only a few exceptions of this were observed when the reduction time was 120 min. This sudden decrease could be due to imperfect dividing of the sample before carbon analysis. Figure 40 shows the mass percentage of carbon in the samples as a function of time at 1100 ˚C.

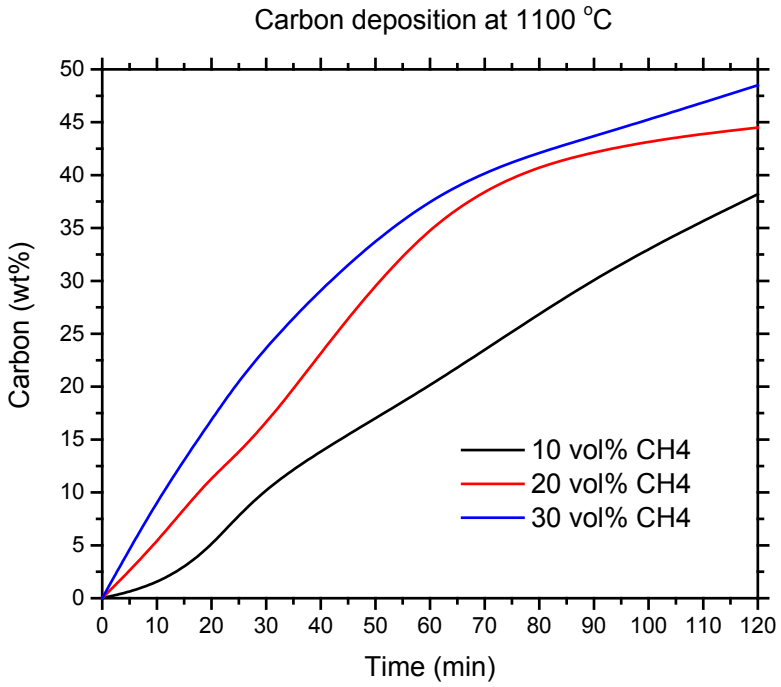

Figure 40 Carbon deposition at 1100˚C

It can be seen that the increase in reduction time increases the amount of carbon deposition regardless of the methane content used in the feed gas mixture. The deposition rate is however faster as the percentage of CH_4 grows. The carbon mass percentage is at its highest at 48.5 wt% when the methane

content was 30 vol%, represented by the blue line, and the reduction time 120 min. Figure 41 shows the same graph, but for experiments done at 1200˚C.

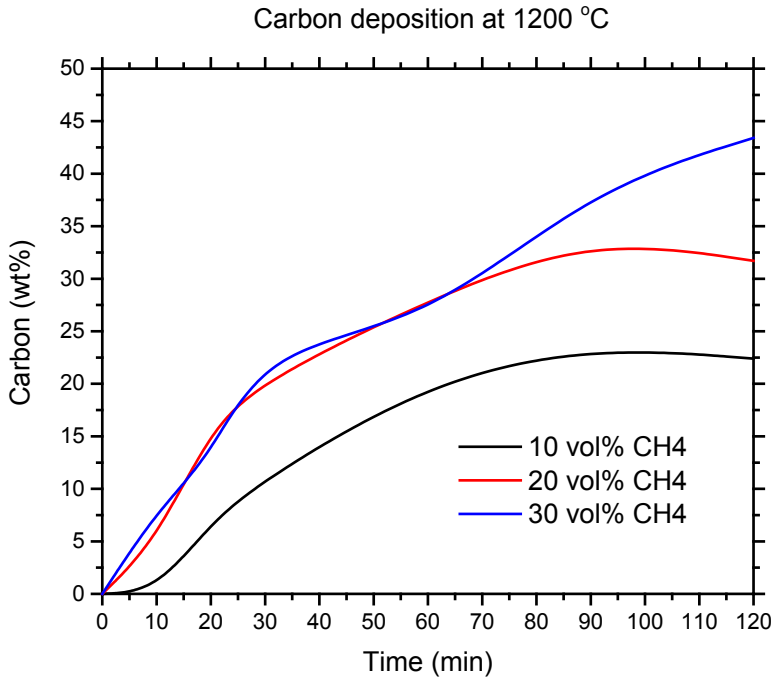

Figure 41 Carbon deposition at 1200˚C

The deposition increases with reduction time, but not as sharply as at 1100˚C. With 10 and 20 vol% CH_4, represented with black and red, the deposition rate levels out after 90 min, but the 30 vol% CH_4 curve in blue continues to rise throughout the time series. Deposition with 20 and 30 vol% CH_4, the deposition rate is similar in the beginning, but as the 20 vol% CH_4 line levels out, the 30 vol% CH_4 line surpasses it. Figure 42 shows the carbon weight-percentage as a function of time at 1300˚C.

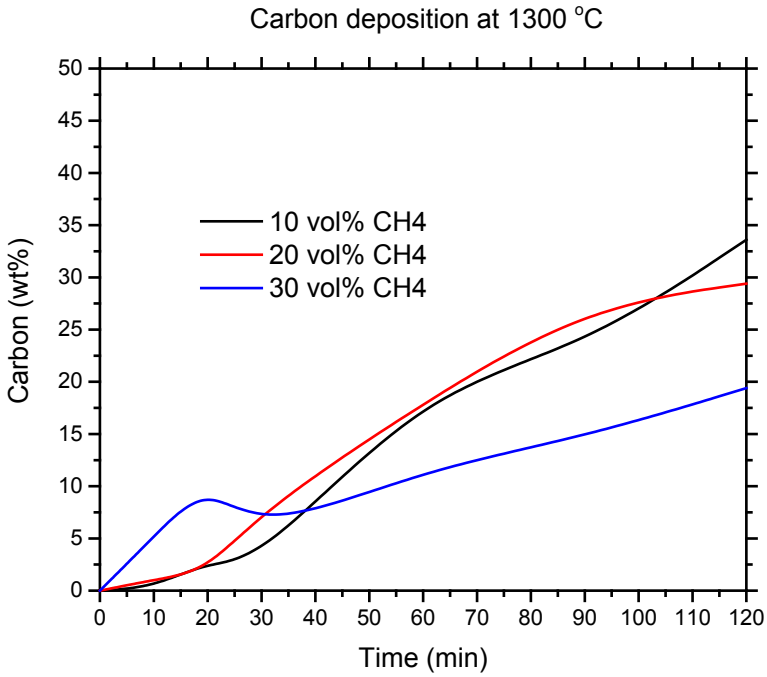

Figure 42 Carbon deposition at 1300˚C

For some reasons, which are not understood, increasing the methane content of the feed gas mixture does not increase the deposition of carbon in this case. The 30 vol% CH_4 curve in blue is actually the lowest of the three. Between 10 and 20 vol% CH_4, represented by black and red, the deposition rate is fairly equal throughout the entire time span. Figure 43 holds the similar graph for 1350˚C, where the same upward trend continues.

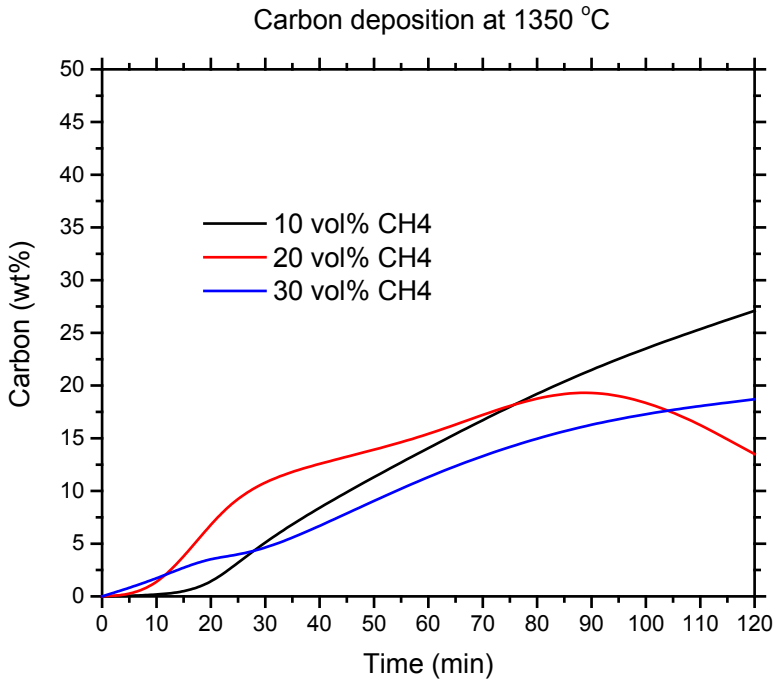

Figure 43 Carbon deposition at 1350˚C

Similar to the results at 1300˚C, the gas composition does not affect the deposition in the same manner as it did at lower temperatures. Now the lines are fairly similar with all the gas compositions. 10 and 30 vol% CH_4 curves in black and blue increase, but the 20 vol% CH_4 curve in red decreases after 90 min. This could only be explained as an error in sample division or as a random error.

Figures 44, 45 and 46 contain the results of carbon deposition with different methane concentrations. All atmospheres, 10, 20 and 30 vol% CH_4 indicate a drop in carbon deposition as the temperature rises.

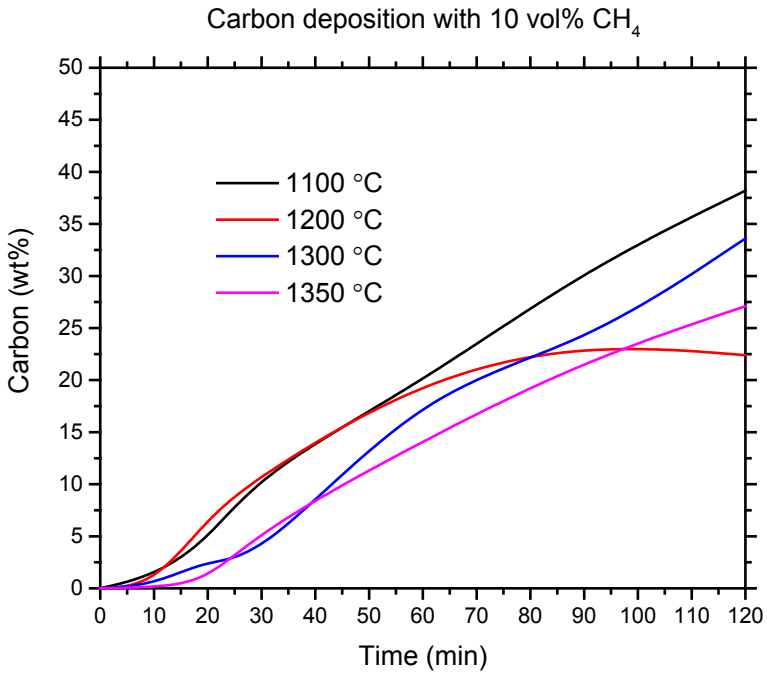

Figure 44 Carbon deposition with 10 vol% CH_4

Figure 44 shows the amount of carbon increasing over time, but as the temperature increases, the amount of carbon slightly decreases. The 1200˚C line in red acts differently from the others as it levels out after 90 min, while the other three continue rising. Figure 45 shows the mass percentage of carbon in the samples when the reducing gas contained 20 vol% of CH_4.

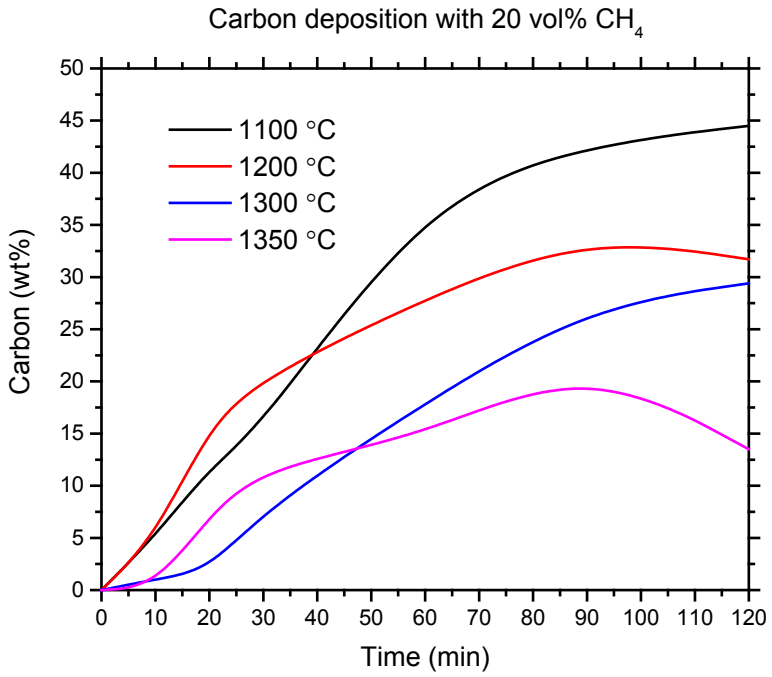

Figure 45 Carbon deposition with 20 vol% CH_4

The decrease in carbon deposition is ever clearer in this graph compared to Figure 44. As the temperature rises, less carbon is deposited on the sample. Also, all the curves either decrease or stay fairly level after 90 min. The decrease in deposition of free carbon is most clear with the 30 vol% CH_4 atmosphere, illustrated in Figure 46.

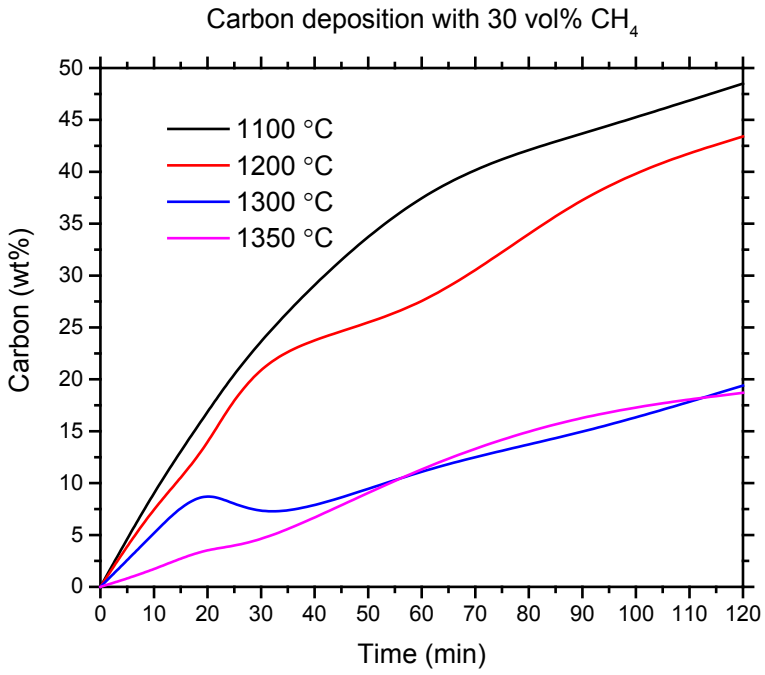

Figure 46 Carbon deposition with 30 vol% CH_4

In Figure 46 it can be seen that when the temperature is 1100˚C, almost 50 % of the weight of the sample is carbon, but at 1300˚C and 1350˚C the percentage does not even reach 20 wt%. Although more methane cracks at higher temperatures, it is possible that the reduction of metals consumes more carbon, thus reversing the apparent carbon deposition amount as temperature rises. Also it is possible, that as the temperature rises, more carbon is deposited, but it deposits elsewhere in the furnace, such as the furnace tube walls and the outer surface of the crucible.

6.4 Mineralogy from XRD Measurements and Rietveld Calculations

For a reliable Rietveld analysis, PANalytical (2015) recommends the highest peak on the diffractogram to be at least 10,000 counts. Unfortunately, the

average count value acquired for the highest peak was approximately 400. It was apparent that the XRD results were not strong enough for a reliable Rietveld analysis. Several reasons were thought to have caused the problem for the analyses. The sample amount was clearly too small for the sample holder and therefore a plastic filler was used to raise the surface of the sample to the level of the sample holder's upper surface. Therefore, the sample layer was much thinner than was designed for the diffractogram. Also the poor results could be partly explained by the fact that a monochromator could not be used during the measurement. Another possible explanation for the low number of counts is an uneven particle size distribution.

Even if no accurate conclusions could be drawn from the XRD and Rietveld results, some trends were confirmed by them. The amount of carbon increases in the samples with reduction time. The values for carbon deposition were however much higher than the ones obtained from the S/C analyses performed by Outotec. This was due to the low number of counts which caused the inaccuracy of the Rietveld calculations.

Also, there is a clear indication that the chromite mineral reduces and the amounts of iron and chromium as metals and carbides increase as reduction time, methane percentage and temperature increase. The Rietveld calculations indicated the presence of FeCr metal alloys and carbides when the reduction temperature reached 1300˚C. For example, when the temperature was 1350˚C and the reduction time 60 min or more, the XRD could find only traces of chromite in the sample and mostly carbon and different combinations of iron and chromium and their carbides. This would indicate total reduction of iron and chromium at the temperature of 1350˚C with 60 min reduction time. Figures 47 and 48 illustrate the amount of chromite at the temperatures of 1300 and 1350˚C. The values are not exact as the XRD analysis in this case can only be seen as suggestive.

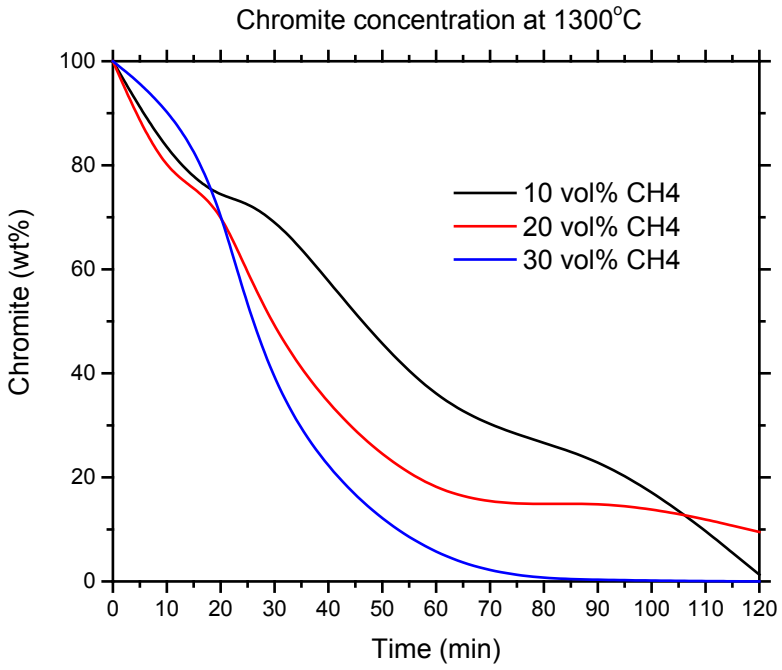

Figure 47 Chromite concentration from XRD analysis and Rietveld calculations at 1300˚C

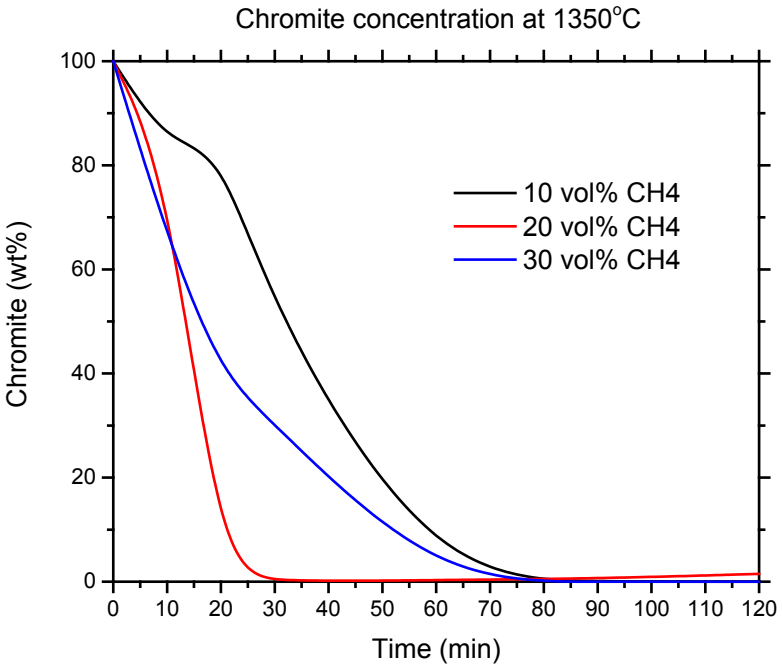

Figure 48 Chromite concentration from XRD analysis and Rietveld calculations at 1350˚C

7 Summary and Conclusions

Chromite concentrate from the Kemi deposit in Finland was reduced in CH_4-H_2 atmospheres to acquire knowledge of the reduction characteristics. Altogether 72 experiments, along with two reference tests, were conducted with three variables; temperature, time and the content of methane in the feed gas mixture. The reduction temperatures were 1100, 1200, 1300 and 1350˚C and the reduction times 10, 20, 30, 60, 90 and 120 minutes. Three methane contents were used; 10, 20 and 30 vol% with H_2, balancing the amount to 100 %.

The samples were analyzed using three different analysis techniques. Mineralogy was defined with XRD and a quantitative phase analysis was performed using the Rietveld method. Particle structure, reaction mechanism and metallization was observed using SEM imaging and EDS analysis of different phases, while the carbon content of the samples was evaluated using an S/C analyzer.

7.1 Reduction Mechanism

The reduction mechanism was observed to proceed mainly through a shrinking core model in two stages. In the first stage, carbon from the methane reduces the iron and some chromium into carbides. After this, and partly at the same time, a second stage of the reduction emerges, where the chromium in the remaining spinel is reduced. Iron was essentially reduced in full after 30 min when the temperature reached 1200 and 1300˚C. As temperature was increased to 1350˚C, the iron was almost completely reduced from the chromite after 20 min reduction.

At the highest temperature 1350˚C, basically all of the chromium was eventually reduced, resulting in residual aluminum and magnesium oxides with varying amounts of silica being left of the original Kemi chromite. The reduced iron and chromium metals started to form two alloys, one iron based and one chromium based. The iron based phase was partly molten, unlike the solid chromium based alloy.

The reduced metals diffused to the surface of the particle and depending on the used temperature, formed partly molten phases with carbon, as carbon lowers the liquidus temperature of the Fe-Cr system. As a result of surface energies between the remaining spinel and the partly molten metal carbide mixture, the reduced material was spherical and formed beads rather than a continuous product layer on the residual chromite surface.

The metallization degree was difficult to define experimentally as no quantitative chemical analysis method was used. However, the metallization was observed to start immediately after chromite was exposed to CH_4-H_2 mixtures as significant reduction to metal was observable after only 10 minutes of reduction time. At the temperatures of 1300˚C and 1350˚C the metallization was seen to be completed within the duration of the experiments, as only very small amounts of iron and chromium remained in the unreacted zones. Therefore, reduction of Kemi chromite with CH_4-H_2 mixture was judged as highly efficient compared to reduction with only solid carbon as the reductant. This was accredited to the high activity of carbon when it is provided by cracking methane in a hydrogen atmosphere.

7.2 Future Work

The results from this Master's thesis are promising, but more research needs to be done on the matter. Accurate quantitative phase analysis needs to be performed on similar samples. This would enable the determination of, i.e. rate controlling factors and an accurate metallization degree.

In order to obtain more information about the mineralogy of the samples, the unsuccessful XRD analyses and Rietveld calculations could be improved in many ways. For example preparing larger quantities of the sample would allow for a more accurate phase analysis, as the sample amount would be suitable for the sample holder. Using a monochromator with the XRD diffractometer would give a more accurate result as the sample contains iron and a monochromator is particularly useful in the analysis of these kinds of samples. Also, the results could be improved via leveling of the sample's particle size distribution by using a grinding mill, as was done by Hem et al. (2009).

After additional information is gained and if the method still seems feasible, small pilot plant scale testing depending on the ractor type chosen is needed to confirm the applicability of the method. Furthermore, the process itself needs to be modified for a larger scale production. In a real production facility, the prereduction would probably be more economic to perform in a continuous process instead of batches. Optimizing a process like this would need even more experiments and studying.

The next step would be to test the applicability of this prereduced product in the SAF and how it acts in that process.

Also, the off-gases of this prereduction method and their combustion value needs to be evaluated as they could be utilized as a heat source, for example in pre-heating the raw material.

During the analyses, carbon deposition was seen to increase over time and as the CH_4 content rose. This was evident also during the actual experiments and was seen as a hazard from the practical point of view. Clogging of the off-gas system was a major issue and the application of this method in large scale production would be challenging as the amount of methane, and therefore depositing carbon, would be increased immensely. Both methane and hydrogen are explosive gases and any clogging of the off-gas system risks the possibility of unwanted gas leaks. This would be a major safety issue in an industrial size facility and needs to be thoroughly considered.

8 References

Alapieti, T. T. & Huhtelin, T. A., 2005. The Kemi Intrusion and Associated Chromite Deposit. In: T. T. Alapieti & A. J. Kärki, eds. *Field Trip Guidebook - Early Palaeoproterozoic (2.5-2.4) Tornio - Näränkävaara Layered Intrusion Belt and Related Chrome and Platinum-Group Element Mineralization, Northern Finland.* Espoo: Geological Survey of Finland, pp. 13-32.

Alapieti, T. T., Kujanpaa, J., Lahtinen, J. J. & Papunen, H., 1989. The Kemi stratiform chromitite deposit, northern Finland. *Economic Geology,* 84(5), pp. 1057-1077.

Anacleto, N. & Ostrovski, O., 2004. Solid-State Reduction of Chromium Oxide by Methane-Containing Gas. *Metallurgical and Materials Transactions B,* 35(4), pp. 609-615.

Arvanitidis, I. et al., 1996. Study of the kinetics of reduction of iron chromate by hydrogen. *Scandinavian Journal of Metallurgy,* 25(4), pp. 141-147.

Basson, J. & Daavittila, J., 2013. Chapter 9 - High Carbon Ferrochrome Technology. In: M. I. Gasik, ed. *Handbook of Ferroalloys.* s.l.:Elsevier, pp. 317-363.

Davies, R. H. et al., 2002. MTDATA - Thermodynamic and Phase Equilibrium Software from the National Physical Laboratory. *Calphad,* 26(2), pp. 229-271.

de Campos, M. & Eric, R. H., 2006. *Reduction behaviour of Chromite in the Presence of a Hydrocarbon Gas.* s.l., Sohn International Symposium; Advanced Processing of Metals and Materials, Vol 1.

Ding, Y. L. & Warner, N. A., 1997. Catalytic Reduction of Carbon-chromite Composite Pellets by Lime. *Thermochimica Acta,* 292(1-2), pp. 85-94.

Duong, H. V. & Johnston, R. F., 2000. Kinetics of solid state silica fluxed reduction of chromite with coal. *Ironmaking & Steelmaking,* 01 June, 27(3), pp. 202-206.

Ebrahimi-Kahrizsangi, R., Zadeh, H. M. & Nemati, V., 2010. Synthesis of chromium carbide by reduction of chromium oxide with methane. *Int. Journal of Refractory Metals & Hard Materials,* 28(3), pp. 412-415.

Halli, P., 2015. *Solid-State Reduction on Vanadium Containing Mustavaara Titano-Magnetite Concentrate.* Master's Thesis: Aalto University, School of Chemical Technology. Espoo. 175p.

Hem, S. R. et al., 2009. *Sample preparation for quantitative Rietveld analysis, phase identification and XRF in one step: automated sample preparation by Centaurus.* s.l., The Southern African Institute of Mining and Metallurgy. The 7th International Heavy Minerals Conference, pp. 49-56.

Huovinen, I., 2007. *Kemin kromiitin Cr/Fe-suhde kromiitin raekoon funktiona Pohjois-Viian, Elijärven ja Elijärven E-malmioissa.* Pro gradu: University of Oulu, Department of Geosciences. Oulu. 104p.

Härkki, J., 1972. *Kromiitin selektiivisesti, kargotermisesti esipelkistetyn raudan pallotus.* Master's Thesis: Helsinki University of Technology, Department of Metallurgy. Espoo. 110p.

International Stainless Steel Forum, 2015. *Meltshop production statistics 2001 to 2014.* [Online] Available at: http://www.worldstainless.org/crude_steel_production/meltshop_production_2001_2014 [Accessed 25.3.2015].

Kekkonen, M., Xiao, Y. & Holappa, L., 1995. *Kinetic Study on Solid State Reduction of Chromite Pellets.* Trondheim, FFF. Proceedings of INFACON 7, pp. 351-360.

Khoshandam, B., Kumar, R. V. & Jamshidi, E., 2006. Producing Chromium Carbide Using Reduction of Chromium Oxide with Methane. *American Institute of Chemical Engineers Journal,* 52(3), pp. 1094-1102.

King, H., 2015. *Geoscience news and information.* [Online] Available at: http://geology.com/minerals/chromite.shtml [Accessed 10.3.2015].

Kojo, M. & Holappa, L., 1991. *Ferrokromin valmistus nyt ja tulevaisuudessa.* 1st ed. Espoo: Teknillinen korkeakoulu.

Kytö, M., 1971. *Raudan Pallotus Esipelkistettäessä Kromiittia Hiilellä.* Master's Thesis: Helsinki University of Technology, Department of Metallurgy. Espoo. 109p.

Lyakishev, N. P. & Gasik, M. I., 1998. *Metallurgy of Chromium.* 1st ed. New York: Allerton Press.

Murthy, Y. R., Tripathy, S. K. & Kumar, C. R., 2011. Chrome ore beneficiation challenges & opportunities – A review. *Minerals Engineering,* 24(5), pp. 375-380.

National Physical Laboratory, 2015. *MTDATA - Databases.* [Online] Available at: http://www.npl.co.uk/science-technology/mathematics-modelling-and-simulation/mtdata/databases/
[Accessed 13.8.2015].

Niayesh, M. J. & Dippenaar, R. J., 1992. *The Solid-state Reduction of Chromite.* Johannesburg, The South African Institute of Mining and Metallurgy. Proceedings of INFACON 6, Cape Town, pp. 57-63.

Ostrovski, O. & Zhang, G., 2006. Reduction and Carburization of Metal Oxides by Methane-Containing Gas. *American Institute of Chemical Engineers Journal,* 52(1), pp. 300-310.

Outokumpu Oyj, 2013. *Handbook of Stainless Steel.* Espoo: Outokumpu Oyj.

PANalytical, 2015. *Total X-ray Powder Pattern Analysis - X'Pert HighScore and X'Pert HighScore Plus.* [Online] Available at: http://www.google.fi/url?sa=t&rct=j&q=&esrc=s&source=web&cd=3&ved=0CDEQFjAC&url=http%3A%2F%2Fwww.panalytical.com%2Fweb%2Ffile%3Fuuid%3Dbb076ba2-b870-446d-bbe2-0c61af604ab7%26owner%3Dce090ecb-1fc6-4295-ab98-fb45920410c2%26contentid%3D2978&ei=Im6SVb-

NBcGvsQ
[Accessed 30.6.2015].

Papp, J. F., 2014. *USGS - Minerals Yearbook - Chromium 2012.* [Online] Available at: http://minerals.usgs.gov/minerals/pubs/commodity/chromium/myb1-2012-chrom.pdf
[Accessed 11.3.2015].

Papp, J. F., 2015. *USGS - Mineral commodity summaries - Chromium 2014.* [Online]
Available at: http://minerals.usgs.gov/minerals/pubs/commodity/chromium/mcs-2015-chrom.pdf
[Accessed 11.3.2015].

Perry, K. P. D., Finn, C. W. P. & King, R. P., 1988. An Ionic Diffusion Mechanism of Chromite Reduction. *Metallurgical Transactions B,* 19(4), pp. 677-684.

Qayyum, M. A. & Reeve, D. A., 1976. Reduction of Chromites to Sponge Ferrochromium in Methane-hydrogen Mixtures. *Canadian Metallurgical Quarterly,* 15(3), pp. 193-200.

Ramakrishna, G., Kadarolkar, A. & Srikakulapu, N. G., 2015. Exergy and Its Efficiency Calculations in Ferrochrome Production. *Metallurgical and Materials Transactions B,* 46(2), pp. 1073-1081.

Read, P. J., Reeve, D. A., Walsh, J. H. & Rehder, J. E., 1974. Reduction of Chromites in Methane-hydrogen Mixtures - Chromium Sesquioxide. *Canadian Metallurgical Quarterly,* 13(4), pp. 587-595.

Soykan, O., Eric, R. H. & King, R. P., 1991a. The Reduction Mechanism of a Natural Chromite at 1416. *Metallurgical Transactions B,* Volume 22B, pp. 53-63.

Soykan, O., Eric, R. H. & King, R. P., 1991b. Kinetics of the Reduction of Bushveld Complex Chromite Ore at 1416 C. *Metallurgical Transactions B,* Volume 22B, pp. 801-810.

Syynimaa, A., 1996. *The Effect of Oxidation State on the Reduction of Sintered Chromite Pellets.* Master's Thesis: Teknillinen korkeakoulu, Materiaali- ja kalliotekniikan osasto. Espoo. 108p.

Taskinen, P., Fabritius, T. & Eric, R. H., 2014. A new FiDiPro project: Sustainable Production of Ferroalloys. *Materia,* I(5), pp. 46-50.

USGS, 2015. *Chromium statistics and information.* [Online] Available at: http://minerals.er.usgs.gov/minerals/pubs/commodity/chromium/index.html [Accessed 29.6.2015].

Weber, P. & Eric, R. H., 1993. The reduction mechanism of chromite in the presence of a silica flux. *Metallurgical Transactions B,* 24(6), pp. 987-995.

Weber, P. & Eric, R. H., 2006. The Reduction of Chromite in the Presence of Silica Flux. *Minerals Engineering,* 19(3), pp. 318-324.

worldsteel association, 2014. *Annual steel production 1980 - 2013.* [Online] Available at: https://www.worldsteel.org/dms/internetDocumentList/statistics-archive/production-archive/steel-archive/steel-annually/steel-annually-1980-2013/document/steel%20annually%201980-2013.pdf
[Accessed 25.2.2015].

Xiao, Y. et al., 2004. *Solid State Reduction of Chromite with CO.* Cape Town, Proceedings of INFACON X, pp. 1-4.

Xiao, Y. et al., 2004. *Solid State Reduction of Chromite With CO.* Cape Town, Proceedings of INFACON X, pp. 1-4.

Appendices

Appendix I

Reference: Chromite production by country 2008-2012, USGS

TABLE 8
CHROMITE: WORLD PRODUCTION, BY COUNTRY[1, 2, 3]

(Metric tons, gross weight)

Country	2008	2009	2010	2011	2012[e]
Afghanistan[e, 4]	6,500	6,700 [r]	5,727 [r, 5]	6,204 [r, 5]	6,000
Albania[6]	225,373 [r]	283,558 [r]	328,322 [r]	330,938 [r]	330,000
Australia	224,809	119,314	180,000 [r]	323,800 [r]	452,300 [5]
Brazil[7]	664,347	365,210	520,129	542,512 [r]	543,000 [p]
China[e]	200,000	200,000	200,000	200,000	200,000
Finland	613,543	246,817	598,000 [r]	692,527 [r]	425,217 [5]
Greece[e, 4]	1,400	1,400	1,400	1,600	1,600
India	3,900,000	3,760,000	3,800,000	3,850,000 [e]	3,900,000
Iran	268,586	268,586 [r]	45,000 [r]	100,000 [r, e]	100,000
Kazakhstan	3,552,000	3,544,000	3,760,000 [e]	3,800,000 [e]	4,000,000
Madagascar	112,613 [r]	133,000 [r]	134,500	66,700 [r]	67,000
Oman	859,748	636,482	801,856	616,700	554,800 [5]
Pakistan	104,000	133,000 [r]	252,000 [r]	250,000 [r, e]	260,000
Philippines	15,268	14,322	14,807	22,794 [r]	23,890 [5]
Russia	913,000	416,194	400,000 [e]	662,000 [r]	660,000
South Africa	9,682,640	7,560,938	10,871,095	10,721,360 [r]	11,000,000
Sudan	27,094	14,087	56,823	64,128 [r]	18,300 [5]
Turkey	1,885,712	1,573,993	1,904,461	2,901,027 [r]	2,500,000
United Arab Emirates	34,350	23,770	25,000	--	--
Vietnam	55,880	37,105	40,000	40,000 [e]	40,000
Zimbabwe	442,584	193,673	510,000	599,079 [r]	550,000
Total	23,800,000	19,500,000 [r]	24,400,000 [r]	25,800,000 [r]	25,600,000

[e]Estimated. [p]Preliminary. [r]Revised. -- Zero.

[1]World totals and estimated data are rounded to no more than three significant digits; may not add to totals shown.

[2]Table includes data available through February 25, 2014.

[3]Figures for all countries represent marketable output.

[4]Gross weight estimated assuming an average grade of 44% chromic oxide (Cr_2O_3).

[5]Reported figure.

[6]Ore grade was 18% to 42% chromic oxide (Cr_2O_3).

[7]Average chromic oxide (Cr_2O_3) content was as follows: 2008—42.5%; 2009—40.0%.; 2010—49.7%; 2011—45.2% (revised); and 2012—45.0% (estimated).

Appendix II

Reference: Alapieti & Huhtelin, 2005

Sample	1	2	3	4	5	6	7	8
				Weight percent				
TiO_2	0,39	0,96	0,4	0,41	0,61	0,57	0,42	0,62
Al_2O_3	14,17	9,63	15,43	14,51	16,98	2,3	0,84	16,79
Cr_2O_3	51,32	42,18	49,03	48,63	42,94	39,65	39,43	45,1
Fe_2O_3	3,90	10,81	5,29	5,69	5,89	23,7	26,49	7,82
V_2O_3	0,22	0,21	0,11	0,15	0,13	0,13	0,14	0,2
FeO	15,52	29,57	18,09	19,06	28,6	29,73	30,36	17,16
MnO	0,31	0,67	0,3	0,32	0,26	0,28	0,26	0,32
MgO	11,71	0,14	10,54	9,67	4,06	1,18	0,78	11,45
ZnO	0,00	3,40	0,08	0,06	0,05	<0.05	0,07	<0.05
NiO	0,17	<0,05	0,11	0,1	0,05	0,17	0,18	0,09
Sum	97,70	97,57	99,34	98,6	99,57	97,71	98,97	99,58
				Number of ions on the basis of 32 oxygen atoms				
Al	4,38	3,333	4,719	4,512	5,385	0,82	0,299	5,067
Cr	10,645	9,794	10,059	10,144	9,135	9,477	9,419	9,128
Fe^{3+}	0,77	2,389	1,025	1,13	1,193	5,392	6,023	1,506
Ti	0,077	0,212	0,078	0,081	0,123	0,13	0,095	0,119
V	0,046	0,049	0,028	0,032	0,028	0,032	0,034	0,043
Mg	4,577	0,061	4,076	0,803	1,628	0,532	0,351	4,37
Ni	0,035		0,023	0,021	0,011	0,041	0,044	0,018
Fe^{2+}	3,404	7,262	3,926	4,205	6,425	7,516	7,671	3,673
Zn	0	0,737	0,015	0,012	0,01		0,016	
Mn	0,068	0,167	0,066	0,072	0,059	0,041	0,067	0,07
				Mole percent				
$(Fe,Mg)Cr_2O_4$	67,4	63,1	63,6	64,3	58,1	60,4	59,8	58,1
$(Fe,Mg)Al_2O_4$	27,7	21,5	29,9	28,6	34,3	5,2	1,9	32,3
Fe_3O_4	4,9	15,4	6,5	7,1	7,6	34,4	38,3	9,6
Cr/Fe	2,37	0,94	1,88	1,77	1,11	0,68	0,64	1,64

Appendices – SEM micrographs

Appendix III

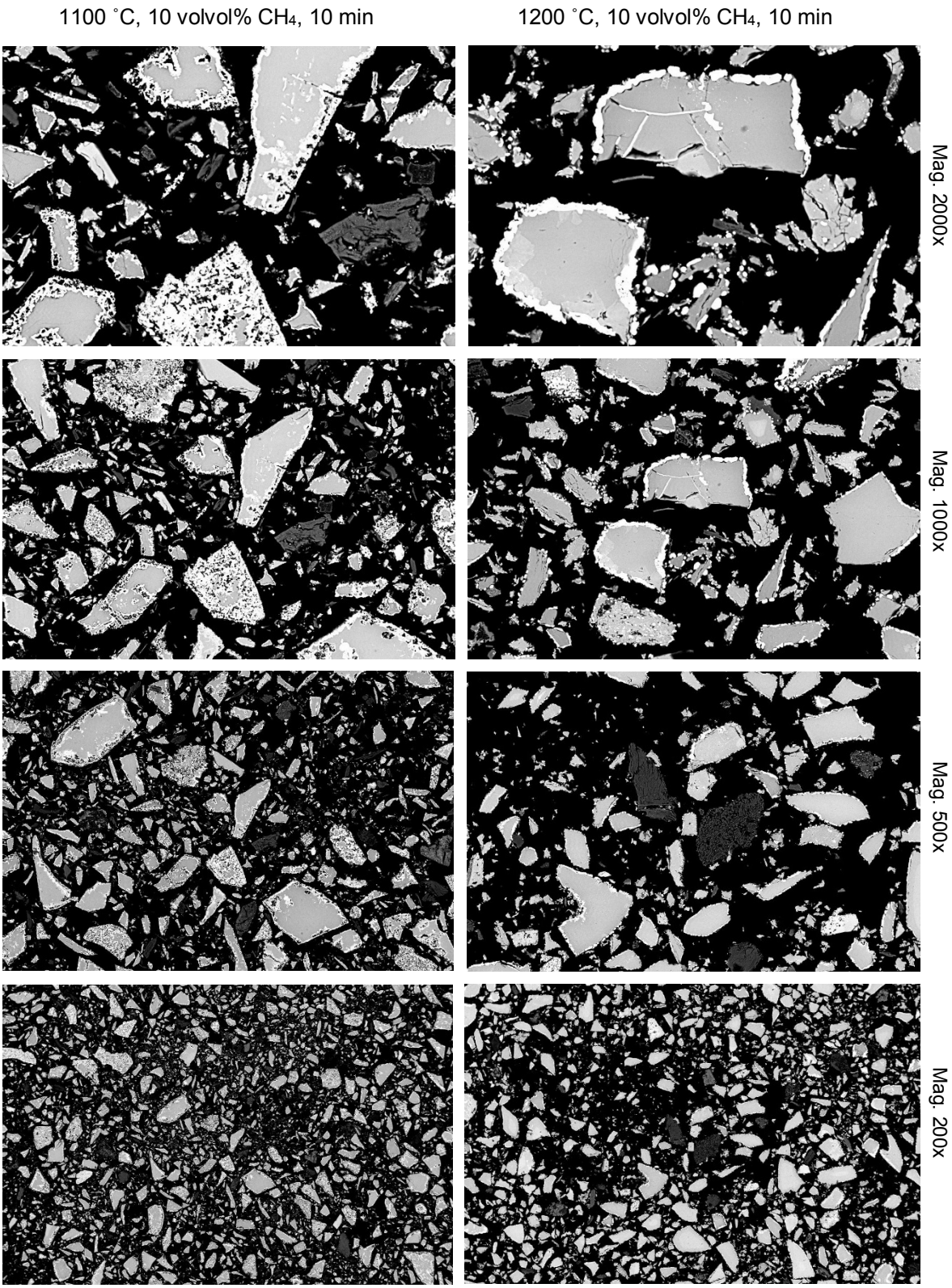

Appendix IV

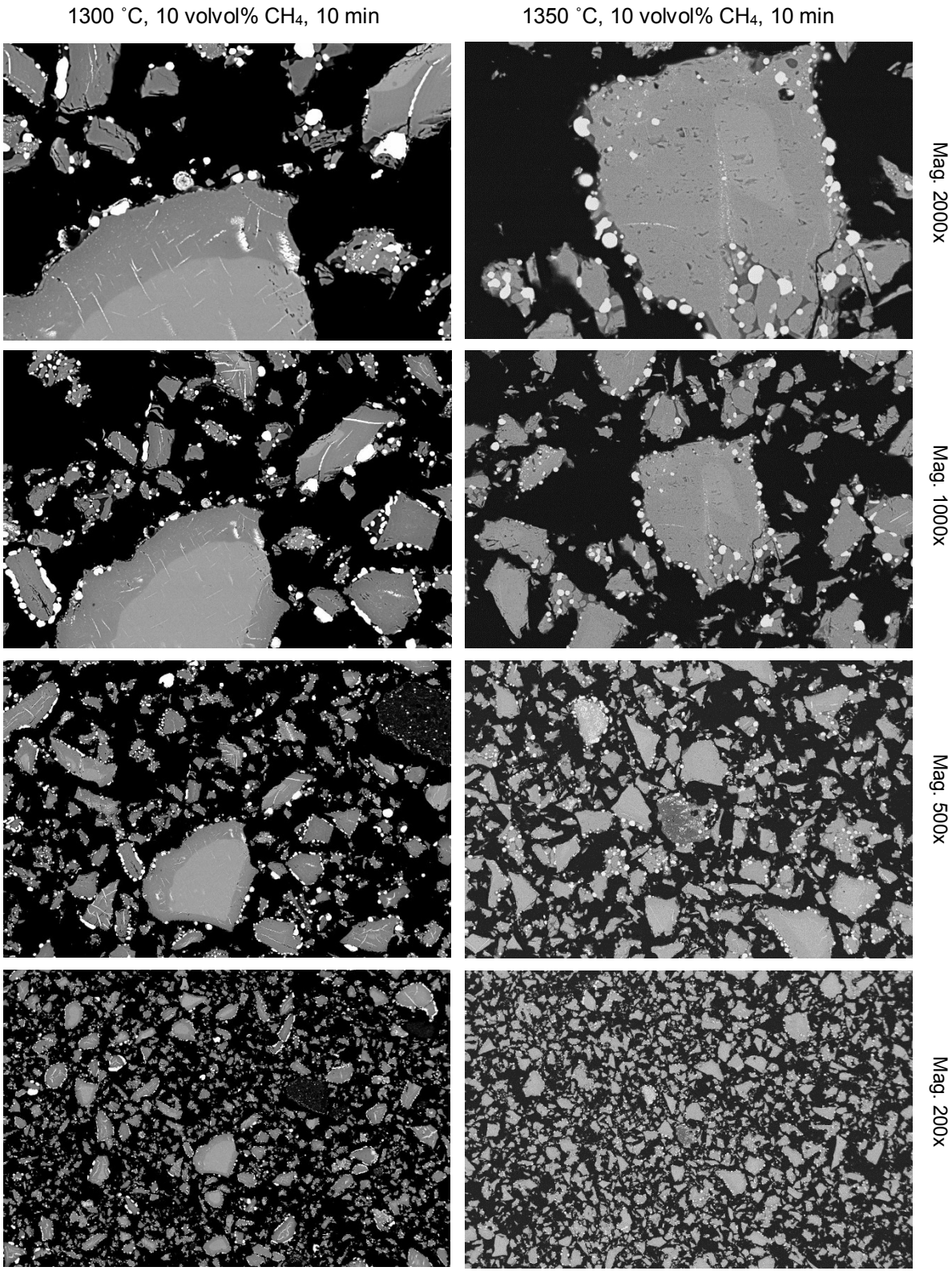
1300 ˚C, 10 volvol% CH_4, 10 min
1350 ˚C, 10 volvol% CH_4, 10 min
Mag. 2000x
Mag. 1000x
Mag. 500x
Mag. 200x

Appendix V

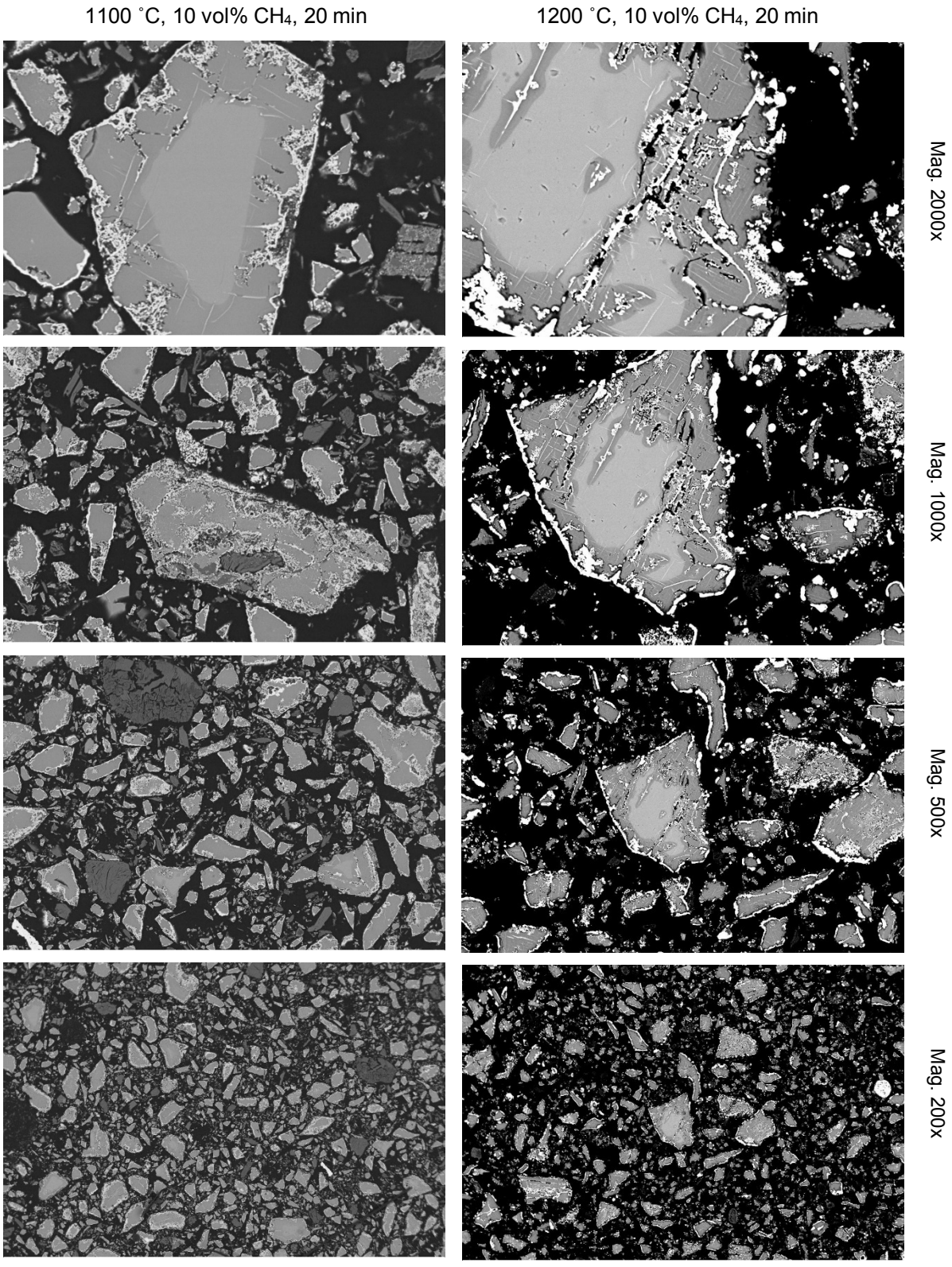
1100 ˚C, 10 vol% CH_4, 20 min
1200 ˚C, 10 vol% CH_4, 20 min
Mag. 2000x
Mag. 1000x
Mag. 500x
Mag. 200x

Appendix VI

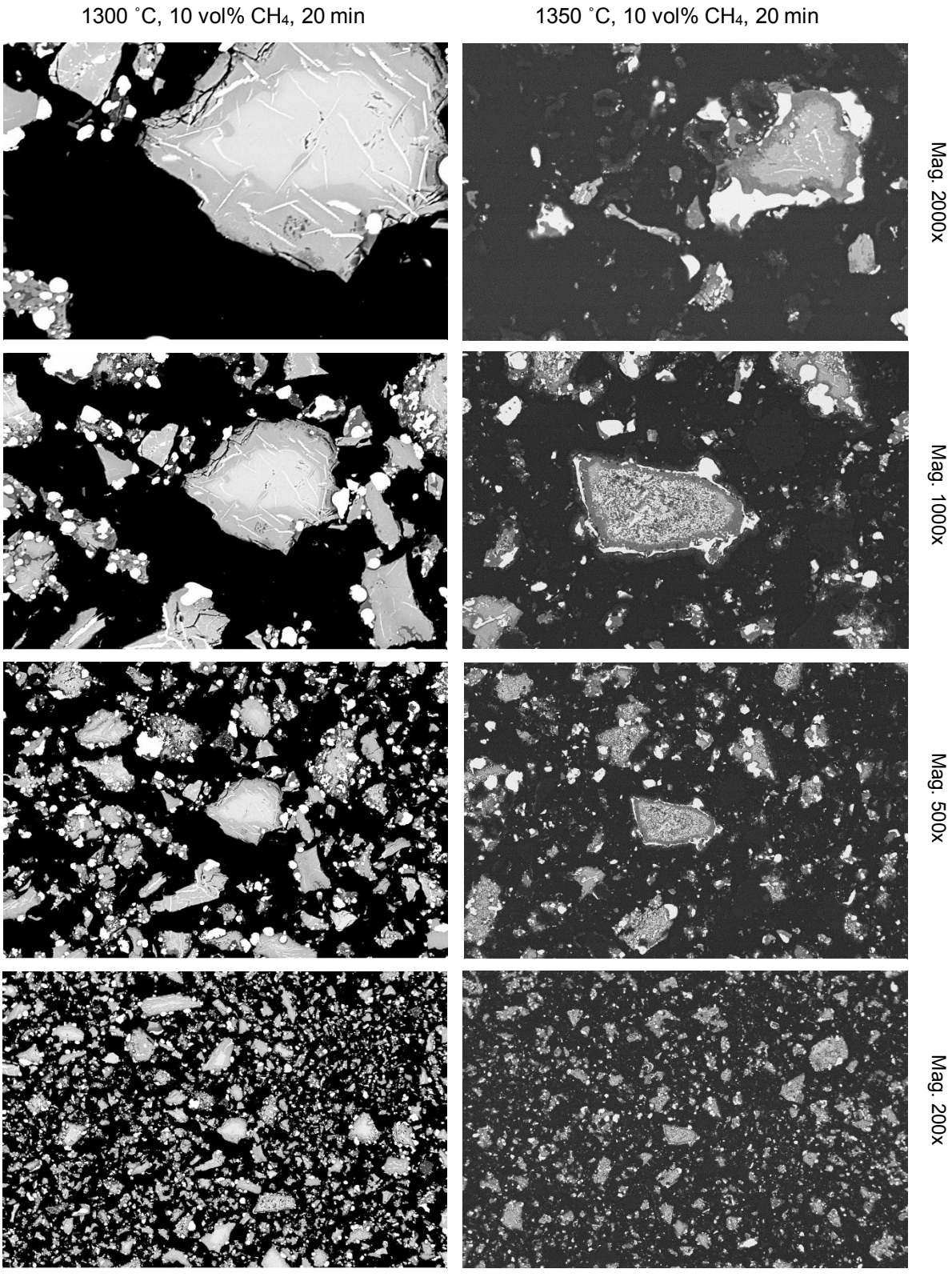
1300 ˚C, 10 vol% CH_4, 20 min
1350 ˚C, 10 vol% CH_4, 20 min
Mag. 2000x
Mag. 1000x
Mag. 500x
Mag. 200x

Appendix VII

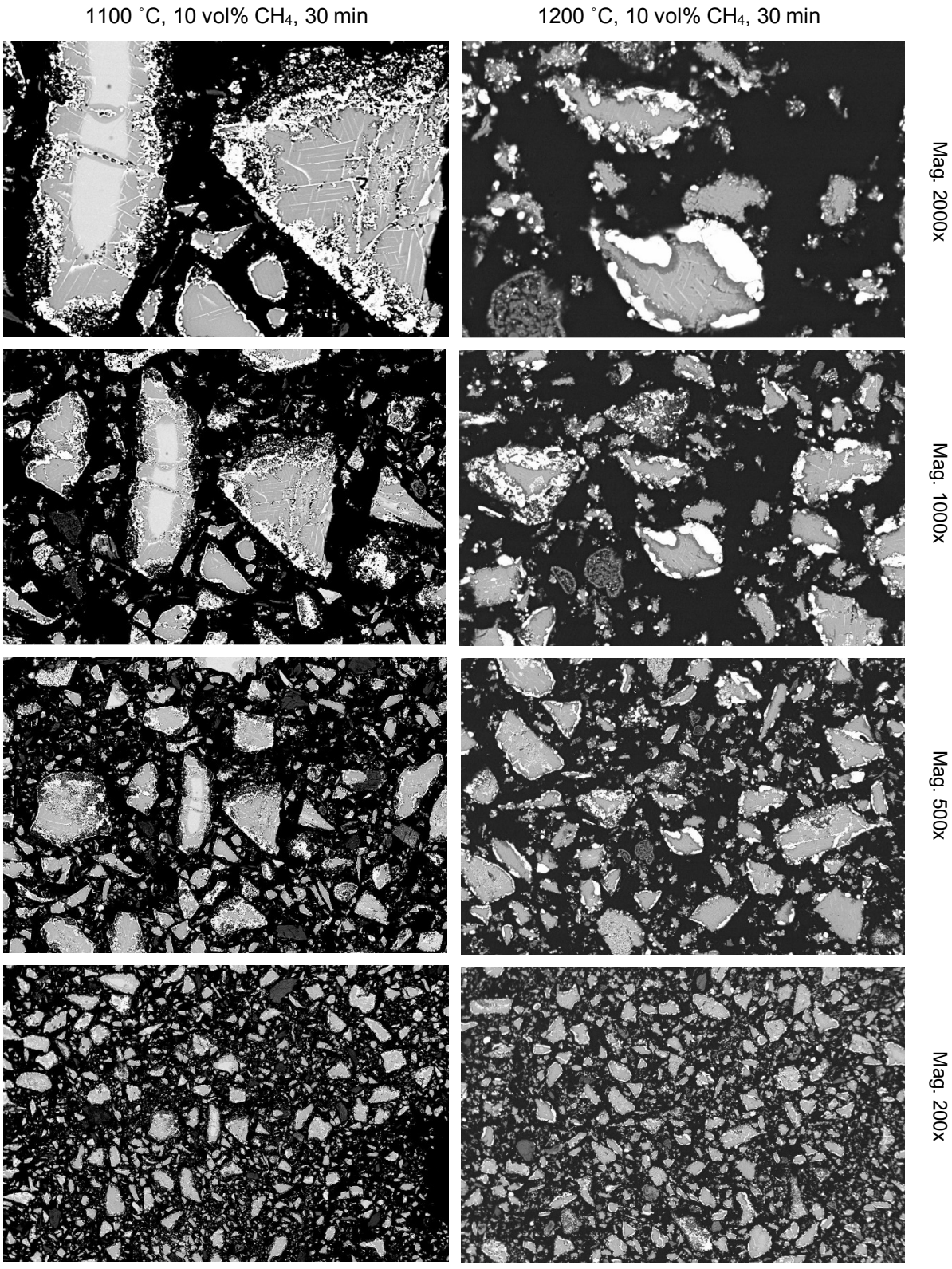

Appendix VIII

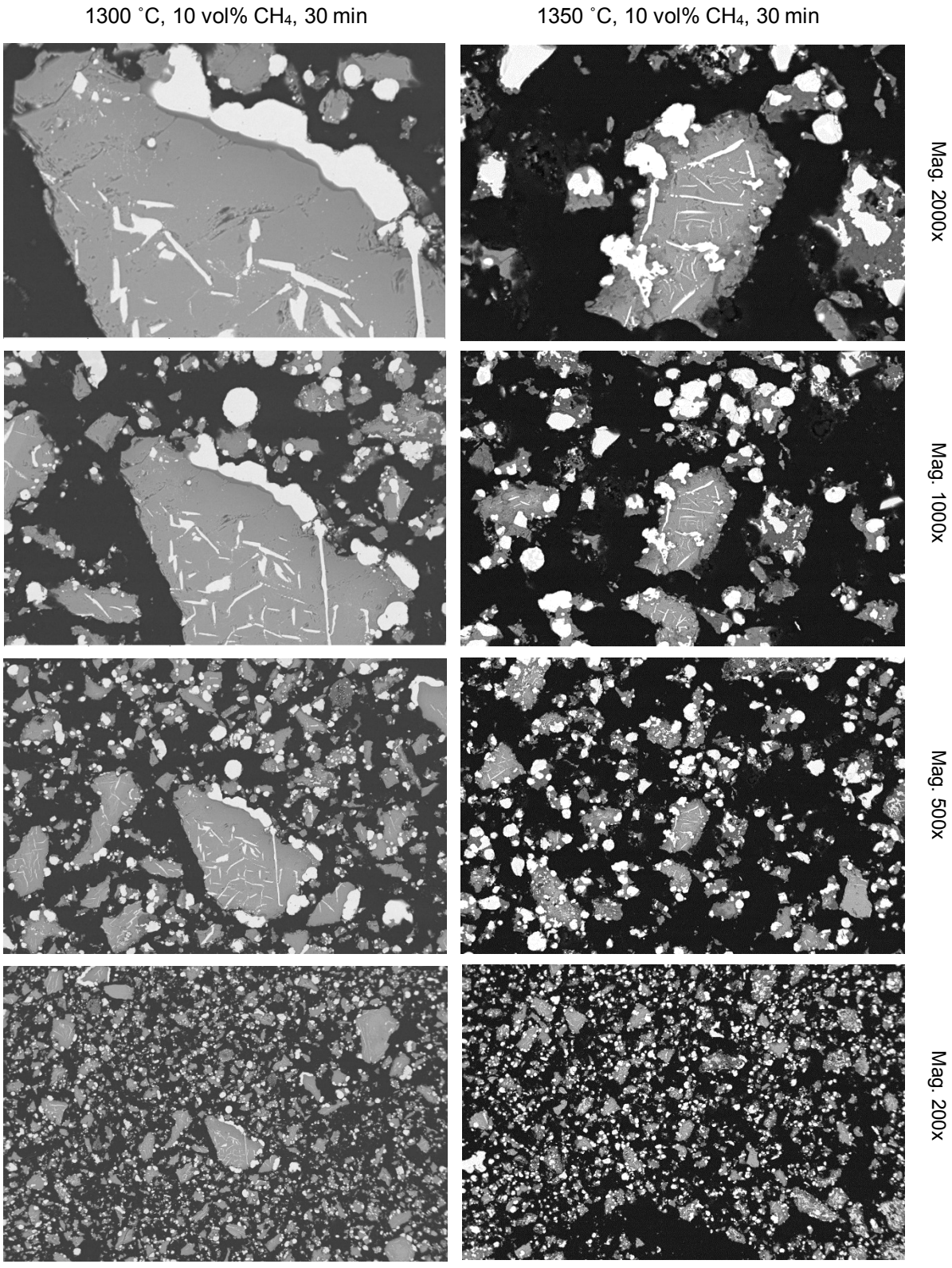

Appendix IX

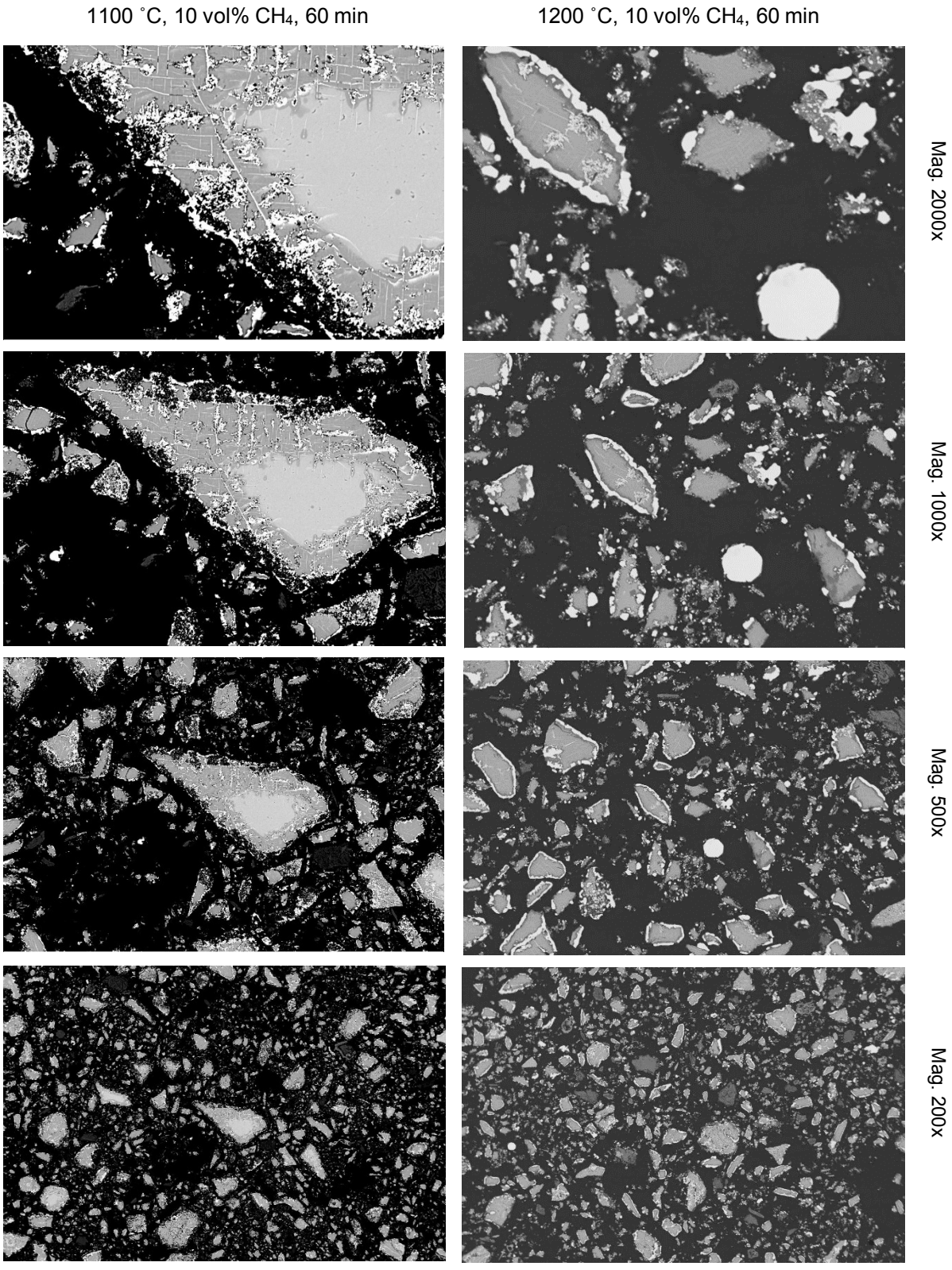
1100 ˚C, 10 vol% CH_4, 60 min
1200 ˚C, 10 vol% CH_4, 60 min
Mag. 2000x
Mag. 1000x
Mag. 500x
Mag. 200x

Appendix X

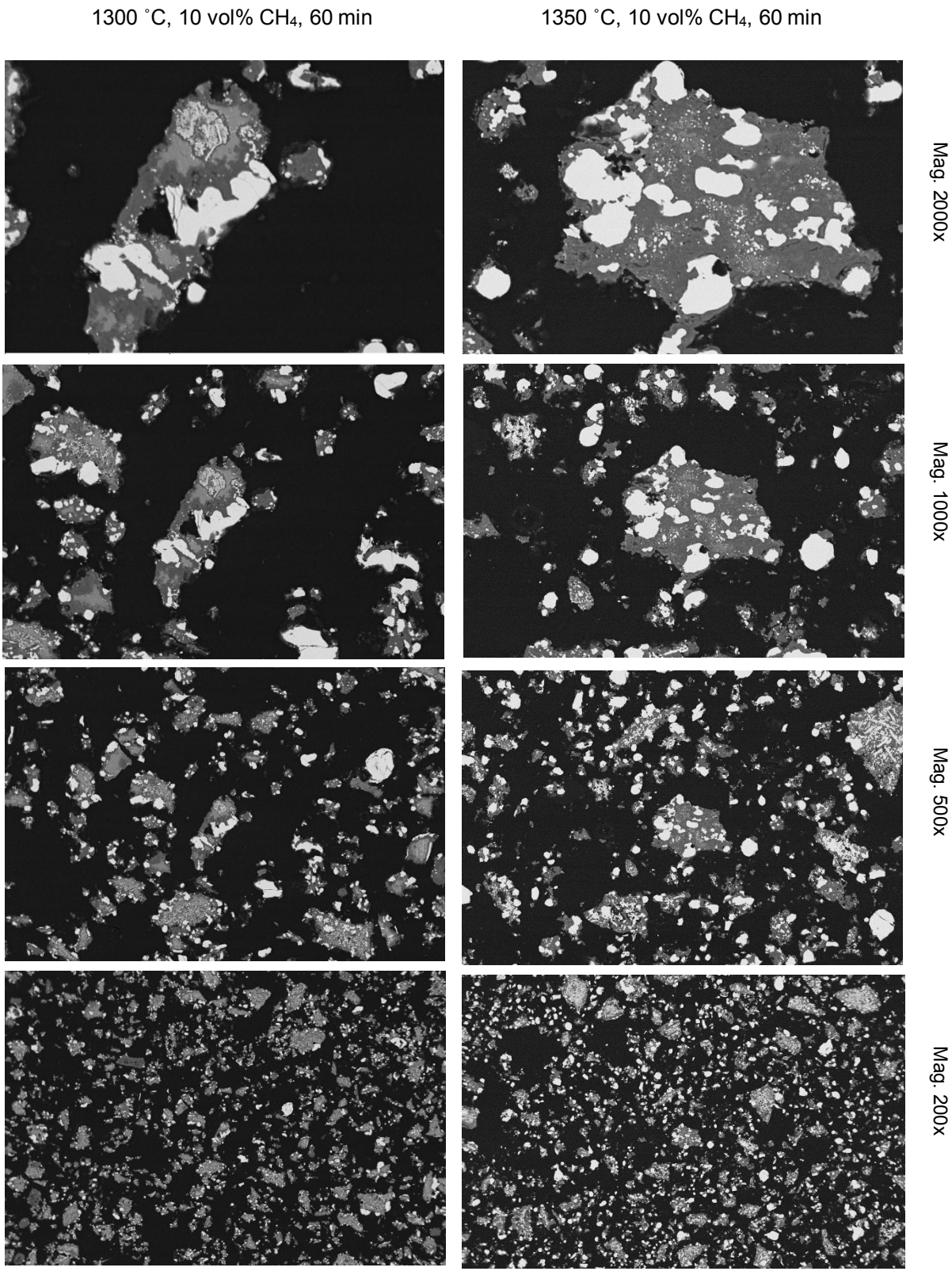
1300 ˚C, 10 vol% CH_4, 60 min
1350 ˚C, 10 vol% CH_4, 60 min
Mag. 2000x
Mag. 1000x
Mag. 500x
Mag. 200x

Appendix XI

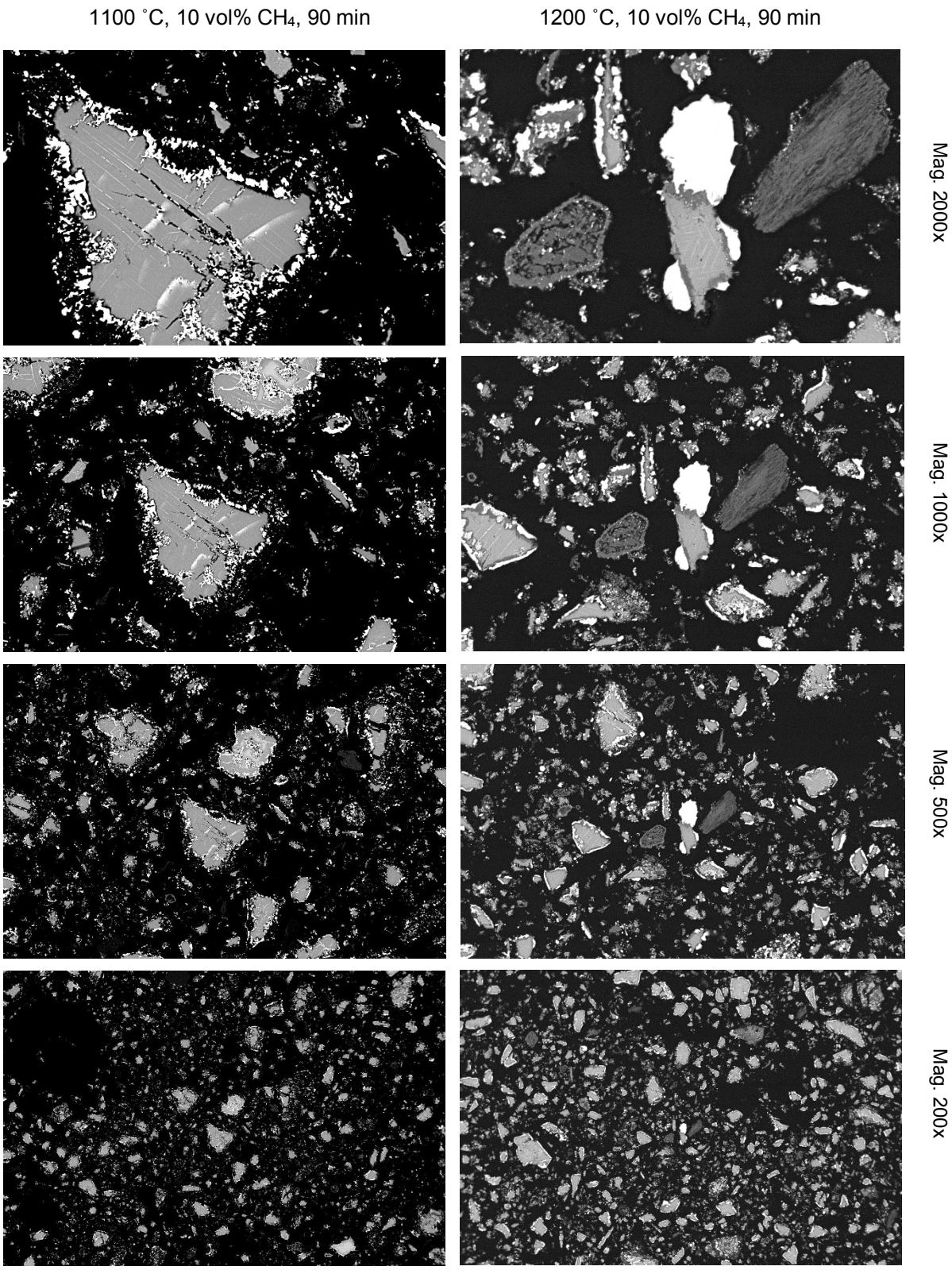
1100 ˚C, 10 vol% CH4, 90 min
1200 ˚C, 10 vol% CH4, 90 min
Mag. 2000x
Mag. 1000x
Mag. 500x
Mag. 200x

Appendix XII

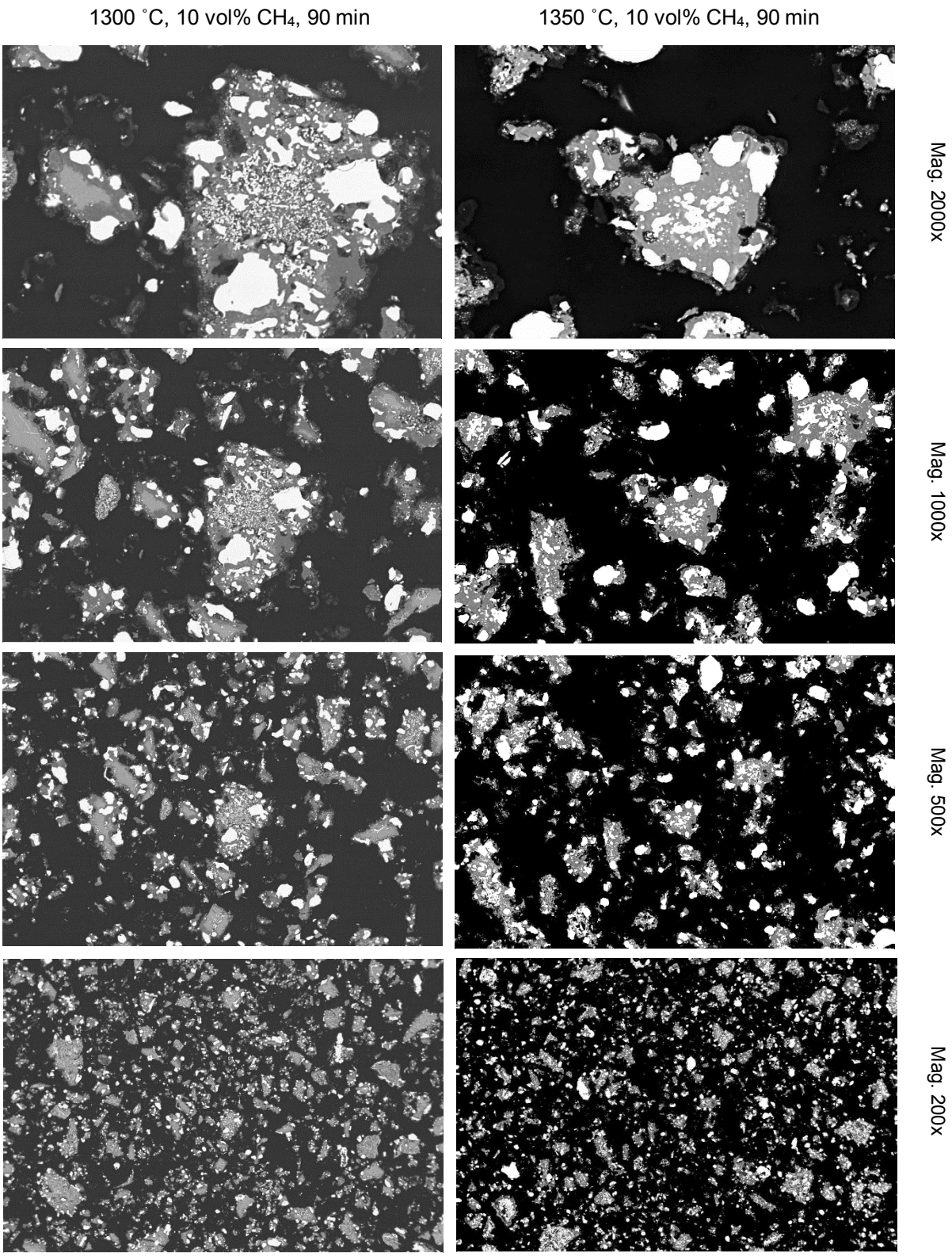

Appendix XIII

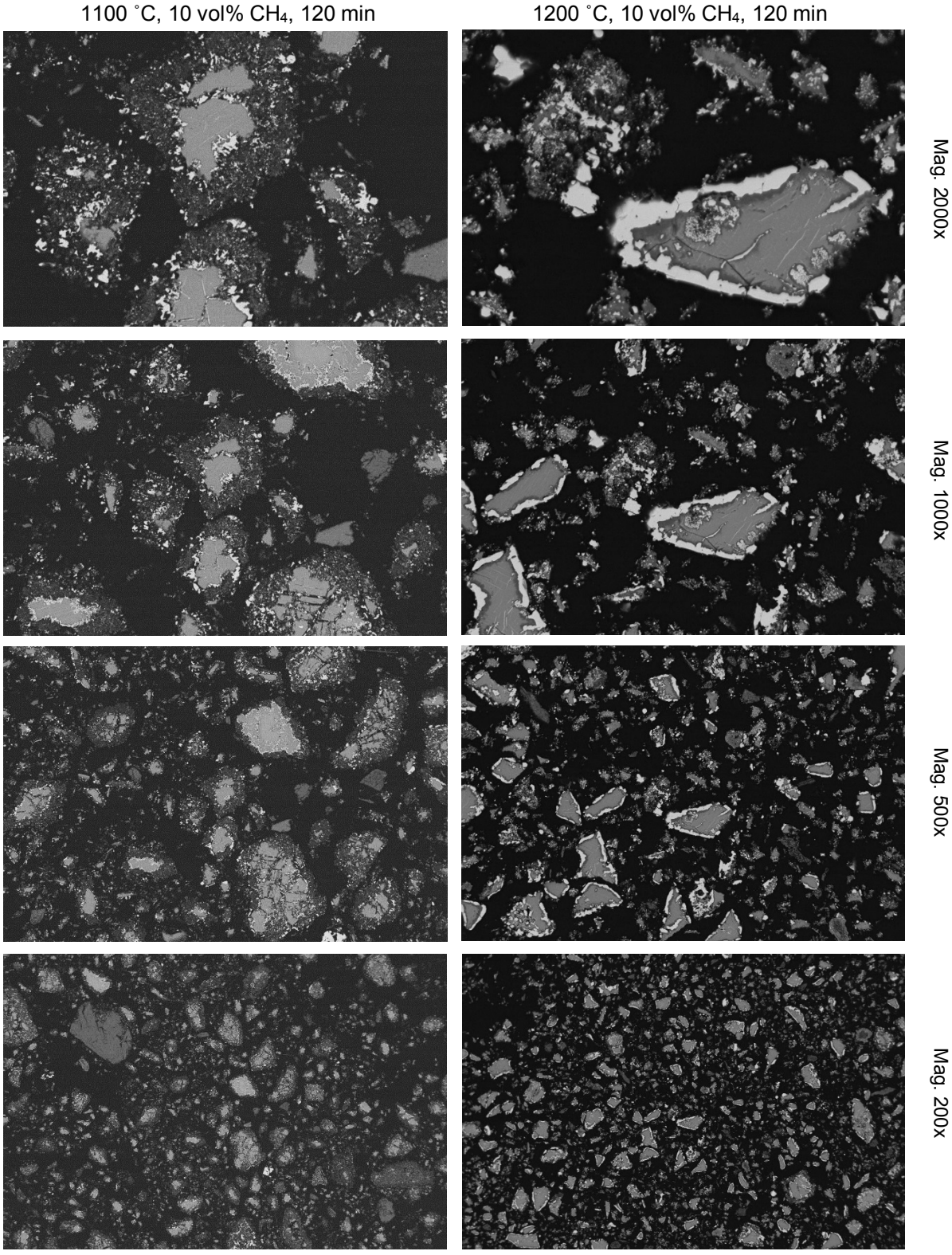

Appendix XIV

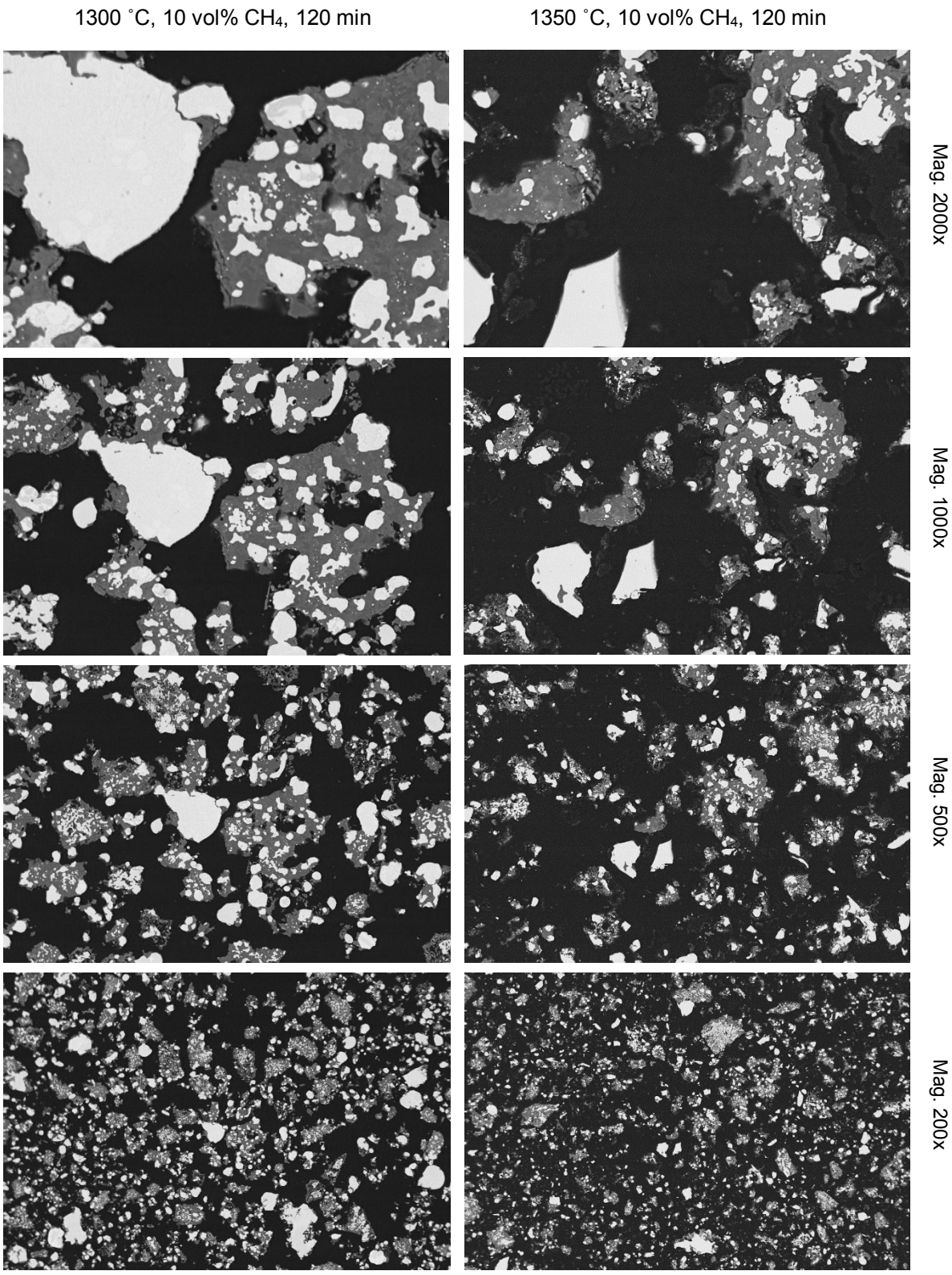

Appendix XV

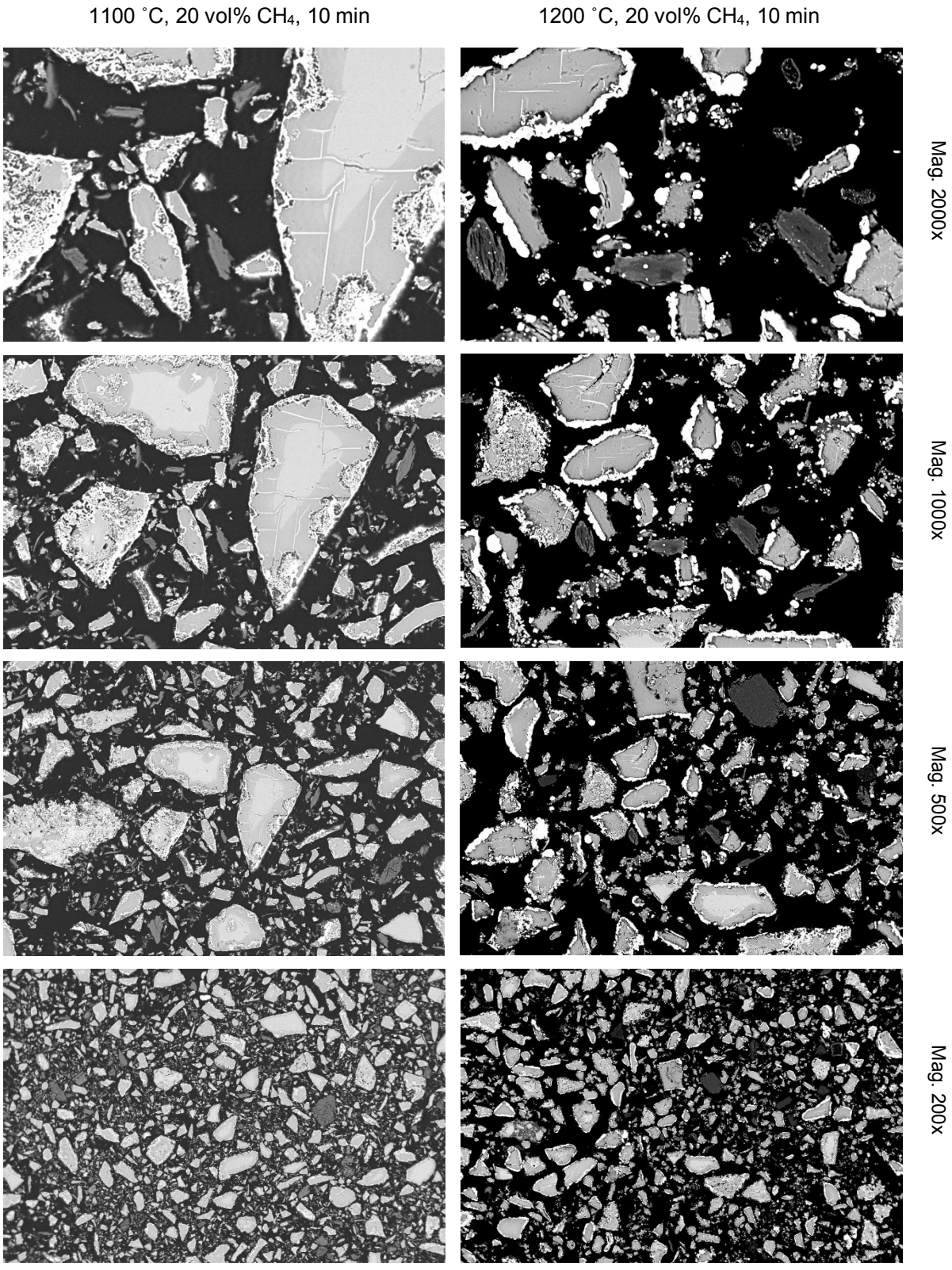
1100 ˚C, 20 vol% CH_4, 10 min
1200 ˚C, 20 vol% CH_4, 10 min
Mag. 2000x
Mag. 1000x
Mag. 500x
Mag. 200x

Appendix XVI

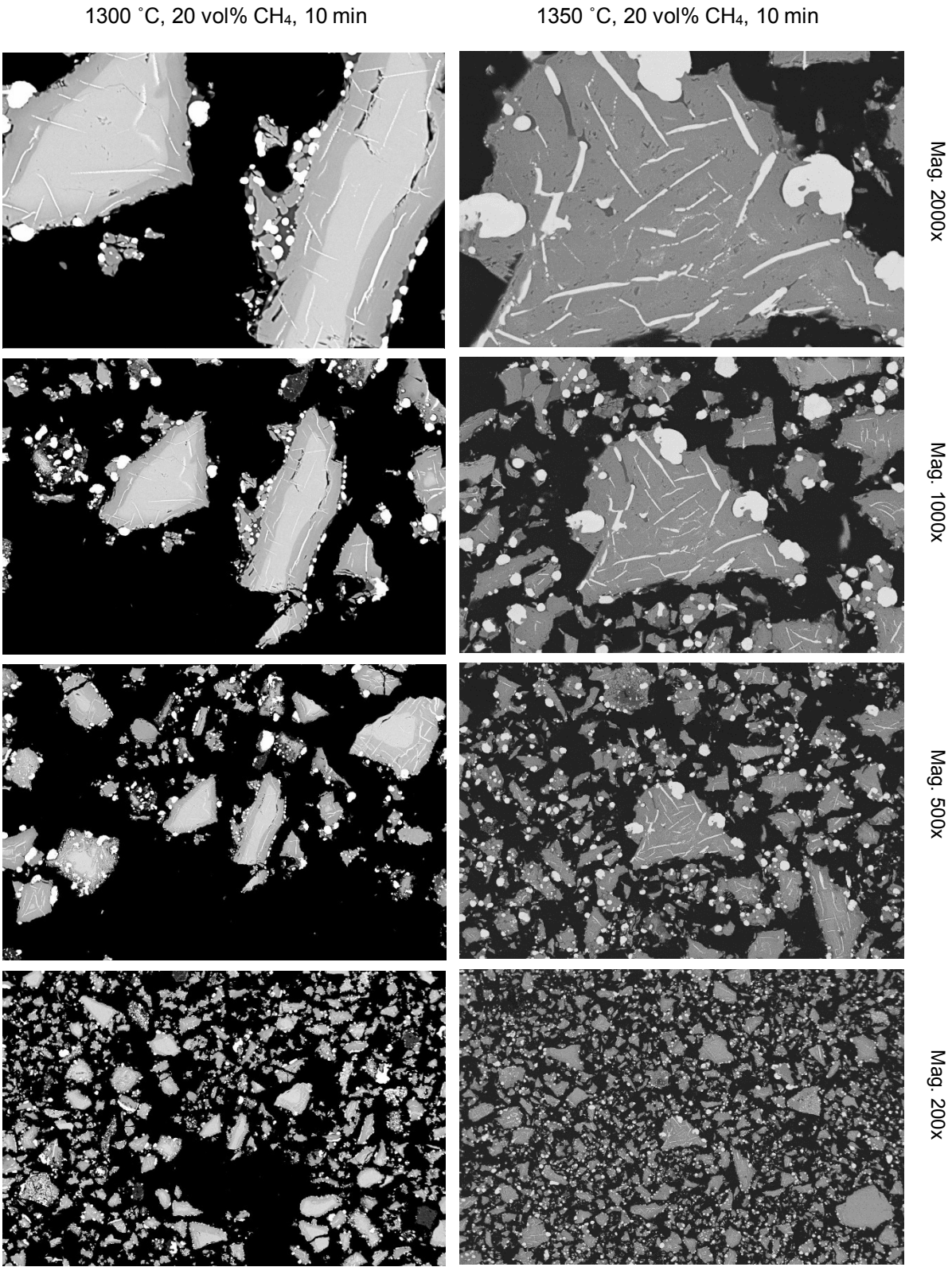

Appendix XVII

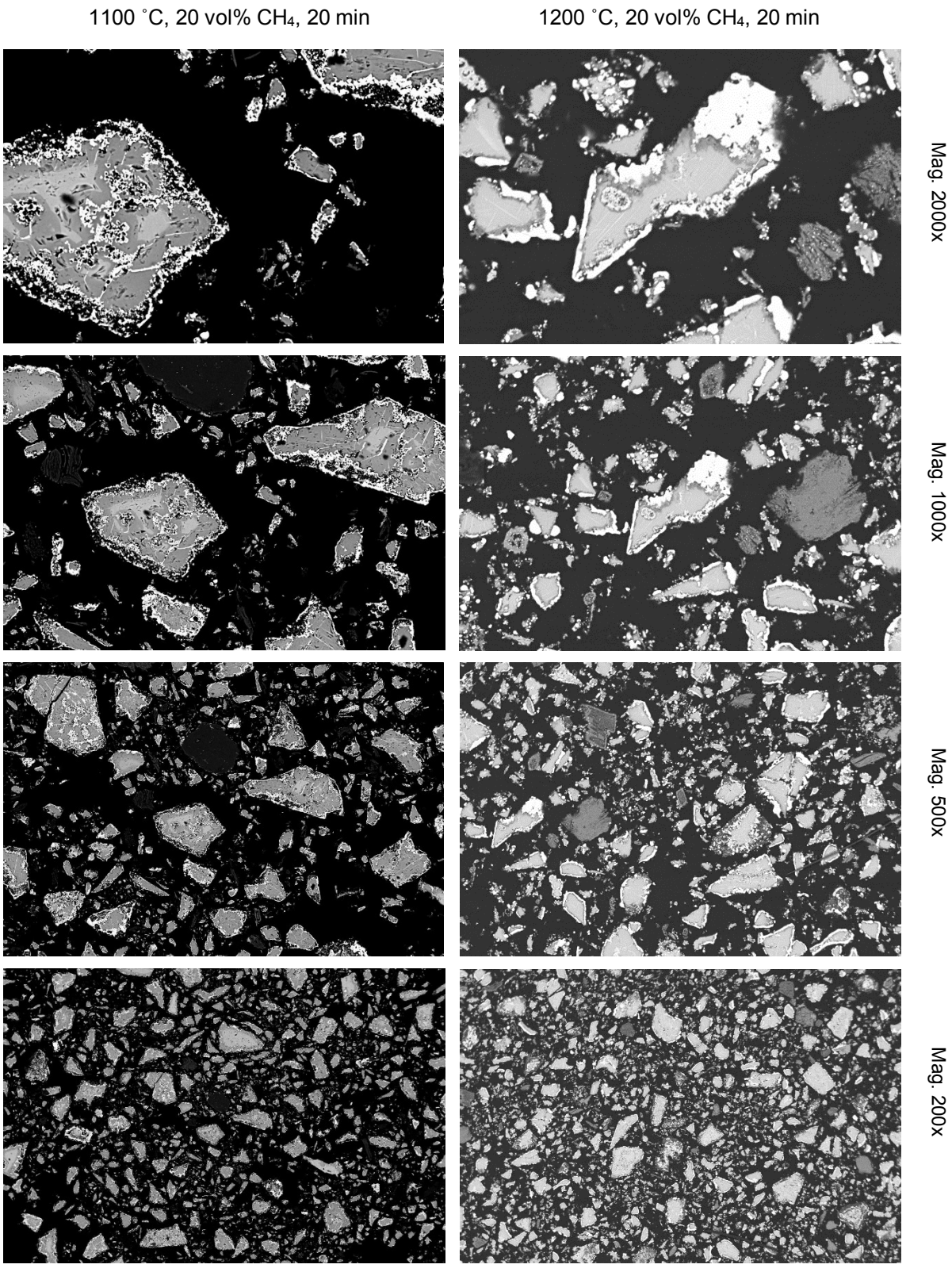

Appendix XVIII

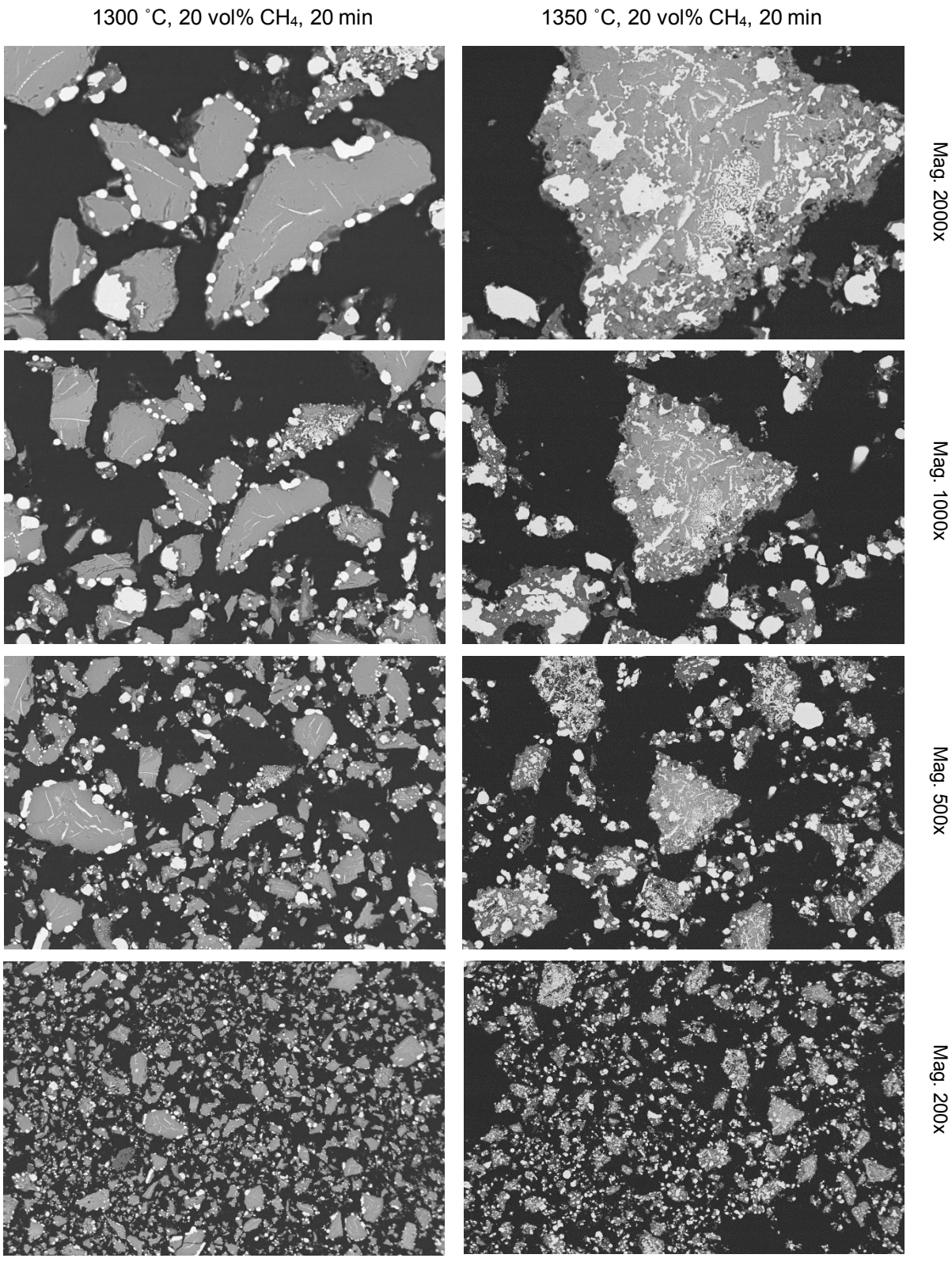

Appendix XIX

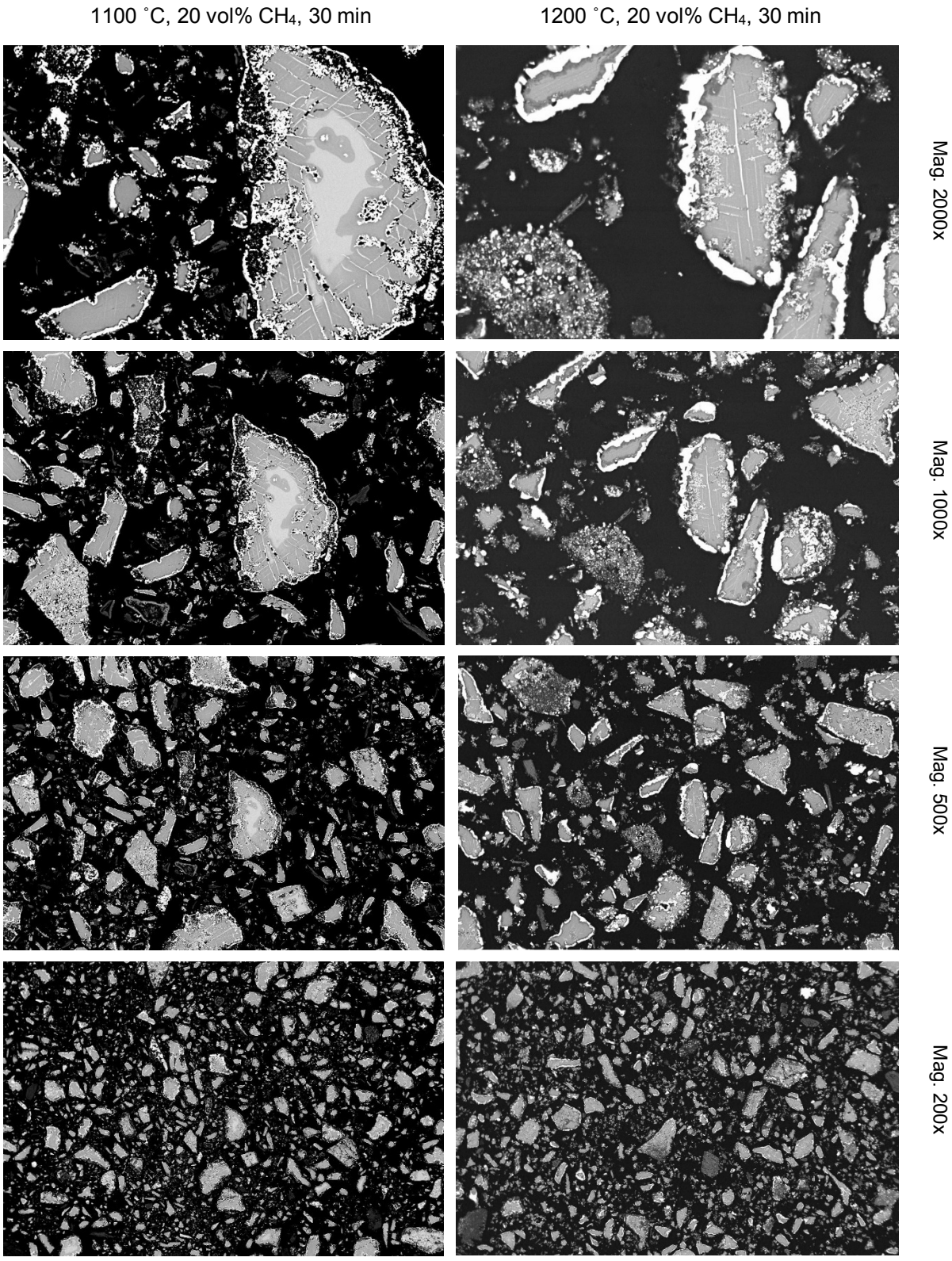

Appendix XX

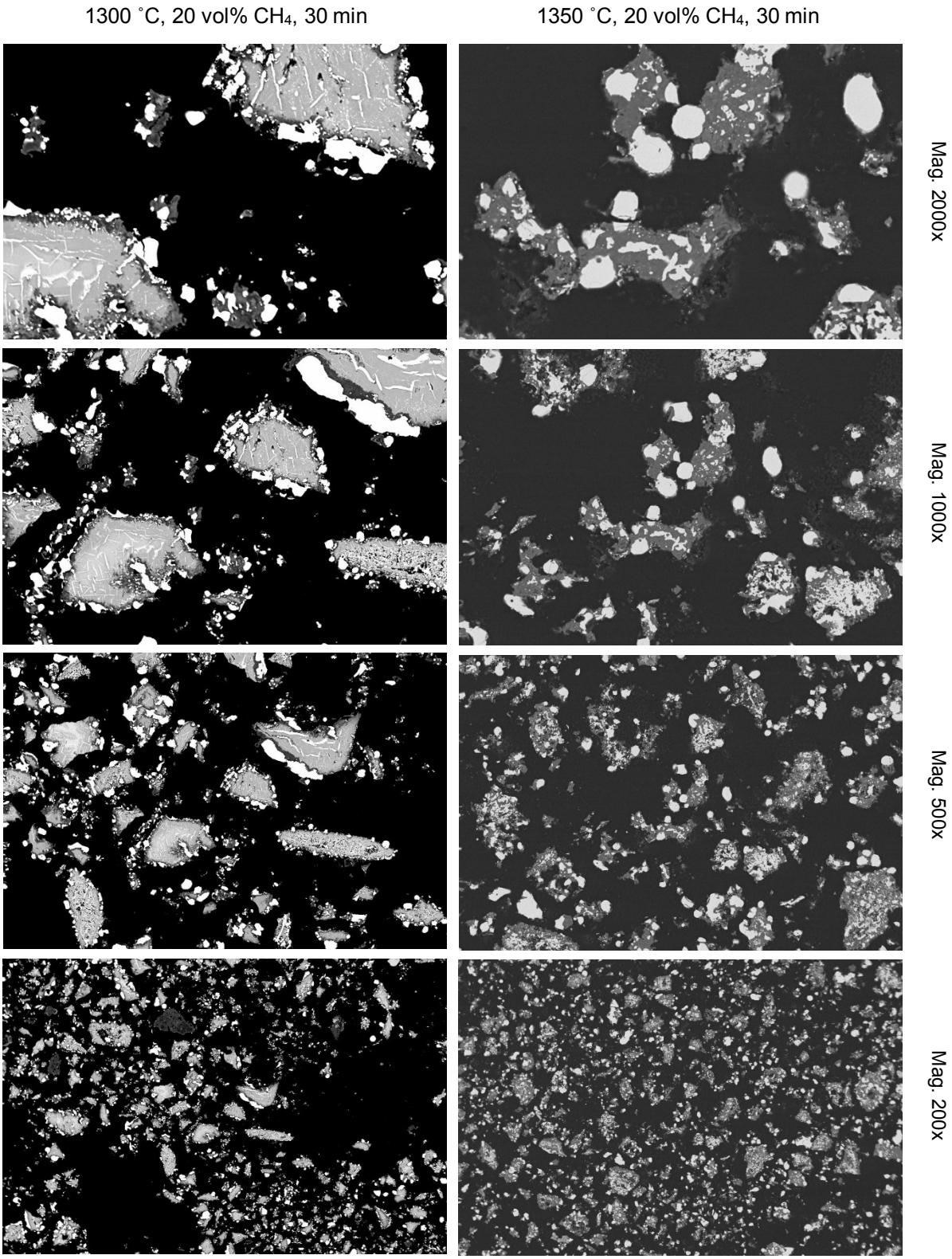
1300 ˚C, 20 vol% CH_4, 30 min
1350 ˚C, 20 vol% CH_4, 30 min
Mag. 2000x
Mag. 1000x
Mag. 500x
Mag. 200x

Appendix XXI

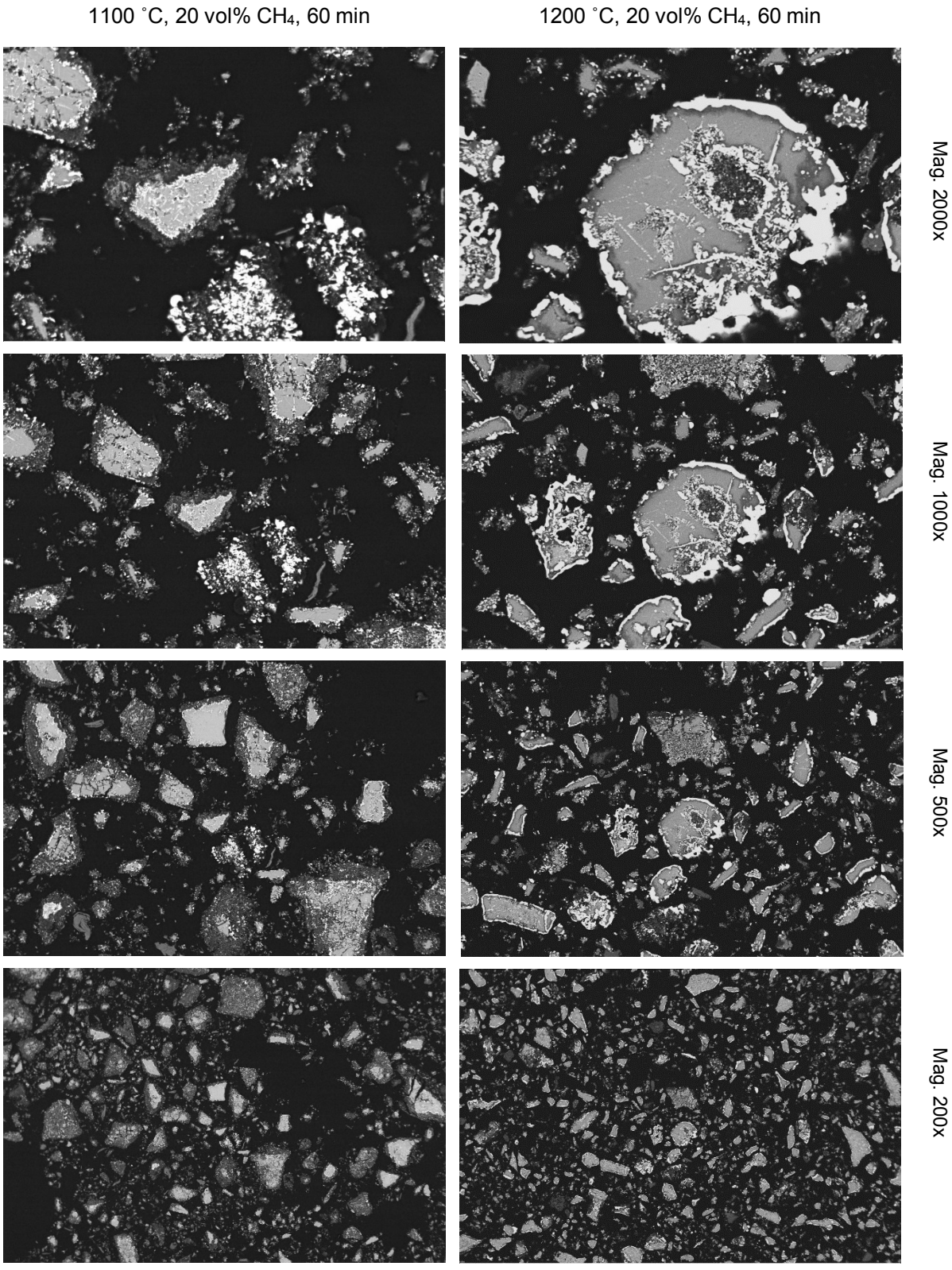

Appendix XXII

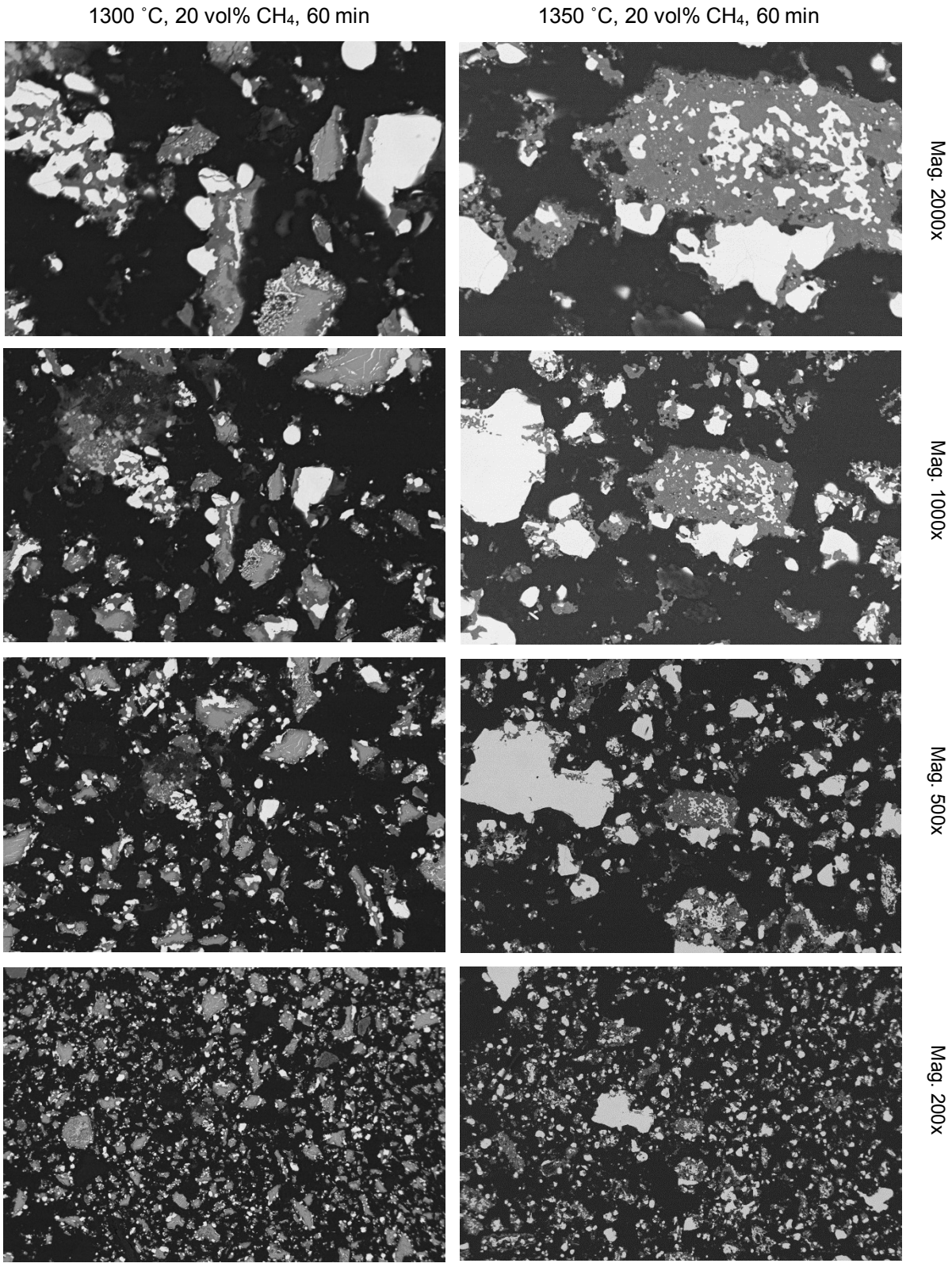

Appendix XXIII

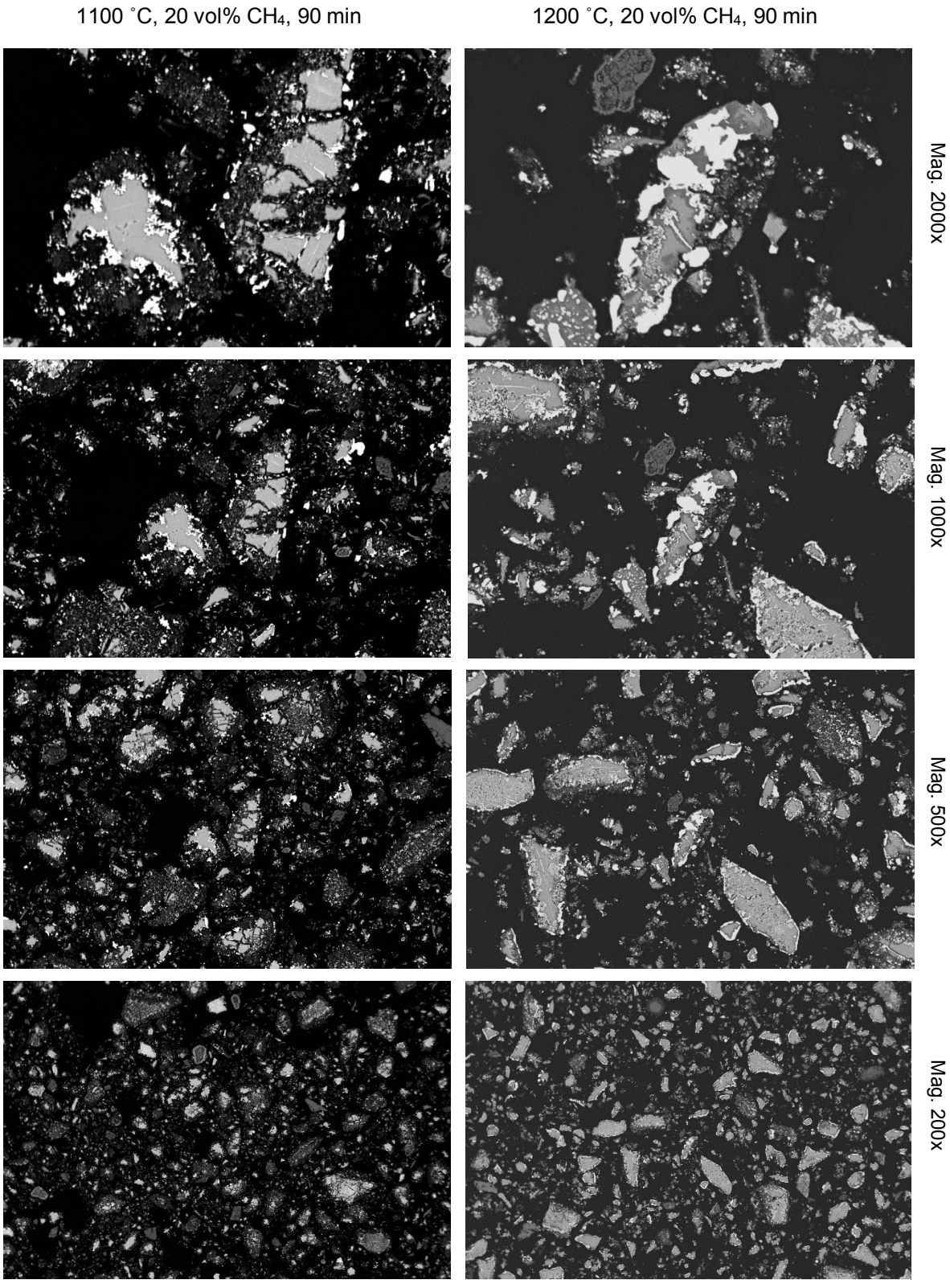

Appendix XXIV

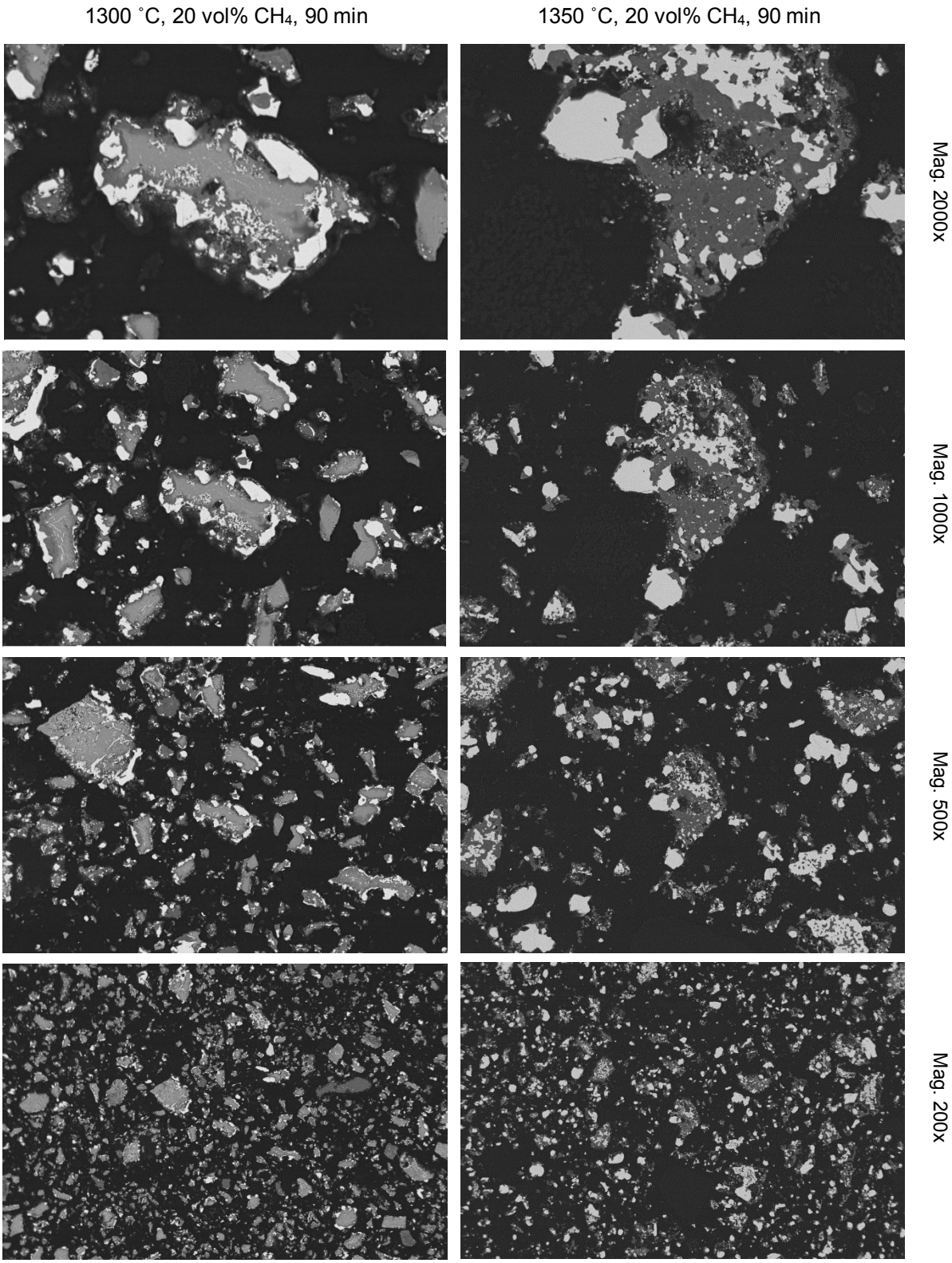

Appendix XXV

1100 ˚C, 20 vol% CH_4, 120 min

1200 ˚C, 20 vol% CH_4, 120 min

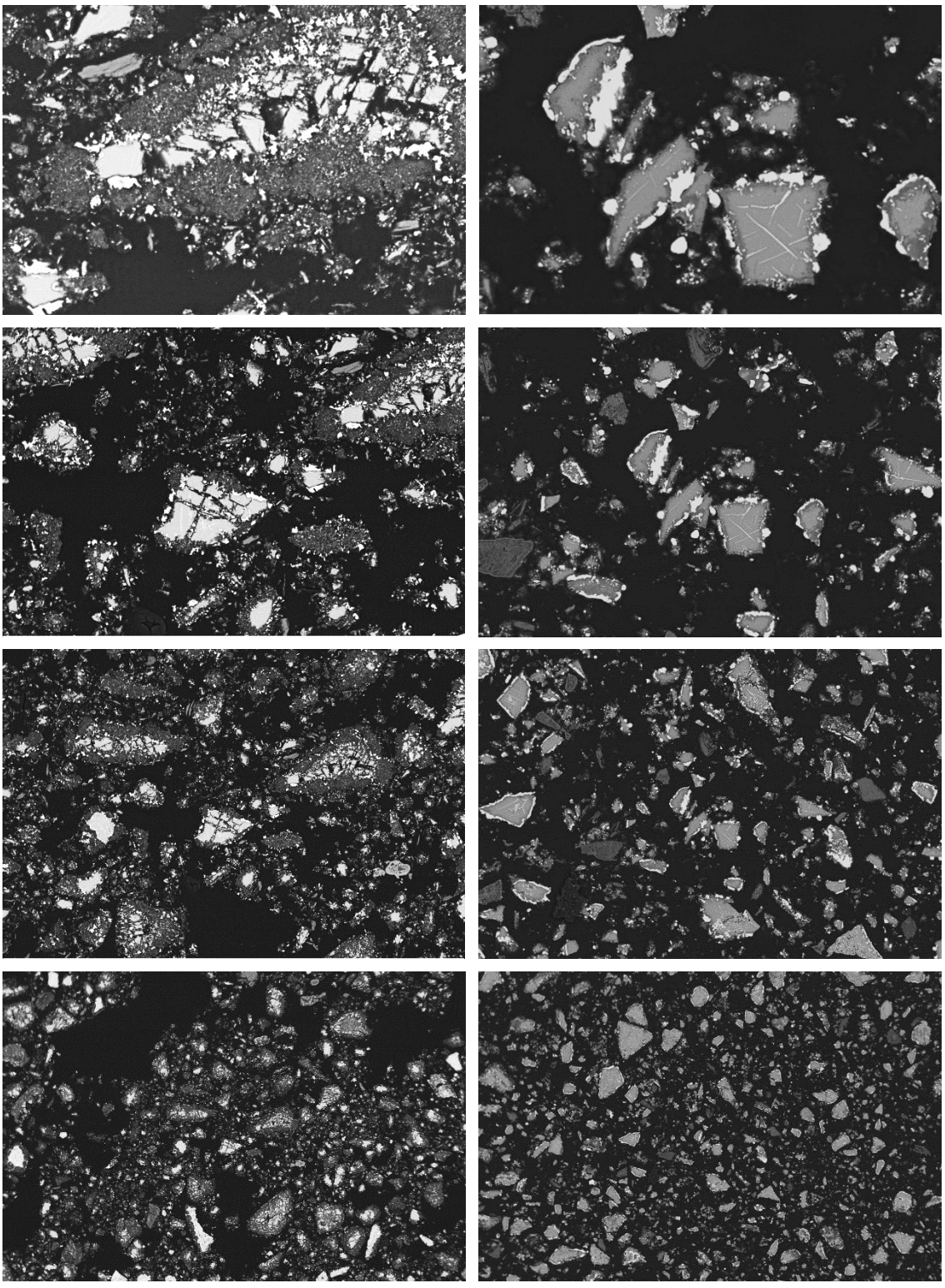

Mag. 2000x

Mag. 1000x

Mag. 500x

Mag. 200x

Appendix XXVI

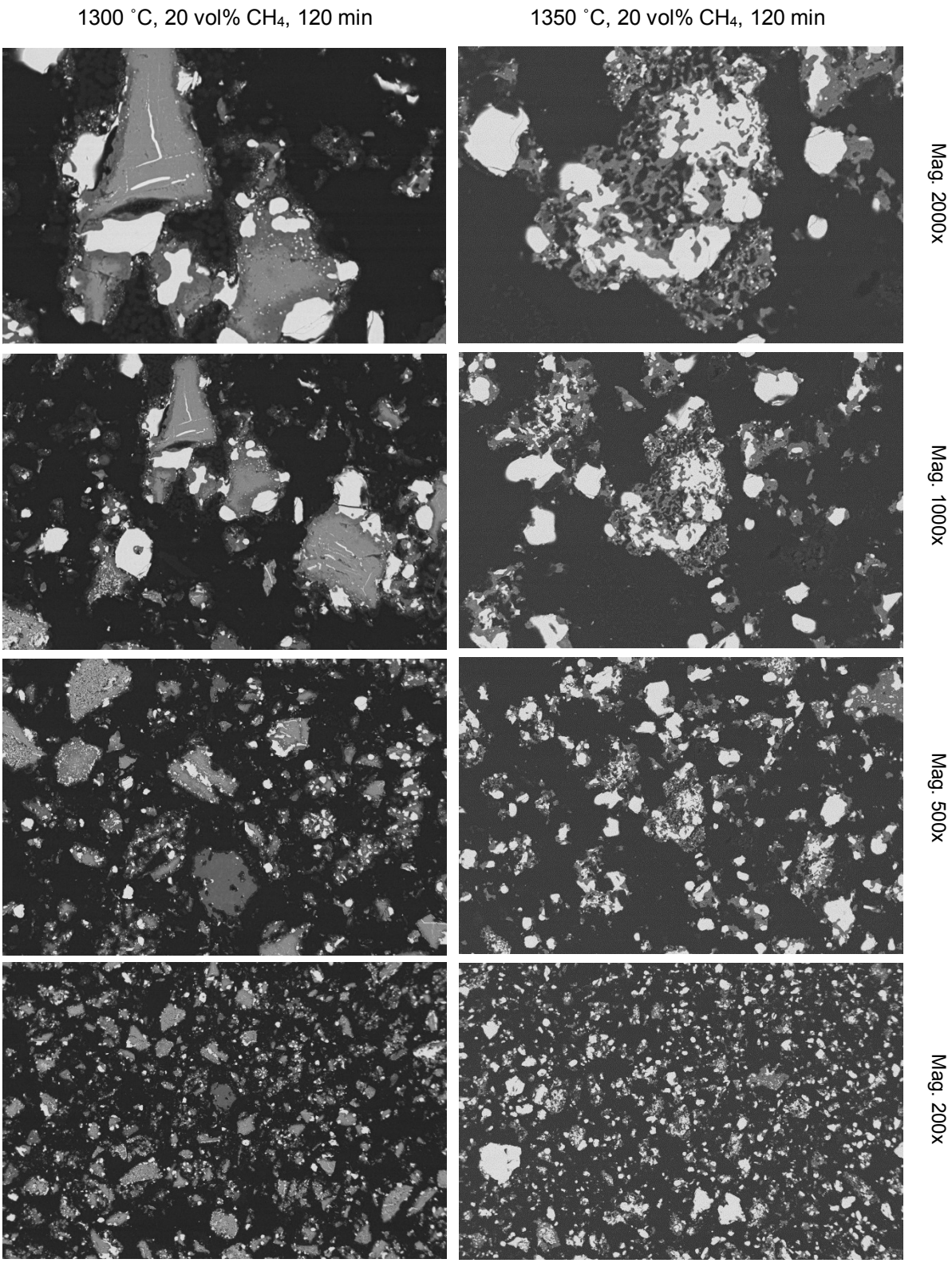

Appendix XXVII

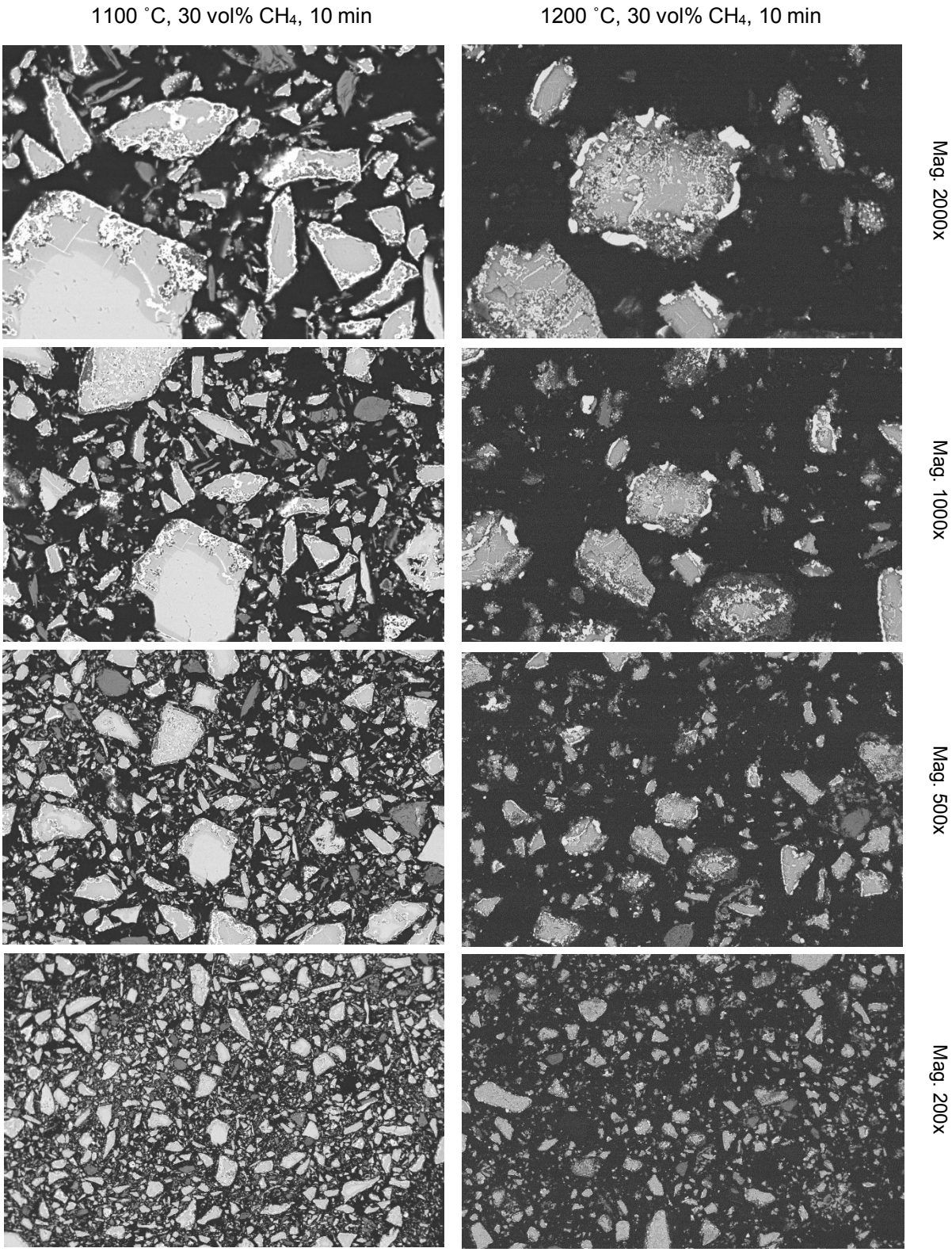

Appendix XXVIII

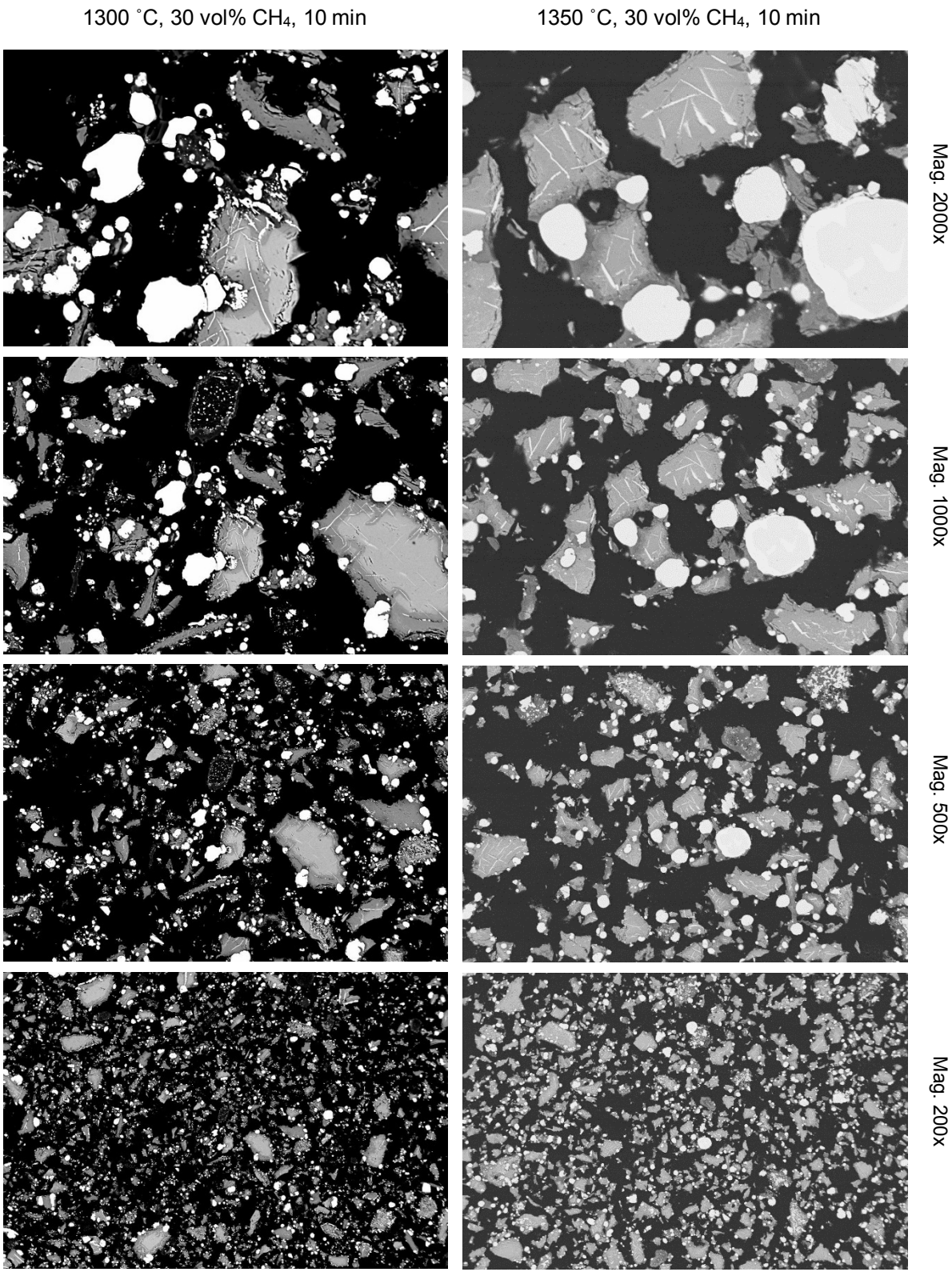

Appendix XXIX

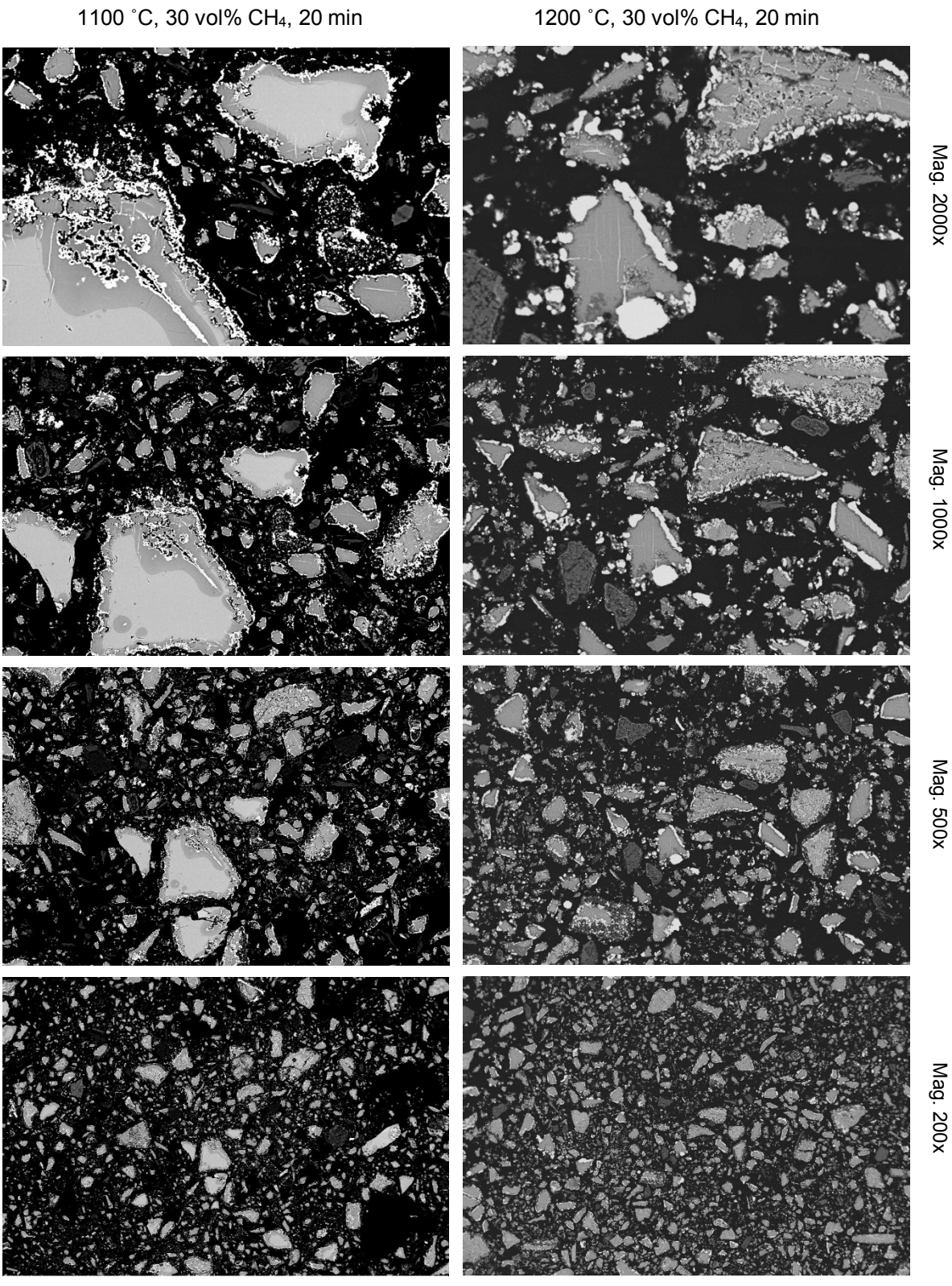

Appendix XXX

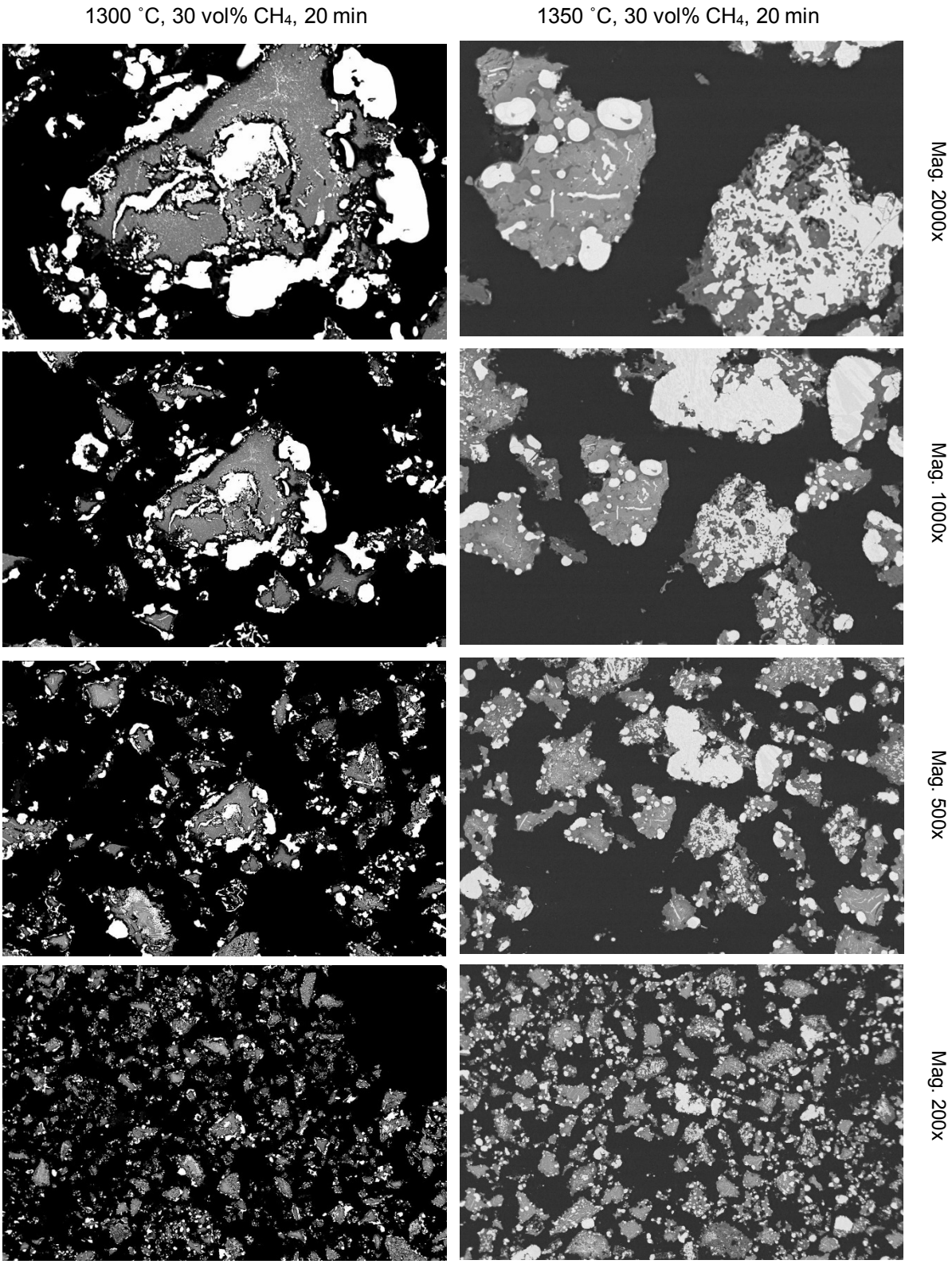

Appendix XXXI

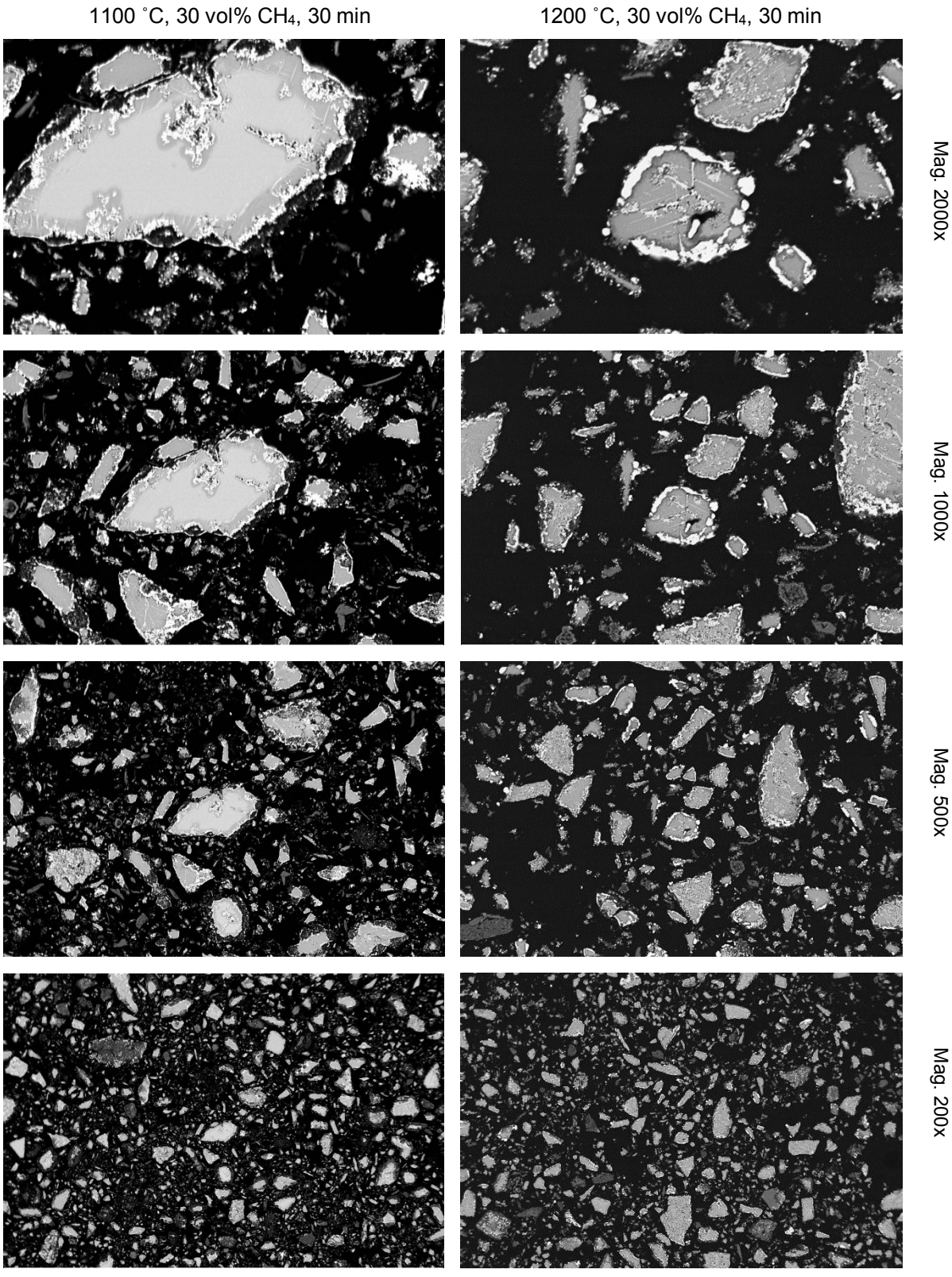

Appendix XXXII

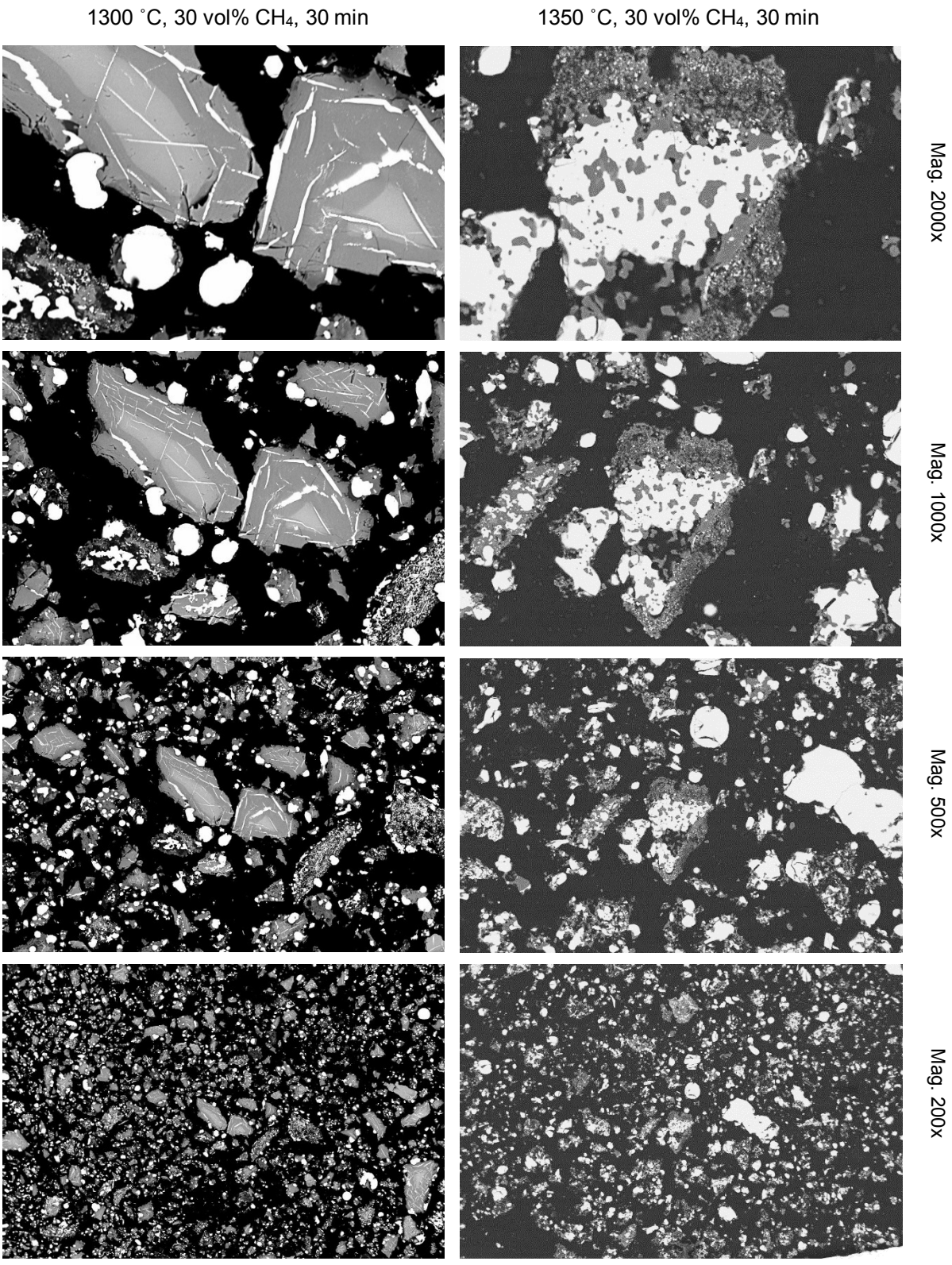

Appendix XXXIII

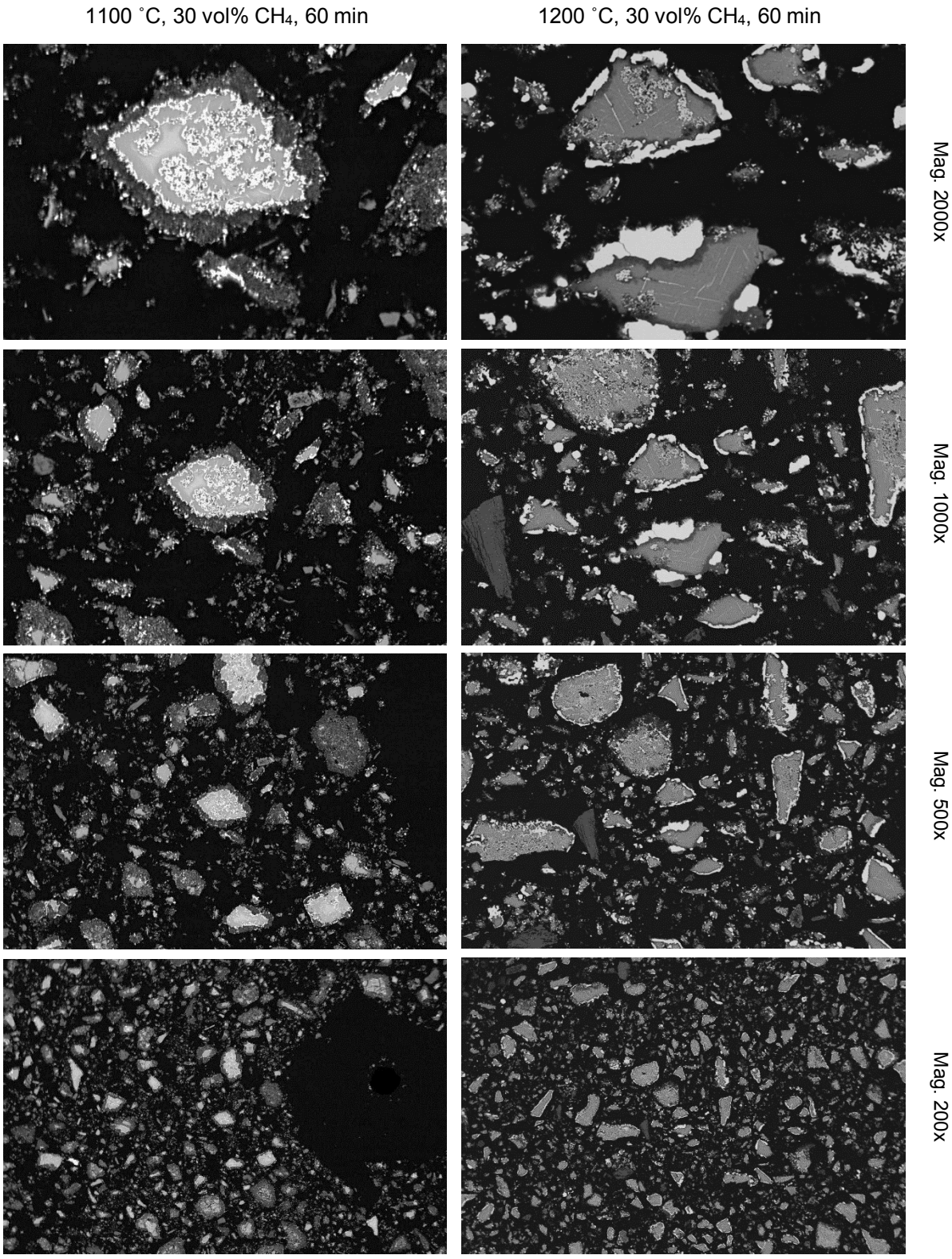

Appendix XXXIV

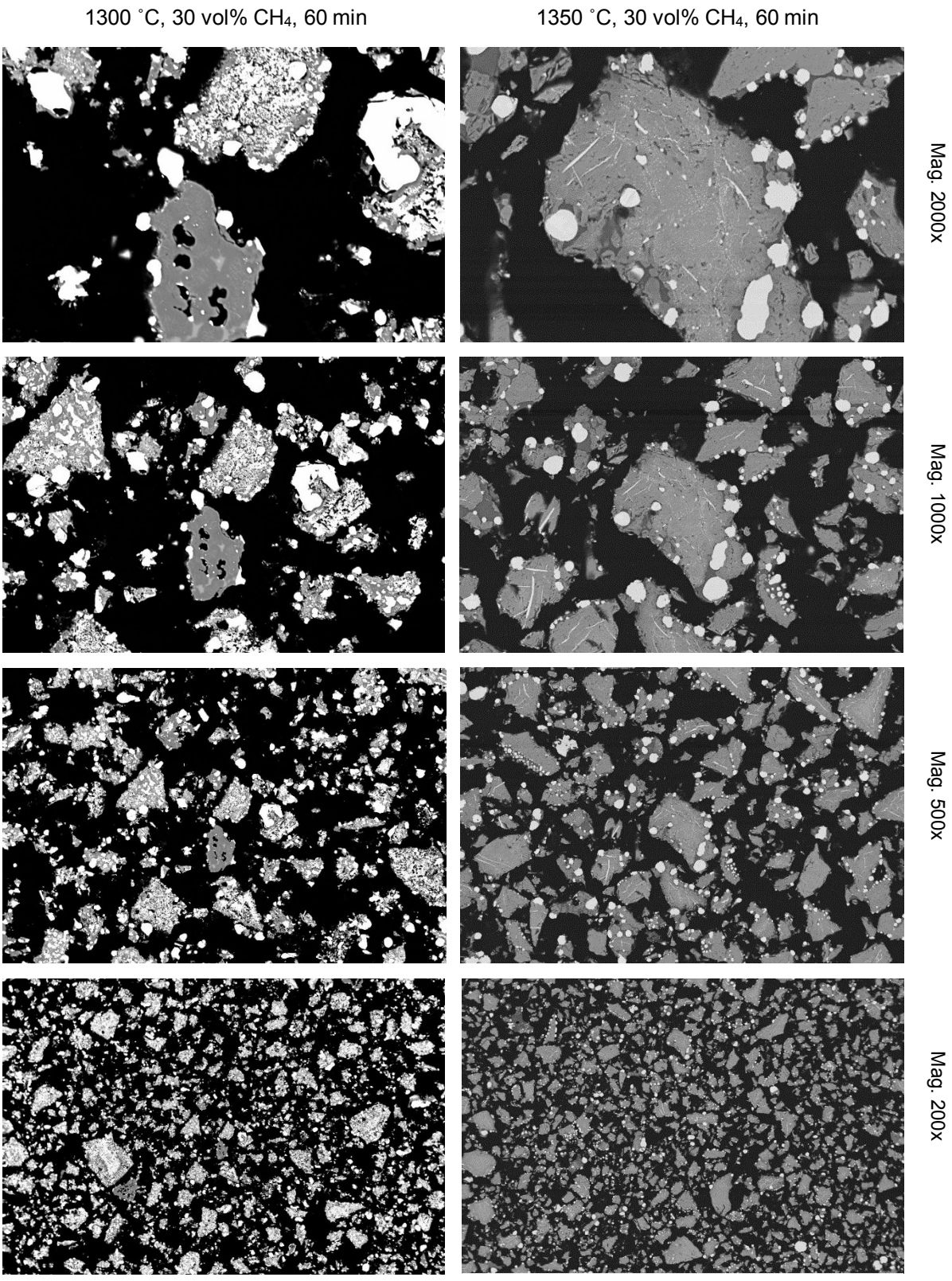

Appendix XXXV

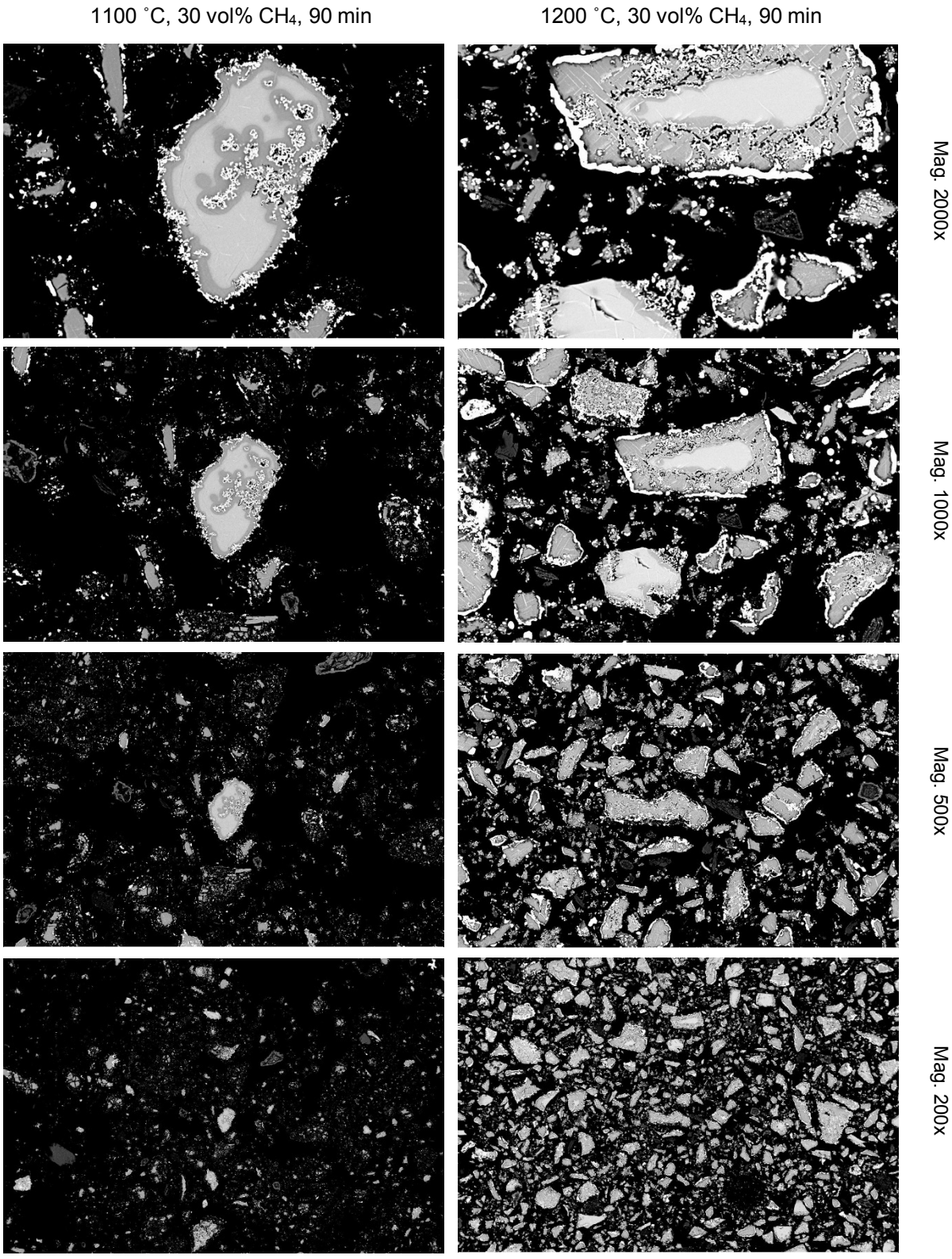

Appendix XXXVI

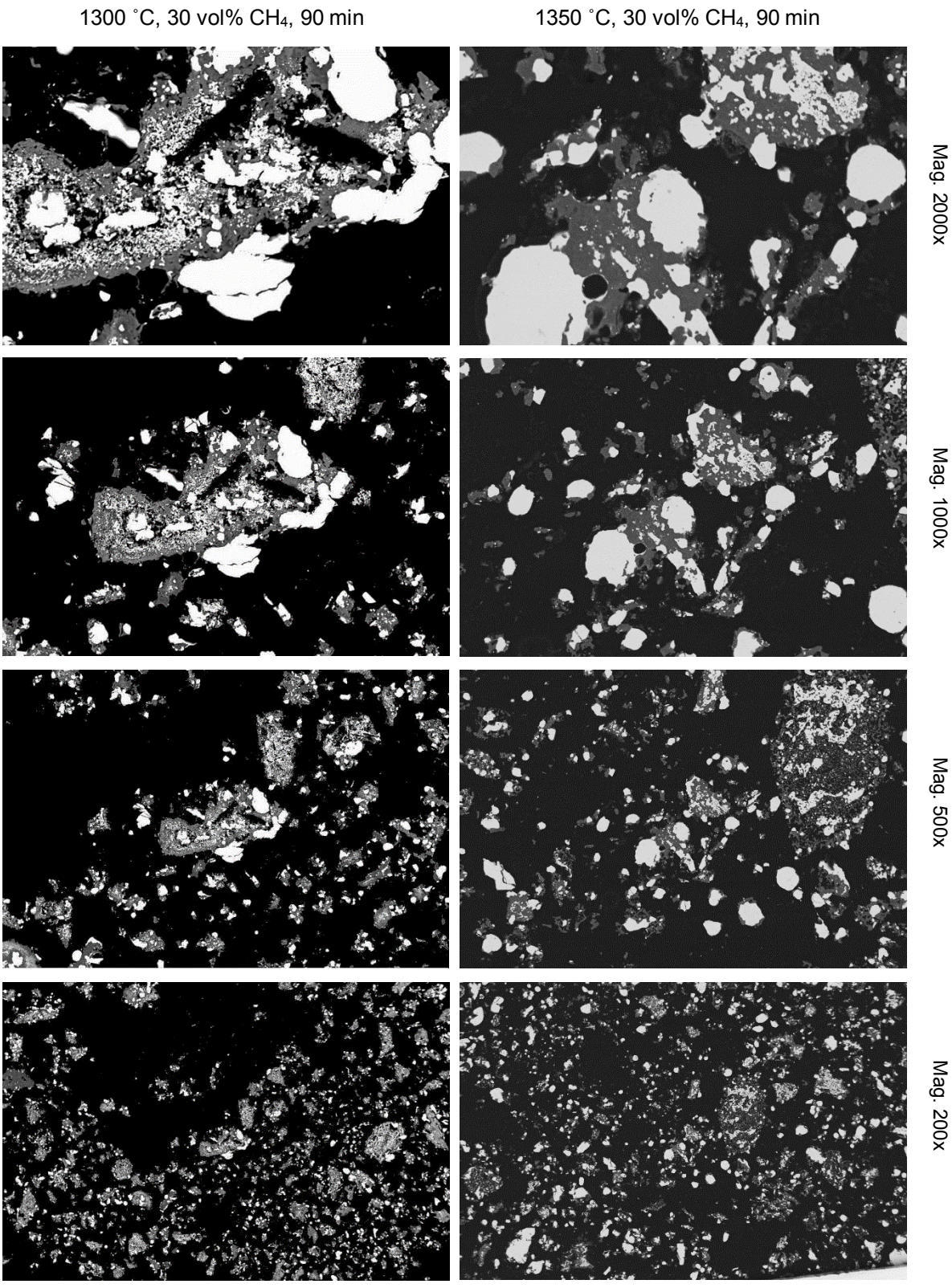

Appendix XXXVII

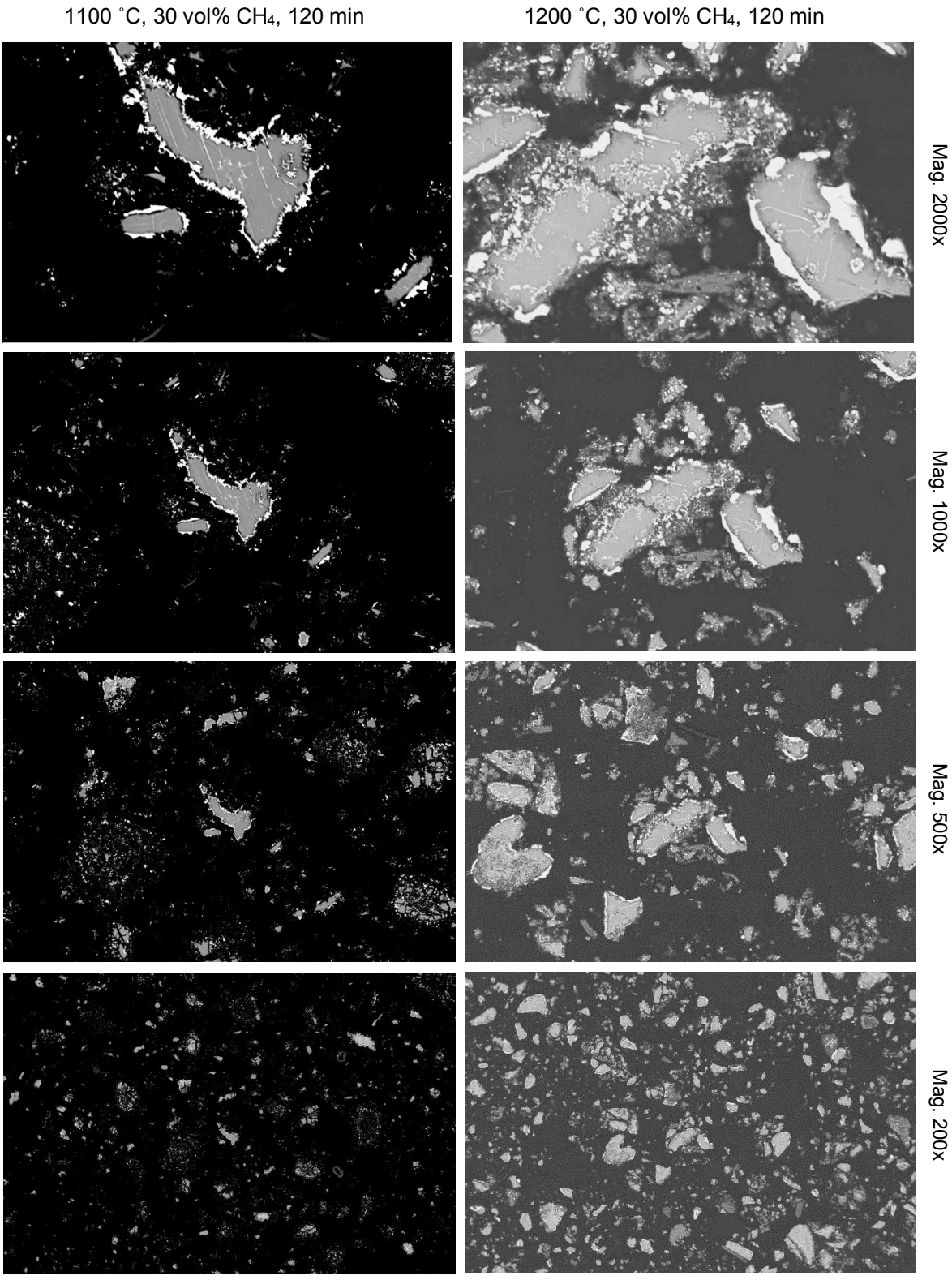

Appendix XXXVIII

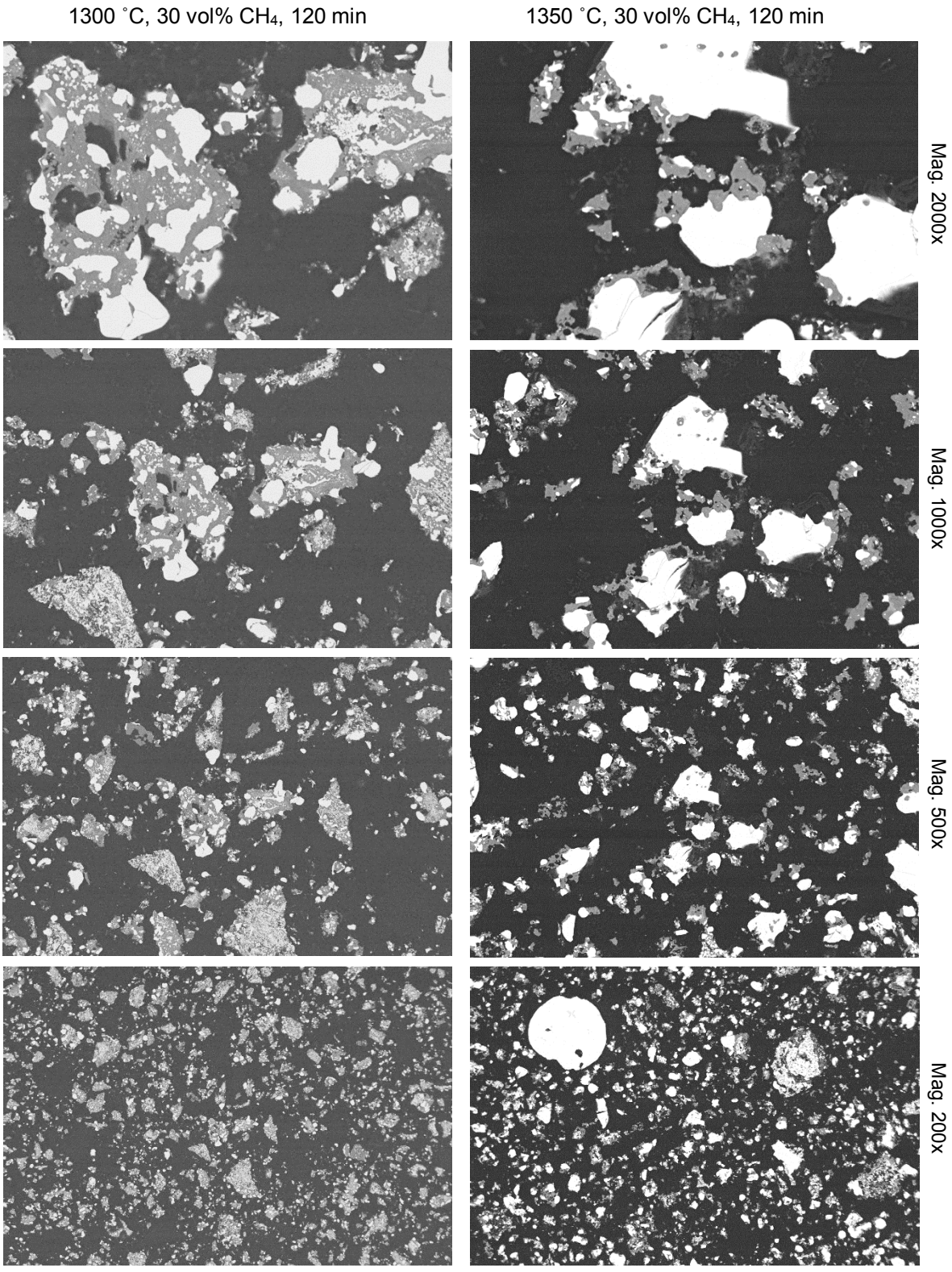

Appendix XXXIX

1300 ˚C, 99,9995 vol% C, 120 min

1300 ˚C, 99,99 vol% H_2, 120 min

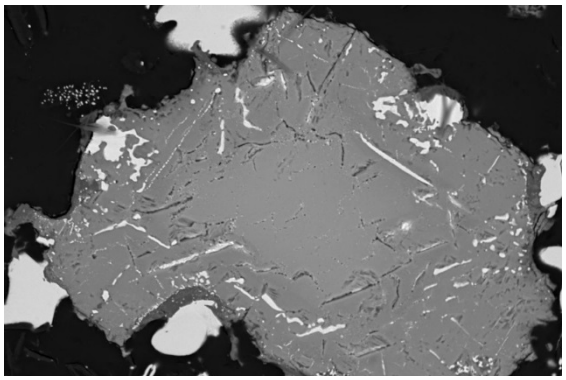

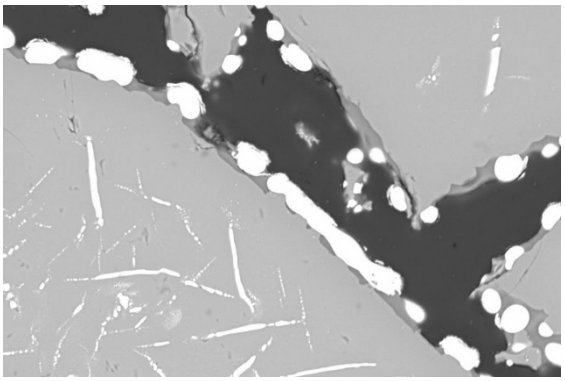

Mag. 2000x

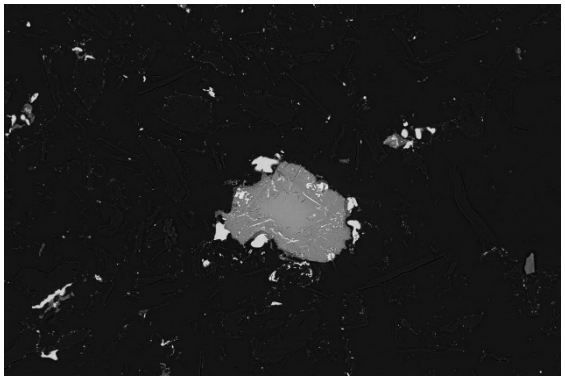

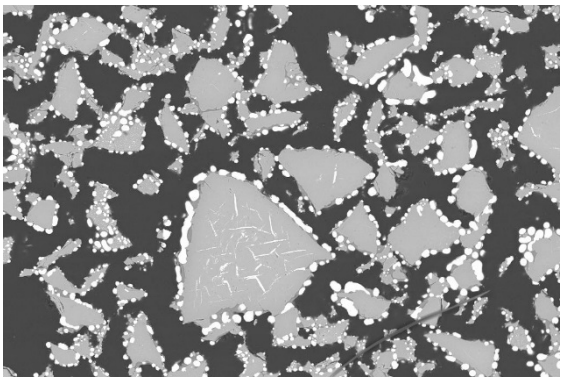

Mag. 500x

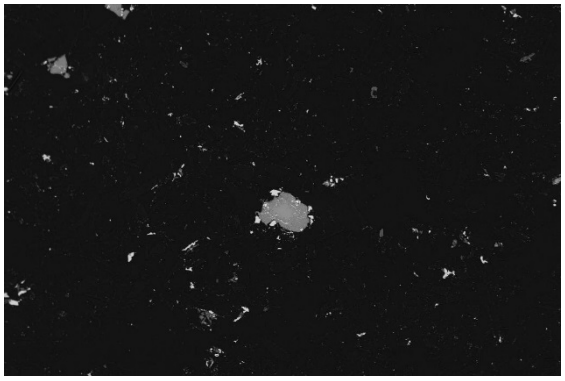

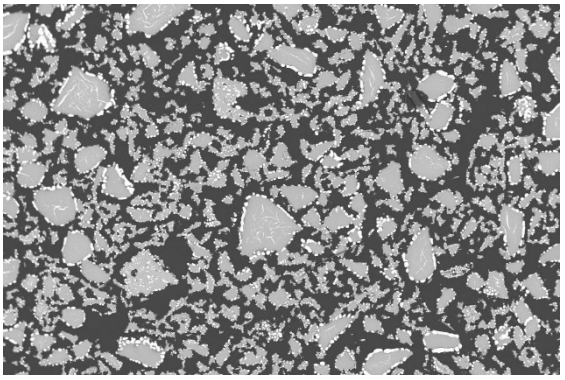

Mag. 200x

Appendix XL

Raw material, Kemi chromite

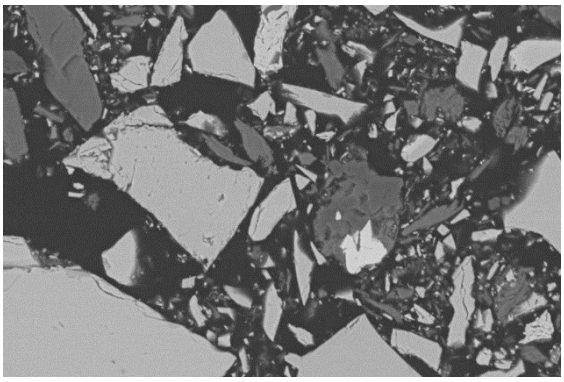

Mag. 200x

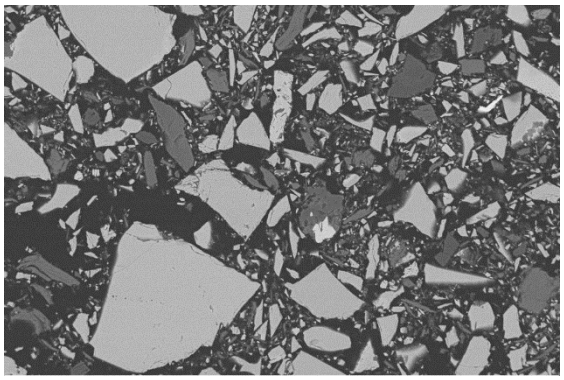

Mag. 500x

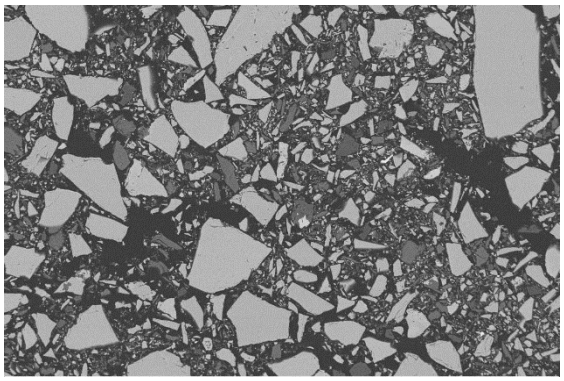

Mag. 1000x

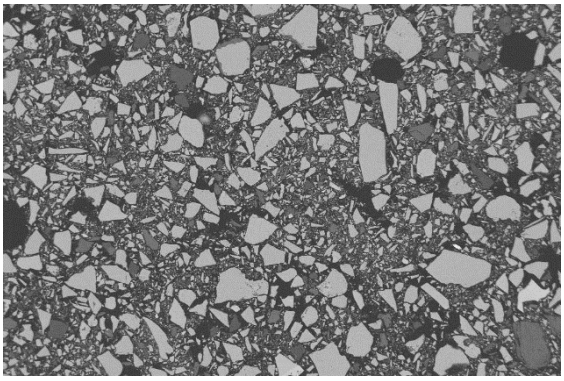

Mag. 2000x

Appendix XLI

1100 ˚C, 10 vol% CH_4, 10 min

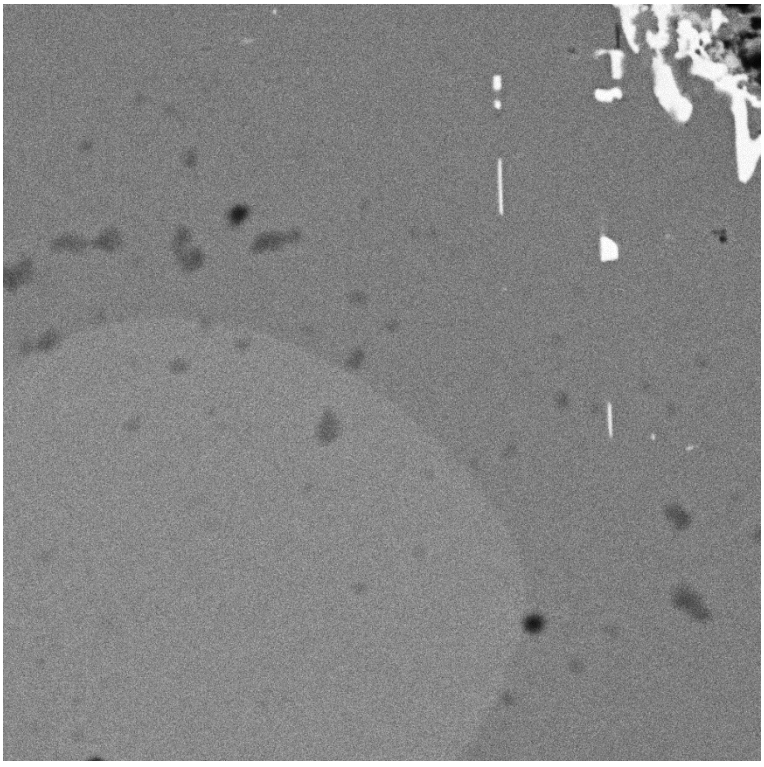

Mag. 10 000x

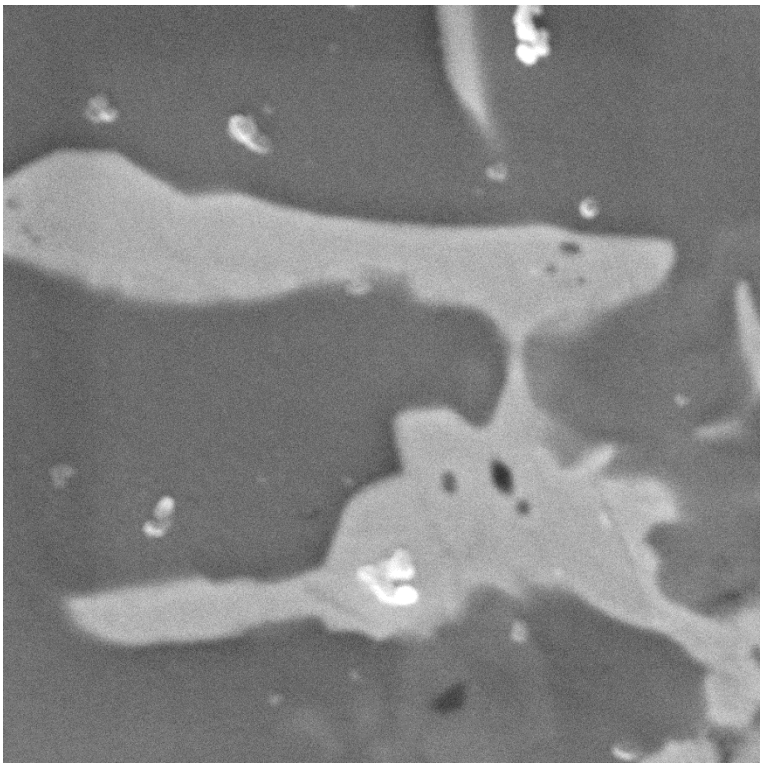

Mag. 36 000x

Appendix XLII

1100 ˚C, 30 vol% CH_4, 120 min

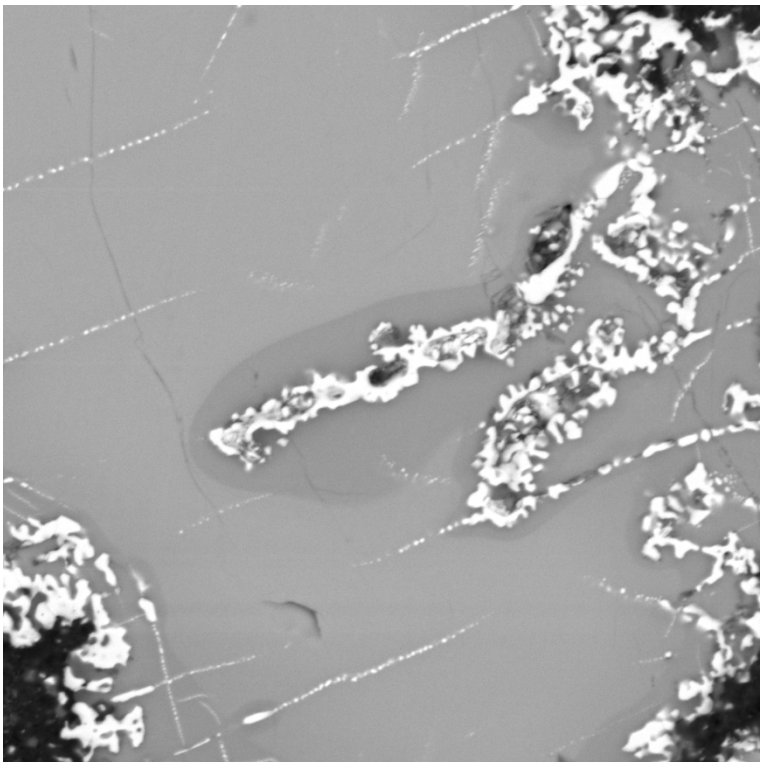

Mag. 10 000x

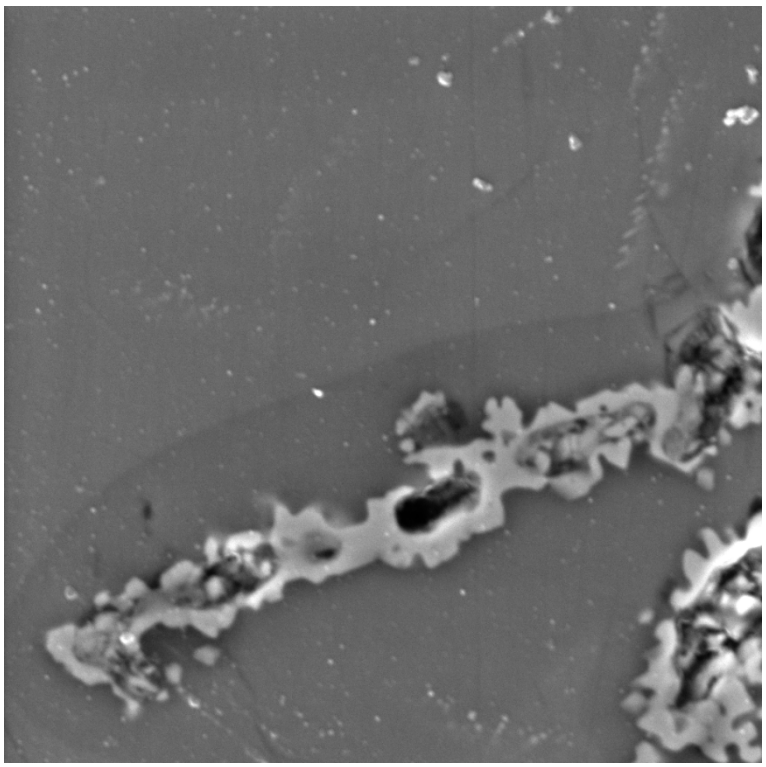

Mag. 22 000x

Appendix XLIII

1350 ˚C, 10 vol% CH_4, 10 min

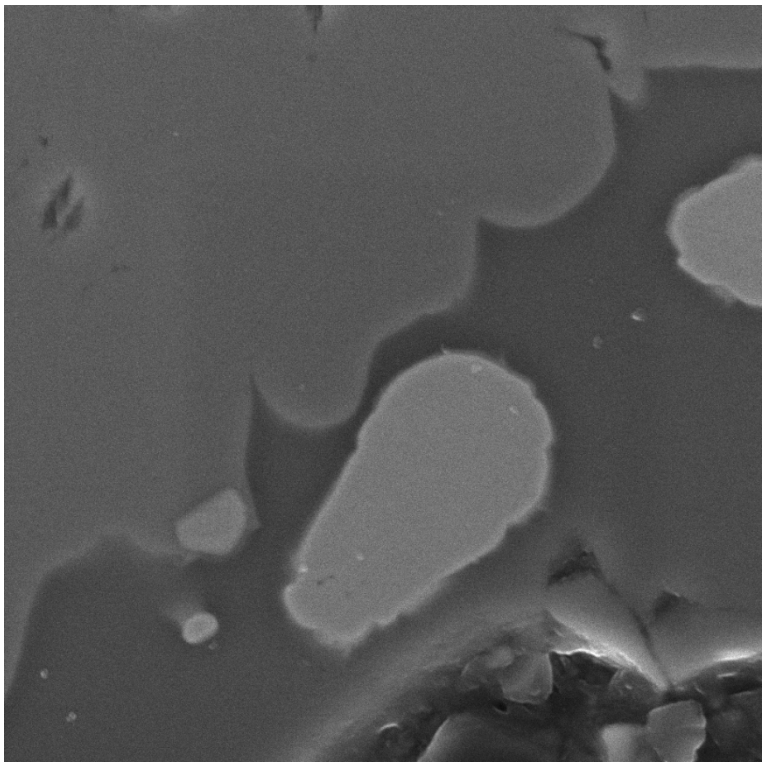

Mag. 20 000x

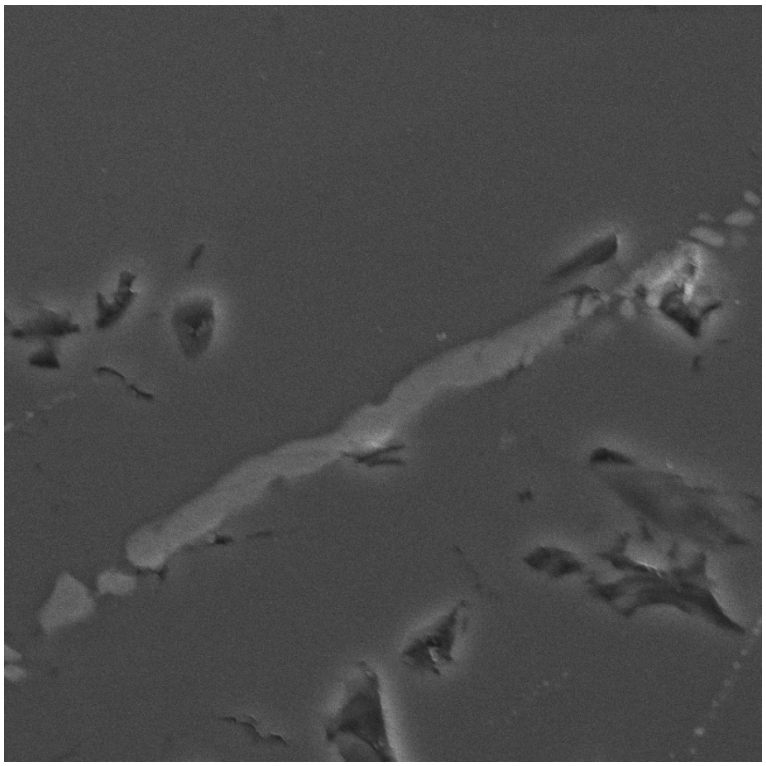

Mag. 20 000x

Appendix XLIV

1350 ˚C, 30 vol% CH_4, 120 min

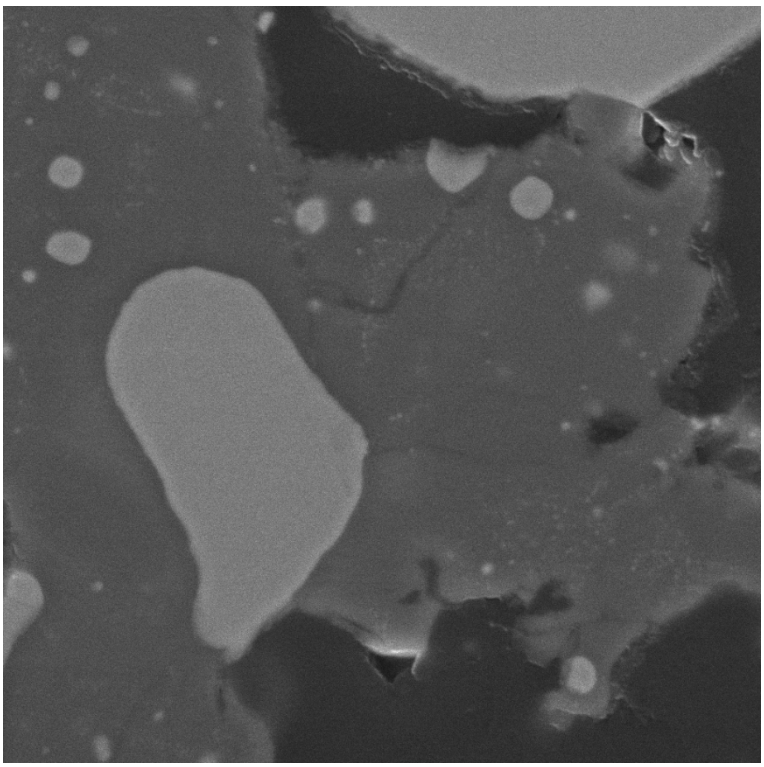

Mag. 20 000x

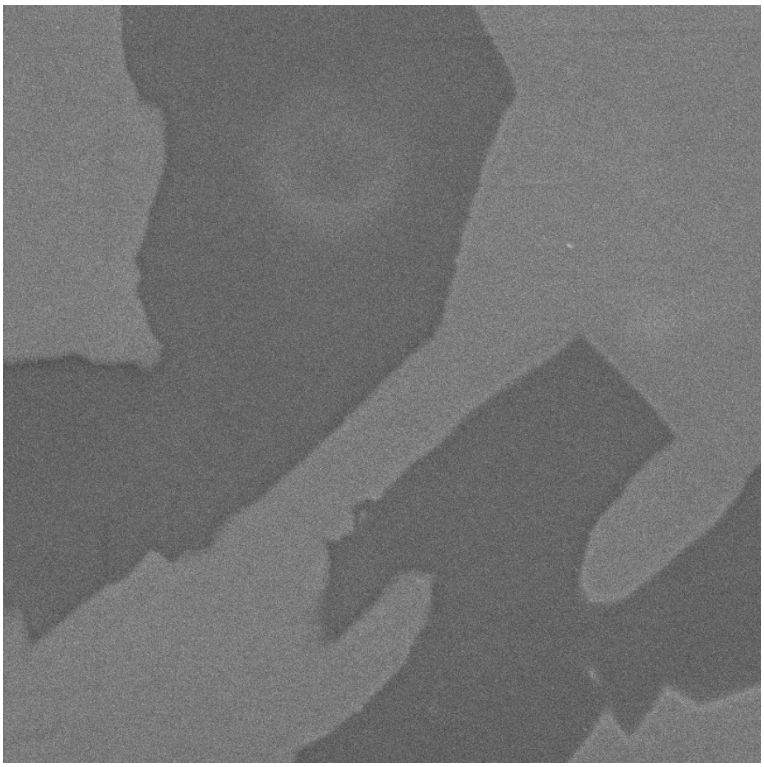

Mag. 20 000x

Appendices – SEM micrographs and SEM-EDS [wt%], C wt% not visible

Appendix XLV

1100 ˚C, 10 vol% CH_4, 10 min

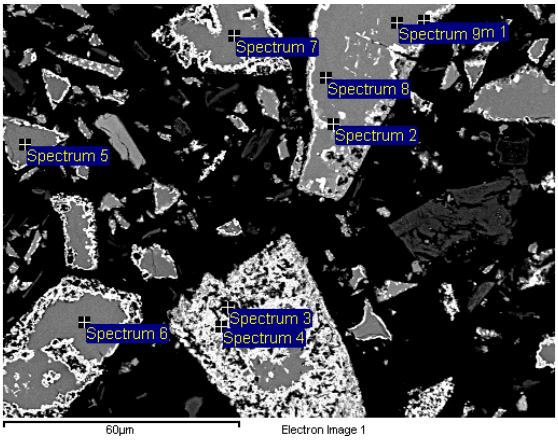

Spec.	O	Mg	Al	Ti	Cr	Fe	Total
1	2.74		0.95		13.84	78.87	**96.40**
2	2.88	0.16	0.70		16.73	77.78	**98.24**
3	7.76		8.11	0.37	27.79	49.79	**93.82**
4	6.28	0.27	6.49	0.19	38.69	38.89	**90.81**
5	34.95	12.58	9.59	0.32	40.14	2.42	**99.99**
6	34.69	12.11	9.36	0.30	40.04	2.74	**99.24**
7	34.74	12.19	9.03	0.20	41.27	2.23	**99.67**
8	34.91	10.52	9.27	0.29	41.99	2.80	**99.78**
9	33.40	10.42	8.99	0.31	42.69	2.71	**98.52**

1100 ˚C, 10 vol% CH_4, 20 min, site 1/2

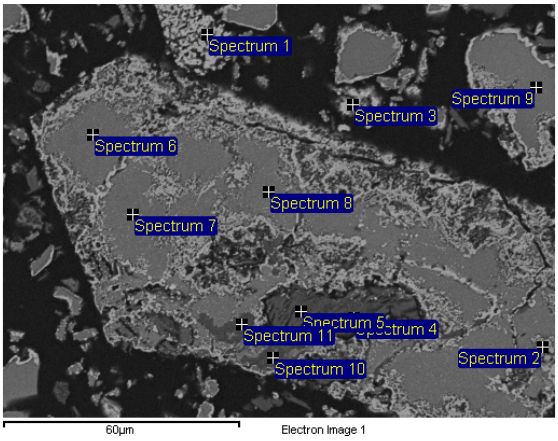

Spec.	O	Mg	Al	Si	Ti	Cr	Fe	Total
1	2.07		0.47		0.42	31.79	50.03	**84.77**
2	5.65	1.16	7.62		0.23	37.80	24.18	**76.62**
3	4.80	0.43	0.62			9.86	56.81	**72.51**
4	30.71	20.20	5.80	15.00		7.17	2.25	**81.13**
5	34.39	23.14	5.89	15.19		4.85	1.16	**84.62**
6	29.29	11.79	8.86		0.56	38.51	4.57	**93.57**
7	31.24	11.88	9.02		0.62	38.48	3.26	**94.51**
8	30.33	11.92	8.13		0.41	39.18	4.07	**94.05**
9	29.62	10.72	5.30			44.58	2.21	**92.44**
10	20.75	9.59	4.97	10.29	0.32	27.21	27.21	**100.35**
11	15.52	7.11	8.78	0.46	0.43	34.30	12.09	**78.70**

Appendix XLVI

1100 ˚C, 10 vol% CH_4, 20 min, site 2/2

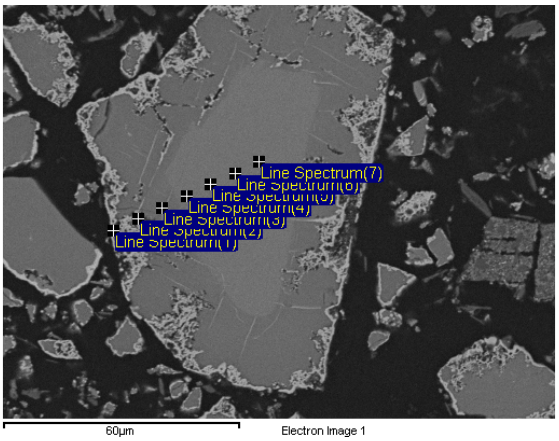

Spec.	O	Mg	Al	Si	Ti	Cr	Fe	Total
1	9.07	0.64	8.47			32.11	36.90	**87.19**
2	9.09	2.73	4.82	0.17		40.55	27.39	**84.76**
3	32.18	11.36	8.00		0.30	40.80	3.52	**96.17**
4	29.71	6.80	7.46		0.33	34.51	16.84	**95.65**
5	29.59	6.84	7.49		0.29	34.57	16.92	**95.71**
6	29.22	6.62	7.44		0.33	34.25	16.77	**94.63**
7	29.20	6.50	7.35		0.27	33.91	16.75	**93.98**

1100 ˚C, 10 vol% CH_4, 30 min

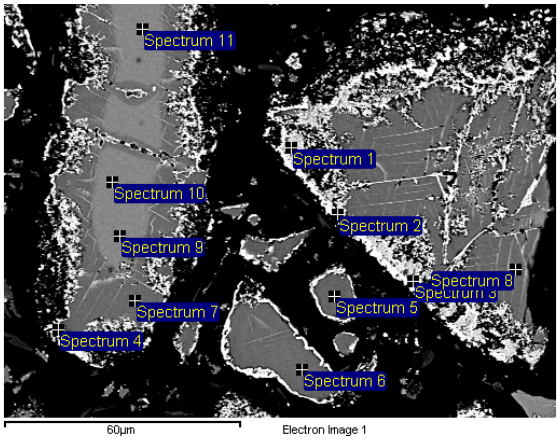

Spec.	O	Mg	Al	Si	Ti	Cr	Fe	Total
1	5.97	0.17	6.59	0.13	0.38	33.83	39.30	**86.37**
2	0.60					30.09	52.56	**83.25**
3	11.65	0.51	9.31	2.70	0.57	25.13	35.79	**85.66**
4	0.83	0.18	0.27			40.81	44.01	**86.11**
5	33.51	12.18	9.04		0.33	38.06	2.58	**95.70**
6	33.96	11.57	8.82		0.32	39.10	2.76	**96.53**
7	34.10	12.31	8.03		0.28	41.09	1.79	**97.59**
8	32.61	11.93	8.24		0.35	39.13	1.39	**93.65**
9	31.59	6.41	7.42		0.25	34.52	17.21	**97.39**
10	31.40	6.37	7.42		0.27	34.23	17.11	**96.80**
11	30.56	6.30	7.25		0.20	34.26	16.89	**95.44**

Appendix XLVII

1100 ˚C, 10 vol% CH_4, 60 min

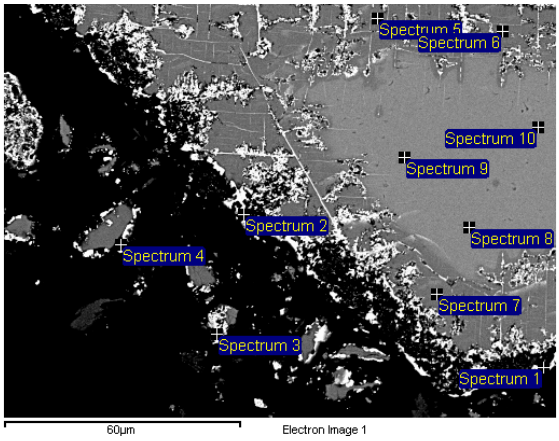

Spec.	O	Mg	Al	Si	Ti	Cr	Fe	Total
1	0.53		0.31			41.13	41.76	**83.73**
2	1.48	0.24	1.91			36.65	39.53	**79.82**
3	6.83	2.43	8.28	0.12	0.22	33.27	32.76	**83.91**
4	0.46			0.89	0.15	44.67	40.81	**86.97**
5	31.18	13.28	8.07		0.30	40.91	2.31	**96.05**
6	30.01	12.80	8.08		0.26	40.82	3.35	**95.32**
7	32.61	13.41	8.36		0.29	41.58	1.28	**97.53**
8	29.86	7.47	7.67		0.25	35.20	15.02	**95.47**
9	29.76	7.46	7.75		0.21	35.18	15.00	**95.36**
10	29.29	7.48	7.63		0.27	34.98	15.57	**95.22**

1100 ˚C, 10 vol% CH_4, 90 min

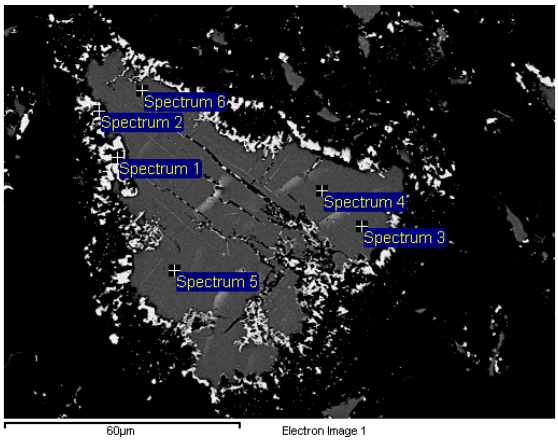

Spec.	O	Mg	Al	Si	Ti	Cr	Fe	Total
1	0.59			2.12		34.90	50.16	**87.77**
2	4.17	1.73	1.85	1.33	0.28	38.27	38.92	**86.55**
3	31.08	12.44	8.57		0.30	39.43	1.28	**93.10**
4	30.51	12.25	8.33		0.36	39.51	1.08	**92.03**
5	34.38	13.22	8.79		0.29	40.27	1.53	**98.49**
6	28.76	11.58	8.84	0.52	0.60	37.16	1.31	**88.77**

Appendix XLIVIII

1100 ˚C, 10 vol% CH_4, 120 min, site 1/3

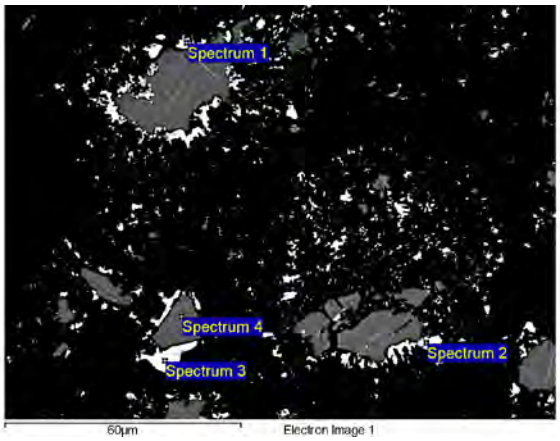

Spec.	O	Mg	Al	Si	Ti	Cr	Fe	Total
1	0.53		0.13	0.90		38.82	44.17	**84.55**
2		0.12	0.26			40.24	36.11	**76.73**
3	0.71			14.27		7.39	73.47	**95.84**
4	36.10	13.52	9.59		0.25	40.80	1.74	**102.01**

1100 ˚C, 10 vol% CH_4, 120 min, site 2/3

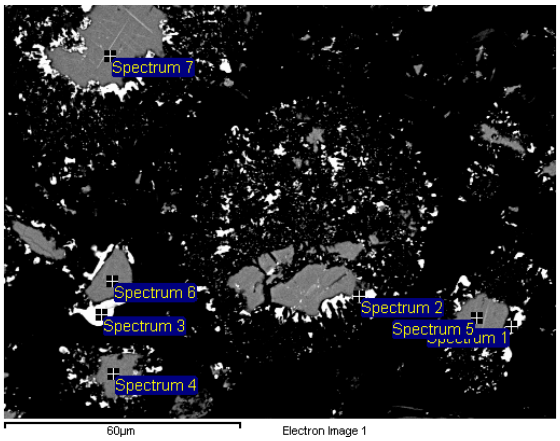

Spec.	O	Mg	Al	Si	Ti	Cr	Fe	Total
1				0.75		42.41	40.02	**83.18**
2			0.14		0.14	40.43	36.48	**77.18**
3	0.78			14.09		7.69	73.89	**96.45**
4	36.15	13.17	10.13		0.13	38.98	1.11	**99.66**
5	34.49	13.13	8.73		0.34	39.69	2.10	**98.49**
6	36.29	13.86	10.03	0.05	0.33	39.09	1.53	**101.17**
7	35.73	13.52	10.39		0.36	38.21	1.16	**99.38**

Appendix XLIX

1100 ˚C, 10 vol% CH_4, 120 min, site 3/3

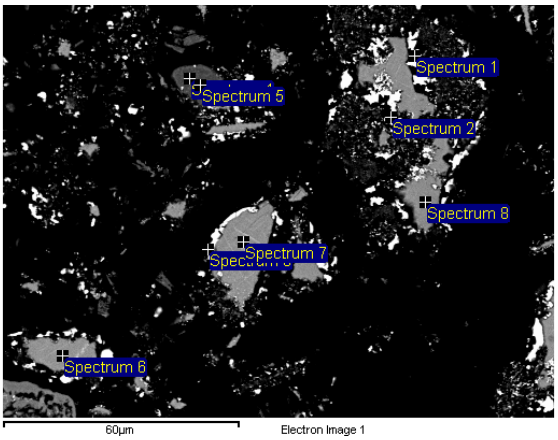

Spec.	O	Mg	Al	Si	Ca	Ti	Cr	Fe	Total
1	0.36					0.13	43.91	39.13	**83.53**
2	0.37						44.96	38.21	**83.54**
3	0.88	0.34	0.12	0.24			47.29	36.18	**85.05**
4	48.29	1.36	10.86	29.32	5.32		0.47	0.26	**95.89**
5	46.56	2.88	10.30	30.05	3.23		0.47	0.32	**93.81**
6	35.61	16.27	9.68	0.19	0.11	0.30	37.84	5.34	**105.36**
7	33.54	12.85	8.70			0.28	39.41	3.03	**97.81**
8	34.73	13.67	11.24	0.07		0.43	35.66	0.77	**96.55**

1100 ˚C, 20 vol% CH_4, 10 min

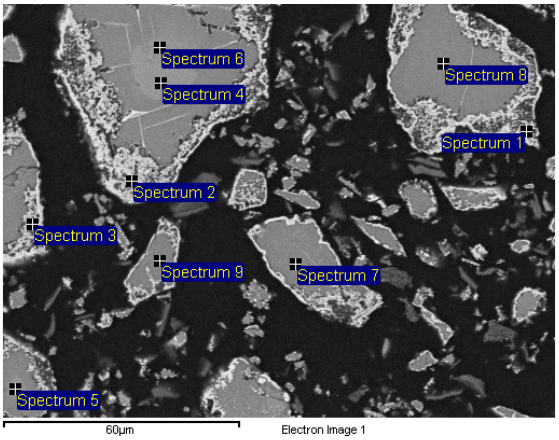

Spec.	O	Mg	Al	Si	Ti	Cr	Fe	Total
1	13.67	1.92	14.77	0.16	0.24	33.64	38.92	**103.33**
2	6.41	0.69	5.93	0.26		42.99	36.48	**92.77**
3	7.70	0.75	9.15		0.22	29.59	28.86	**76.26**
4	34.87	6.34	8.13		0.21	38.56	19.64	**107.76**
5	35.69	7.59	8.47		0.29	37.55	19.62	**109.20**
6	34.92	6.45	8.29		0.27	38.71	19.51	**108.16**
7	38.22	12.81	9.12	0.26	0.34	44.46	3.32	**108.52**
8	37.36	11.54	8.99		0.40	44.91	3.87	**107.06**
9	37.93	13.12	9.41		0.38	44.59	2.68	**108.11**

Appendix L

1100 ˚C, 20 vol% CH_4, 20 min, site 1/2

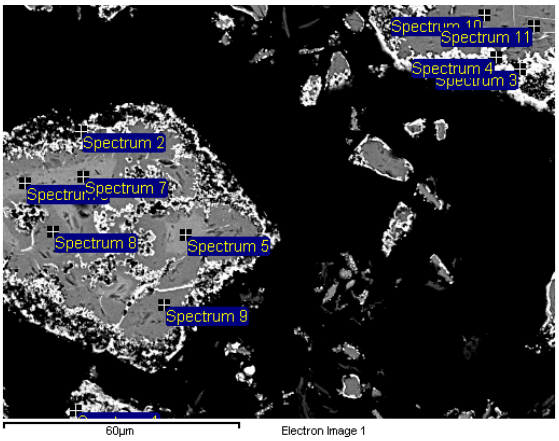

Spec.	O	Mg	Al	Si	Ti	Cr	Fe	Total
1	9.70	0.17	9.90	0.35	0.70	37.04	31.32	**89.19**
2	0.84		0.25	0.12		41.05	44.86	**87.12**
3	0.97		0.84			37.93	46.69	**86.43**
4	5.32	0.42	4.88			35.50	42.60	**88.72**
5	31.01	6.28	7.81		0.69	33.29	17.89	**96.96**
6	30.13	6.32	7.80		0.24	33.99	17.95	**96.43**
7	31.02	6.40	7.99		0.25	33.78	17.98	**97.41**
8	32.36	11.26	8.55		0.34	35.79	15.85	**104.14**
9	35.97	12.73	8.86		0.33	40.99	2.22	**101.09**
10	31.00	11.31	8.26	0.10	0.33	38.86	5.41	**95.26**
11	28.29	11.34	8.25		0.38	40.79	6.12	**95.18**

1100 ˚C, 20 vol% CH_4, 20 min, site 2/2

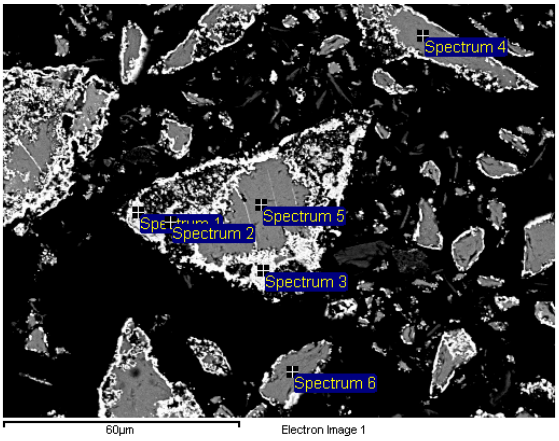

Spec.	O	Mg	Al	Si	Ti	Cr	Fe	Total
1	7.25		8.03	0.15	0.40	34.45	37.88	**88.16**
2	8.84		9.41	0.12	0.52	37.55	34.21	**90.65**
3	8.20	0.22	8.24	0.20	0.73	34.32	38.26	**90.17**
4	35.93	12.58	9.29		0.41	39.79	2.35	**100.34**
5	33.34	11.28	8.58		0.42	40.60	2.76	**96.97**
6	34.42	12.48	9.31		0.34	39.58	2.19	**98.31**

Appendix LI

1100 ˚C, 20 vol% CH_4, 30 min

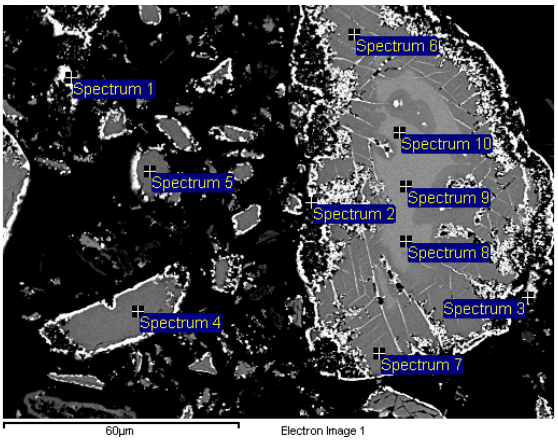

Spec.	O	Mg	Al	Si	Ti	Cr	Fe	Total
1	0.40		0.19			40.09	45.10	**85.79**
2	2.35	0.96	2.26	0.16		34.51	39.25	**79.49**
3	2.42	0.98	2.15	0.47	0.19	36.00	34.03	**76.24**
4	33.20	12.00	9.06		0.28	39.53	2.61	**96.66**
5	34.05	12.60	9.98		0.38	38.05	1.46	**96.52**
6	32.65	12.10	7.61		0.29	41.20	1.83	**95.68**
7	33.95	12.49	7.79		0.27	41.25	1.49	**97.25**
8	30.27	6.34	7.08		0.19	34.75	16.95	**95.59**
9	30.45	6.18	7.08		0.24	34.83	16.99	**95.77**
10	30.51	6.62	7.11		0.22	35.17	15.88	**95.51**

1100 ˚C, 20 vol% CH_4, 60 min

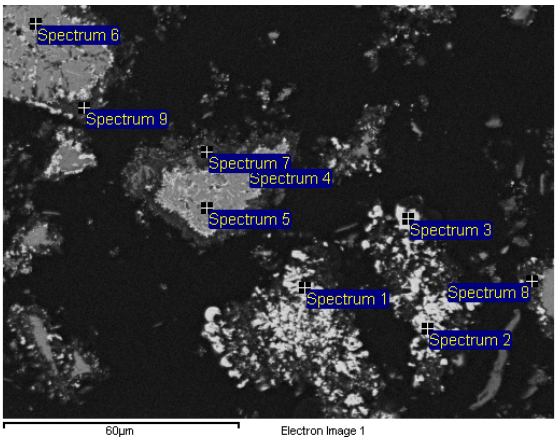

Spec.	O	Mg	Al	Si	Ca	Ti	Cr	Fe	Total
1	1.98	0.38	0.83	0.41		0.24	44.46	42.37	**90.67**
2							46.86	44.95	**91.80**
3							47.44	43.79	**91.23**
4	28.20	13.30	7.63		0.22	0.31	40.24	9.84	**99.73**
5	31.53	13.70	8.54			0.28	38.87	7.46	**100.39**
6	25.84	10.42	10.01			0.37	39.61	13.54	**99.80**
7	0.99	0.71	0.89	0.96			3.07	8.01	**14.63**
8	1.70	2.35	6.73	0.38			4.34	3.85	**19.35**
9	2.72	2.41	6.54	0.19			4.89	3.95	**20.71**

Appendix LII

1100 ˚C, 20 vol% CH_4, 90 min

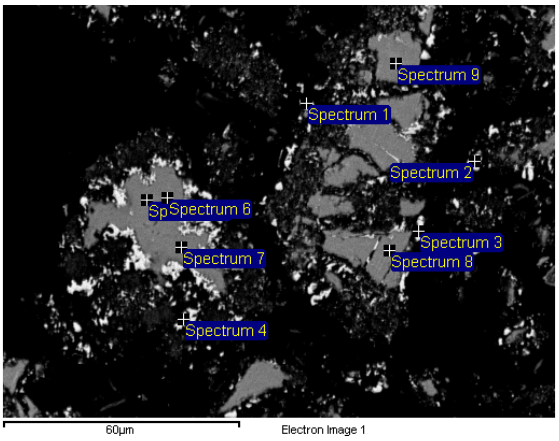

Spec.	O	Mg	Al	Si	Ca	Ti	Cr	Fe	Total
1				13.86			8.18	74.02	**96.06**
2	0.57			11.03			17.99	65.77	**95.36**
3							46.52	38.40	**84.92**
4	1.31		0.43	0.31	0.17		39.68	39.80	**81.69**
5	32.26	12.60	8.79			0.39	39.69	2.24	**95.98**
6	32.22	12.53	8.62			0.36	40.63	1.48	**95.85**
7	33.06	12.71	9.08			0.42	39.89	1.29	**96.46**
8	32.58	12.75	9.10			0.37	39.33	1.45	**95.59**
9	32.64	12.72	8.40			0.36	40.36	1.89	**96.36**

1100 ˚C, 20 vol% CH_4, 120 min, site 1/2

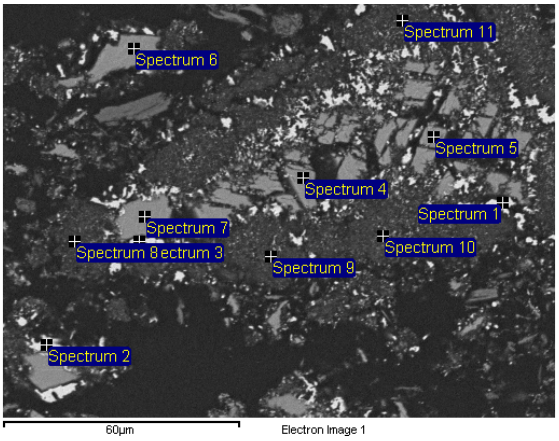

Spec.	O	Mg	Al	Si	Ca	Ti	Cr	Fe	Total
1							43.92	40.50	**84.42**
2	0.48						46.24	38.54	**85.27**
3	3.52	2.74	1.66	1.12	0.32	0.27	30.53	25.54	**65.69**
4	24.64	10.53	6.95			0.20	38.82	1.17	**82.30**
5	26.34	11.26	7.33			0.25	38.70	1.24	**85.12**
6	28.65	12.03	8.82			0.39	37.34	1.67	**88.92**
7	28.73	12.04	7.95			0.30	39.69	1.62	**90.33**
8	0.89	0.71	1.37	0.18			6.69	4.83	**14.67**
9	0.75	0.59	1.28				4.75	5.06	**12.43**
10	1.06	0.99	3.16	0.56			5.72	10.44	**21.92**
11	1.87	1.09	2.89				7.54	6.86	**20.24**

Appendix LIII

1100 ˚C, 20 vol% CH_4, 120 min, site 2/2

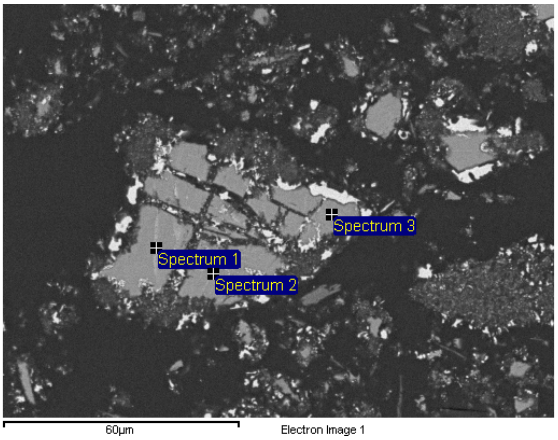

Spec.	O	Mg	Al	Si	Ti	Cr	Fe	Total
1	25.92	11.27	7.51	0.42	0.34	38.97	5.96	**90.38**
2	29.10	12.24	7.55		0.33	39.27	1.85	**90.34**
3	29.12	11.98	8.01		0.34	37.83	2.39	**89.67**

1100 ˚C, 30 vol% CH_4, 10 min

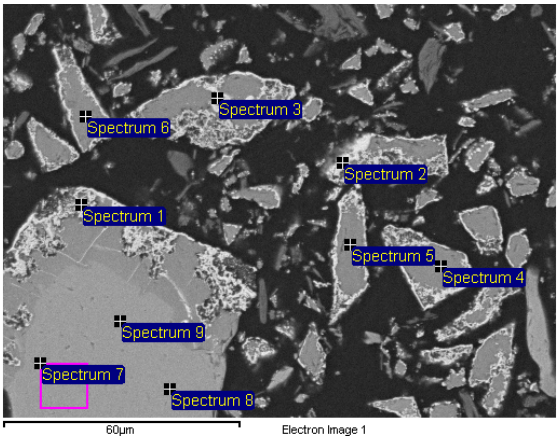

Spec.	O	Mg	Al	Ti	Cr	Fe	Total
1	5.84	1.14	6.26		38.50	41.59	**93.33**
2	0.79		0.43		42.52	47.95	**91.69**
3	4.19	0.29	4.37		33.45	36.48	**78.78**
4	32.60	11.66	9.00	0.55	42.63	3.49	**99.93**
5	33.71	12.32	10.42	0.49	41.18	2.65	**100.77**
6	33.89	12.82	8.51	0.38	44.11	2.24	**101.96**
7	31.65	7.01	8.07	0.28	37.54	18.02	**102.57**
8	31.54	7.01	8.18	0.27	37.48	18.01	**102.49**
9	31.43	7.06	8.07	0.36	37.18	18.14	**102.23**

Appendix LIV

1100 ˚C, 30 vol% CH_4, 20 min

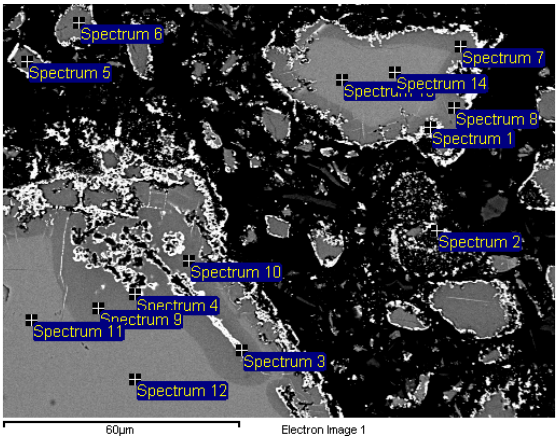

Spec.	O	Mg	Al	Si	Ti	Cr	Fe	Total
1	1.90	0.56	1.50			35.72	46.09	**85.77**
2	1.34	0.20	0.87	0.29	0.15	38.69	41.45	**83.00**
3	2.63	0.59	1.67			12.05	79.00	**95.95**
4	1.03		0.16			21.37	73.95	**96.51**
5	26.34	12.33	9.34		0.34	37.87	3.47	**89.70**
6	25.29	11.19	7.45		0.26	39.87	3.79	**87.85**
7	23.96	11.28	6.68		0.32	41.06	1.65	**84.95**
8	24.02	9.95	6.33		0.34	40.39	4.33	**85.34**
9	25.35	9.91	8.84		0.36	40.30	3.97	**88.73**
10	24.87	10.95	8.26		0.34	40.69	1.24	**86.35**
11	24.32	6.49	7.76		0.30	34.13	17.08	**90.07**
12	24.00	6.40	7.73		0.28	33.83	17.24	**89.49**
13	23.71	6.03	7.00		0.28	33.99	17.19	**88.19**
14	23.03	5.74	6.84		0.28	33.95	17.22	**87.06**

1100 ˚C, 30 vol% CH_4, 30 min

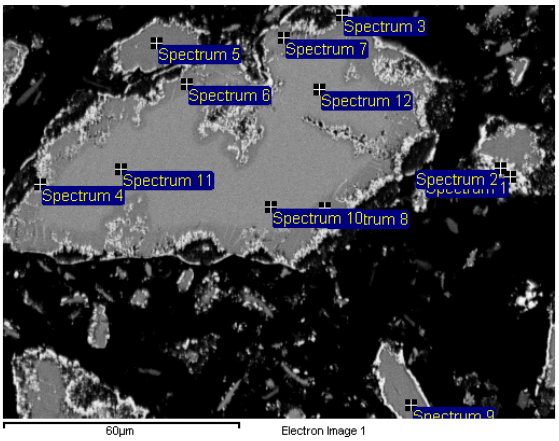

Spec.	O	Mg	Al	Si	Ti	Cr	Fe	Total
1	0.47		0.22			40.83	40.94	**82.46**
2	0.75		0.32	0.17		41.64	42.82	**85.70**
3	5.01	2.73	6.72			36.93	31.27	**82.67**
4	7.01	3.07	4.61		0.22	42.92	30.79	**88.63**
5	32.99	11.80	8.58		0.33	40.37	2.32	**96.39**
6	31.93	11.40	7.36		0.22	41.49	3.11	**95.50**
7	31.27	11.80	7.04		0.23	41.11	4.75	**96.20**
8	33.11	12.08	7.38		0.26	41.83	2.06	**96.73**
9	32.66	11.48	7.82		0.24	41.21	2.87	**96.28**
10	31.43	6.85	7.14		0.28	35.99	16.08	**97.77**
11	30.88	6.80	7.19			36.19	16.24	**97.30**
12	30.53	6.70	7.02		0.19	35.88	16.08	**96.42**

Appendix LV

1100 ˚C, 30 vol% CH_4, 60 min, site 1/2

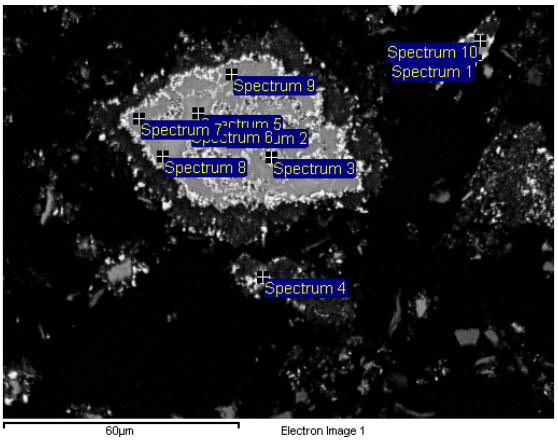

Spec.	O	Mg	Al	Si	Ca	Ti	Cr	Fe	Total
1	2.13	0.47	0.59	0.16			37.69	38.56	**79.60**
2	6.06	2.11	5.09			0.25	36.73	32.38	**82.61**
3	4.80	1.97	4.42				39.52	35.80	**86.51**
4	0.75	0.23	0.67	0.23			34.57	32.34	**68.79**
5	31.08	6.54	8.11		0.19	0.30	33.15	17.77	**97.15**
6	31.80	7.74	8.20			0.50	33.88	15.84	**97.95**
7	31.49	12.39	10.37	0.17		1.24	36.00	3.51	**95.18**
8	24.29	9.67	8.81	0.11		1.02	36.36	8.51	**88.76**
9	24.60	10.30	9.09	0.21		0.97	35.89	6.27	**87.32**
10	6.67	3.56	2.01	1.38	0.24		33.62	31.85	**79.33**

1100 ˚C, 30 vol% CH_4, 60 min, site 2/2

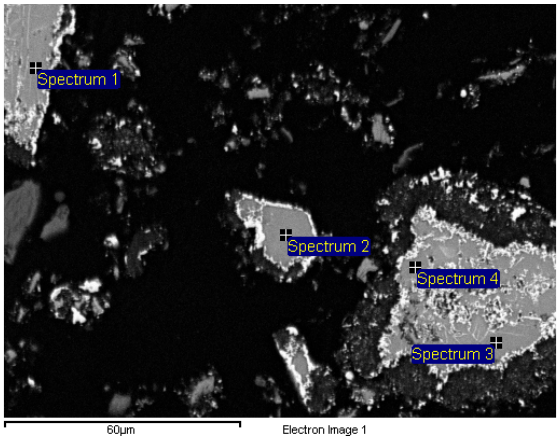

Spec.	O	Mg	Al	Ti	Cr	Fe	Total
1	33.31	11.96	7.99	0.30	41.79	2.83	**98.19**
2	33.40	12.09	8.86	0.29	40.33	2.36	**97.32**
3	33.98	12.71	8.78	0.48	40.26	1.36	**97.57**
4	33.95	12.74	8.32	0.36	40.94	1.04	**97.35**

Appendix LVI

1100 ˚C, 30 vol% CH_4, 90 min, site 1/2

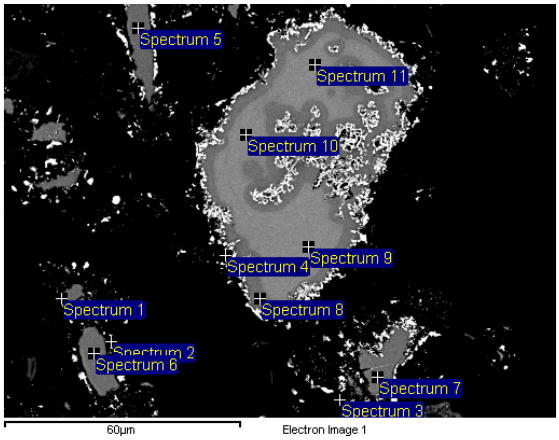

Spec.	O	Mg	Al	Si	Ti	Cr	Fe	Total
1	0.65		0.16			43.97	41.34	**86.12**
2	0.52			5.64		29.98	53.79	**89.93**
3	0.45	0.19	0.29			44.53	38.16	**83.62**
4	0.64		0.29			42.55	40.09	**83.57**
5	34.74	12.95	9.96	0.13	0.39	37.39	1.64	**97.21**
6	34.39	12.95	8.99		0.43	38.53	3.05	**98.35**
7	34.04	12.78	8.50		0.42	38.90	4.30	**98.94**
8	36.84	12.89	8.65		0.29	40.33	1.66	**100.68**
9	32.49	7.25	7.71		0.30	33.98	15.80	**97.54**
10	32.12	7.15	7.69		0.24	34.16	15.47	**96.85**
11	31.26	7.15	7.58		0.28	34.16	15.24	**95.67**

1100 ˚C, 30 vol% CH_4, 90 min, site 2/2

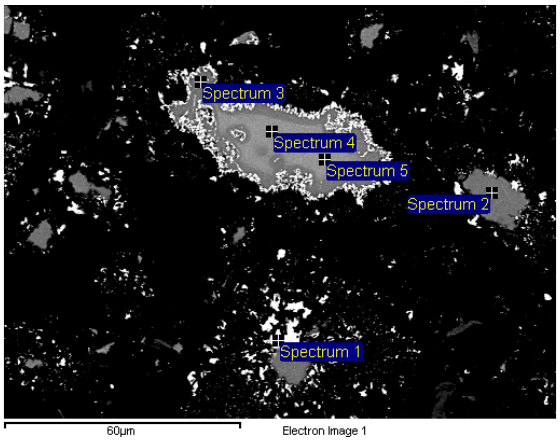

Spec.	O	Mg	Al	Ti	Cr	Fe	Total
1	0.36				44.71	40.11	**85.18**
2	33.00	12.53	8.47	0.38	38.81	3.17	**96.37**
3	33.76	12.33	8.23	0.37	40.03	1.37	**96.09**
4	30.95	6.03	7.00	0.23	34.57	17.10	**95.89**
5	31.25	5.91	7.04	0.25	34.61	17.23	**96.28**

Appendix LVII

1100 ˚C, 30 vol% CH_4, 120 min

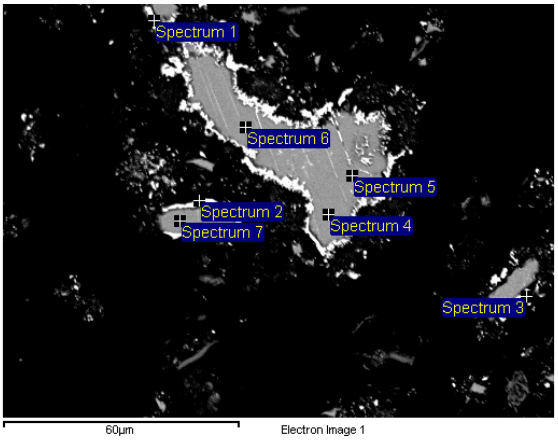

Spec.	O	Mg	Al	Si	Ti	Cr	Fe	Total
1	0.82	0.33	0.31	0.20		45.44	40.72	**87.82**
2	0.50					44.01	40.93	**85.45**
3	0.48		0.15	0.13		44.48	36.79	**82.04**
4	35.13	12.87	8.92		0.36	40.31	1.31	**98.91**
5	34.05	12.89	8.94	0.10	0.40	39.68	0.67	**96.74**
6	34.59	13.09	8.79		0.42	40.48	1.27	**98.64**
7	33.33	12.65	9.39		0.38	39.04	4.65	**99.44**

1200 ˚C, 10 vol% CH_4, 10 min, site 1/2

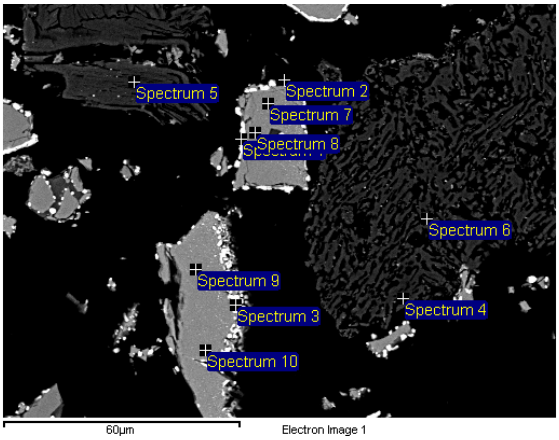

Spec.	O	Mg	Al	Si	Ca	Ti	Cr	Fe	Total
1	1.59		0.16				9.90	86.70	**98.35**
2	1.70			0.11			6.14	58.05	**66.00**
3	4.71	0.48	1.13	1.55	0.68	0.15	20.57	28.60	**57.88**
4	44.09	25.61		25.04			0.46	0.75	**95.95**
5	48.10	20.71		31.28			0.50	0.37	**100.96**
6	44.28	29.60		22.53	0.13		0.29	0.76	**97.59**
7	33.84	8.45	9.49			0.37	42.52	5.10	**99.77**
8	34.39	8.56	9.48			0.40	42.47	5.28	**100.57**
9	33.32	8.85	8.58			0.33	41.64	6.90	**99.62**
10	32.64	8.79	7.79			0.25	42.02	9.00	**100.48**

Appendix LVIII

1200 ˚C, 10 vol% CH_4, 10 min, site 2/2

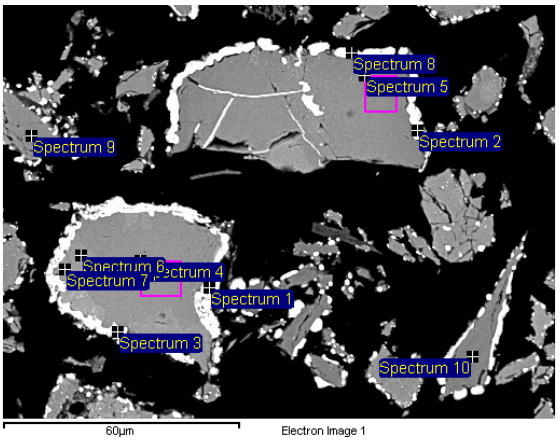

Spec.	O	Mg	Al	Si	Ca	Ti	Cr	Fe	Total
1	0.80			0.34			7.80	92.20	**101.14**
2	0.79		0.21				15.63	81.87	**98.50**
3							8.49	93.95	**102.44**
4	34.71	8.15	8.72			0.21	44.01	6.86	**102.67**
5	34.56	9.31	9.77			0.42	43.36	3.36	**100.79**
6	35.29		9.70			0.66	57.24	0.51	**103.41**
7	36.96		10.93			0.66	55.87	0.69	**105.11**
8	26.16	0.83	5.87	16.18	1.56	0.22	11.90	25.16	**87.88**
9	36.01	10.03	9.76			0.45	41.72	5.04	**103.01**
10	35.15	10.96	10.92			0.53	40.78	1.39	**99.73**

1200 ˚C, 10 vol% CH_4, 20 min

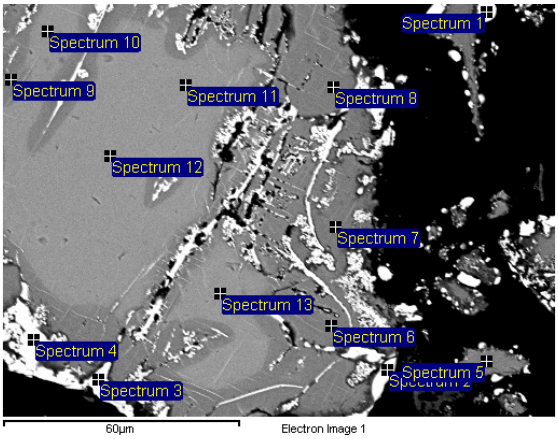

Spec.	O	Mg	Al	Si	Ca	Ti	Cr	Fe	Total
1	0.86			7.03			14.18	71.60	**93.67**
2	0.69						42.59	41.07	**84.35**
3	0.65						43.30	42.37	**86.32**
4	2.03	0.86	1.48	0.52			42.70	41.28	**88.86**
5	28.12	12.77	7.83	0.13	0.10	0.30	39.74	1.36	**90.35**
6	27.51	12.15	7.75			0.37	39.82	3.10	**90.69**
7	27.69	12.54	8.23			0.39	39.51	0.79	**89.15**
8	27.17	12.34	7.79	0.09		0.33	40.32	0.83	**88.86**
9	28.52	11.62	8.55			0.44	39.81	2.16	**91.08**
10	25.90	6.90	7.58			0.26	33.66	16.10	**90.39**
11	25.58	6.84	7.32			0.31	33.52	16.11	**89.69**
12	26.18	6.85	7.50			0.29	34.18	16.27	**91.26**
13	26.02	6.70	7.37			0.29	33.80	16.41	**90.59**

Appendix LIX

1200˚C, 10 vol% CH_4, 30 min, site 1/2

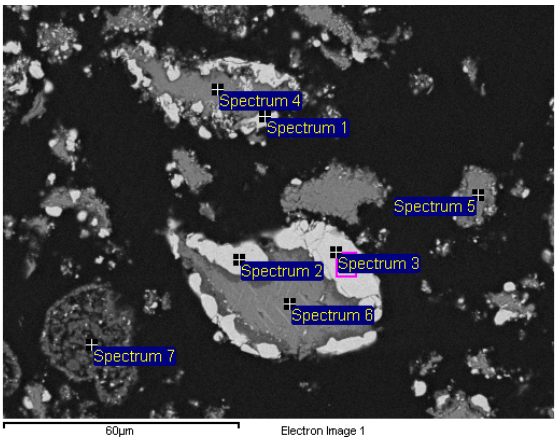

Spec.	O	Mg	Al	Si	Ca	Ti	Cr	Fe	Total
1	0.41						43.90	39.59	**83.91**
2				0.89			43.48	40.92	**85.28**
3				0.65			39.73	44.40	**84.77**
4	30.75	12.17	9.68			0.33	38.95	1.36	**93.22**
5	31.30	12.78	10.12			0.51	36.30	1.14	**92.16**
6	32.42	12.59	8.30			0.47	39.15	0.40	**93.33**
7	15.49	34.50	0.39	0.82	0.27		1.12	1.38	**53.97**

1200˚C, 10 vol% CH_4, 30 min, site 2/2

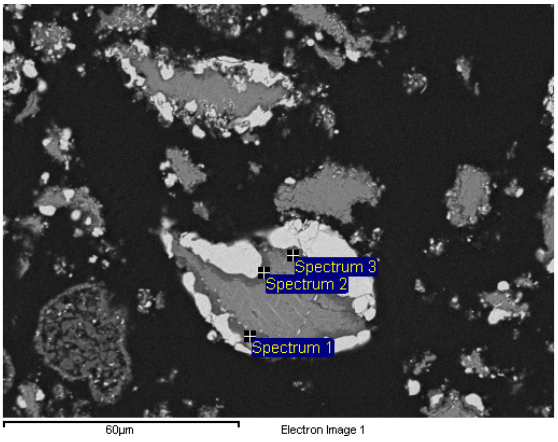

Spec.	O	Mg	Al	Si	Ca	Ti	Cr	Fe	Total
1	39.67	17.46	25.69	3.27	0.91	0.30	9.81	0.56	**97.66**
2	39.29	15.90	20.46	9.37	2.27	0.26	7.48	0.48	**95.51**
3	36.18	14.23	21.18	2.66	0.50	0.42	16.08	0.49	**91.74**

Appendix LX

1200˚C, 10 vol% CH_4, 60 min

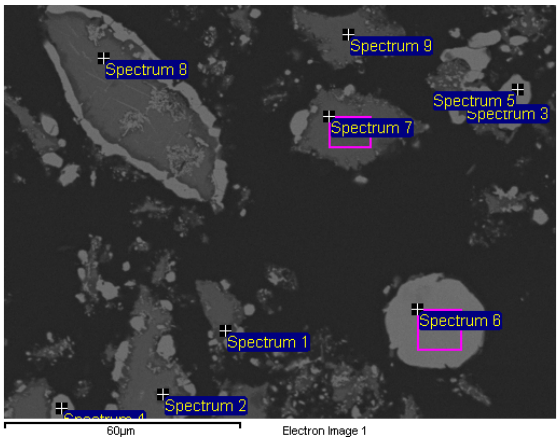

Spec.	O	Mg	Al	Si	Ca	Ti	Cr	Fe	Total
1	41.64	24.59	16.80	10.70	0.61	0.39	4.46	1.04	**100.24**
2	40.36	30.28	1.82	16.05	0.36		8.69	0.56	**98.13**
3	36.09	15.13	20.49	5.06	4.88	0.26	14.68	7.50	**104.09**
4	0.48						40.86	46.96	**88.30**
5	0.55						42.41	42.51	**85.46**
6	0.82			7.89			11.87	74.38	**94.96**
7	33.52	13.13	9.43			0.39	39.80	1.02	**97.29**
8	34.09	13.20	8.97			0.43	40.30	0.72	**97.70**
9	32.80	13.06	10.18		0.24	0.60	37.67	0.53	**95.09**

1200˚C, 10 vol% CH_4, 90 min, site 1/2

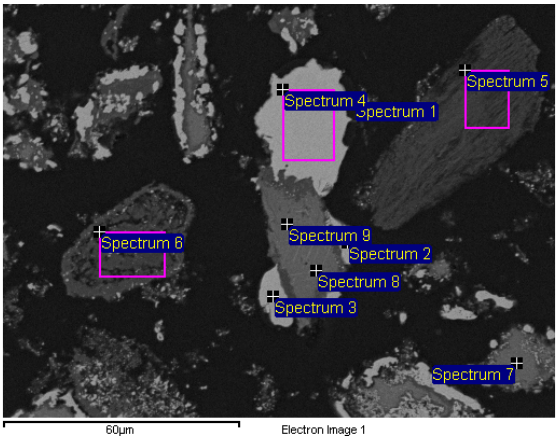

Spec.	O	Mg	Al	Si	Ca	Ti	Cr	Fe	Total
1	0.88	0.13	0.16	0.26			0.58	0.52	**2.52**
2	0.47						39.18	45.55	**85.20**
3							40.28	44.87	**85.15**
4				1.47			32.99	52.50	**86.96**
5	27.90	21.43		19.54	0.34		0.45	0.51	**70.16**
6	26.45	42.18		4.12			1.26	3.84	**77.85**
7	33.65	12.81	8.84			0.52	39.83	0.67	**96.32**
8	33.30	12.75	10.17			0.43	37.40	1.27	**95.31**
9	33.90	13.15	9.91			0.50	37.47	0.68	**95.60**

Appendix LXI

1200˚C, 10 vol% CH_4, 90 min, site 2/2

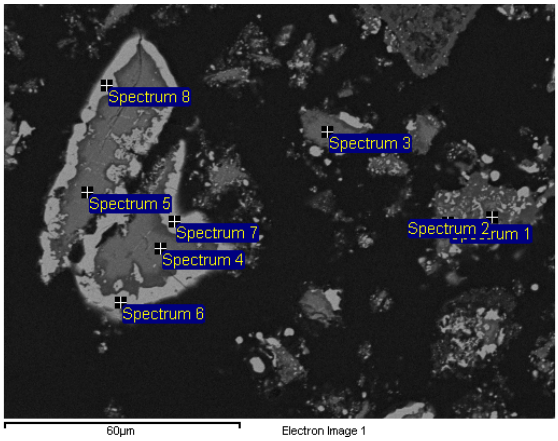

Spec.	O	Mg	Al	Si	Ca	Ti	Cr	Fe	Total
1	33.50	15.48	8.38	3.28	0.76	0.42	34.04	1.65	**97.52**
2	38.49	26.86	5.81	12.70	1.00	0.41	13.60	0.95	**99.80**
3	33.13	12.57	9.34			0.35	37.94	0.84	**94.17**
4	33.72	12.53	8.94			0.46	39.68	0.50	**95.82**
5	33.17	12.35	7.64			0.39	41.50	1.92	**96.97**
6							45.22	39.58	**84.80**
7							45.22	40.22	**85.44**
8							44.06	40.33	**84.40**

1200˚C, 10 vol% CH_4, 120 min, site 1/2

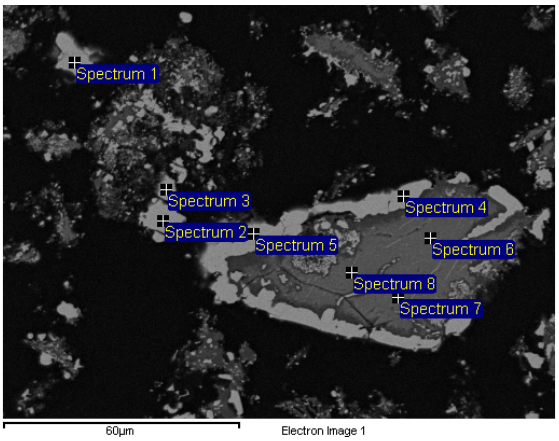

Spec.	O	Mg	Al	Si	Ca	Ti	Cr	Fe	Total
1				0.38	0.40		48.28	36.28	**85.34**
2	0.60						46.72	40.06	**87.37**
3							47.62	39.42	**87.03**
4							44.32	41.45	**85.77**
5							45.52	40.99	**86.50**
6	32.83	12.28	8.08			0.36	40.88	2.07	**96.48**
7	33.45	12.37	8.02			0.41	42.28	1.54	**98.07**
8	34.21	12.54	8.30			0.45	41.48	1.35	**98.33**

1200˚C, 10 vol% CH_4, 120 min, site 2/2

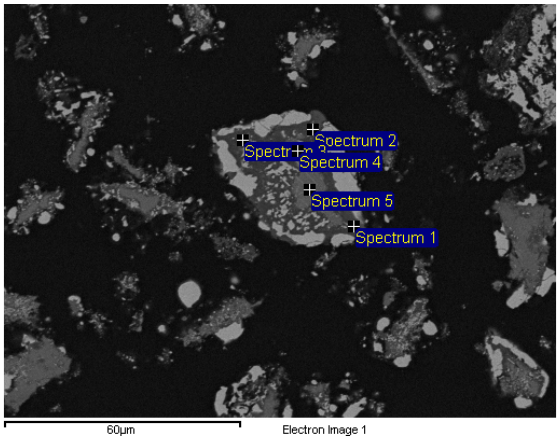

Spec.	O	Mg	Al	Si	Ca	Ti	Cr	Fe	Total
1	42.86	20.83	20.46	8.34	1.93		1.82	0.99	**97.23**
2	45.39	10.94	20.96	10.26	6.94	0.19	2.64	1.06	**98.38**
3	33.35	13.64	19.84	5.72	2.48	0.28	15.54	11.71	**102.56**
4	32.59	12.82	9.22	0.36		0.52	38.02	0.70	**94.23**
5	32.95	12.65	8.72			0.50	39.63	0.83	**95.27**

1200 ˚C, 20 vol% CH_4, 10 min, site 1/2

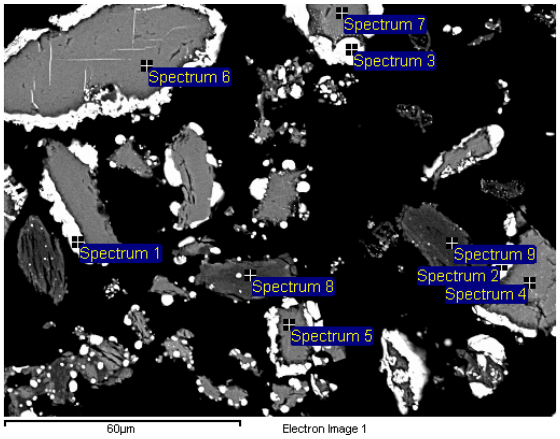

Spec.	O	Mg	Al	Si	Ca	Ti	Cr	Fe	Total
1	0.86		0.16	1.21			28.19	70.49	**100.91**
2	0.57			0.12			43.47	46.43	**90.59**
3	0.40			0.69			38.73	57.04	**96.86**
4	33.70	12.57	8.61	0.12		0.42	42.26	2.18	**99.85**
5	36.56	13.45	10.53	0.11		0.34	40.87	0.60	**102.46**
6	35.79	12.67	9.52	0.11		0.38	42.49	1.10	**102.07**
7	35.51	12.38	9.37	0.14		0.39	42.52	1.27	**101.58**
8	50.62	3.55	22.49	19.63	7.03	0.22	0.57	0.32	**104.42**
9	46.25	20.74	1.12	28.31	0.81		3.58	0.42	**101.22**

Appendix LXIII

1200 ˚C, 20 vol% CH_4, 10 min, site 2/2

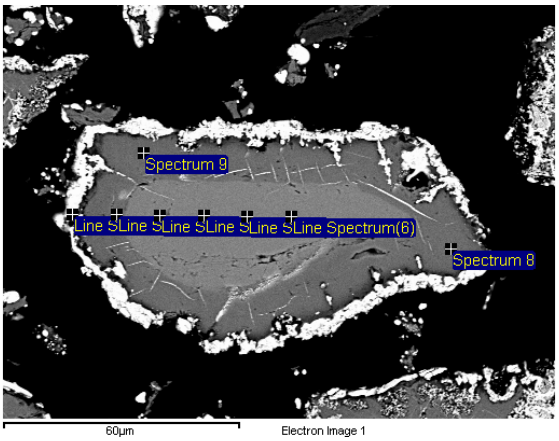

Spec.	O	Mg	Al	Si	Ti	Cr	Fe	Total
1	0.92		0.29	0.18		59.56	31.67	**92.62**
2	37.10	13.37	8.89		0.28	43.76	2.18	**105.57**
3	31.26	7.36	7.44		0.26	37.55	15.57	**99.45**
4	33.34	7.80	7.76		0.22	37.90	15.60	**102.62**
5	33.23	7.87	7.67		0.27	37.52	15.37	**101.93**
6	33.11	7.79	7.77			37.70	15.24	**101.61**
8	34.60	12.32	8.29		0.35	43.46	1.23	**100.25**
9	35.08	12.34	8.32		0.31	43.85	1.94	**101.85**

1200˚C, 20 vol% CH_4, 20 min, site 1/2

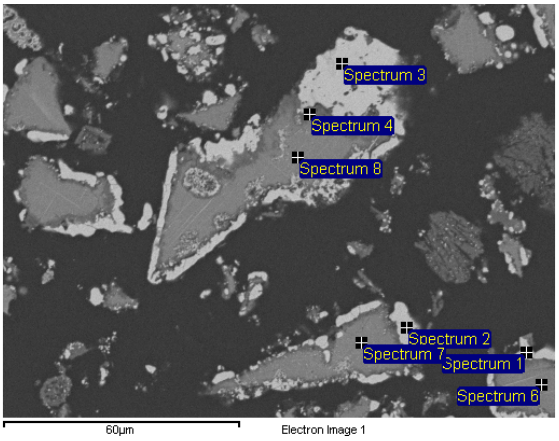

Spec.	O	Mg	Al	Si	Ca	Ti	Cr	Fe	Total
1							43.17	42.63	**85.80**
2							42.63	43.32	**85.95**
3							42.72	42.68	**85.40**
4	37.32	15.23	24.09	3.20	0.86	0.47	9.26	1.48	**91.90**
6	32.30	12.36	8.78			0.40	39.63	1.03	**94.49**
7	30.43	11.80	8.16			0.45	41.45	2.36	**94.65**
8	31.28	12.32	8.54	0.22		0.50	39.60	2.03	**94.49**

Appendix LXIV

1200˚C, 20 vol% CH_4, 20 min, site 2/2

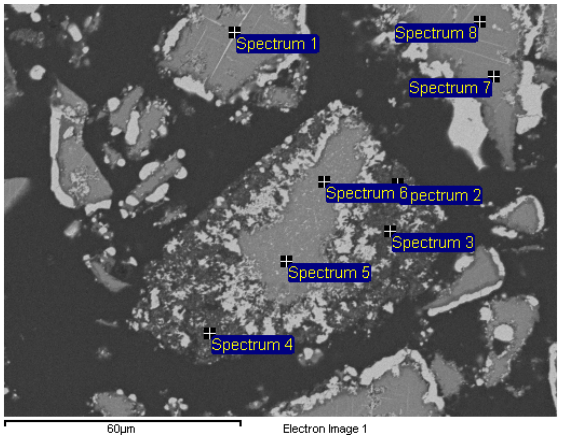

Spec.	O	Mg	Al	Si	Ti	Cr	Fe	Total
1	3.79	1.44	1.79	0.13		16.70	5.73	**29.58**
2	2.89	1.54	4.86	0.29	0.24	14.08	12.58	**36.49**
3	3.27	1.22	6.53	0.23	0.39	8.62	7.91	**28.18**
4	3.85	1.98	9.35	0.46	0.45	6.53	5.19	**27.82**
5	31.72	11.86	8.55		0.73	38.86	4.14	**95.86**
6	31.05	11.52	8.49		0.75	38.41	4.23	**94.44**
7	32.22	12.47	8.84		0.36	39.39	1.13	**94.41**
8	32.12	12.00	8.56		0.26	39.46	1.21	**93.61**

1200˚C, 20 vol% CH_4, 30 min, site 1/2

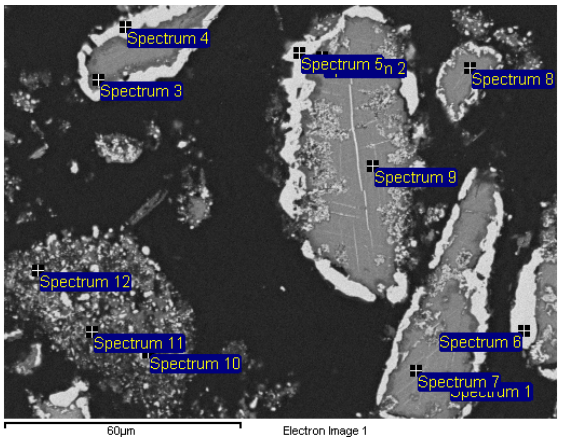

Spec.	O	Mg	Al	Si	Ca	Ti	Cr	Fe	Total
1	25.82	16.80	10.51	5.27		0.21	22.61	15.59	**96.81**
2	37.80	14.68	12.40	16.97	0.38	0.89	2.52	0.95	**86.59**
3	35.92	16.82	19.40	4.53	0.23	0.43	9.83	0.86	**88.03**
4							44.20	38.72	**82.92**
5	0.47						40.65	42.32	**83.45**
6							40.52	41.38	**81.90**
7	30.51	12.10	7.67			0.38	39.74	1.13	**91.54**
8	29.39	12.15	8.04			0.29	39.21	2.45	**91.52**
9	29.91	11.76	8.19			0.43	38.23	0.98	**89.51**
10	6.06	6.53	0.53	3.10			8.33	6.44	**30.98**
11	13.76	10.06	7.83	5.44	0.46	0.27	8.06	11.43	**57.31**
12	1.44	3.05	2.02	1.22	0.22		17.13	9.03	**34.12**

Appendix LXV

1200˚C, 20 vol% CH_4, 30 min, site 2/2

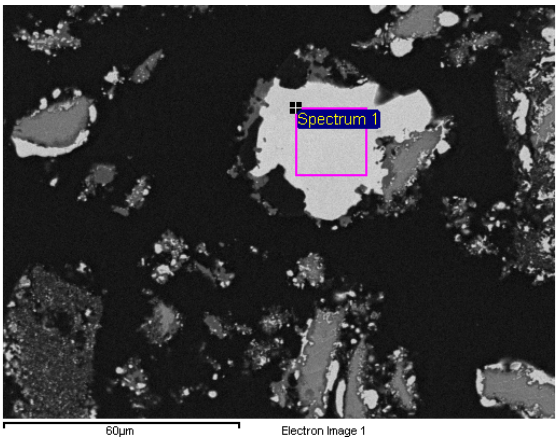

Spec.	O	Si	Cr	Fe	Total
1	0.62	1.27	18.17	65.87	**85.93**

1200˚C, 20 vol% CH_4, 60 min, site 1/3

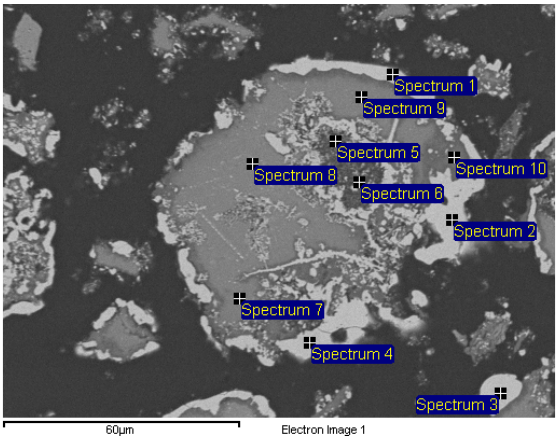

Spec.	O	Mg	Al	Si	Ti	Cr	Fe	Total
1						40.18	45.20	**85.38**
2	0.43					40.90	43.83	**85.16**
3						37.23	47.86	**85.10**
4	2.35	0.94	2.12			40.81	37.63	**83.85**
5	2.96	0.44	9.98	0.16	0.26	13.99	9.40	**37.21**
6	5.64	2.03	11.07	0.17	0.45	9.00	5.77	**34.13**
7	32.10	12.66	10.01		0.55	37.72	1.32	**94.36**
8	30.95	11.94	8.54		0.51	39.57	1.16	**92.66**
9	30.52	11.97	9.16		0.60	37.56	2.70	**92.51**
10	33.68	13.56	17.80		0.84	25.45	1.15	**92.49**

1200˚C, 20 vol% CH_4, 60 min, site 2/3

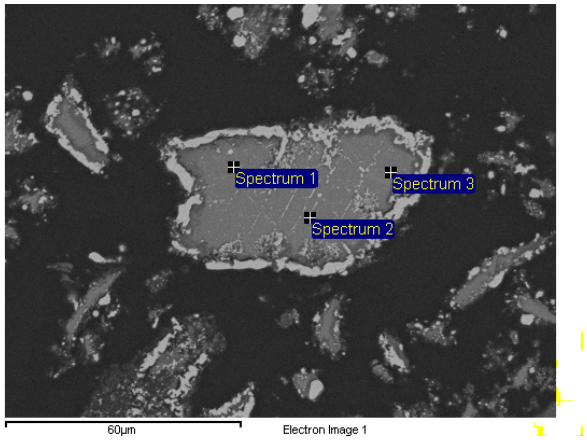

Spec.	O	Mg	Al	Ti	Cr	Fe	Total
1	31.28	12.25	8.84	0.35	39.14	1.00	**92.86**
2	31.35	11.99	8.58	0.49	39.87	1.62	**93.90**
3	30.22	11.88	8.51	0.36	38.84	2.70	**92.52**

1200˚C, 20 vol% CH_4, 60 min, site 3/3

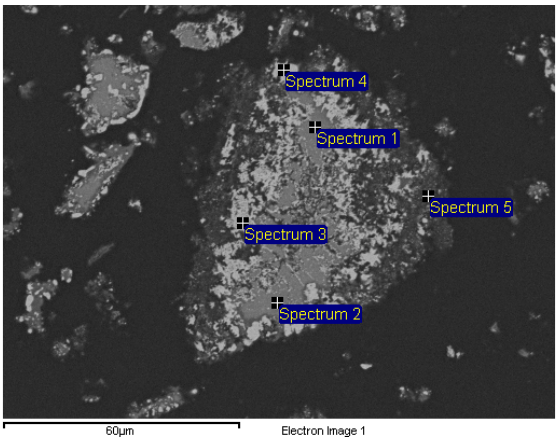

Spec.	O	Mg	Al	Si	Ti	Cr	Fe	Total
1	30.60	11.88	7.51		0.40	40.19	1.59	**92.18**
2	28.39	10.95	7.54	0.21	0.97	38.52	4.91	**91.51**
3	3.48		4.22			43.48	36.09	**87.27**
4						39.58	41.90	**81.48**
5	7.39	0.55	12.18	0.27	0.56	5.94	4.92	**31.81**

Appendix LXVII

1200˚C, 20 vol% CH_4, 90 min, site 1/2

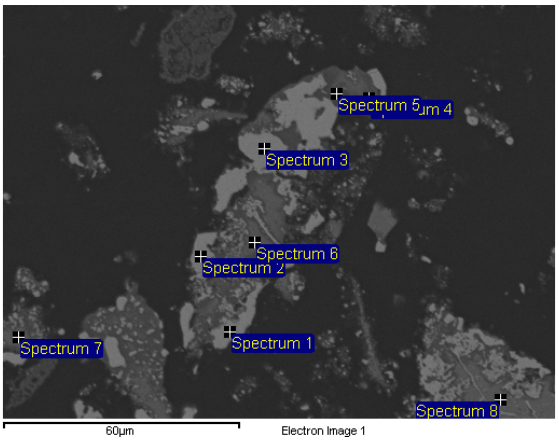

Spec.	O	Mg	Al	Si	Ca	Ti	Cr	Fe	Total
1							47.33	39.61	**86.93**
2	0.59						47.17	39.67	**87.42**
3							45.03	41.07	**86.11**
4	41.23	15.37	25.07	4.51	2.29	0.37	7.25	0.80	**96.89**
5	38.28	18.49	23.32	3.36	0.18	0.67	12.10	0.52	**96.91**
6	32.38	12.76	10.88			0.42	37.61	1.48	**95.53**
7	31.59	12.80	8.61			0.51	41.65	2.35	**97.51**
8	29.64	12.27	7.57	0.35		0.45	39.60	6.07	**95.95**

1200˚C, 20 vol% CH_4, 90 min, site 2/2

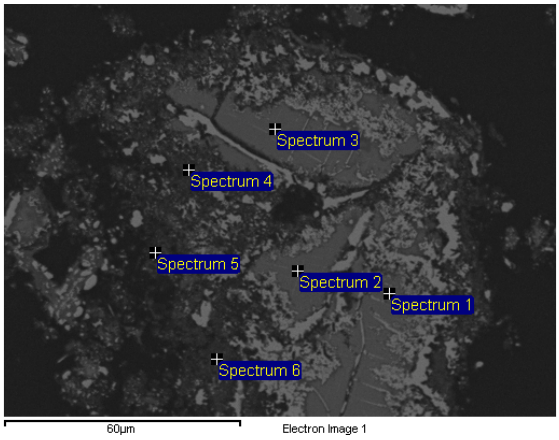

Spec.	O	Mg	Al	Si	Ti	Cr	Fe	Total
1	31.19	12.39	8.65		0.39	38.82	1.65	**93.09**
2	29.00	11.79	8.24		0.46	40.51	3.75	**93.75**
3	31.81	12.56	8.28		0.34	40.15	0.78	**93.92**
4	4.45	4.34	10.38	0.16	0.80	7.28	5.40	**32.81**
5	2.07	2.36	5.75	0.86		0.75	2.59	**14.38**
6	8.24	4.27	9.59	1.17		3.83	7.91	**35.02**

Appendix LXVIII

1200˚C, 20 vol% CH_4, 120 min, site 1/2

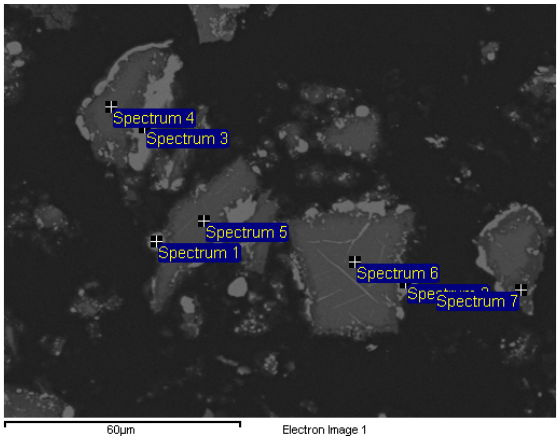

Spec.	O	Mg	Al	Si	Ca	Ti	Cr	Fe	Total
1							46.94	40.54	**87.48**
2	0.49		0.16				46.12	40.72	**87.49**
3							46.28	40.95	**87.23**
4	34.78	12.91	10.20			0.62	37.43	0.88	**96.83**
5	35.05	13.24	8.92			0.36	39.96	0.53	**98.06**
6	34.45	12.61	7.96			0.33	41.22	0.94	**97.50**
7	43.63	10.84	11.74	15.98	12.81	1.53	2.49	0.33	**99.34**

1200˚C, 20 vol% CH_4, 120 min, site 2/2

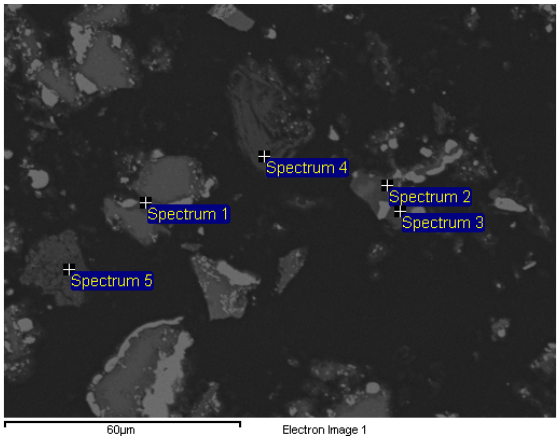

Spec.	O	Mg	Al	Si	Ca	Ti	Cr	Fe	Total
1	41.24	0.78	14.99	17.89	12.59		4.04	2.80	**94.33**
2	42.47	26.42	11.34	12.85	0.26		4.01	0.44	**97.80**
3	39.24	17.96	15.22	3.35	0.13	0.74	24.41	1.22	**102.29**
4	46.39	20.26	0.60	29.28	0.32		0.48	0.69	**98.03**
5	21.56	42.07		0.16			0.72	10.94	**75.45**

Appendix LXIX

1200 ˚C, 30 vol% CH_4, 10 min, site 1/2

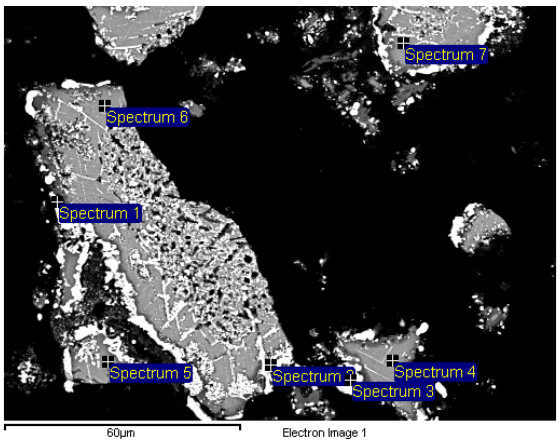

Spec.	O	Mg	Al	Si	Ti	Cr	Fe	Total
1	0.36					44.43	39.11	**83.90**
2						43.93	39.65	**83.59**
3	0.40					40.77	42.91	**84.07**
4	33.14	13.15	8.55	0.07	0.45	38.52	1.36	**95.24**
5	34.48	13.00	9.05		0.52	39.23	1.00	**97.28**
6	33.53	13.01	8.77		0.41	39.59	1.52	**96.83**
7	33.52	12.93	8.72		0.53	38.11	2.34	**96.15**

1200 ˚C, 30 vol% CH_4, 10 min, site 2/2

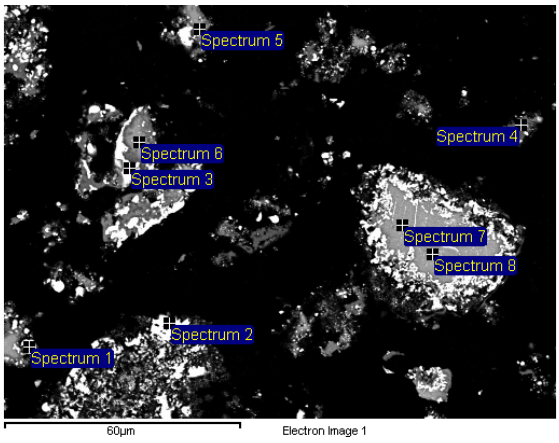

Spec.	O	Mg	Al	Si	Ca	Ti	Cr	Fe
1	0.32						45.54	**39.34**
2			0.11				47.53	**34.70**
3	0.48		0.15	0.15			46.25	**36.67**
4	38.13	31.13	0.62	17.29	0.29	0.13	6.81	**3.86**
5	34.00	13.82	10.22	0.14		0.58	37.00	**1.09**
6	34.00	13.68	9.58	0.08		0.55	38.14	**0.65**
7	33.63	12.71	8.59			0.43	38.57	**2.26**

Appendix LXX

1200 ˚C, 30 vol% CH_4, 20 min, site 1/2

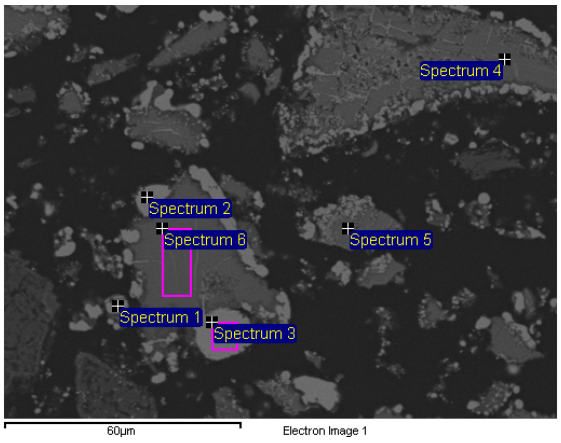

Spec.	O	Mg	Al	Si	Ti	Cr	Fe	Total
1						44.79	41.30	**86.09**
2	0.41					38.47	48.23	**87.11**
3	0.58			0.27		34.38	51.22	**86.45**
4	26.80	11.15	7.24		0.47	40.73	6.53	**92.92**
5	29.76	11.90	7.56		0.54	40.82	3.41	**94.00**
6	31.17	12.08	8.06		0.36	40.91	1.62	**94.19**

1200 ˚C, 30 vol% CH_4, 20 min, site 2/2

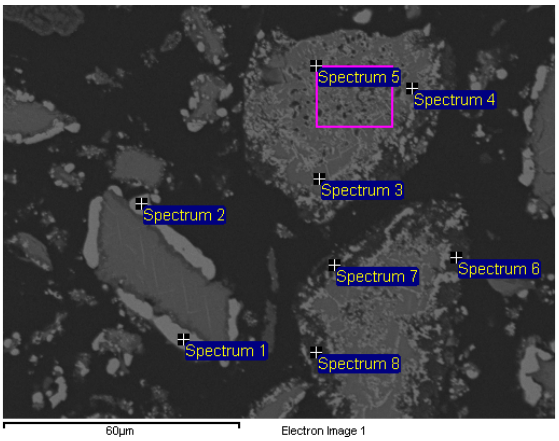

Spec.	O	Mg	Al	Si	Ti	Cr	Fe	Total
1	0.51					36.35	50.78	**87.64**
2	0.90					45.48	39.09	**85.47**
3	30.96	11.95	7.51		0.34	40.79	1.66	**93.21**
4	30.61	11.74	7.85	0.20	0.61	40.11	3.41	**94.51**
5	13.65	6.61	7.77		0.31	34.30	18.43	**81.06**
6	4.14	2.80	8.20	0.31		2.98	3.80	**22.24**
7	6.03	3.59	10.84	0.29		6.14	4.52	**31.41**
8	4.05	1.17	8.55	0.21		4.06	3.34	**21.37**

Appendix LXXI

1200˚C, 30 vol% CH_4, 30 min, site 1/2

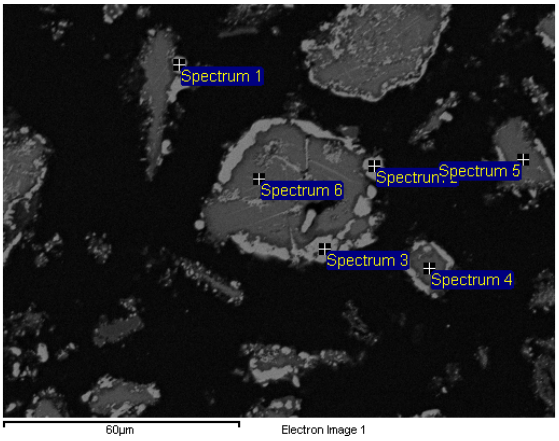

Spec.	O	Mg	Al	Si	Ca	Ti	Cr	Fe	Total
1							42.57	41.15	**83.71**
2	0.66		0.25				35.23	43.82	**79.96**
3	1.52	0.46	1.10				41.43	38.83	**83.35**
4	31.52	12.50	12.21	2.80	0.17	0.84	26.68	1.47	**88.19**
5	11.64	6.42	8.74	0.50			33.88	25.52	**86.70**
6	27.25	11.97	8.47	0.41		0.58	38.44	2.94	**90.06**

1200˚C, 30 vol% CH_4, 30 min, site 2/2

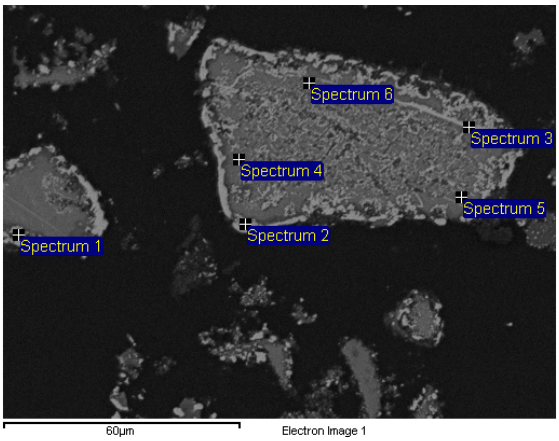

Spec.	O	Mg	Al	Si	Ti	Cr	Fe	Total
1	3.38	1.45	3.25	0.26		42.80	35.22	**86.37**
2	4.36	2.15	2.96	0.28		39.50	39.42	**88.67**
3	17.18	7.84	13.23	0.47	0.44	30.42	18.89	**88.46**
4	28.67	11.76	7.57		0.32	38.53	4.80	**91.65**
5	25.40	11.24	8.93		0.69	36.43	5.19	**87.87**
6	28.75	12.51	8.82	1.08	0.81	34.75	2.61	**89.32**

Appendix LXXII

1200˚C, 30 vol% CH_4, 60 min, site 1/2

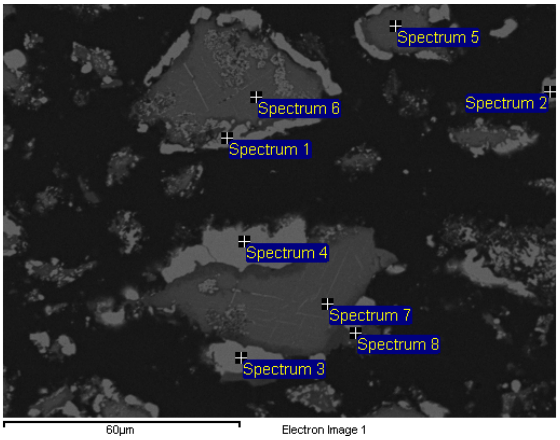

Spec.	O	Mg	Al	Si	Ca	Ti	Cr	Fe	Total
1							44.24	40.95	**85.20**
2							38.41	45.68	**84.10**
3	0.51						38.08	48.15	**86.74**
4	0.41						38.05	47.52	**85.98**
5	30.39	11.69	7.36			0.37	40.06	2.45	**92.33**
6	29.68	11.49	8.05			0.44	39.60	2.95	**92.20**
7	31.18	12.15	8.81			0.29	38.55	3.11	**94.09**
8	38.33	10.68	20.62	12.17	3.26	0.36	2.18	0.78	**88.38**

1200˚C, 30 vol% CH_4, 60 min, site 2/2

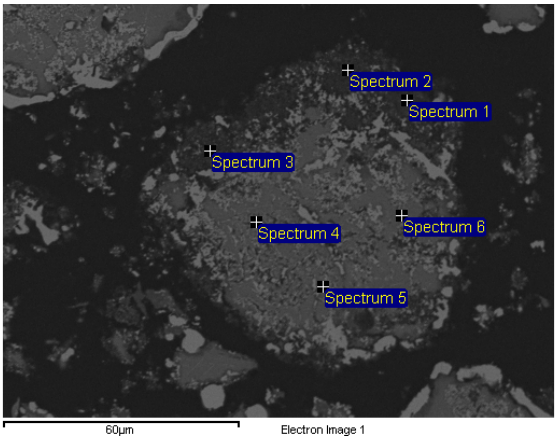

Spec.	O	Mg	Al	Si	Ti	Cr	Fe	Total
1	1.96	2.01	4.21	0.45		7.32	7.85	23.79
2	1.82	2.16	4.69	0.25	0.14	6.46	5.76	21.29
3	0.87	0.91	1.90	0.55		8.02	9.80	22.05
4	13.44	7.86	8.62	0.13	0.34	29.65	15.53	75.56
5	15.71	7.57	8.95	0.17	0.27	38.31	21.44	92.43
6	29.03	11.94	8.07		0.31	37.99	3.93	91.27

Appendix LXXIII

1200 ˚C, 30 vol% CH_4, 90 min, site 2/2

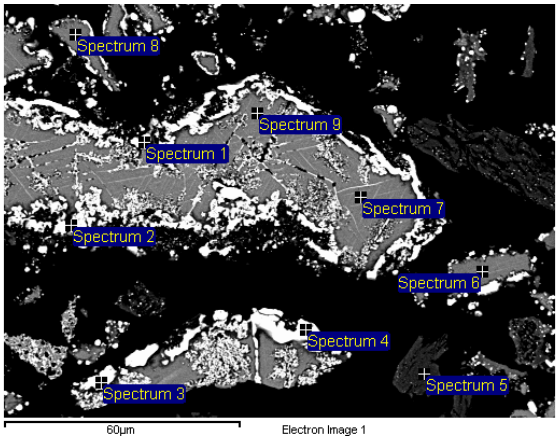

Spec.	O	Mg	Al	Si	Ca	Ti	Cr	Fe	Total
1	0.44		0.15				40.37	46.45	**87.40**
2	0.53						39.07	48.98	**88.58**
3	0.46					0.18	38.35	49.61	**88.60**
4	0.49					0.17	33.47	53.21	**87.34**
5	43.79	28.55	1.81	22.05	0.26		0.98	0.83	**98.27**
6	33.47	12.80	8.72			0.34	41.18	1.29	**97.79**
7	32.45	12.16	8.14			0.38	41.26	1.70	**96.10**
8	34.40	13.12	8.43			0.32	42.23	1.09	**99.58**
9	32.51	12.35	8.34			0.31	41.27	1.41	**96.19**

1200 ˚C, 30 vol% CH_4, 90 min, site 1/2

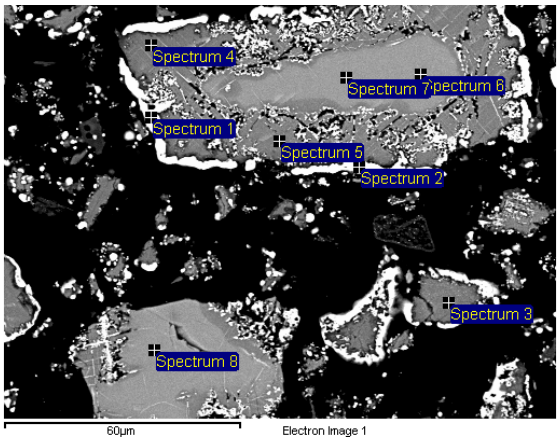

Spec.	O	Mg	Al	Si	Ti	Cr	Fe	Total
1	0.47			0.75		31.48	62.43	**95.13**
2	0.47			0.62		40.49	50.18	**91.76**
3	31.90	12.29	9.31		0.59	38.88	4.40	**97.38**
4	33.26	12.24	8.98	0.08	0.46	41.24	2.23	**98.49**
5	33.92	12.83	8.07	0.18	0.40	41.58	2.20	**99.17**
6	31.03	6.24	7.05		0.30	35.84	17.14	**97.61**
7	31.06	6.35	7.28		0.27	35.44	17.07	**97.46**
8	31.76	6.83	7.33		0.27	35.33	17.30	**98.82**

Appendix LXXIV

1200˚C, 30 vol% CH_4, 120 min

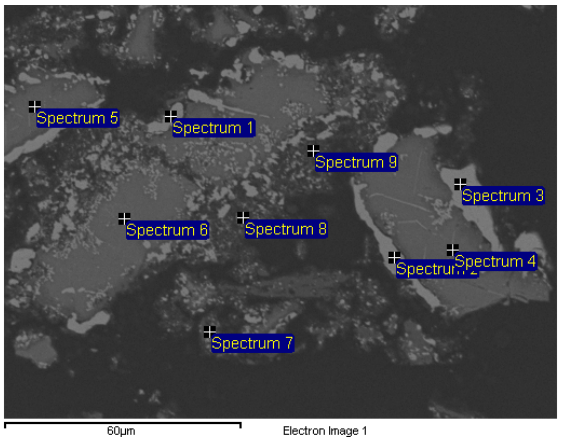

Spec.	O	Mg	Al	Si	Ca	Ti	Cr	Fe	Total
1							48.94	36.69	**85.63**
2							47.23	38.84	**86.07**
3	0.47						42.65	40.99	**84.11**
4	28.42	11.12	7.91			0.43	40.26	2.78	**90.91**
5	34.80	13.03	9.67	0.35		0.73	38.23	0.67	**97.47**
6	31.22	11.96	8.61			0.29	36.59	7.05	**95.72**
7	1.38	2.43	0.88	1.04	0.25		7.70	5.83	**19.51**
8	1.91		4.34				10.68	6.53	**23.45**
9	4.72	2.39	6.70	0.58	0.21		11.19	6.67	**32.46**

1300 ˚C, 10 vol% CH_4, 10 min

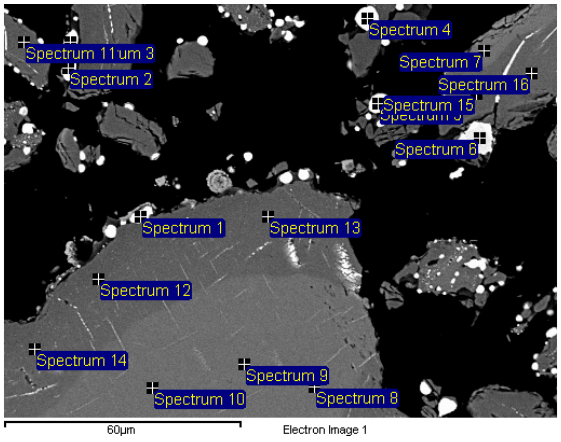

Spec.	O	Mg	Al	Si	Ti	Cr	Fe	Total
1	0.59			0.24		18.60	78.42	**97.85**
2	0.48			0.20		21.40	76.23	**98.31**
3	0.43			0.15		21.48	76.43	**98.49**
4	0.55			0.27		27.33	68.51	**96.67**
5	0.53			0.28		27.12	68.91	**96.84**
6	0.38					47.67	41.19	**89.24**
7	28.59	5.72	7.27	0.10	0.37	32.65	18.81	**93.51**
8	29.14	6.96	7.15		0.26	35.50	15.64	**94.65**
9	29.65	7.07	7.23		0.37	35.41	15.51	**95.24**
10	29.98	7.07	7.46		0.25	35.74	15.50	**96.01**
11	32.79	11.28	8.17		0.38	41.98	2.93	**97.53**
12	31.42	9.55	8.72		0.39	41.15	4.57	**95.81**
13	30.40	9.37	7.77		0.38	42.45	3.59	**93.96**
14	31.59	9.38	8.25		0.37	42.03	4.71	**96.32**
15	32.48	9.15	8.58		0.47	41.82	4.31	**96.81**
16	31.76	8.93	8.11		0.44	42.22	4.50	**95.95**

Appendix LXXV

1300 ˚C, 10 vol% CH_4, 20 min, site 1/2

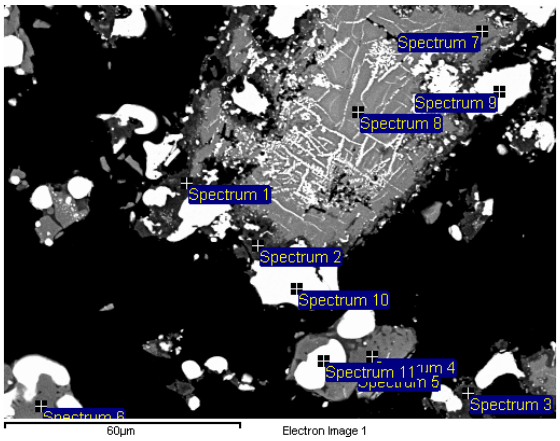

Spec.	O	Mg	Al	Si	Ca	Ti	Cr	Fe	Total
1	41.25	19.52	27.35	3.26	0.46	0.40	5.98	0.45	**98.67**
2	40.29	30.82	2.16	17.17	0.49	0.14	3.45	0.40	**94.93**
3	39.34	24.49	11.18	12.40	3.24	0.40	2.54	0.57	**94.17**
4	33.61	13.09	13.57	0.12		0.51	32.51	0.56	**93.97**
5	33.24	12.61	11.31	0.72	0.24	0.40	33.83	3.01	**95.36**
6	34.97	12.47	14.44	1.30	0.34	0.56	31.63	1.05	**96.76**
7	30.14	12.09	7.65			0.34	40.13	0.80	**91.15**
8	28.92	7.80	7.46			0.27	34.34	14.50	**93.29**
9							70.47	14.00	**84.47**
10	0.36					0.15	52.76	32.13	**85.40**
11	0.54			0.89			36.48	58.63	**96.55**

1300 ˚C, 10 vol% CH_4, 20 min, site 2/2

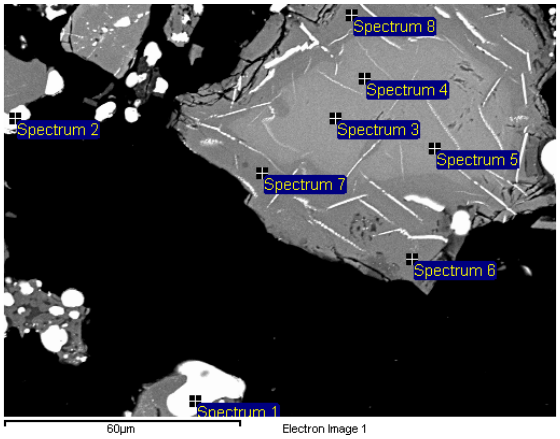

Spec.	O	Mg	Al	Si	Ti	Cr	Fe	Total
1	0.61			0.36		26.95	68.65	**96.58**
2	0.66			0.34		25.19	70.06	**96.25**
3	29.79	6.84	7.87		0.22	33.78	15.86	**94.36**
4	29.44	6.73	7.68		0.28	33.57	15.73	**93.43**
5	29.15	6.86	7.61		0.29	33.79	15.39	**93.09**
6	32.79	12.50	8.36		0.39	40.15	0.79	**94.98**
7	33.88	12.51	8.88		0.31	39.50	2.24	**97.33**
8	31.52	12.17	8.44		0.31	40.16	1.00	**93.60**

Appendix LXXVI

1300˚C, 10 vol% CH_4, 30 min, site 1/2

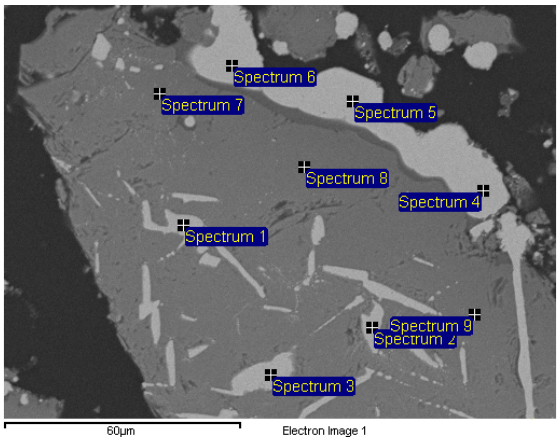

Spec.	O	Mg	Al	Si	Ti	Cr	Fe	Total
1	0.60					31.34	64.37	**96.32**
2	0.71			0.20		30.42	65.14	**96.47**
3	0.73					28.88	65.32	**94.93**
4	0.51			0.42		33.44	58.30	**92.68**
5	0.42			0.51		34.17	59.15	**94.25**
6	0.46			0.53		34.95	58.44	**94.38**
7	30.68	10.14	11.93		0.45	36.11	1.34	**90.65**
8	31.37	9.96	11.93		0.50	35.68	0.91	**90.35**
9	30.62	9.45	12.15		0.35	35.38	1.06	**89.02**

1300˚C, 10 vol% CH_4, 30 min, site 2/2

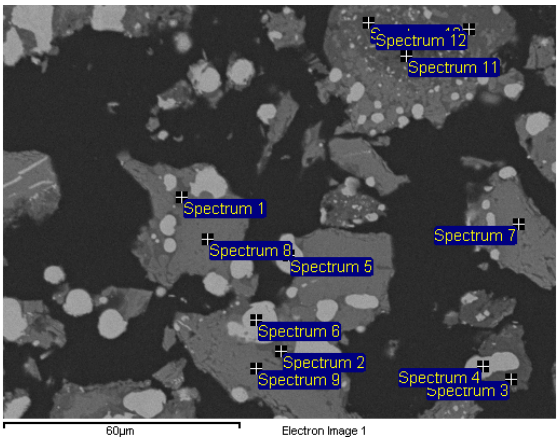

Spec.	O	Mg	Al	Si	Ca	Ti	Cr	Fe	Total
1	39.03	6.56	9.60	20.34	5.92	0.59	7.69		**89.73**
2	44.36	6.08	8.88	23.42	6.82	0.56	5.14	0.47	**95.73**
3	36.69	22.56	14.71	9.34	1.45	0.39	2.16	0.36	**87.67**
4							54.71	27.06	**81.77**
5	0.44			0.70			32.24	60.88	**94.27**
6	0.49			0.79			32.97	59.12	**93.36**
7	30.59	11.28	8.08			0.43	39.23	1.14	**90.77**
8	33.87	12.51	9.39			0.35	38.67	0.68	**95.46**
9	32.41	10.97	10.17	1.49	0.47	0.40	34.15	0.66	**90.73**
10	31.61	21.64	2.66	10.32		0.51	18.38	4.20	**89.31**
11	20.19	40.15	0.50				4.25	0.95	**66.05**
12	31.99	14.19	9.87	3.78	0.66	0.60	28.39	1.76	**91.24**

Appendix LXXVII

1300˚C, 10 vol% CH_4, 60 min, site 1/2

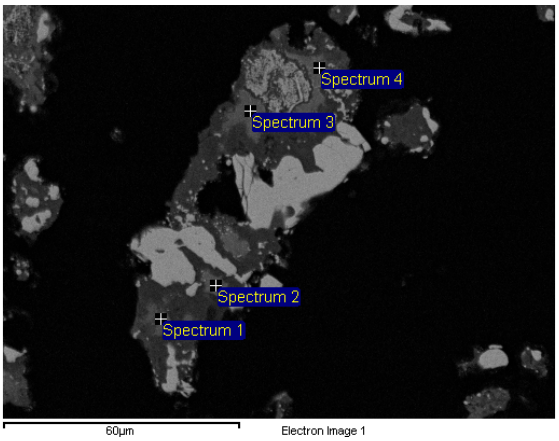

Spec.	O	Mg	Al	Si	Ca	Ti	Cr	Fe	Total
1	32.33	13.61	9.34	0.41		1.19	38.17	0.61	**95.67**
2	33.49	14.36	12.16	1.81		0.87	29.84	1.01	**93.54**
3	29.25	14.20	11.82	2.33		0.65	36.69	1.91	**96.85**
4	33.36	15.95	17.03	2.67	0.25	0.95	19.53	1.65	**91.40**

1300˚C, 10 vol% CH_4, 60 min, site 2/2

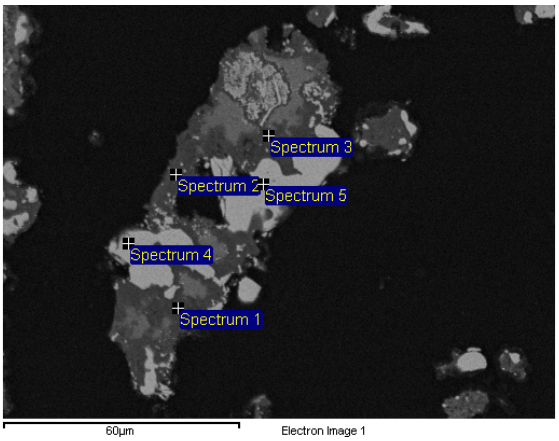

Spec.	O	Mg	Al	Si	Ca	Ti	Cr	Fe	Total
1	39.89	25.58	9.91	14.22	1.10		0.68		**91.39**
2	44.72	11.31	17.93	16.55	5.75	0.38	1.16	1.57	**99.37**
3	38.42	21.33	19.26	5.71		0.72	12.52	1.24	**99.21**
4						0.31	46.45	39.29	**86.05**
5	1.14	0.41	0.86				42.51	37.74	**82.65**

Appendix LXXVIII

1300˚C, 10 vol% CH_4, 90 min, site 1/2

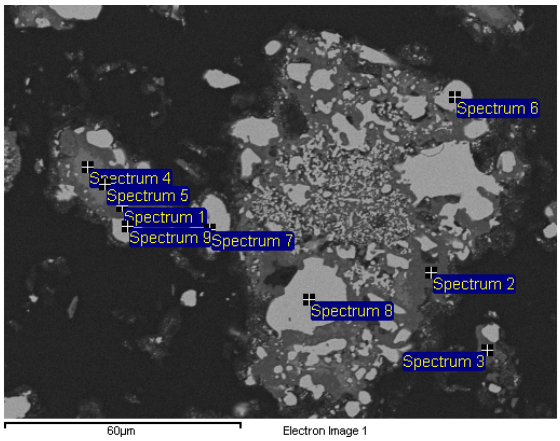

Spec.	O	Mg	Al	Si	Ca	Ti	Cr	Fe	Total
1	39.85	31.20	0.97	18.26	1.53		0.97		**92.78**
2	40.39	22.87	19.86	7.77	0.84	0.38	2.29	0.35	**94.74**
3	37.21	25.07	9.21	12.05	1.47	0.32	1.53	0.31	**87.17**
4	31.13	12.47	8.12			0.36	39.78	1.30	**93.16**
5	31.51	12.48	8.27			0.44	39.77	0.77	**93.23**
6							51.76	31.57	**83.32**
7							49.50	35.46	**84.96**
8							59.31	24.26	**83.57**
9							47.99	35.94	**83.93**

1300˚C, 10 vol% CH_4, 90 min, site 2/2

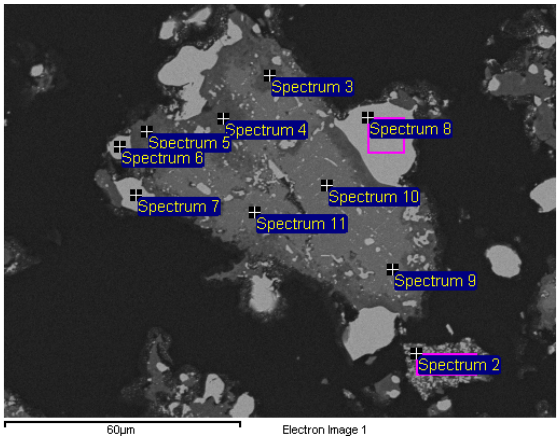

Spec.	O	Mg	Al	Si	Ca	Ti	Cr	Fe	Total
2	9.72	9.19	8.14			0.38	29.73	13.97	**71.14**
3	38.46	17.20	28.30	1.49	0.22	0.45	4.64		**90.77**
4	41.34	16.15	30.78	1.10	1.21	0.42	4.12		**95.12**
5	38.26	19.12	19.66	4.35	0.63	0.61	12.22	0.80	**95.64**
6							45.25	37.95	**83.19**
7							45.45	38.02	**83.46**
8							42.64	39.82	**82.46**
9	29.72	11.89	8.53			0.38	37.75	1.92	**90.19**
10	30.69	12.25	8.49			0.37	37.97	0.77	**90.54**
11	31.57	12.60	9.62			0.47	36.50	0.97	**91.73**

Appendix LXXIX

1300˚C, 10 vol% CH_4, 120 min, site 1/2

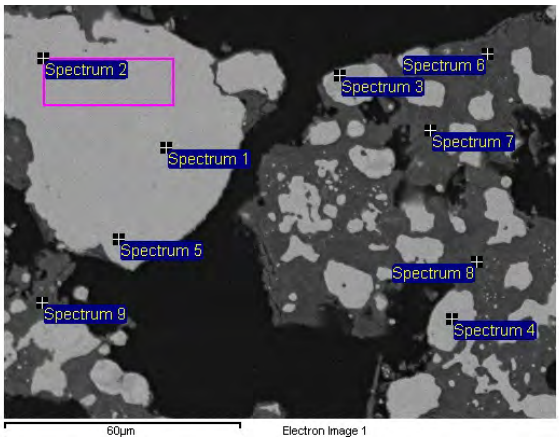

Spec.	O	Mg	Al	Si	Ca	Ti	Cr	Fe	Total
1				2.16			48.84	44.05	**95.05**
2				1.29			56.79	33.44	**91.51**
3							74.14	8.88	**83.02**
4				0.84			57.01	31.87	**89.71**
5				2.17			51.26	42.89	**96.32**
6	36.94	32.31	15.15	0.42	0.37	0.74	6.23		**92.16**
7	40.81	23.61	12.86	10.15	1.60	0.59	3.98		**93.60**
8	40.83	34.56	2.98	11.71	2.60	0.43	1.60		**94.72**
9	39.82	16.23	25.68	0.18		1.05	12.84		**95.80**

1300˚C, 10 vol% CH_4, 120 min, site 2/2

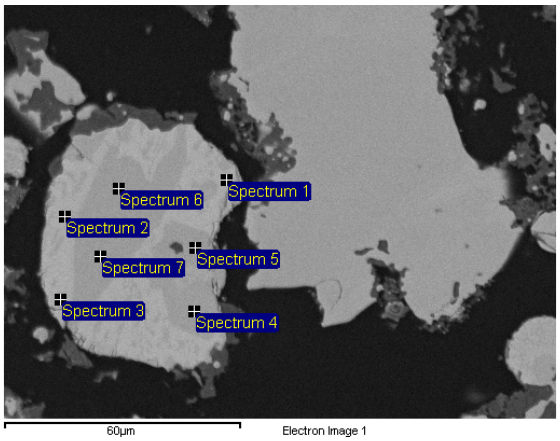

Spec.	O	Si	Cr	Fe	Total
1	0.59	4.15	39.98	49.76	**94.47**
2	0.53	4.28	40.28	49.55	**94.65**
3	0.56	3.82	40.82	50.94	**96.13**
4			70.17	14.11	**84.29**
5			74.02	9.98	**84.01**
6			71.61	12.94	**84.55**
7			74.68	9.98	**84.66**

1300 ˚C, 20 vol% CH_4, 10 min, site 1/2

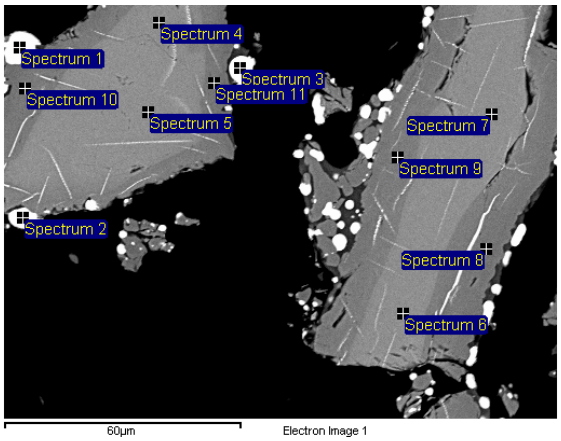

Spec.	O	Mg	Al	Si	Ti	Cr	Fe	Total
1	0.59			0.32		25.43	69.86	**96.19**
2	0.54			0.24		22.29	71.88	**94.94**
3	0.55			0.25		25.85	68.66	**95.32**
4	29.58	6.61	7.32		0.32	34.31	16.23	**94.36**
5	30.05	6.72	7.38		0.27	34.48	16.34	**95.24**
6	30.73	6.45	7.63		0.38	33.53	17.24	**95.97**
7	29.02	6.07	7.27		0.28	33.37	17.17	**93.16**
8	31.70	10.17	8.93		0.44	40.32	2.18	**93.72**
9	31.90	9.81	7.87		0.44	40.85	3.72	**94.59**
10	33.22	11.23	8.68		0.42	41.29	1.75	**96.59**
11	30.79	10.49	7.98		0.33	39.98	3.33	**92.90**

1300 ˚C, 20 vol% CH_4, 10 min, site 2/2

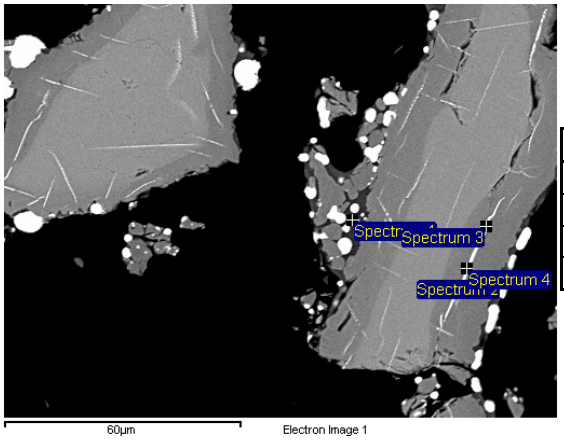

Spec.	O	Mg	Al	Si	Ca	Ti	Cr	Fe	Total
1	42.75	1.56	10.16	22.91	7.14	0.62	7.49	0.73	**93.36**
2	34.71	0.93	9.54	19.58	6.80	0.48	7.39	0.64	**80.08**
3	13.62	5.14	3.54				20.44	63.04	**105.77**
4	11.22	3.98	2.95				18.72	66.64	**103.51**

Appendix LXXXI

1300 ˚C, 20 vol% CH_4, 20 min, site 1/2

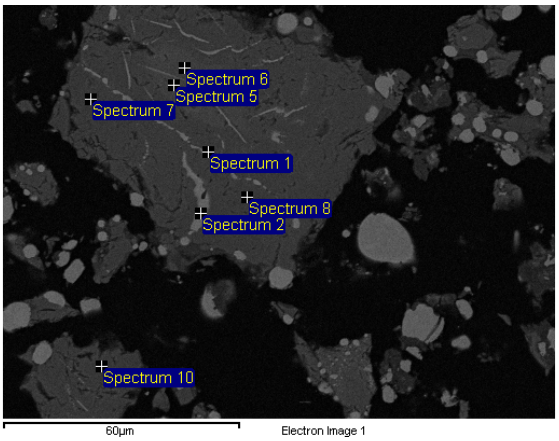

Spec.	O	Mg	Al	Ti	Cr	Fe	Total
1	1.84	0.61	0.28		21.18	77.22	**101.13**
2	4.96	1.97	1.58		24.12	72.42	**105.05**
5	30.47	6.51	7.66	0.39	35.61	18.47	**99.11**
6	30.04	6.11	7.85		35.25	18.72	**97.97**
7	35.20	11.95	8.96	0.42	44.03	1.83	**102.40**
8	33.59	11.39	8.56	0.37	43.69	1.71	**99.31**
10	32.81	11.84	8.57	0.45	43.13	1.33	**98.13**

1300 ˚C, 20 vol% CH_4, 20 min, site 2/2

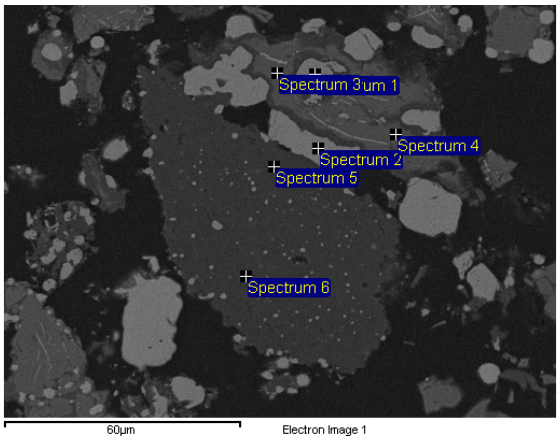

Spec.	O	Mg	Al	Si	Ca	Ti	Cr	Fe	Total
1							49.43	36.29	**85.72**
2							41.64	44.69	**86.33**
3	30.76	12.86	8.90			0.61	38.10	4.04	**95.27**
4	32.05	13.66	9.92	0.41		0.76	37.56	1.95	**96.30**
5	41.10	31.13	1.61	19.72	0.78		0.78	2.26	**97.37**
6	42.35	25.58	4.12	21.06	2.22		0.40		**95.73**

Appendix LXXXII

1300 ˚C, 20 vol% CH_4, 30 min, site 1/2

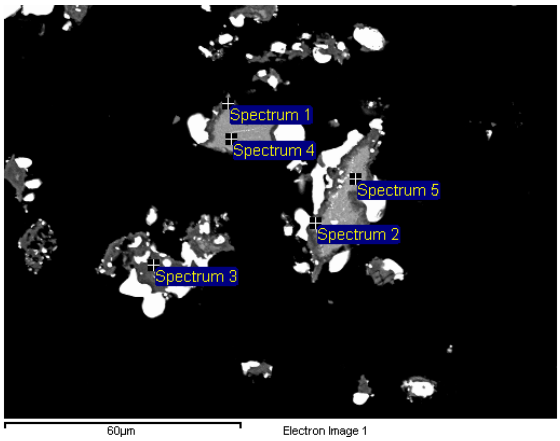

Spec.	O	Mg	Al	Si	Ca	Ti	Cr	Fe	Total
1	38.47	19.15	20.12	4.76	0.48	0.86	9.19	0.36	**93.38**
2	38.35	18.80	14.59	4.34	0.45	0.83	20.16	0.56	**98.07**
3	39.76	27.03	9.37	11.68	0.39	0.53	10.14	0.51	**99.40**
4	33.24	13.18	9.37			0.45	39.48	1.59	**97.32**
5	31.88	12.96	9.08			0.42	37.21	3.85	**95.40**

1300 ˚C, 20 vol% CH_4, 30 min, site 2/2

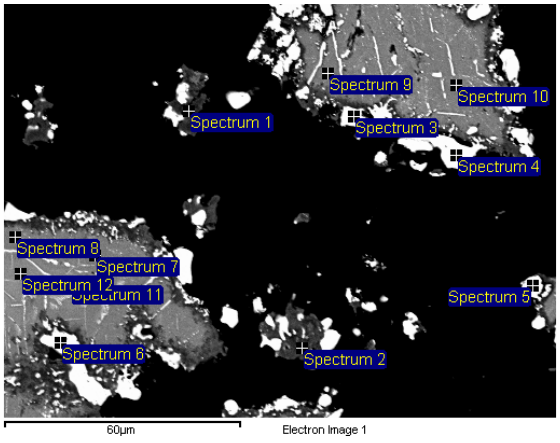

Spec.	O	Mg	Al	Si	Ca	Ti	Cr	Fe	Total
1	42.56	18.28	32.09	1.54	0.18	0.61	3.64	0.78	**99.67**
2	41.31	18.05	27.98	2.91	0.62	0.67	5.81	0.48	**97.83**
3	0.59						47.03	38.46	**86.08**
4	0.54						42.17	42.71	**85.43**
5	0.46						41.41	43.64	**85.50**
6	0.42						56.65	30.10	**87.17**
7	32.88	12.68	8.33			0.28	40.44	2.28	**96.88**
8	32.46	12.73	8.20			0.33	41.07	1.74	**96.53**
9	33.37	12.95	9.10			0.45	38.69	4.07	**98.63**
10	32.53	12.52	9.12			0.40	39.17	2.74	**96.48**
11	31.13	9.57	7.66			0.30	34.27	15.89	**98.83**
12	30.66	9.73	7.73			0.30	35.58	13.10	**97.09**

Appendix LXXXIII

1300˚C, 20 vol% CH_4, 60 min, site 1/2

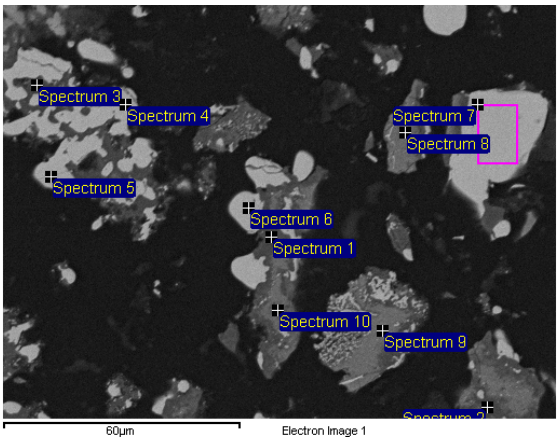

Spec.	O	Mg	Al	Si	Ca	Ti	Cr	Fe	Total
1	38.72	14.91	27.39	3.55	2.21		3.68	0.55	**91.00**
2	42.49	21.02	20.13	6.67	0.84	0.32	4.25	0.50	**96.22**
3	41.95	29.37	4.52	15.08	0.64	0.46	4.45	0.34	**96.81**
4	0.66			0.22			51.11	33.06	**85.04**
5	0.90			0.31			52.17	31.95	**85.33**
6	0.59			0.26			46.43	38.12	**85.40**
7	0.62			0.24			49.44	33.42	**83.71**
8	34.40	12.19	7.59	0.25		0.33	39.34	0.68	**94.77**
9	32.20	11.62	7.57	0.28		0.38	37.78	5.28	**95.10**
10	36.24	13.38	10.82	0.99	0.75	1.36	32.76	0.68	**96.97**

1300˚C, 20 vol% CH_4, 60 min, site 2/2

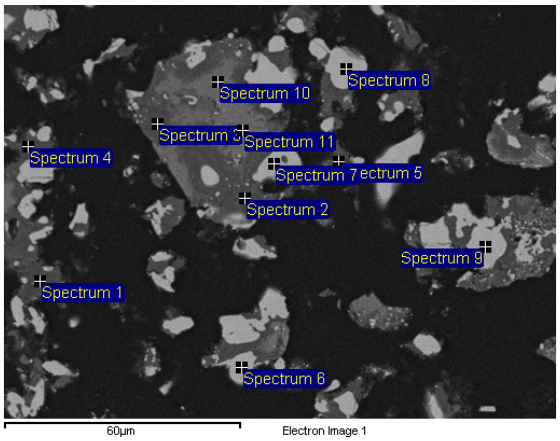

Spec.	O	Mg	Al	Si	Ca	Ti	Cr	Fe	Total
1	42.80	18.97	24.54	4.44	0.60	0.36	4.42	0.35	**96.48**
2	42.80	29.87	4.08	16.40	1.26		2.34	0.85	**97.60**
3	39.11	16.53	18.85	2.12	0.31	0.84	19.25	0.50	**97.51**
4	43.13	19.34	22.97	5.46	0.64	0.36	4.28	0.50	**96.68**
5	41.72	22.14	15.77	7.67	0.90	0.74	6.95	0.78	**96.68**
6	0.72			0.31			48.22	34.71	**83.96**
7	0.62			0.29			46.62	36.86	**84.39**
8	0.58			0.28			48.19	33.55	**82.61**
9	0.72			0.23			46.77	34.03	**81.75**
10	31.98	11.30	8.12	0.24		0.40	38.85	1.94	**92.83**
11	33.02	13.04	8.83	0.38		0.41	36.93	1.73	**94.34**

Appendix LXXXIV

1300˚C, 20 vol% CH_4, 90 min

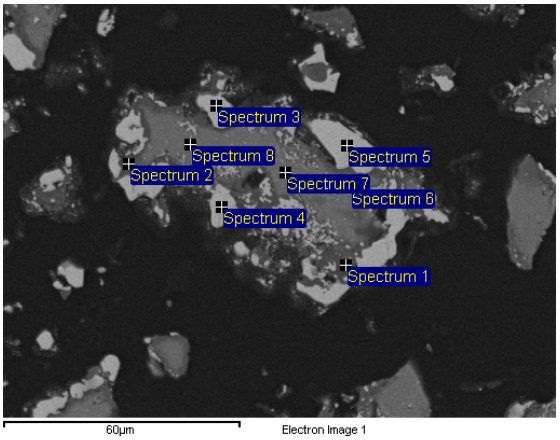

Spec.	O	Mg	Al	Si	Ca	Ti	Cr	Fe	Total
1	39.64	15.34	30.64	0.31	0.22	0.64	4.49	0.71	**91.98**
2	41.34	15.00	27.51	2.05	1.67	0.76	5.83		**94.15**
3							44.07	38.10	**82.16**
4	0.59						45.11	36.46	**82.17**
5	0.49						42.40	39.43	**82.32**
6	30.52	11.85	7.92			0.31	38.03	1.22	**89.85**
7	31.79	11.98	8.02			0.39	38.33	2.32	**92.83**
8	31.98	12.10	8.35			0.46	37.81	1.12	**91.81**

1300˚C, 20 vol% CH_4, 120 min

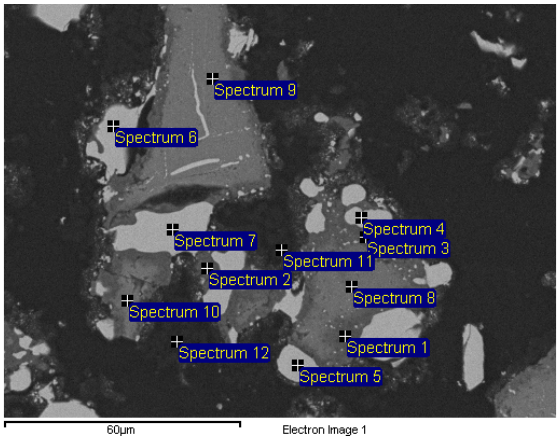

Spec.	O	Mg	Al	Si	Ca	Ti	Cr	Fe	Total
1	35.14	15.39	28.94	0.59	0.19	0.69	5.00	0.34	**86.27**
2	37.09	29.15	3.01	15.76	0.65	0.22	2.63	1.32	**89.84**
3	34.43	15.27	23.90	1.41		0.86	10.70	0.92	**87.48**
4							44.51	37.28	**81.79**
5	0.52						45.68	38.50	**84.70**
6	0.67						45.03	38.22	**83.91**
7	0.51						43.25	39.91	**83.66**
8	30.24	12.54	10.05			0.83	35.24	1.30	**90.20**
9	29.71	12.20	8.54			0.44	37.90	0.51	**89.30**
10	31.54	12.76	9.76	0.19		0.86	35.89	0.47	**91.46**
11	0.92						0.38		**1.30**
12	2.04						0.21		**2.25**

Appendix LXXXV

1300 ˚C, 30 vol% CH_4, 10 min

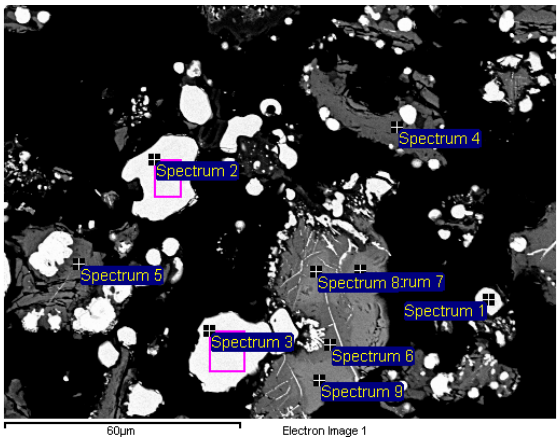

Spec.	O	Mg	Al	Si	Ti	Cr	Fe	Total
1	0.38					54.23	31.43	**86.04**
2	0.51			0.19		50.53	36.49	**87.72**
3	0.62		0.13	0.44		42.66	43.79	**87.64**
4	35.38	13.43	12.46	0.14	0.43	34.71	0.77	**97.32**
5	18.50	7.57	5.27	0.18	0.34	39.61	2.64	**74.12**
6	30.14	5.86	6.97		0.29	34.59	18.73	**96.57**
7	29.18	5.02	6.84		0.20	33.90	19.30	**94.44**
8	28.43	5.14	6.77		0.28	33.48	19.11	**93.23**
9	30.59	5.37	6.99		0.33	34.47	19.39	**97.14**

1300 ˚C, 30 vol% CH_4, 20 min

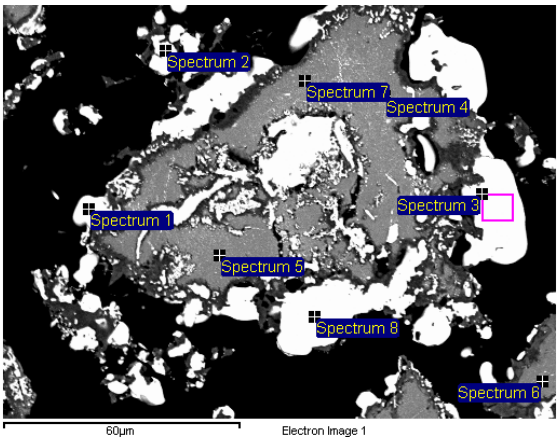

Spec.	O	Mg	Al	Ti	Cr	Fe	Total
1	0.47				45.86	42.46	**88.80**
2	0.49				51.35	35.73	**87.57**
3	0.35				55.36	31.21	**86.92**
4	30.49	11.60	7.90	0.35	41.44	5.18	**96.96**
5	32.63	12.43	8.91	0.40	42.13	4.60	**101.10**
6	34.40	12.94	9.15	0.41	40.63	1.07	**98.60**
7	30.66	11.67	8.16	0.39	41.25	6.12	**98.25**
8	0.41				47.15	41.15	**88.71**

Appendix LXXXVI

1300 ˚C, 30 vol% CH_4, 30 min

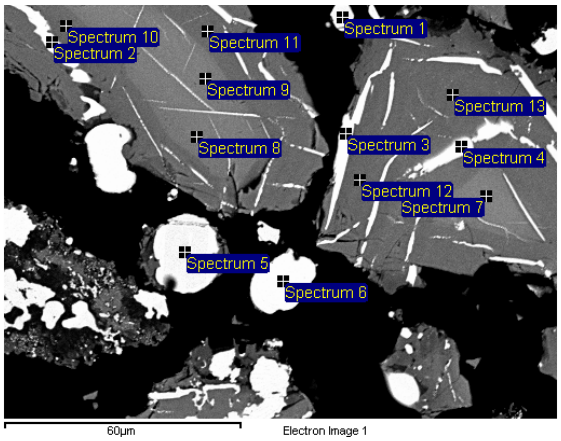

Spec.	O	Mg	Al	Si	Ti	Cr	Fe	Total
1	0.38				0.16	60.25	24.54	**85.33**
2	0.57			0.52		29.21	68.01	**98.30**
3	0.54			0.62		29.75	65.53	**96.45**
4						7.74	88.08	**95.83**
5						68.14	19.00	**87.14**
6	0.48			0.66		30.12	66.03	**97.29**
7	30.82	6.76	7.90		0.30	32.57	17.53	**95.88**
8	32.38	8.19	8.20		0.27	34.14	15.50	**98.68**
9	31.61	7.73	8.14		0.38	34.06	15.64	**97.57**
10	34.16	11.39	9.12		0.40	40.41	3.85	**99.31**
11	32.81	11.76	8.46		0.40	41.12	1.64	**96.20**
12	34.02	12.38	8.86		0.39	41.11	0.93	**97.69**
13	32.57	12.05	8.61		0.40	40.23	1.93	**95.79**

1300 ˚C, 30 vol% CH_4, 60 min

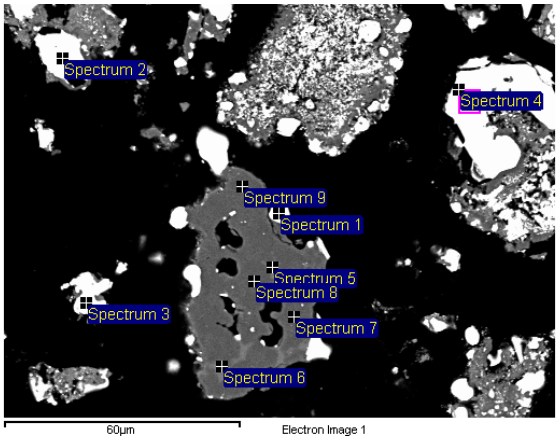

Spec.	O	Mg	Al	Si	Ca	Ti	Cr	Fe	Total
1				0.19		0.20	61.08	25.14	**86.61**
2	0.36					0.21	57.69	31.12	**89.37**
3	0.45			0.13		0.26	51.35	36.75	**88.95**
4	0.51			0.16		0.26	54.62	32.36	**87.91**
5	38.35	19.46	0.14	17.70	17.61		5.20	6.61	**105.06**
6	41.63	19.05	0.18	17.85	21.37		0.42		**100.51**
7	41.96	33.72		18.95	0.16		3.52	0.51	**98.81**
8	42.09	33.71		19.01	0.16		3.74	0.36	**99.08**
9	42.06	33.59		19.21	0.11		3.02	0.52	**98.52**

Appendix LXXXVII

1300 ˚C, 30 vol% CH_4, 90 min

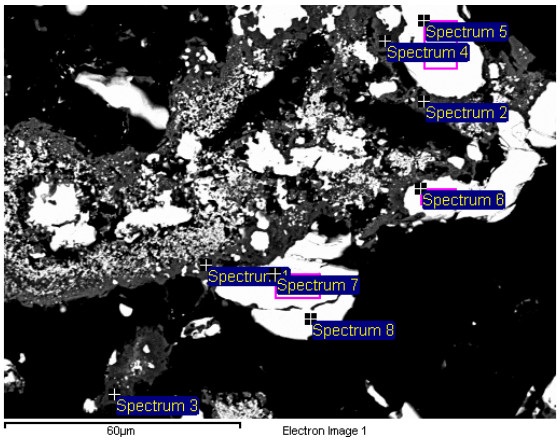

Spec.	O	Mg	Al	Si	Ca	Ti	Cr	Fe	Total
1	39.17	17.61	27.32	0.14		0.78	12.29	0.43	**97.74**
2	34.98	20.24	22.86	0.18		0.64	15.88	2.13	**96.91**
3	41.64	27.99	10.82	12.95	1.34		0.74		**95.47**
4	40.95	17.54	28.28	1.63	0.18	0.92	6.31	0.25	**96.06**
5	0.64					0.17	47.10	38.56	**86.47**
6	0.55					0.18	47.51	38.16	**86.40**
7	0.71					0.18	44.75	40.98	**86.63**
8	0.61					0.20	45.94	39.92	**86.68**

1300 ˚C, 30 vol% CH_4, 120 min, site 1/2

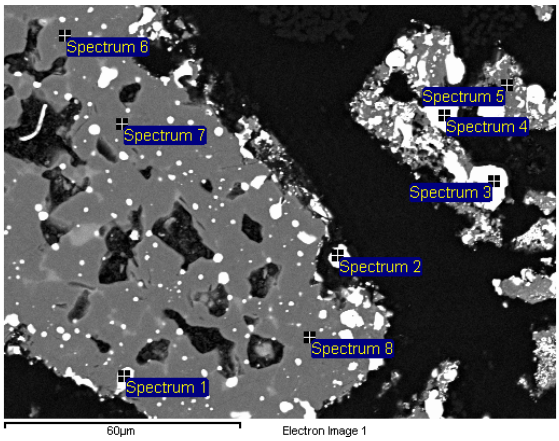

Spec.	O	Mg	Al	Si	Ca	Ti	Cr	Fe	Total
1	0.50			11.73	0.14	0.19	58.47	17.73	**88.77**
2					0.09	0.18	58.09	25.87	**84.23**
3						0.23	53.18	30.75	**84.15**
4						0.19	53.36	30.81	**84.36**
5	34.33	21.89	8.71	13.74	1.33		1.47	0.92	**82.39**
6	43.59	35.21		20.13	0.42		0.39	0.29	**100.02**
7	44.08	35.26		19.89	0.55		0.21	0.22	**100.21**
8	43.60	34.80	0.12	19.77	0.71		0.31	0.25	**99.55**

Appendix LXXXVIII

1300 ˚C, 30 vol% CH_4, 120 min, site 2/2

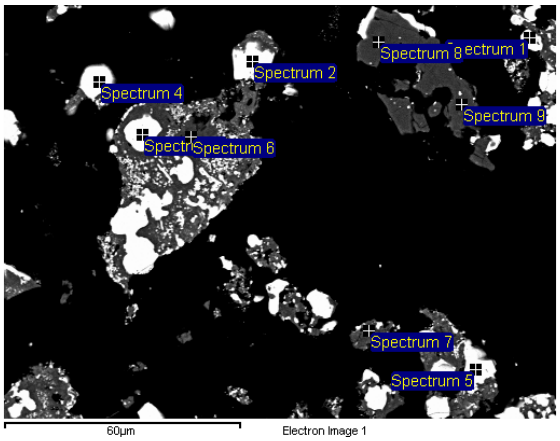

Spec.	O	Mg	Al	Si	Ca	Ti	Cr	Fe	Total
1						0.21	53.14	30.54	**83.89**
2						0.24	52.14	32.56	**84.94**
3						0.19	49.47	36.09	**85.75**
4	0.38					0.17	50.42	35.83	**86.81**
5	0.51					0.24	50.80	34.85	**86.40**
6	43.15	21.21	28.59	4.74	0.44		0.99	0.23	**99.35**
7	37.15	20.66	5.41	13.53	11.49		0.74	0.30	**89.27**
8	42.68	34.43	0.15	19.41	0.24		1.65	0.21	**98.78**
9	43.29	34.01	0.22	19.69	1.37		0.50	0.21	**99.29**

1350 ˚C, 10 vol% CH_4, 10 min, site 1/3

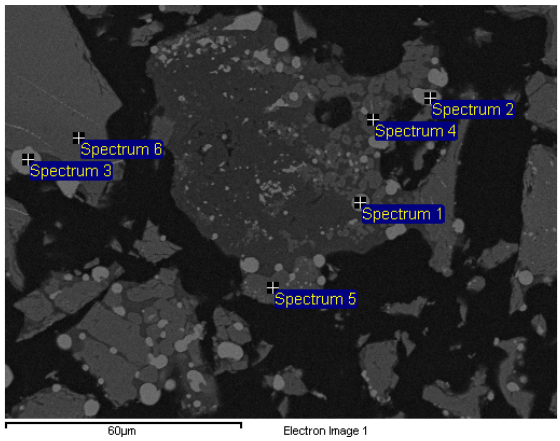

Spec.	O	Mg	Al	Si	Ca	Ti	Cr	Fe	Total
1							2.91	93.82	**96.74**
2	1.12						5.23	93.35	**99.70**
3	3.40	0.82	0.79				16.24	79.04	**100.28**
4	24.58	8.23	6.25	4.78	0.81	0.37	32.81	3.63	**81.46**
5	34.16	12.27	11.18	0.22		0.57	34.98	4.06	**97.44**
6	30.60	7.35	7.65				35.71	16.11	**97.42**

Appendix LXXXIX

1350 ˚C, 10 vol% CH_4, 10 min, site 2/3

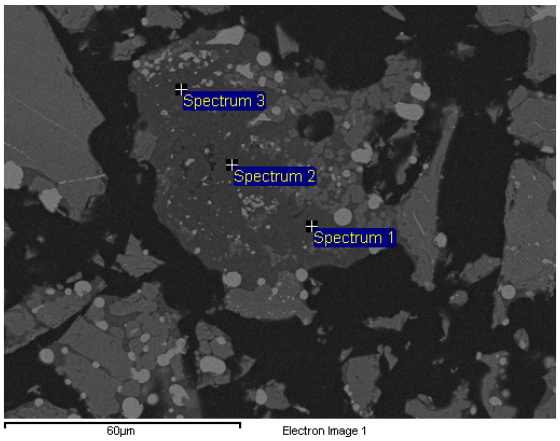

Spec.	O	Mg	Al	Si	Ca	Cr	Fe	Total
1	42.30	31.91		19.21		3.36	2.06	**98.84**
2	42.62	32.78	0.40	18.59	2.07		2.36	**98.82**
3	42.50	32.06	1.38	18.01	1.22	0.66	3.28	**99.11**

1350 ˚C, 10 vol% CH_4, 10 min, site 3/3

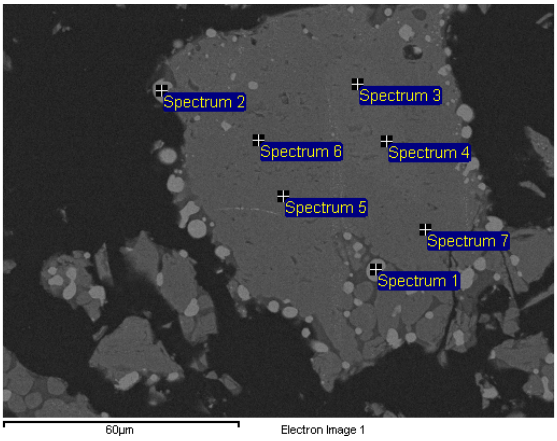

Spec.	O	Mg	Al	Ti	Cr	Fe	Total
1					8.24	90.94	**99.18**
2					8.86	90.27	**99.12**
3	29.51	6.02	7.86		32.59	18.16	**94.15**
4	30.00	5.92	7.81	0.35	32.31	19.03	**95.43**
5	32.24	8.27	8.33	0.47	40.08	8.48	**97.86**
6	32.30	8.30	8.50	0.41	39.65	7.93	**97.09**
7	31.64	8.90	8.27	0.56	39.59	7.16	**96.13**

Appendix XC

1350 ˚C, 10 vol% CH_4, 20 min, site 1/2

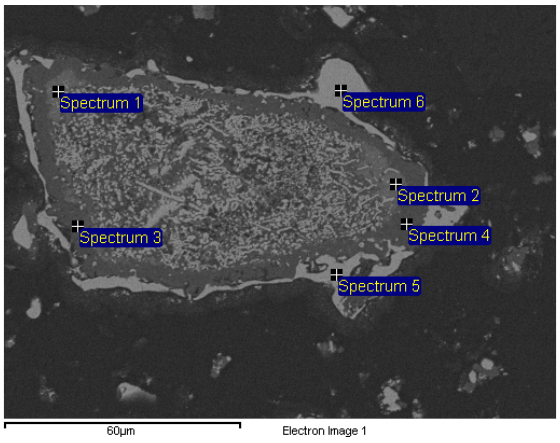

Spec.	O	Mg	Al	Si	Ca	Ti	Cr	Fe	Total
1	31.91	12.81	8.68			0.37	40.70	2.05	**96.53**
2	30.93	13.09	8.65			0.37	39.41	1.41	**93.86**
3	39.89	24.73	13.89	10.45	1.51	0.58	3.43	0.72	**95.21**
4	40.42	16.86	33.69			0.68	2.81		**94.45**
5							53.46	33.31	**86.77**
6							52.88	34.98	**87.86**

1350 ˚C, 10 vol% CH_4, 20 min, site 2/2

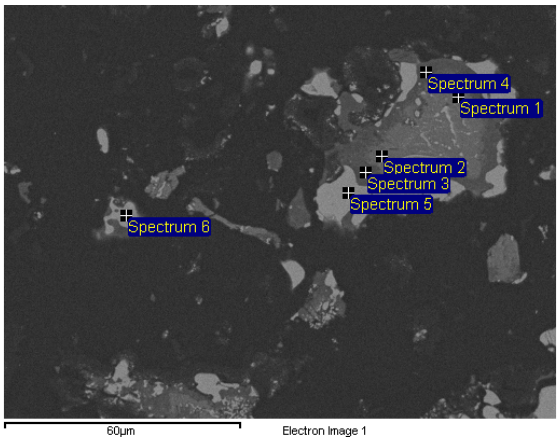

Spec.	O	Mg	Al	Si	Ca	Ti	Cr	Fe	Total
1	29.86	12.19	7.82			0.29	40.37	2.97	**93.50**
2	31.16	12.62	7.92			0.41	39.97	4.72	**96.80**
3	39.90	16.99	31.57	0.77	0.25	0.47	4.54		**94.47**
4	37.72	24.66	8.77	12.96	2.83		2.85		**89.80**
5							51.31	34.87	**86.18**
6							51.27	34.99	**86.25**

Appendix XCI

1350˚C, 10 vol% CH_4, 30 min, site 1/2

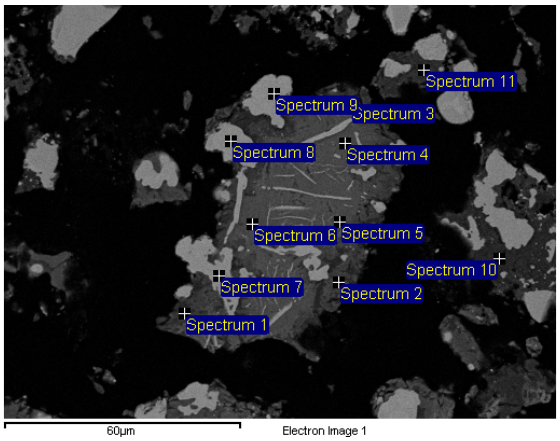

Spec.	O	Mg	Al	Si	Ca	Ti	Cr	Fe	Total
1	37.90	15.40	22.90	0.72	0.35	0.73	17.44	0.73	**96.18**
2	35.35	13.87	17.62	0.96	0.70	0.63	23.35		**92.47**
3	35.08	14.44	21.90	0.54	0.48	1.14	16.81		**90.38**
4	28.37	15.32	7.71			0.30	30.98	10.74	**93.42**
5	30.56	12.22	8.83	0.35	0.29	0.46	34.37	6.60	**93.70**
6	24.78	9.71	7.30			0.32	38.95	2.34	**83.41**
7				0.77			43.77	51.59	**96.13**
8	0.60			0.58			38.95	56.43	**96.57**
9	0.53			0.53			37.16	57.30	**95.52**
10	39.93	29.53	3.28	16.66	3.94		0.60		**93.95**
11	38.89	16.92	19.35	6.43	6.71	0.69	4.31		**93.31**

1350˚C, 10 vol% CH_4, 30 min, site 2/2

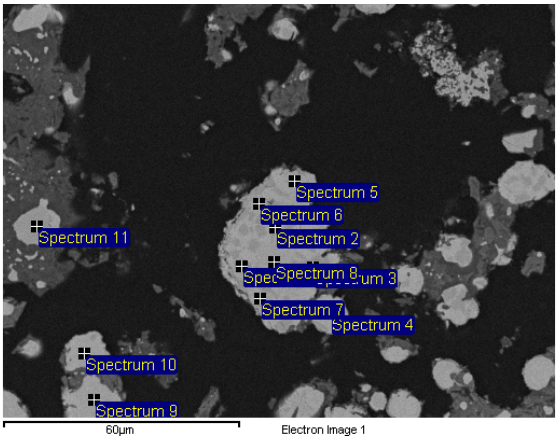

Spec.	O	Si	Cr	Fe	Total
1			73.74	10.04	**83.79**
2			72.22	10.95	**83.17**
3			72.41	11.03	**83.44**
4			69.68	12.93	**82.60**
5	0.66	0.38	34.36	59.13	**94.53**
6	0.59	0.51	34.92	58.43	**94.45**
7	0.61	0.44	34.93	58.02	**94.00**
8		0.20	48.75	40.97	**89.93**
9		0.85	45.14	48.76	**94.74**
10	0.49	0.64	42.85	50.46	**94.44**
11			71.19	12.76	**83.95**

Appendix XCII

1350 ˚C, 10 vol% CH_4, 60 min, site 1/3

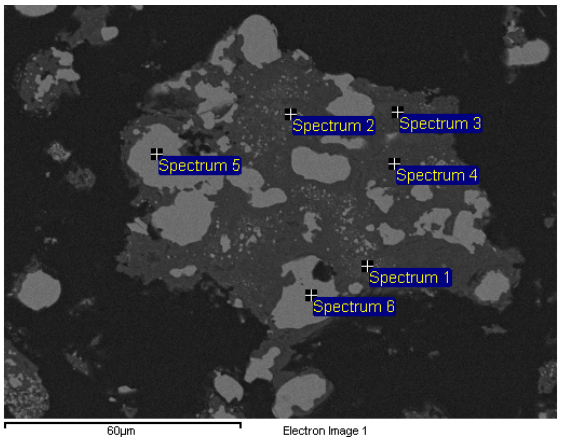

Spec.	O	Mg	Al	Si	Ca	Ti	Cr	Fe	Total
1	35.87	15.96	19.38	0.26		0.77	22.11		**94.35**
2	34.97	18.85	20.89	0.45	0.33	0.93	19.04	0.51	**95.98**
3	37.68	27.32	8.69	14.18	1.29		1.07		**90.23**
4	39.96	28.70	6.51	15.18	1.63	0.34	1.74		**94.06**
5							62.45	23.23	**85.68**
6	0.77						55.92	29.09	**85.78**

1350 ˚C, 10 vol% CH_4, 60 min, site 2/3

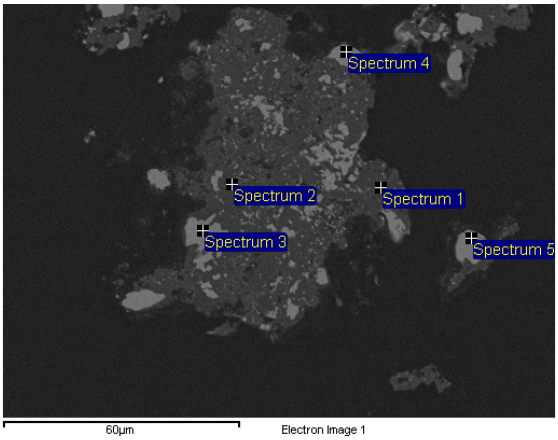

Spec.	O	Mg	Al	Si	Ca	Ti	Cr	Fe	Total
1	36.48	21.34	23.07	1.24	0.42	0.44	14.44	1.27	**98.70**
2	30.74	23.31	7.58	9.08	1.58		26.79	13.26	**112.36**
3							56.21	29.44	**85.65**
4							51.99	32.23	**84.22**
5						0.30	52.01	33.20	**85.51**

Appendix XCIII

1350 ˚C, 10 vol% CH_4, 60 min, site 3/3

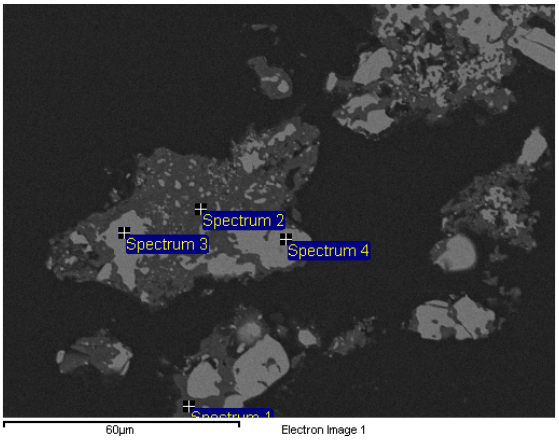

Spec.	O	Mg	Al	Si	Ca	Ti	Cr	Fe	Total
1	39.57	18.92	27.62	0.48	0.37	0.81	9.76		**97.53**
2	40.20	20.63	25.41	6.09	0.97		0.78		**94.08**
3							52.87	32.46	**85.33**
4							53.90	31.23	**85.13**

1350 ˚C, 10 vol% CH_4, 90 min, site 1/2

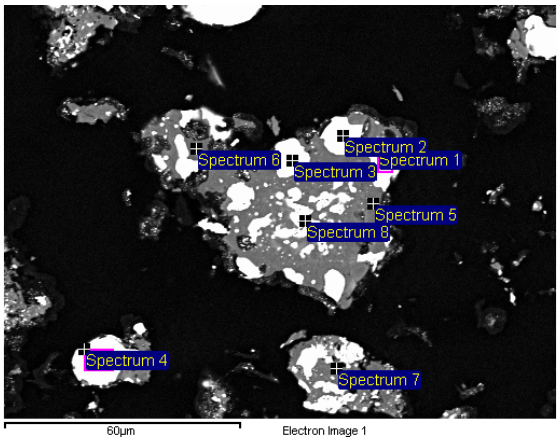

Spec.	O	Mg	Al	Si	Ca	Ti	Cr	Fe	Total
1	0.45			0.23			57.48	32.70	**90.86**
2						0.23	57.22	30.86	**88.32**
3	0.55				0.11	0.18	57.66	30.84	**89.35**
4						0.20	56.60	34.60	**91.40**
5	44.43	34.38	1.32	19.45	0.77		0.58		**100.94**
6	43.60	17.31	34.69	0.47	0.39	0.57	3.36	0.34	**100.73**
7	40.79	23.44	24.77	3.49	0.57	0.50	6.32	9.36	**109.24**
8	2.01	0.86	1.30	0.36		0.18	56.09	31.38	**92.16**

1350 ˚C, 10 vol% CH_4, 90 min, site 2/2

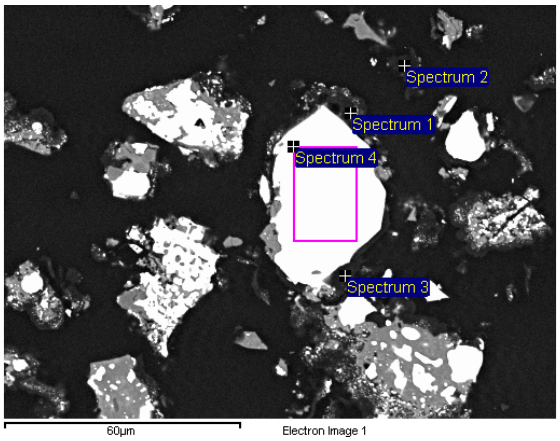

Spec.	O	Mg	Al	Si	Ca	Cr	Fe	Total
1	2.37	0.61	0.40	0.96	0.92	0.32	0.22	**5.79**
2	0.64					0.28	0.15	**1.06**
3	1.51				0.19	0.61		**2.31**
4	0.54					62.32	28.70	**91.55**

1350 ˚C, 10 vol% CH_4, 120 min, site 1/3

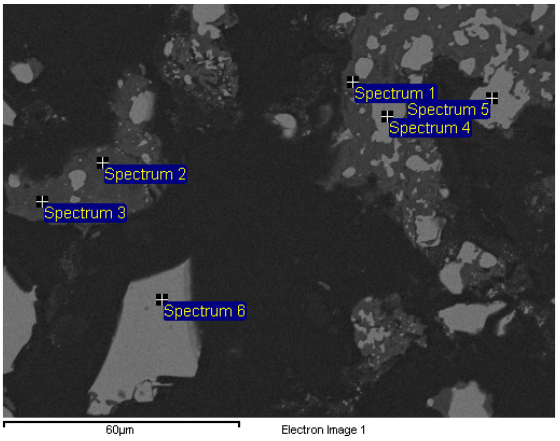

Spec.	O	Mg	Al	Si	Ca	Cr	Fe	Total
1	44.85	33.31	1.07	19.10	2.35	0.62		**101.30**
2	38.90	31.34	0.49	18.25	1.99	0.40		**91.38**
3	37.27	30.30	1.30	16.12	1.45	11.37	5.03	**102.83**
4						48.54	33.10	**81.64**
5						51.81	31.63	**83.45**
6						53.72	29.90	**83.62**

Appendix XCV

1350 ˚C, 10 vol% CH_4, 120 min, site 2/3

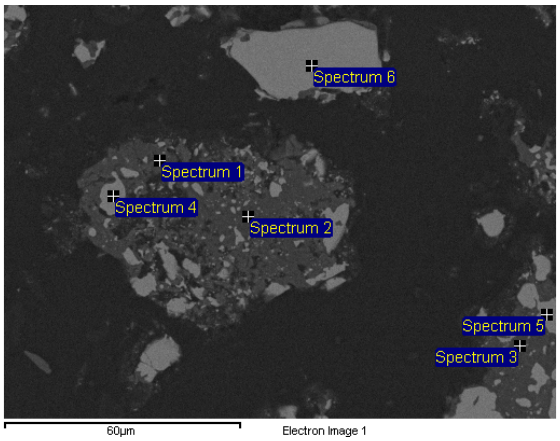

Spec.	O	Mg	Al	Si	Ca	Ti	Cr	Fe	Total
1	35.66	20.00	16.77	6.82	0.71		2.72	1.15	**83.84**
2	37.85	27.22	6.19	13.28	1.47	0.30	1.67	1.11	**89.09**
3	38.97	25.44	10.85	11.80	3.10		1.13		**91.30**
4						0.29	53.06	30.93	**84.29**
5							50.18	31.73	**81.91**
6							52.83	30.68	**83.51**

1350 ˚C, 10 vol% CH_4, 120 min, site 3/3

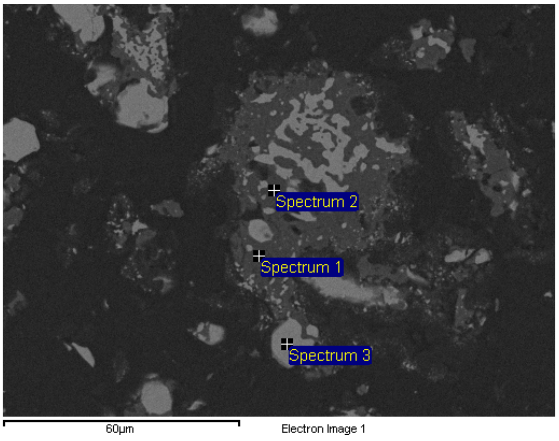

Spec.	O	Mg	Al	Si	Ca	Ti	Cr	Fe	Total
1	40.36	29.89	3.30	15.97	1.97		5.66	2.55	**99.71**
2	40.72	30.24	2.17	16.65	2.60		0.66	0.54	**93.59**
3						0.30	51.46	31.01	**82.77**

Appendix XCVI

1350 ˚C, 20 vol% CH_4, 10 min, site 1/2

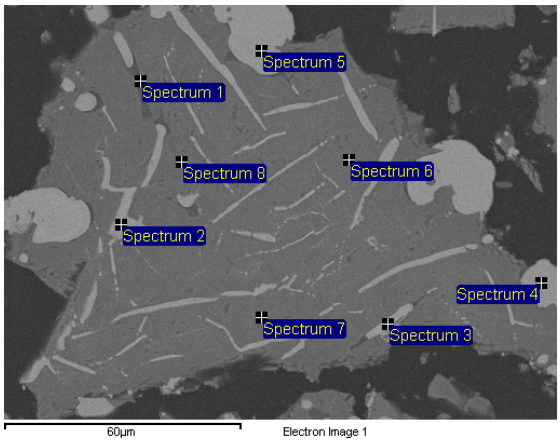

Spec.	O	Mg	Al	Si	Ca	Ti	Cr	Fe	Total
1	41.19	2.75	10.05	21.30	5.11	0.67	11.91		**92.98**
2	4.19	0.88	1.35				26.75	56.83	**90.01**
3	5.64	1.82	1.73	0.42			27.05	60.02	**96.68**
4	0.77			0.24			21.51	73.62	**96.15**
5	0.81			0.33			25.01	70.67	**96.83**
6	31.35	10.37	8.19			0.41	41.90	2.04	**94.26**
7	29.34	9.72	7.99			0.28	40.77	3.49	**91.60**
8	33.47	10.90	8.71			0.49	42.32	2.04	**97.93**

1350 ˚C, 20 vol% CH_4, 10 min, site 2/2

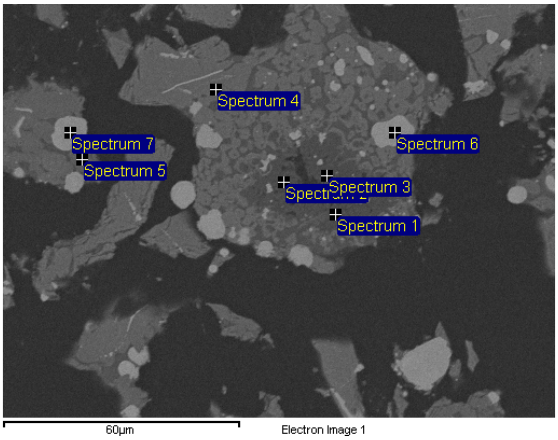

Spec.	O	Mg	Al	Si	Ca	Ti	Cr	Fe	Total
1	36.23	32.96	0.84	15.29	0.94		1.64	1.59	**89.50**
2	36.84	54.47	0.26	1.38			5.35	1.91	**100.22**
3	35.89	53.46		1.31			4.27	1.83	**96.76**
4	31.57	12.37	8.13			0.46	40.99	0.75	**94.28**
5	33.50	12.92	11.62			0.35	36.49	0.79	**95.67**
6	0.85			0.28			19.62	74.95	**95.70**
7							41.56	47.48	**89.04**

Appendix XCVII

1350 ˚C, 20 vol% CH_4, 20 min, site 1/2

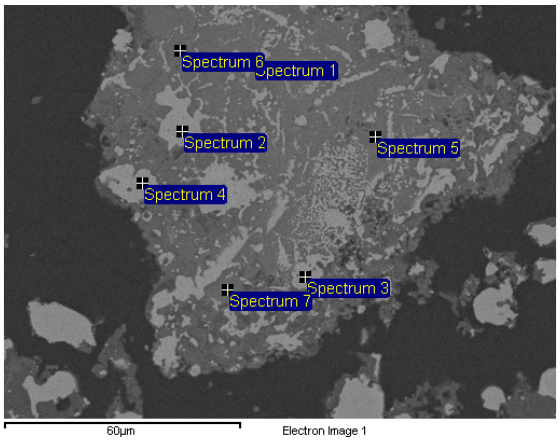

Spec.	O	Mg	Al	Si	Ti	Cr	Fe	Total
1	0.78			0.36		39.44	54.47	**95.05**
2						56.28	35.00	**91.28**
3	0.59			0.28		38.80	57.11	**96.79**
4	0.66					57.83	33.62	**92.11**
5	33.05	11.18	8.79		0.43	38.86	1.31	**93.61**
6	34.64	12.11	9.31		0.46	38.45	1.11	**96.09**
7	34.11	12.79	8.88		0.52	39.10	1.85	**97.25**

1350 ˚C, 20 vol% CH_4, 20 min, site 2/2

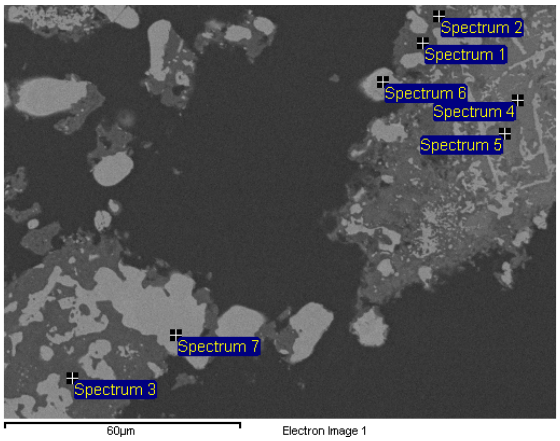

Spec.	O	Mg	Al	Si	Ca	Ti	Cr	Fe	Total
1	43.34	18.81	29.79	2.51		0.32	2.67		**97.43**
2	36.55	20.61	19.47	5.64	0.46	0.31	5.51		**88.54**
3	41.46	31.03	1.11	16.94	4.62	0.31	0.81		**96.29**
4	32.29	11.33	7.72			0.34	40.30	1.32	**93.30**
5	31.45	11.17	7.57			0.37	39.86	3.81	**94.22**
6							63.39	20.65	**84.03**
7							55.46	28.92	**84.38**

Appendix XCVIII

1350˚C, 20 vol% CH_4, 30 min

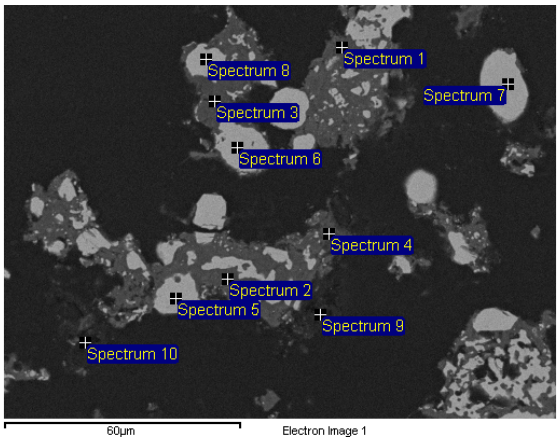

Spec.	O	Mg	Al	Si	Ca	Ti	Cr	Fe	Total
1	36.59	18.58	24.76	4.68	0.77	0.34	2.44	1.59	**89.75**
2	31.81	23.74	9.24	11.00	2.19		1.52	0.49	**79.97**
3	36.97	18.74	28.39	0.47	0.36	0.85	2.78		**88.56**
4	32.08	21.31	12.86	10.34	2.13	0.20	1.22	0.36	**80.49**
5						0.24	53.28	29.23	**82.75**
6							51.82	29.83	**81.65**
7	0.48						57.91	23.04	**81.43**
8	0.49						51.68	29.18	**81.35**
9	0.24	0.27	0.26	0.37	0.46		3.94	2.42	**7.97**
10	1.22	0.18	0.28	0.39	0.26		0.61	0.29	**3.23**

1350 ˚C, 20 vol% CH_4, 60 min, site 1/2

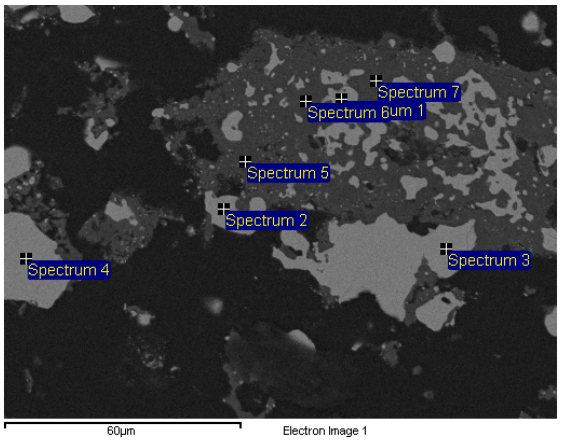

Spec.	O	Mg	Al	Si	Ca	Ti	Cr	Fe	Total
1						0.36	56.13	29.50	**85.98**
2						0.28	55.64	30.49	**86.41**
3							57.21	28.58	**85.79**
4							66.08	22.40	**88.47**
5	39.55	22.00	25.02	3.69	0.47	0.46	7.51	0.67	**99.37**
6	41.27	29.16	6.06	15.00	2.56		0.70		**94.75**
7	41.21	28.60	6.73	14.22	2.59		0.58		**93.93**

Appendix XCIX

1350 ˚C, 20 vol% CH_4, 60 min, site 2/2

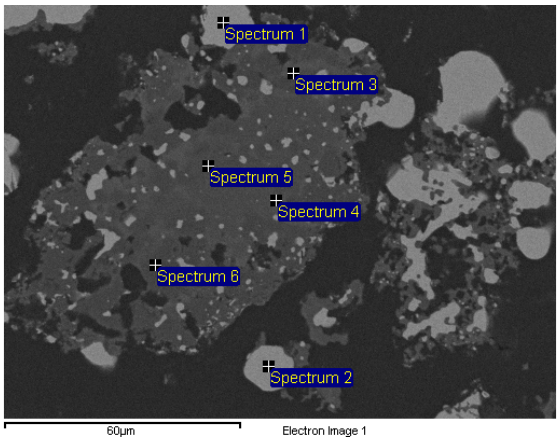

Spec.	O	Mg	Al	Si	Ca	Ti	Cr	Fe	Total
1							56.53	29.89	**86.42**
2						0.30	64.11	22.27	**86.68**
3	39.46	19.64	2.44	15.60	17.43		0.67	0.61	**95.85**
4	39.41	23.35	0.32	15.81	18.12				**97.01**
5	43.15	30.72	0.72	18.56	4.74				**97.88**
6	37.11	60.03							**97.14**

1350 ˚C, 20 vol% CH_4, 90 min, site 1/2

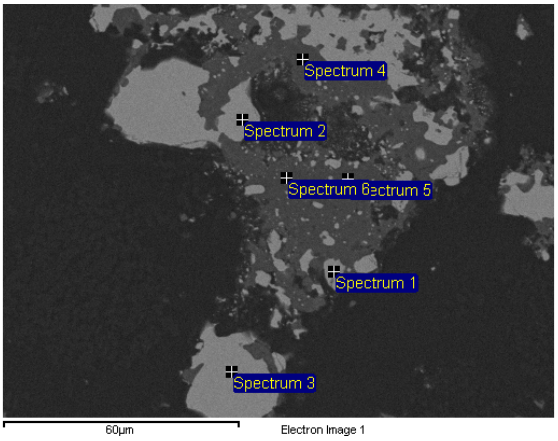

Spec.	O	Mg	Al	Si	Ca	Ti	Cr	Fe	Total
1							55.16	27.59	**82.74**
2							56.75	26.46	**83.21**
3						0.26	58.19	26.65	**85.10**
4	40.67	16.56	29.99	2.43	1.18		2.62	0.77	**94.22**
5	42.12	29.46	5.59	16.17	2.31		1.34		**96.99**
6	43.02	17.50	32.32	0.53		0.51	3.81	0.55	**98.24**

Appendix C

1350 ˚C, 20 vol% CH_4, 90 min, site 2/2

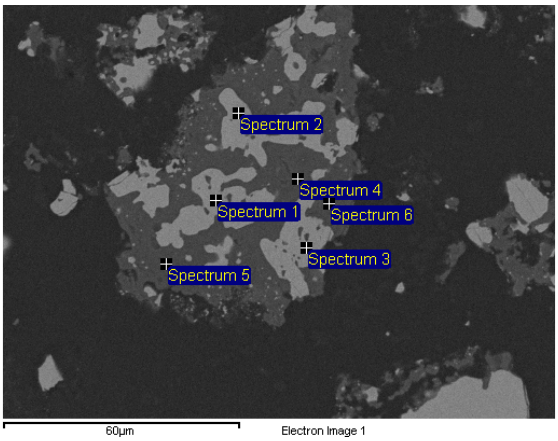

Spec.	O	Mg	Al	Si	Ca	Ti	Cr	Fe	Total
1							57.15	26.10	**83.25**
2							56.28	25.26	**81.55**
3							56.72	26.03	**82.75**
4	40.94	28.77	6.30	15.56	2.33		0.81		**94.71**
5	43.92	24.16	20.59	7.69	1.56	0.41	2.28	0.55	**101.16**
6	39.36	30.97	3.02	14.87	2.45		0.51		**91.18**

1350 ˚C, 20 vol% CH_4, 120 min, site 1/3

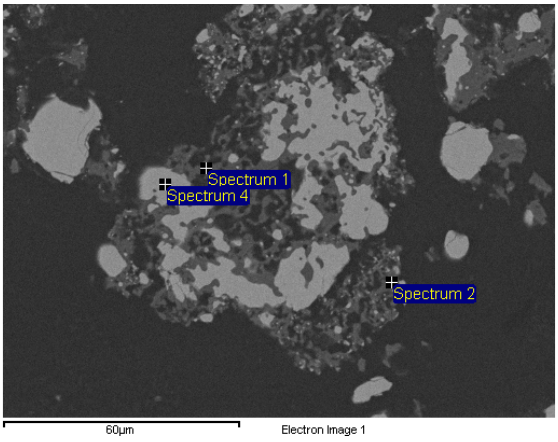

Spec.	O	Mg	Al	Si	Ti	Cr	Fe	Total
1	39.00	16.49	29.38		0.82	2.61		**88.31**
2	38.06	15.35	30.76	0.28		1.63	0.49	**86.57**
4						55.12	23.36	**78.47**

Appendix CI

1350 ˚C, 20 vol% CH_4, 120 min, site 2/3

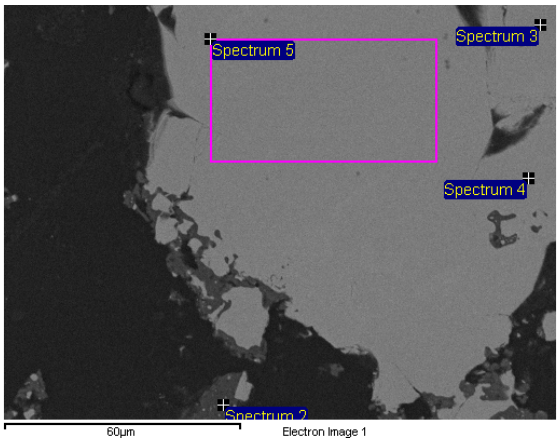

Spec.	O	Mg	Al	Ti	Cr	Fe	Total
2	38.59	15.33	30.30	0.47	2.59	0.38	**87.67**
3					60.99	15.15	**76.14**
4					50.58	25.32	**75.90**
5					55.81	21.30	**77.11**

1350 ˚C, 20 vol% CH_4, 120 min, site 3/3

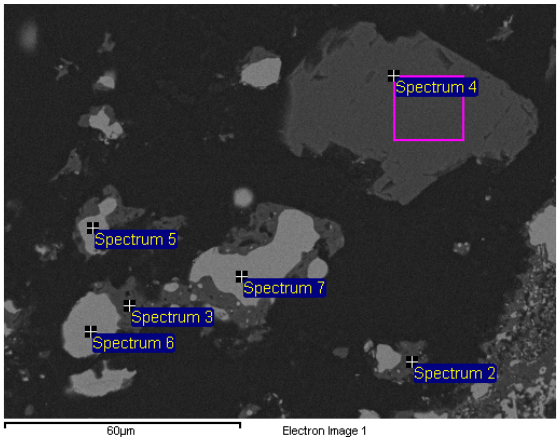

Spec.	O	Mg	Al	Si	Ca	Ti	Cr	Fe	Total
2	37.74	16.36	27.18	0.21	0.20	0.79	3.92		**86.40**
3	37.61	14.86	28.51	0.16		0.81	4.08	0.53	**86.55**
4	36.89	27.35		16.26			0.36	5.11	**85.98**
5							51.89	24.75	**76.64**
6							54.54	21.77	**76.31**
7							55.16	21.15	**76.30**

Appendix CII

1350 ˚C, 30 vol% CH_4, 10 min, site 1/3

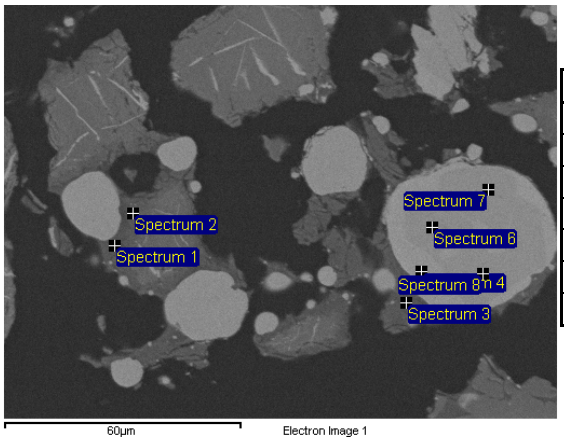

Spec.	O	Mg	Al	Si	Ca	Ti	Cr	Fe	Total
1	43.32	18.88	5.14	22.10	4.77	0.57	4.34	0.63	**99.76**
2	41.12	13.05	8.51	16.12	4.89	0.94	8.99	1.08	**94.70**
3	42.06	8.92	10.85	16.23	5.09	1.09	10.21	0.90	**95.36**
4	0.68			0.29			19.84	74.90	**95.70**
6							56.80	28.92	**85.71**
7							58.64	26.80	**85.45**
8							57.46	28.80	**86.26**

1350 ˚C, 30 vol% CH_4, 10 min, site 2/3

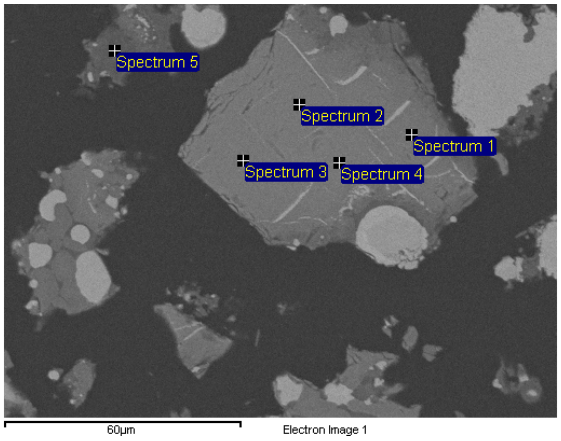

Spec.	O	Mg	Al	Si	Ca	Ti	Cr	Fe	Total
1	30.07	8.15	7.39			0.28	32.29	15.61	**93.78**
2	29.46	5.84	7.49			0.26	32.27	17.40	**92.73**
3	30.27	5.87	7.42				32.03	18.31	**93.90**
4	29.49	5.74	7.51				32.88	17.77	**93.39**
5	23.85	18.65	3.09	12.47	0.97		3.54		**62.57**

Appendix CIII

1350 ˚C, 30 vol% CH_4, 10 min, site 3/3

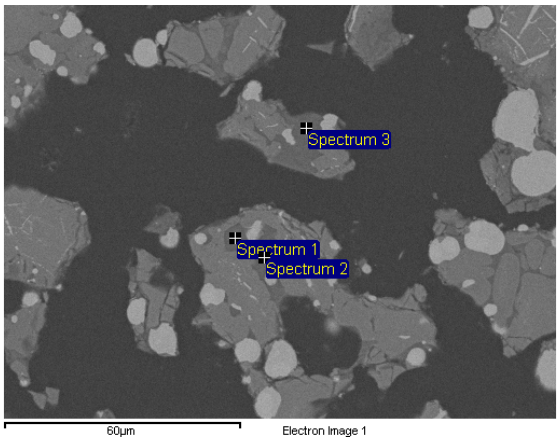

Spec.	O	Mg	Al	Si	Ca	Ti	Cr	Fe	Total
1	41.36	2.12	9.91	22.71	6.28	0.74	7.49	0.57	**91.19**
2	41.29	1.96	9.85	22.04	6.33	0.78	8.03	0.55	**90.82**
3	33.95	6.04	7.15	20.52	4.77	0.67	6.40	0.48	**79.98**

1350˚C, 30 vol% CH_4, 20 min, site 1/2

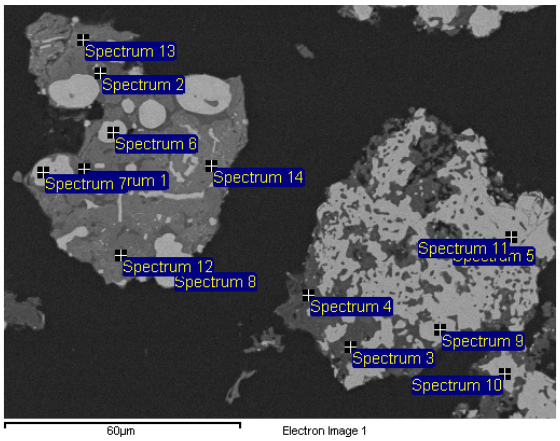

Spec.	O	Mg	Al	Si	Ca	Ti	Cr	Fe	Total
1	38.33	7.99	4.95	21.31	6.91	0.52	6.70		**86.70**
2	39.39	9.27	5.54	21.93	4.90	0.61	6.69	0.39	**88.73**
3	28.62	15.66	19.61	2.62	0.87	0.70	5.31	7.87	**81.26**
4	40.86	20.02	7.85	11.93	13.52		1.90	0.62	**96.71**
5	37.25	15.51	27.87	2.17	2.66	0.35	1.76	0.41	**88.00**
6	0.62			0.37			24.93	64.98	**90.89**
7				0.37			36.11	50.98	**87.45**
8							42.49	43.59	**86.08**
9	0.56						57.22	23.90	**81.69**
10						0.28	61.27	18.41	**79.96**
11							56.70	23.42	**80.12**
12	33.05	12.19	12.74	2.16	0.79	0.47	27.13	0.49	**89.02**
13	21.66	8.89	6.52	0.35		0.43	33.07	22.15	**93.07**
14	28.09	11.47	6.87			0.34	38.78	2.89	**88.44**

Appendix CIV

1350˚C, 30 vol% CH_4, 20 min, site 2/2

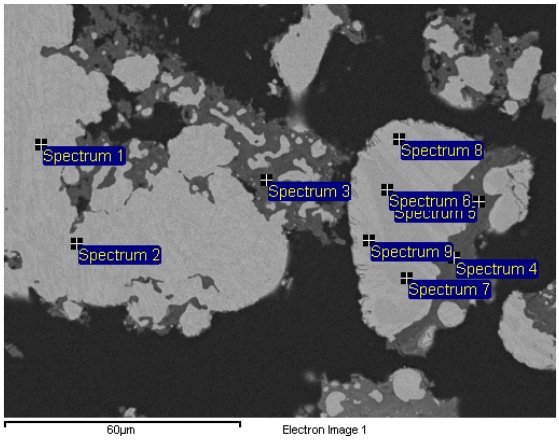

Spec.	O	Mg	Al	Si	Ca	Ti	Cr	Fe	Total
1	0.63			2.06			39.76	48.79	**91.24**
2							68.62	11.93	**80.55**
3	38.15	19.60	11.88	8.36	11.23	0.78	2.33	0.99	**93.32**
4	36.13	14.19	29.18	1.33	1.31	0.81	3.41		**86.37**
5	32.96	9.55	22.43	6.71	5.93	1.05	4.54		**83.18**
6							70.22	10.33	**80.55**
7	0.52						65.80	15.16	**81.48**
8				3.13			35.35	50.50	**88.99**
9				3.39			35.78	50.24	**89.40**

1350 ˚C, 30 vol% CH_4, 30 min, site 1/2

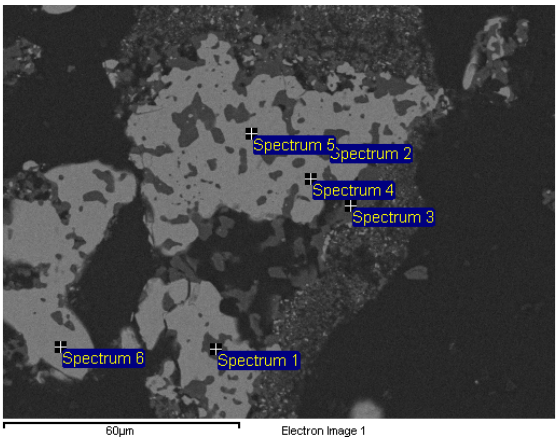

Spec.	O	Mg	Al	Si	Ca	Ti	Cr	Fe	Total
1	39.39	15.84	33.94	0.83	1.14		0.96		**92.10**
2	27.95	14.21	31.15	0.55	0.50		1.38		**75.74**
3	39.59	15.97	33.09	0.59	1.40		2.03	0.79	**93.46**
4			0.23	0.59		0.30	58.25	26.58	**85.95**
5						0.34	58.94	27.06	**86.34**
6	4.55	2.41	4.95				49.93	21.92	**83.76**

Appendix CV

1350 ˚C, 30 vol% CH_4, 30 min, site 2/2

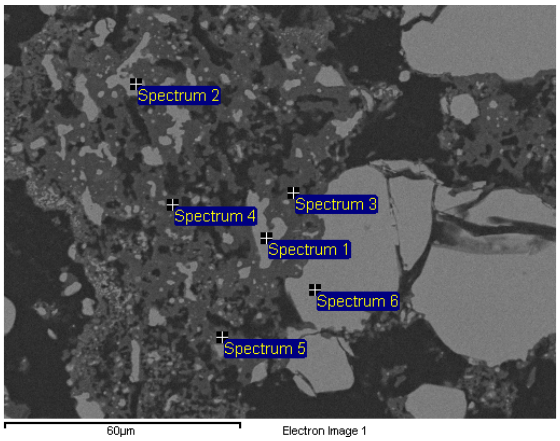

Spec.	O	Mg	Al	Si	Ca	Ti	Cr	Fe	Total
1		0.30	0.27			0.28	62.65	19.58	**83.09**
2	5.45	4.03	5.34			0.43	54.84	16.69	**86.77**
3	34.36	12.84	24.57	5.70	6.15	0.33	4.24	0.65	**88.84**
4	30.86	14.01	20.48	3.00	4.28	0.30	1.80	1.13	**75.87**
5	6.82	3.76	5.13	0.45	0.33	0.27	8.07	2.47	**27.31**
6							61.86	22.14	**84.00**

1350 ˚C, 30 vol% CH_4, 60 min, site 1/2 – categorized as a failed experiment

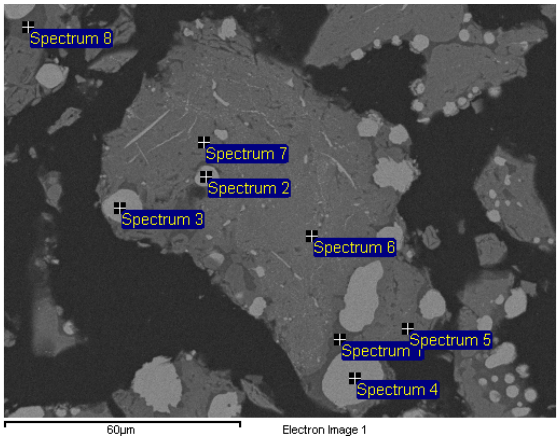

Spec.	O	Mg	Al	Si	Ca	Ti	Cr	Fe	Total
1	41.47	6.06	8.13	22.63	5.08	0.64	6.29		**90.30**
2	1.24			0.31			17.80	73.85	**93.19**
3	0.61						29.87	59.03	**89.51**
4							37.56	49.52	**87.08**
5	31.80	10.90	7.99			0.50	38.87	1.95	**92.01**
6	29.74	7.79	7.68				32.92	14.45	**92.59**
7	34.72	12.10	8.24			0.29	38.79	5.35	**99.48**
8	39.68	3.02	7.37	18.58	5.99	0.65	7.12	0.50	**82.90**

Appendix CVI

1350 ˚C, 30 vol% CH_4, 60 min, site 2/2 – categorized as a failed experiment

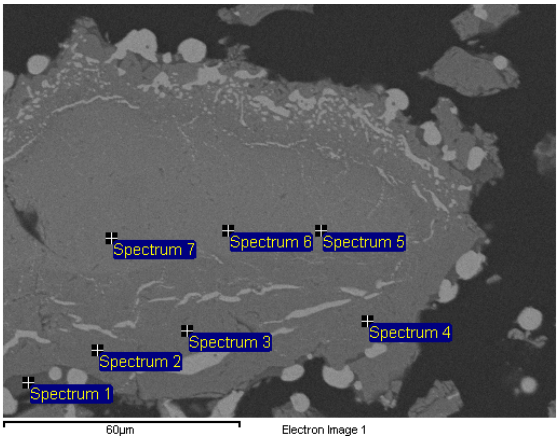

Spec.	O	Mg	Al	Si	Ca	Ti	Cr	Fe	Total
1	42.30	1.02	11.48	22.66	5.79	0.75	7.14	1.20	**92.34**
2	31.47	7.38	9.12			0.42	37.30	6.14	**91.83**
3	31.21	7.21	8.76			0.32	38.28	6.28	**92.05**
4	30.91	7.84	8.68			0.36	37.73	6.24	**91.75**
5	27.67	1.71	7.40			0.29	27.18	26.32	**90.57**
6	27.83	1.58	7.41			0.30	27.36	26.13	**90.62**
7	27.58	1.63	7.75				27.38	26.31	**90.65**

1350 ˚C, 30 vol% CH_4, 90 min, site 1/2

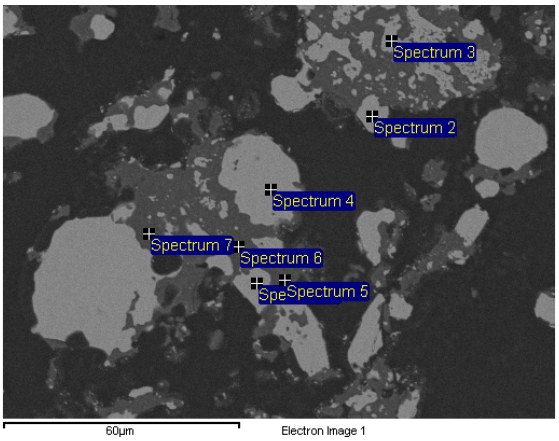

Spec.	O	Mg	Al	Si	Ca	Ti	Cr	Fe	Total
1							49.74	34.00	**83.73**
2	0.66					0.32	55.41	29.40	**85.79**
3						0.29	53.37	29.12	**82.77**
4						0.32	55.63	29.44	**85.39**
5	38.50	16.15	30.54	0.87		0.34	11.47	11.03	**108.90**
6	42.45	31.29	2.81	17.18	1.76		0.84	0.60	**96.92**
7	41.65	24.74	16.21	10.19	0.94		0.83		**94.57**

Appendix CVII

1350 ˚C, 30 vol% CH_4, 90 min, site 2/2

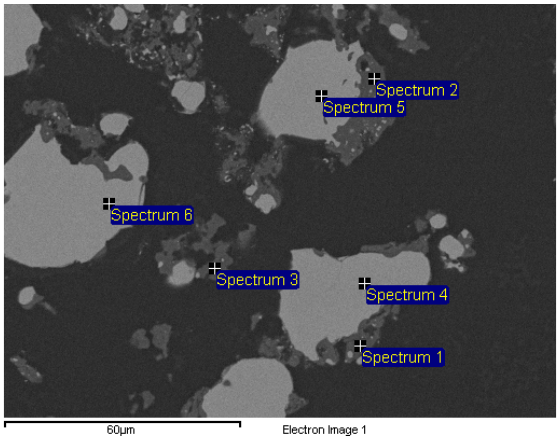

Spec.	O	Mg	Al	Si	Ca	Ti	Cr	Fe	Total
1	39.63	14.52	32.06	0.27	0.19		2.95	0.84	**90.46**
2	41.05	22.76	11.28	11.86	4.32	0.27	1.19		**92.73**
3	41.80	16.57	31.68	0.19		0.94	4.46		**95.66**
4							66.10	17.87	**83.97**
5							56.34	27.43	**83.77**
6						0.31	59.16	24.74	**84.21**

1350 ˚C, 30 vol% CH_4, 120 min, site 1/3

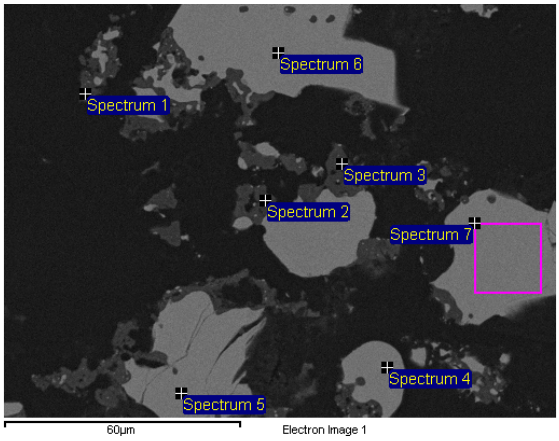

Spec.	O	Mg	Al	Si	Ti	Cr	Fe	Total
1	32.56	12.13	28.63			8.35		**81.67**
2	33.84	15.32	26.03		0.80	8.46		**84.44**
3	33.83	13.49	26.61		0.91	4.56	0.40	**79.80**
4						52.97	21.91	**74.88**
5				5.25	0.27	40.77	29.52	**75.81**
6						52.04	21.72	**73.76**
7						51.92	21.40	**73.32**

Appendix CVIII

1350 ˚C, 30 vol% CH_4, 120 min, site 2/3

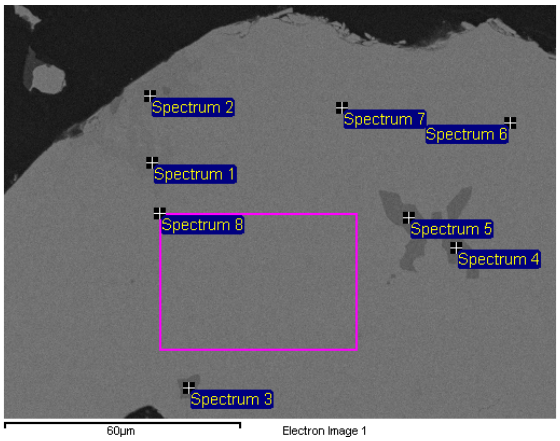

Spec.	O	Al	Si	Ti	Cr	Fe	Total
1			14.46	0.98	37.48	25.78	**78.69**
2			14.39	0.85	37.62	25.57	**78.43**
3				32.18	33.57	1.25	**66.99**
4				33.56	30.76	0.97	**65.28**
5				31.09	33.95	1.05	**66.10**
6			8.53	0.38	30.48	37.39	**76.78**
7		0.43	9.81		22.05	47.53	**79.82**
8	0.67	0.33	7.27	0.32	29.82	39.98	**78.39**

1350 ˚C, 30 vol% CH_4, 120 min, site 3/3

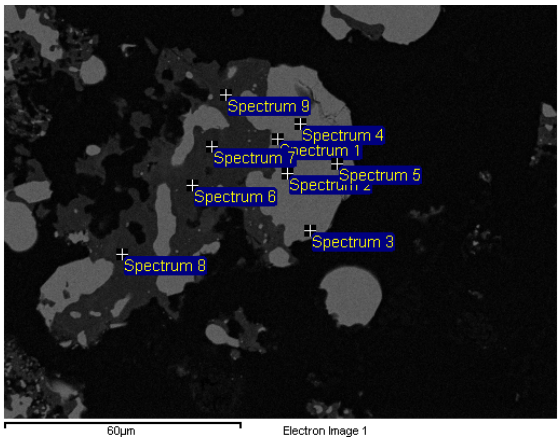

Spec.	O	Mg	Al	Si	Ca	Ti	Cr	Fe	Total
1	0.67			13.03			20.16	46.00	**79.85**
2	0.70			12.86		0.25	16.00	51.43	**81.24**
3				12.92			15.32	51.73	**79.97**
4							52.64	19.98	**72.62**
5							55.93	16.41	**72.34**
6	34.00	28.17	0.69	14.60	2.31		0.35	0.36	**80.48**
7	34.71	26.00	2.87	12.54	5.41		0.45		**81.97**
8	32.74	20.99	13.83	8.52	1.17		0.89	0.38	**78.52**
9	33.57	13.98	28.86	0.26			0.70		**77.36**

Appendix CIX

1300 ˚C, 99,9995 wt% C, 120 min, site 1/3

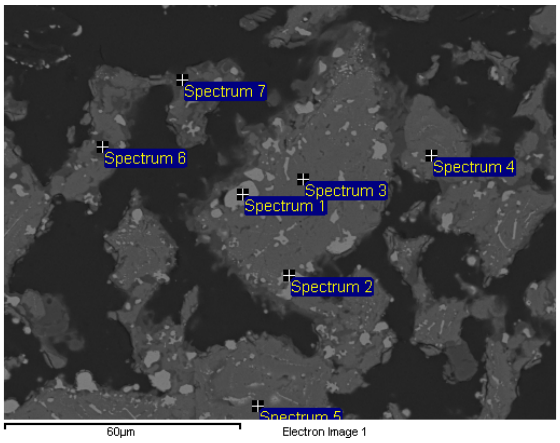

Spec.	O	Mg	Al	Si	Ca	Ti	Cr	Fe	Total
1	0.67						17.99	78.84	**97.50**
2	0.64			0.10			17.25	80.43	**98.41**
3	33.97	14.47	8.42			0.28	36.87	3.28	**97.29**
4	35.21	13.38	8.71			0.30	39.86	1.59	**99.06**
5	33.07	16.42	7.88			0.29	34.19	8.28	**100.13**
6	41.45	31.43		18.66	0.24		3.26	0.36	**95.40**
7	41.53	30.05	0.46	17.70	0.58		2.83	0.32	**93.46**

1300 ˚C, 99,9995 wt% C, 120 min, site 2/3

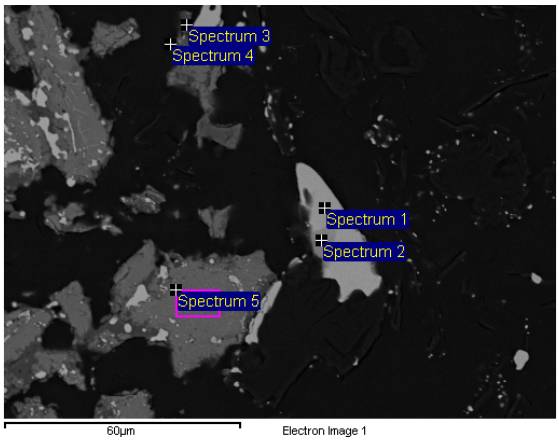

Spec.	O	Mg	Al	Si	Ca	Ti	Cr	Fe	Total
1	0.33						54.73	32.85	**87.91**
2	0.13						49.37	28.51	**78.01**
3	46.20	17.33	37.21	0.14			1.65	0.29	**102.82**
4	57.57	22.12	18.08	2.30	0.21	0.64	27.31	0.30	**128.54**
5	33.96	12.96	8.63			0.39	39.80	4.06	**99.79**

Appendix CX

1300 ˚C, 99,9995 wt% C, 120 min, site 3/3

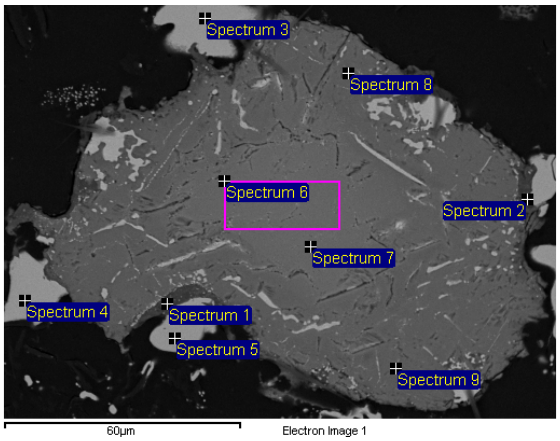

Spec.	O	Mg	Al	Si	Ca	Ti	Cr	Fe	Total
1	48.99	14.26	41.43	0.29	0.15		1.96	0.43	**107.50**
2	33.37	12.87	27.38			1.08	20.56	1.74	**97.01**
3	0.26					0.13	50.65	37.05	**88.09**
4	0.23					0.20	53.98	34.64	**89.05**
5	0.38					0.12	54.65	33.98	**89.14**
6	32.21	6.62	7.28			0.34	34.24	18.65	**99.33**
7	31.45	6.58	7.06			0.37	34.72	17.75	**97.94**
8	33.91	12.42	7.64			0.38	41.53	1.27	**97.16**
9	35.14	12.99	7.99			0.40	40.58	4.03	**101.12**

1300 ˚C, 99,99 vol% H_2, 120 min, site 1/3

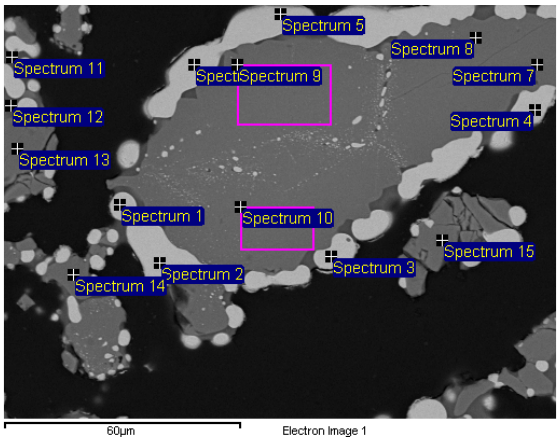

Spec.	O	Mg	Al	Si	Ca	Ti	Cr	Fe	Total
1	0.52			0.44			30.07	63.86	**94.89**
2	0.48			0.52			30.02	63.54	**94.56**
3	0.52			0.51			29.75	63.13	**93.91**
4	0.47			0.51			29.40	62.28	**92.66**
5	0.51			0.45			29.12	62.46	**92.54**
6	0.55			0.48			29.74	63.21	**93.97**
7	33.76	11.98	11.22			0.41	35.08	0.59	**93.05**
8	31.63	11.38	10.46				35.67	0.60	**89.74**
9	32.92	11.36	9.15			0.46	38.89	0.87	**93.65**
10	34.79	11.91	10.00			0.43	38.22	0.92	**96.28**
11	28.28	2.14	6.43	16.50	4.80	0.60	9.21	1.74	**69.70**
12	26.67	10.12	9.95	0.41		0.42	34.06	1.59	**83.22**
13	33.27	12.01	11.45			0.46	35.57	0.63	**93.39**
14	41.58	14.18	14.12				34.79	0.70	**105.36**
15	37.59	13.05	12.12	0.09		0.39	35.39	0.84	**99.46**

Appendix CXI

1300 ˚C, 99,99 vol% H_2, 120 min, site 2/3

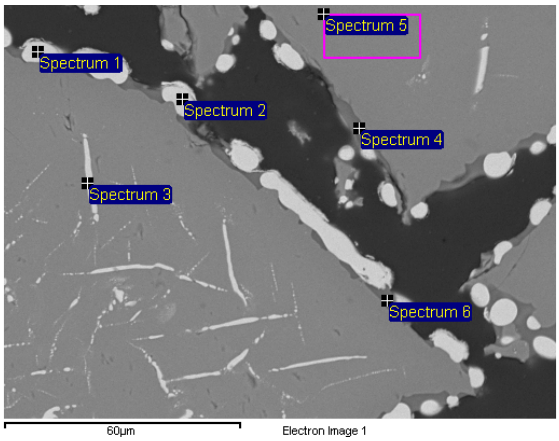

Spec.	O	Mg	Al	Si	Ca	Ti	Cr	Fe	Total
1	0.44			0.44			30.50	61.90	**93.28**
2	0.49			0.41			29.95	61.46	**92.31**
3	22.75	9.28	6.10			0.28	36.47	26.64	**101.52**
4	61.94	4.33	10.86	26.27	6.26	0.62	7.85	0.78	**118.90**
5	33.67	11.53	9.81			0.46	37.84	0.71	**94.03**
6	26.55	2.77	5.68	11.29	3.90	0.42	14.07	0.37	**65.06**

1300 ˚C, 99,99 vol% H_2, 120 min, site 3/3

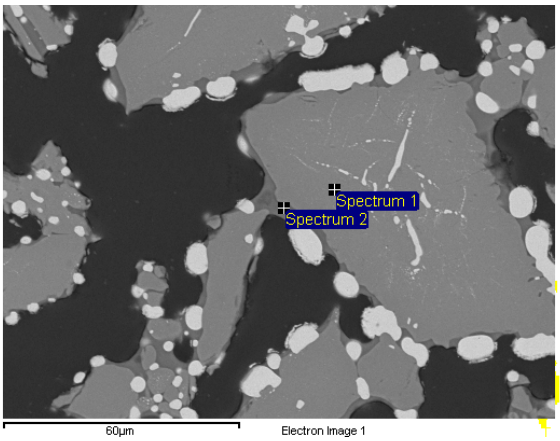

Spec.	O	Mg	Al	Si	Ca	Ti	Cr	Fe	Total
1	33.65	11.67	8.64			0.46	39.77	0.70	**94.89**
2	48.92	4.28	9.60	24.64	6.41	0.56	7.18	0.42	**101.99**

Appendix CXII

Raw material; chromite ore, site 1/2

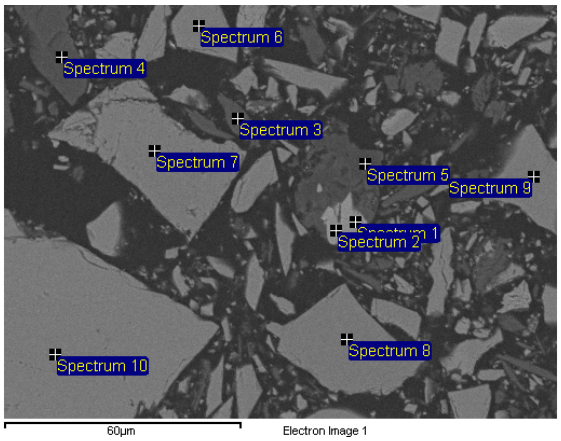

Spec.	O	Mg	Al	Si	Ti	Cr	Fe	Total
1	25.28					2.99	66.87	**95.14**
2	26.20			0.38		2.83	66.81	**96.22**
3	48.89	18.85	0.99	25.95		1.03	0.77	**96.48**
4	34.95	20.86				0.81	10.96	**67.58**
5	38.20	23.61				0.62	6.30	**68.73**
6	32.36	6.28	7.49			33.99	16.96	**97.08**
7	32.98	5.81	7.18		0.34	32.81	18.70	**97.82**
8	32.01	6.86	7.52			34.35	15.47	**96.21**
9	32.43	6.26	7.20			33.86	16.66	**96.40**
10	32.87	5.31	6.73		0.36	34.28	18.78	**98.34**

Raw material; chromite ore, site 2/2

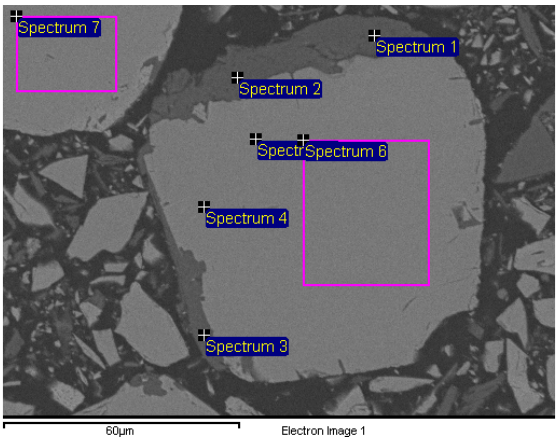

Spec.	O	Mg	Al	Si	Ti	Cr	Fe	Total
1	47.07	19.79	6.09	13.34		4.59	0.74	**91.62**
2	46.22	19.40	5.97	13.12		5.41	0.59	**90.71**
3	47.85	19.85	6.92	13.27		5.17	0.79	**93.86**
4	31.46	6.17	7.15			32.49	16.07	**93.33**
5	30.24	5.87	6.94			32.02	16.13	**91.20**
6	31.22	6.03	6.94		0.26	32.45	16.61	**93.52**
7	31.47	5.33	7.46		0.38	31.40	17.90	**93.95**

Appendices – XRD patterns and Rietveld analyses

Appendix CXIII

Sample: 1100 ˚C, 10 vol% CH_4, 10 min

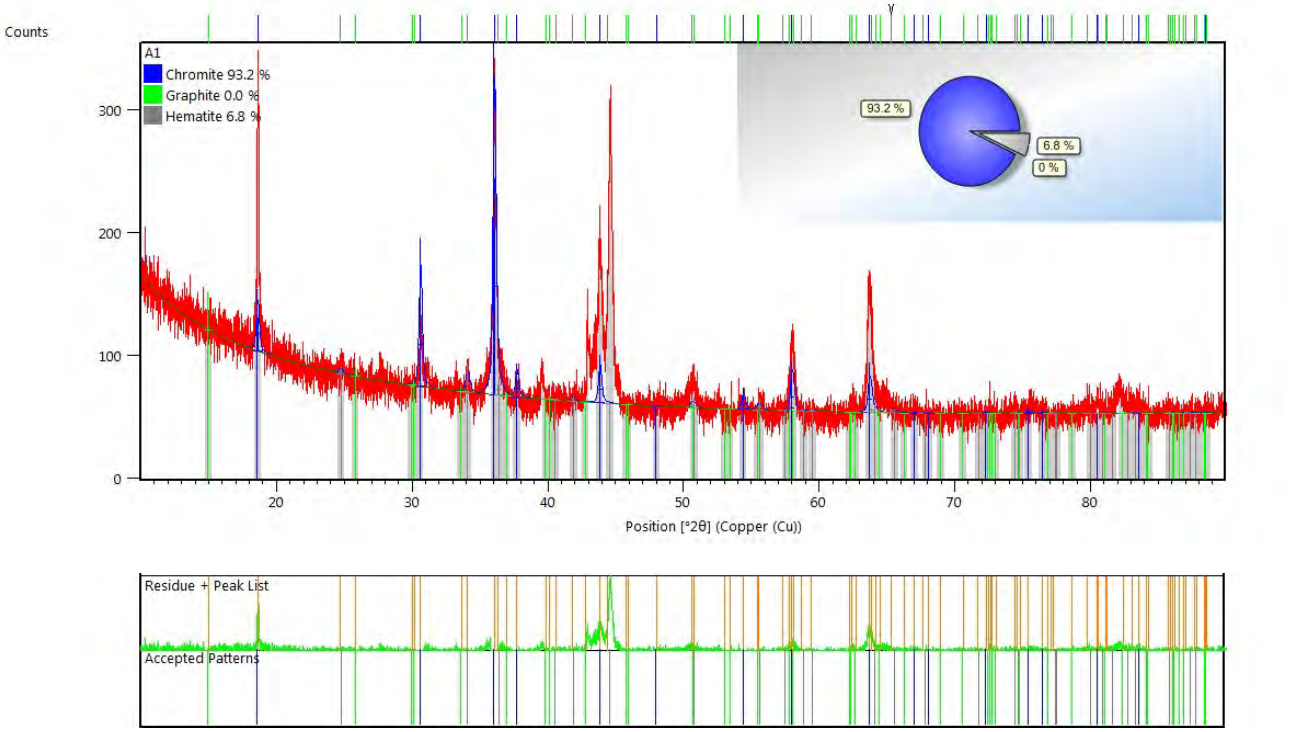

Sample: 1100 ˚C, 10 vol% CH_4, 20 min

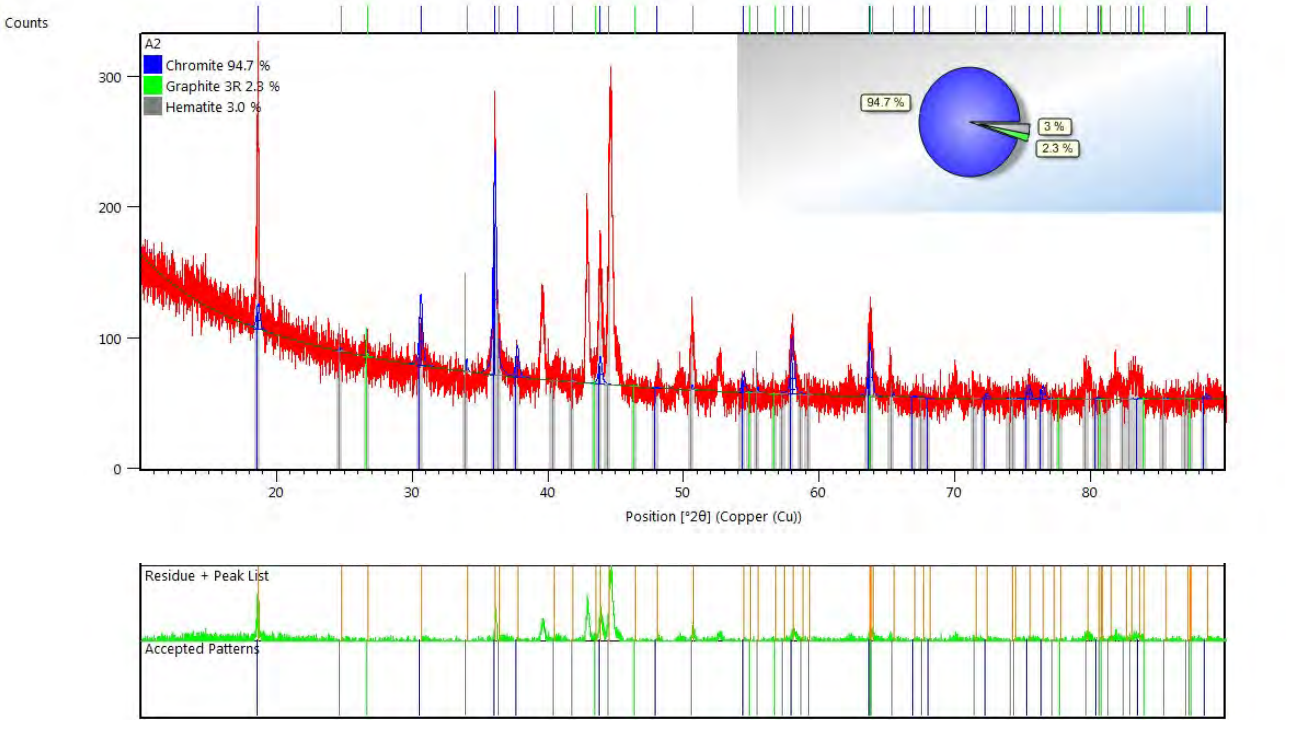

Appendix CXIV

Sample: 1100 ˚C, 10 vol% CH_4, 30 min

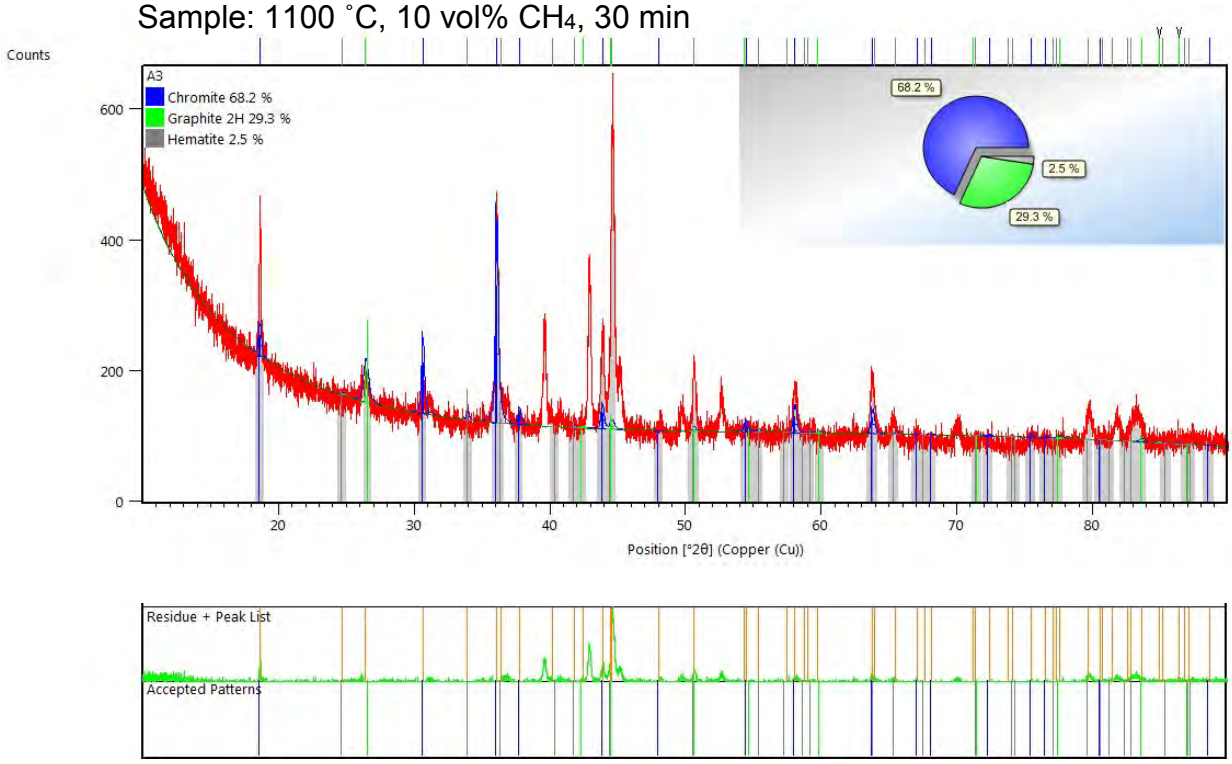

Sample: 1100 ˚C, 10 vol% CH_4, 60 min

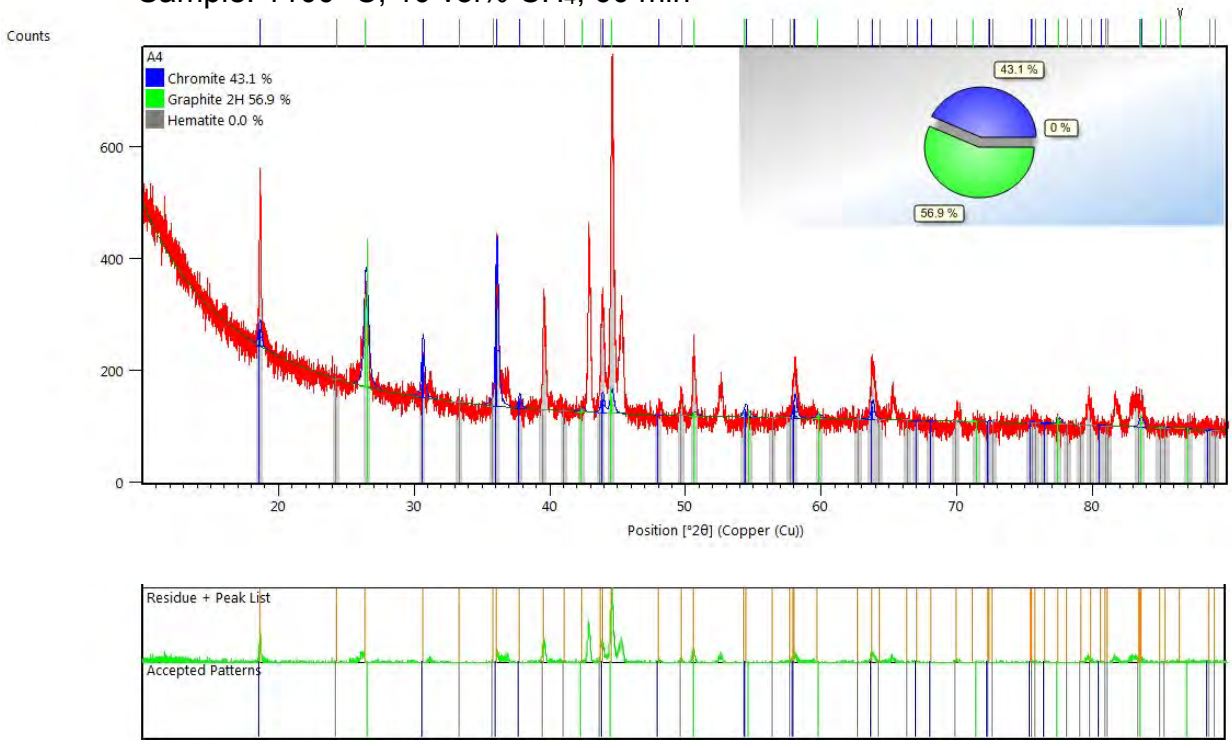

Appendix CXV

Sample: 1100 ˚C, 10 vol% CH_4, 90 min

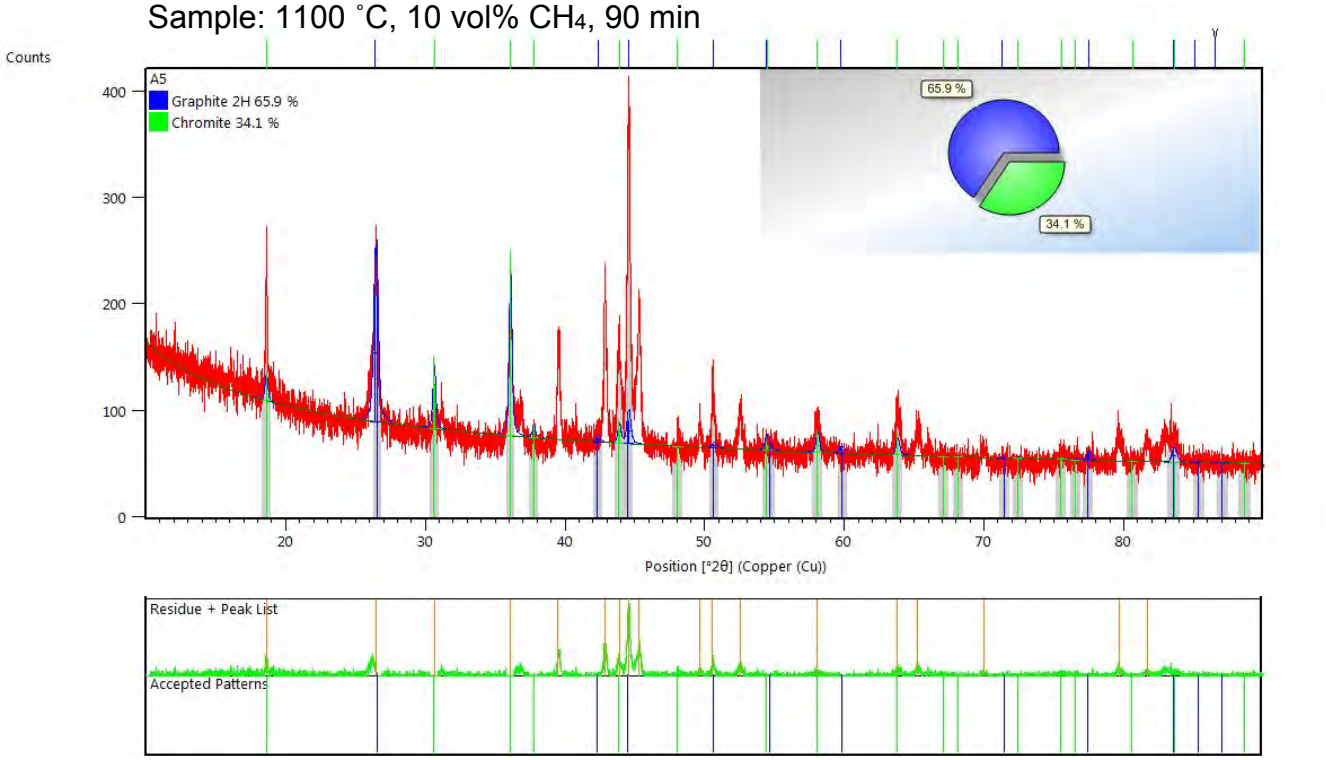

Sample: 1100 ˚C, 10 vol% CH_4, 120 min

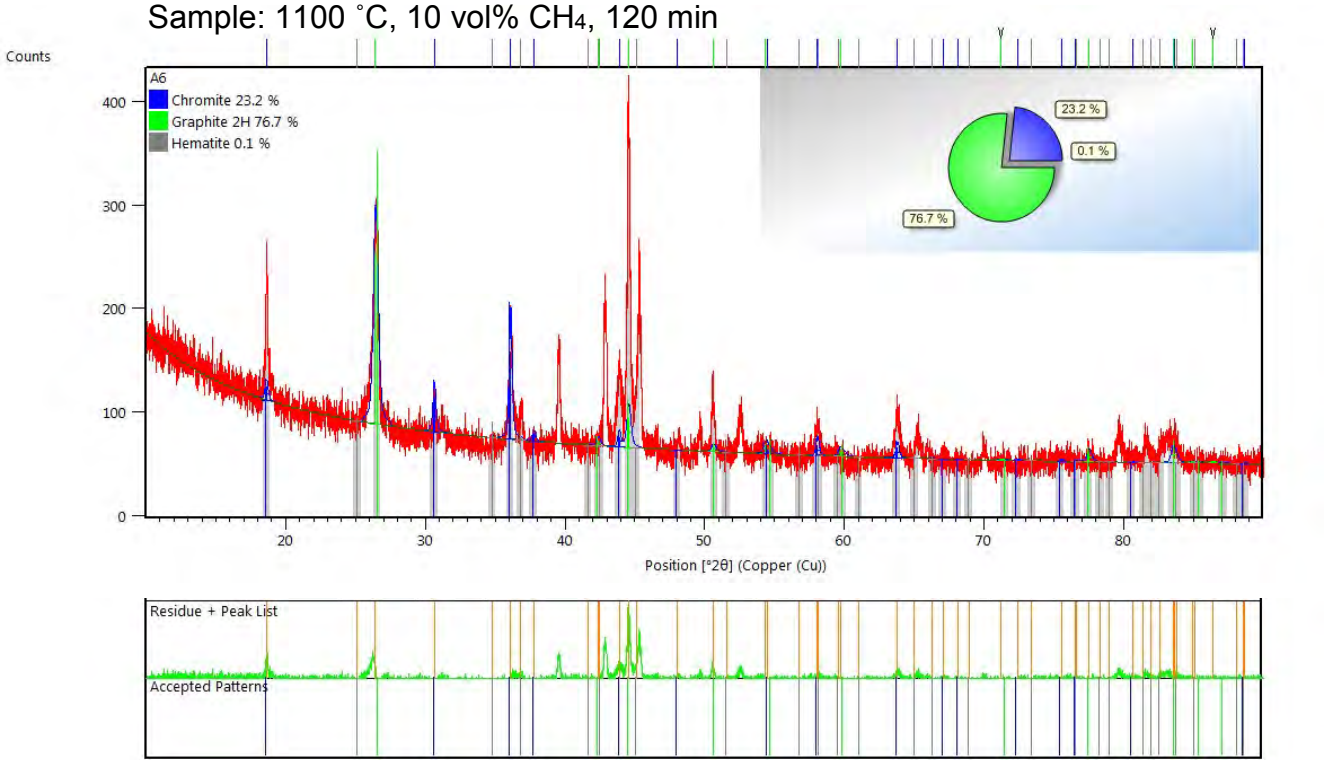

Appendix CXVI

Sample: 1100 ˚C, 20 vol% CH_4, 10 min

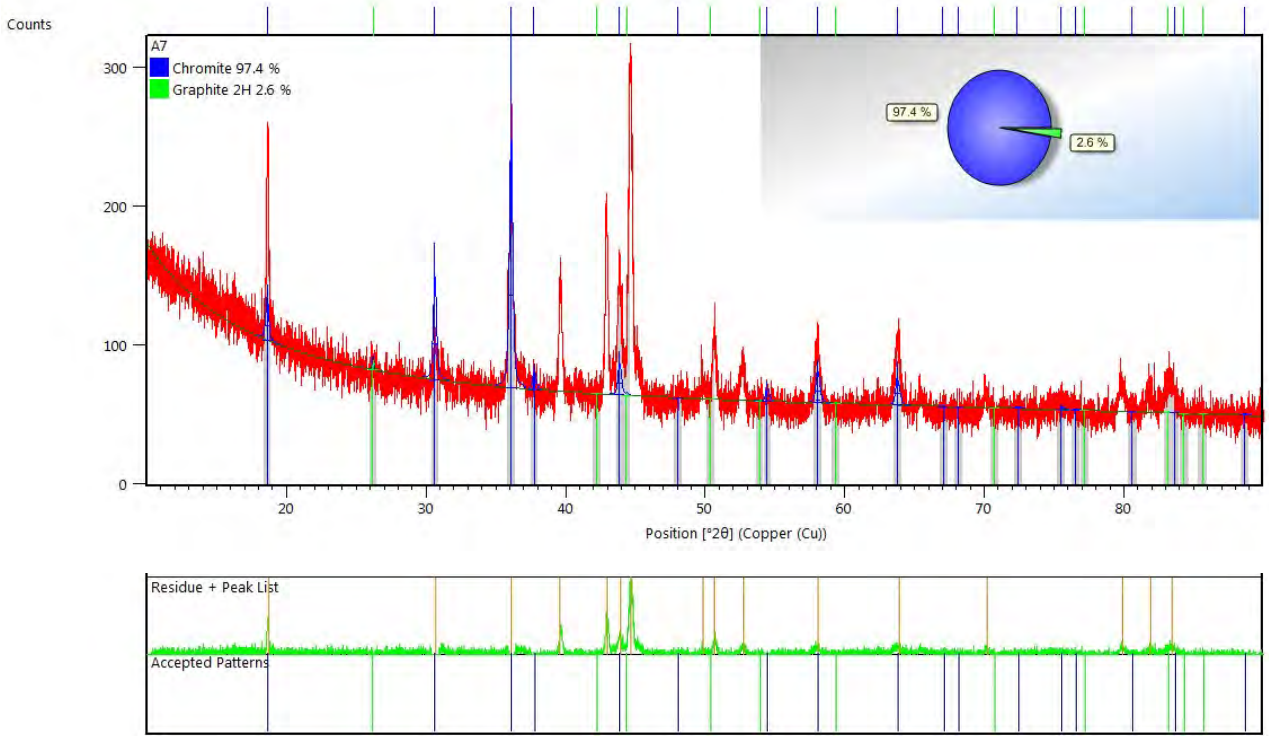

Sample: 1100 ˚C, 20 vol% CH_4, 20 min

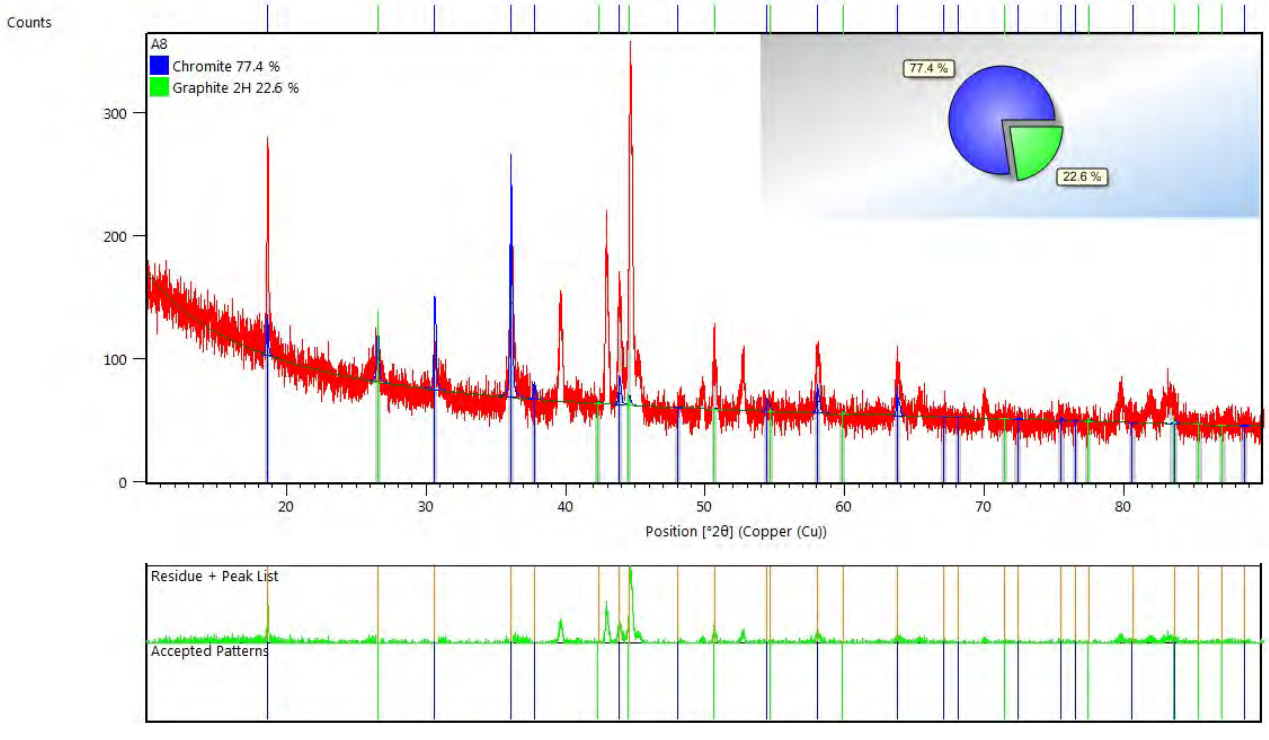

Appendix CXVII

Sample: 1100 ˚C, 20 vol% CH_4, 30 min

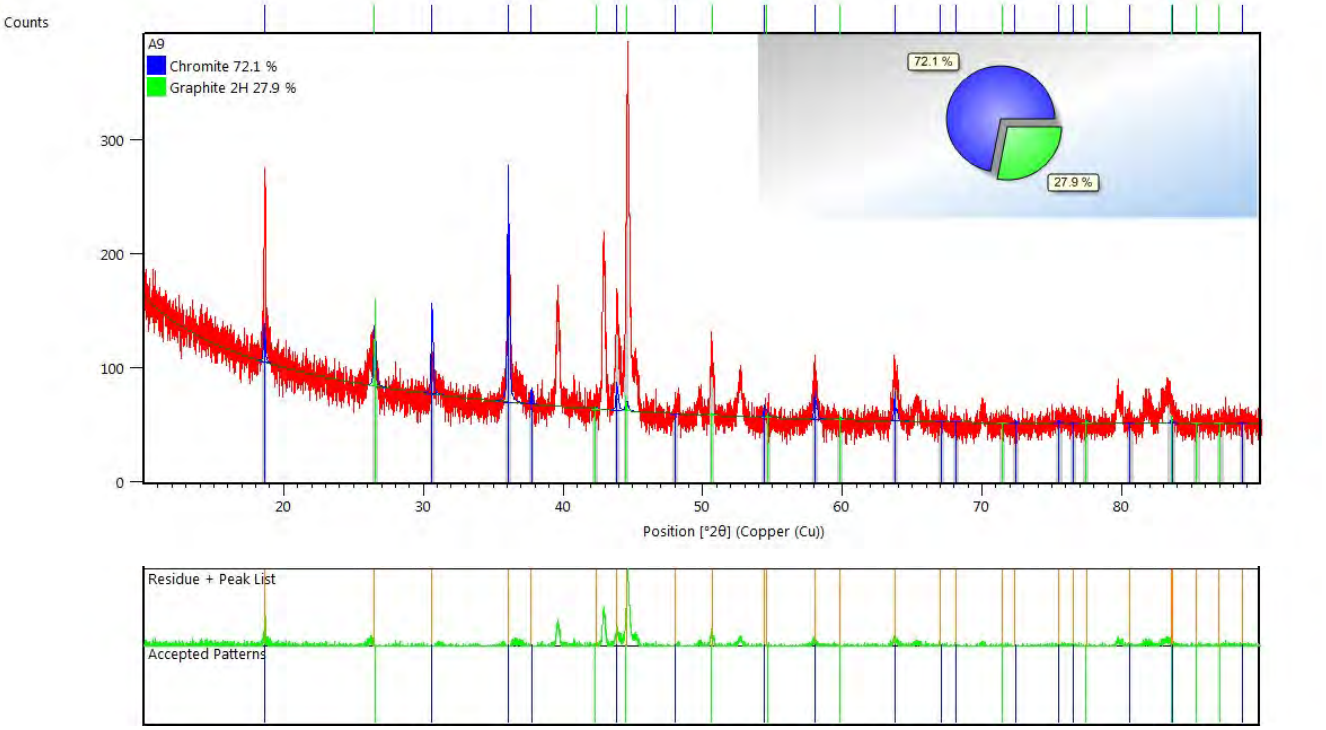

Sample: 1100 ˚C, 20 vol% CH_4, 60 min

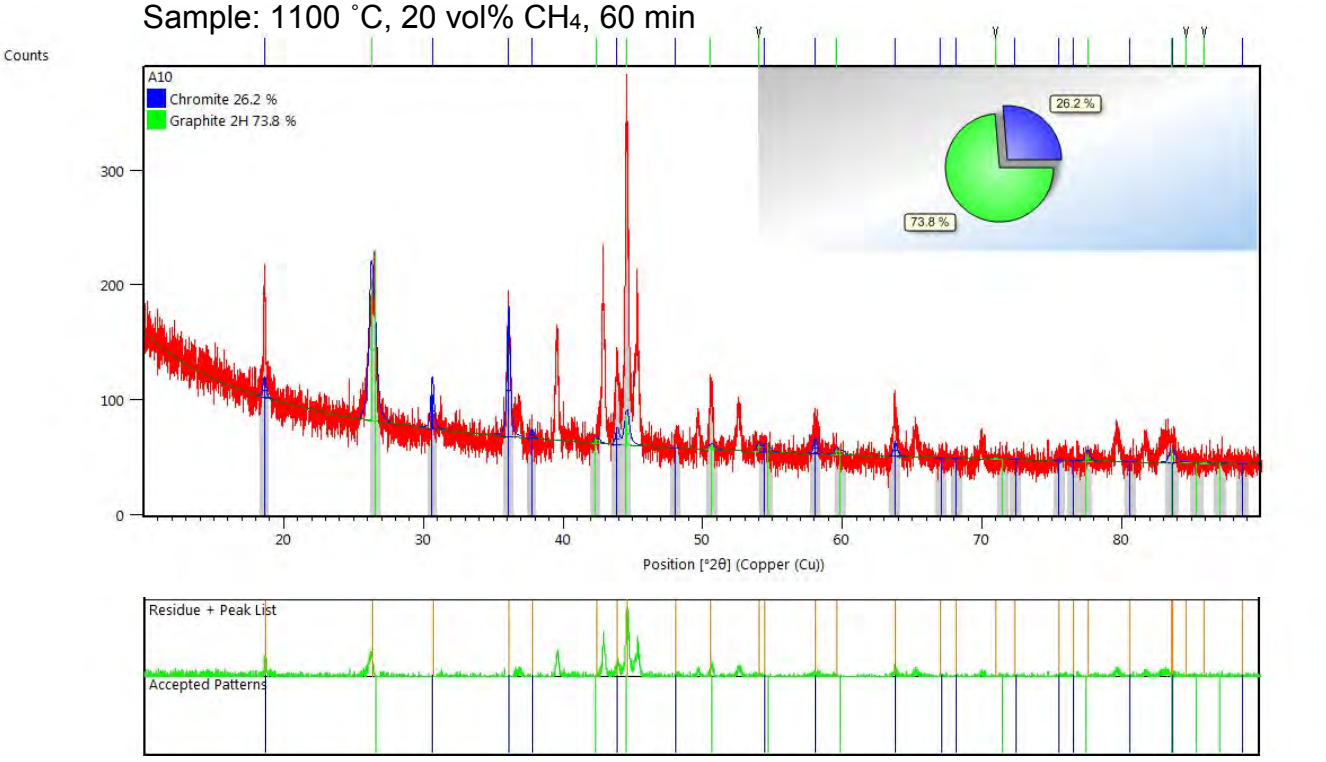

Appendix CXVIII

Sample: 1100 ˚C, 20 vol% CH_4, 90 min

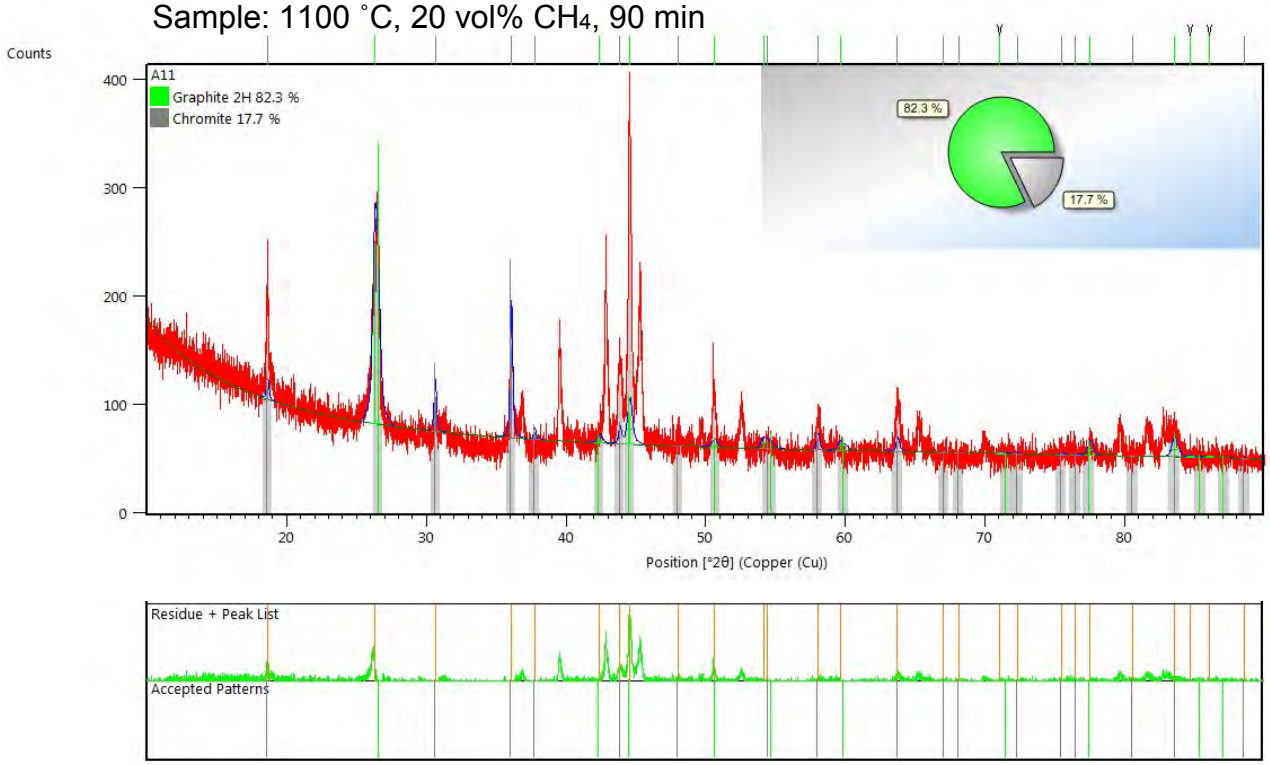

Sample: 1100 ˚C, 20 vol% CH_4, 120 min

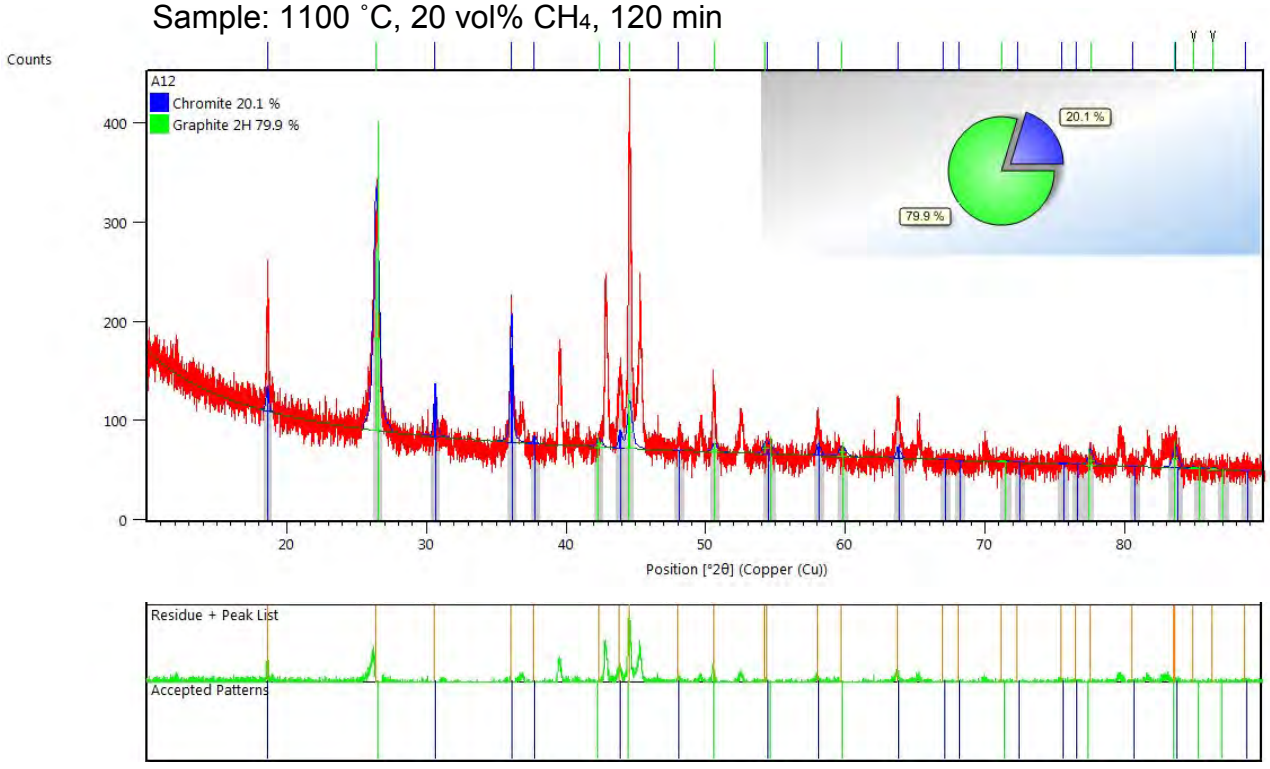

Appendix CXIX

Sample: 1100 ˚C, 30 vol% CH_4, 10 min

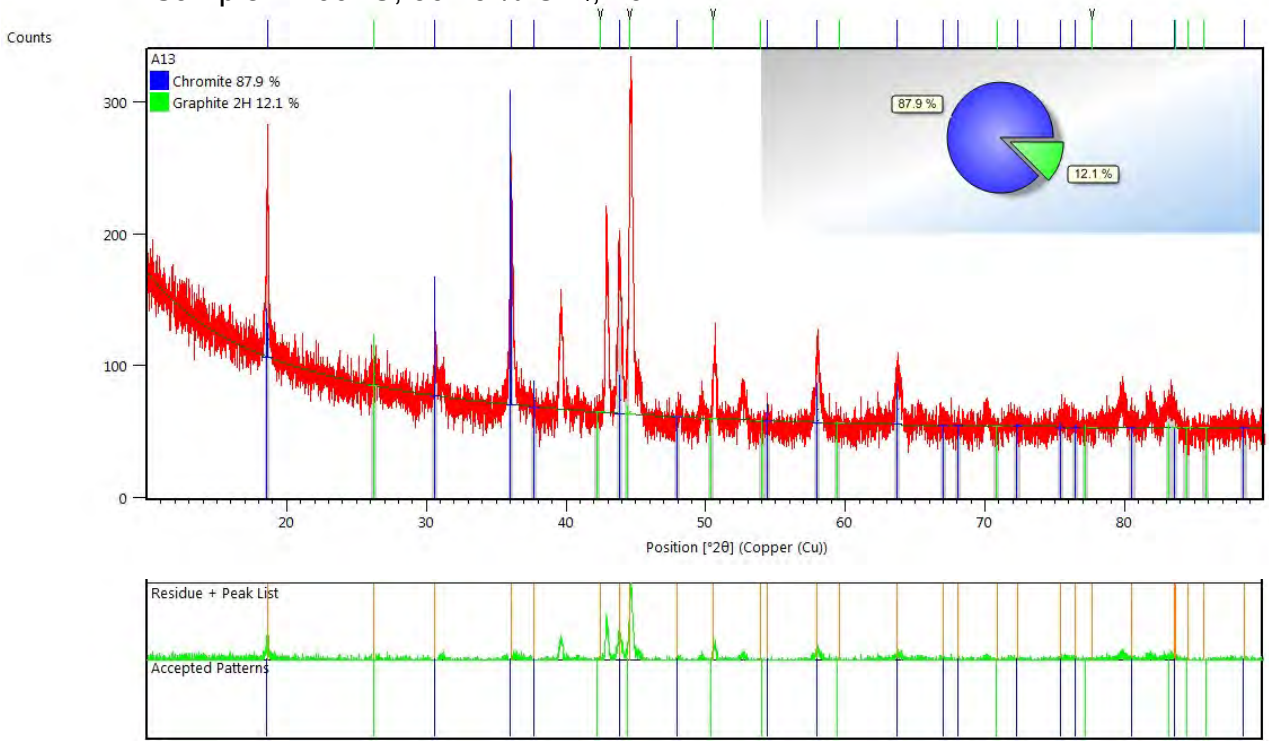

Sample: 1100 ˚C, 30 vol% CH_4, 20 min

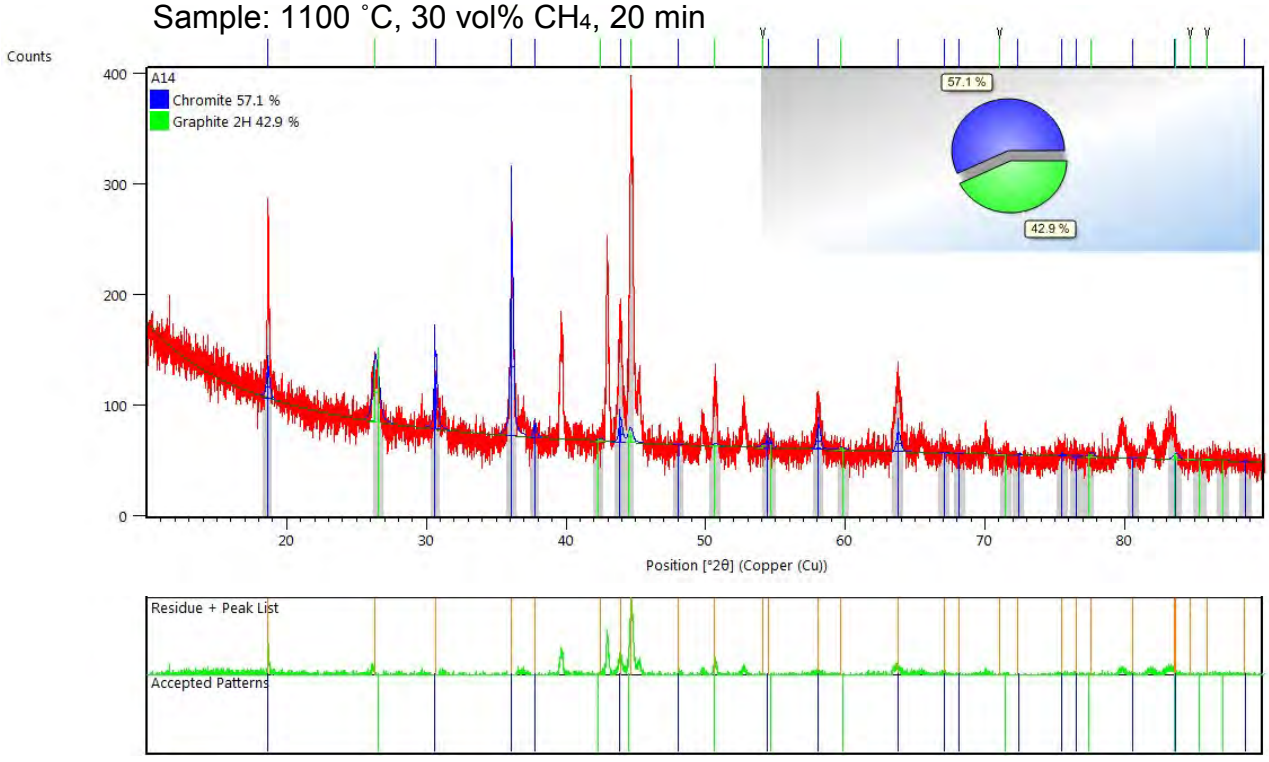

Appendix CXX

Sample: 1100 ˚C, 30 vol% CH_4, 30 min

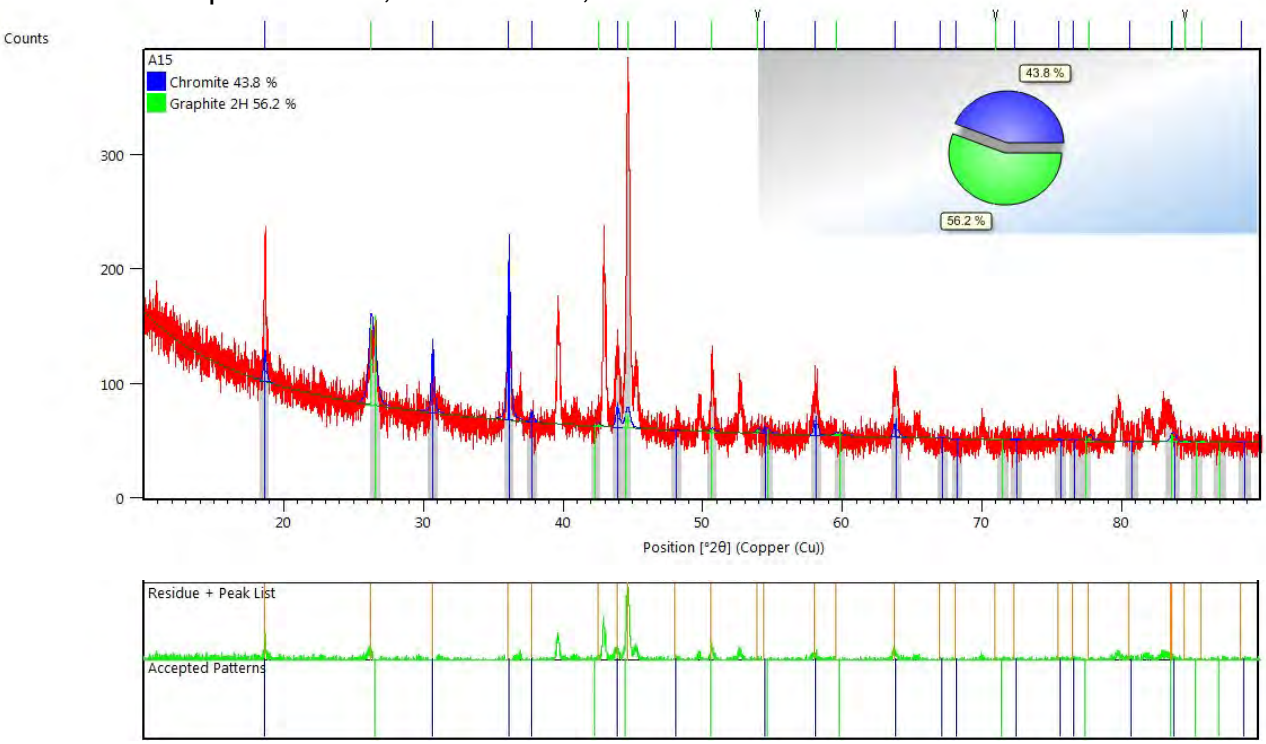

Sample: 1100 ˚C, 30 vol% CH_4, 60 min

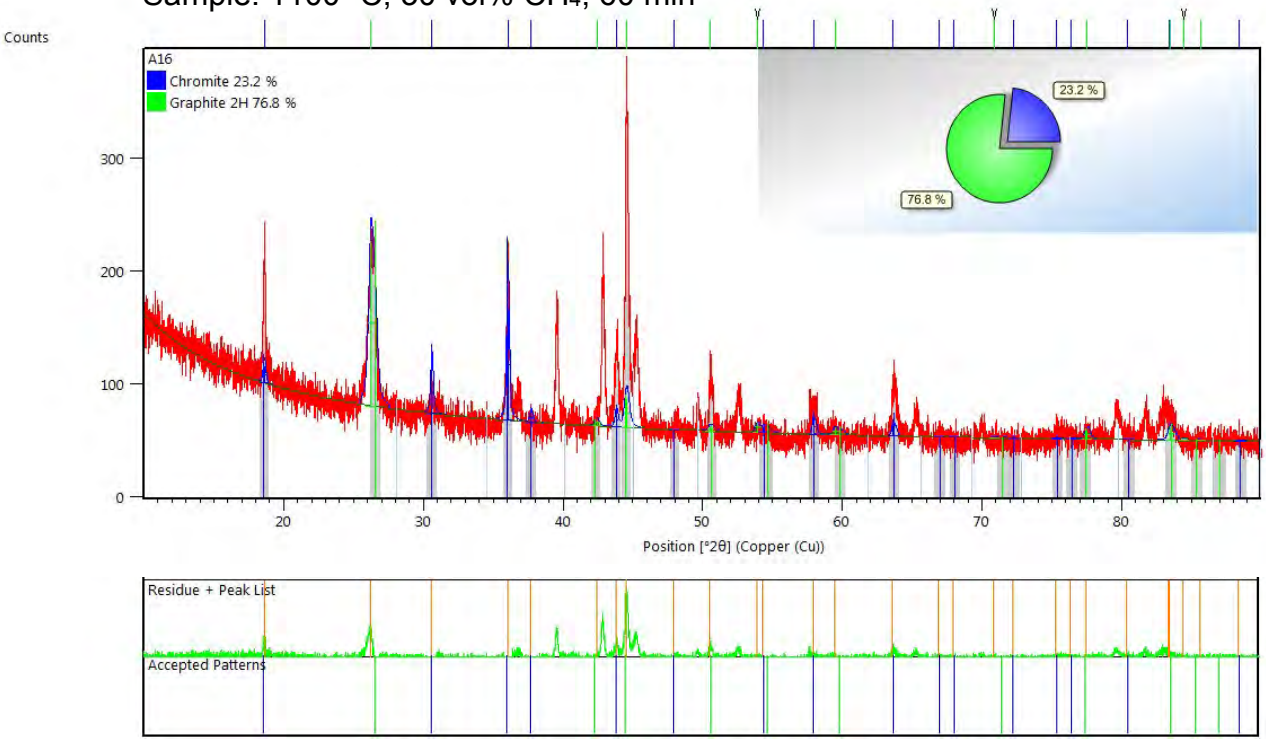

Appendix CXXI

Sample: 1100 ˚C, 30 vol% CH_4, 90 min

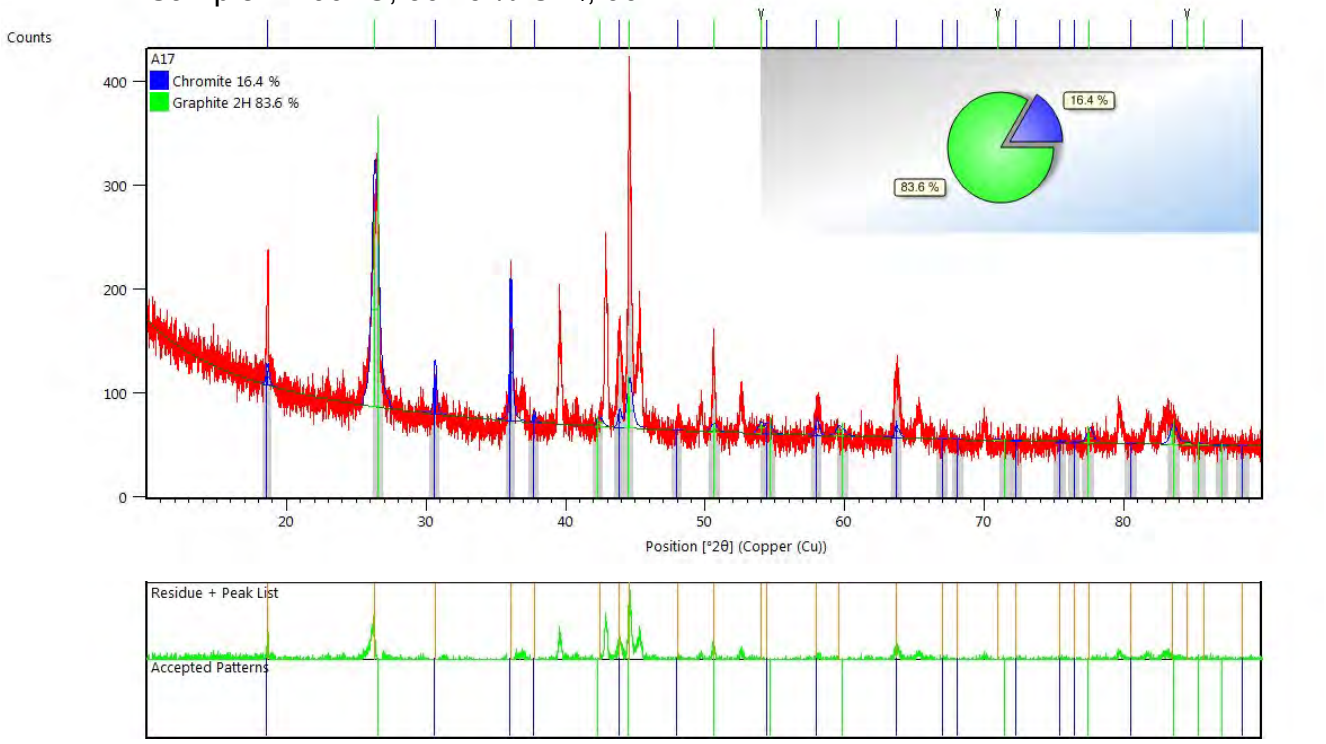

Sample: 1100 ˚C, 30 vol% CH_4, 120 min

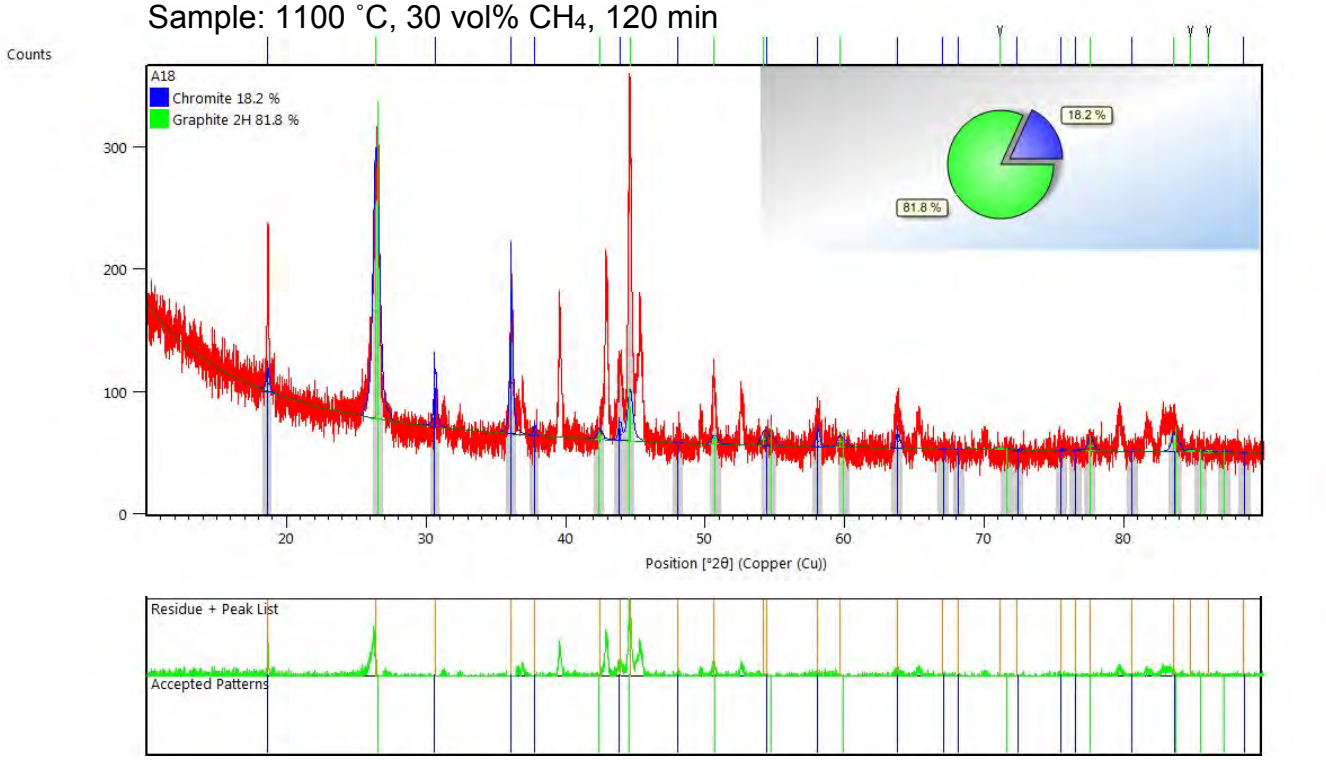

Appendix CXXII

Sample: 1200 ˚C, 10 vol% CH_4, 10 min

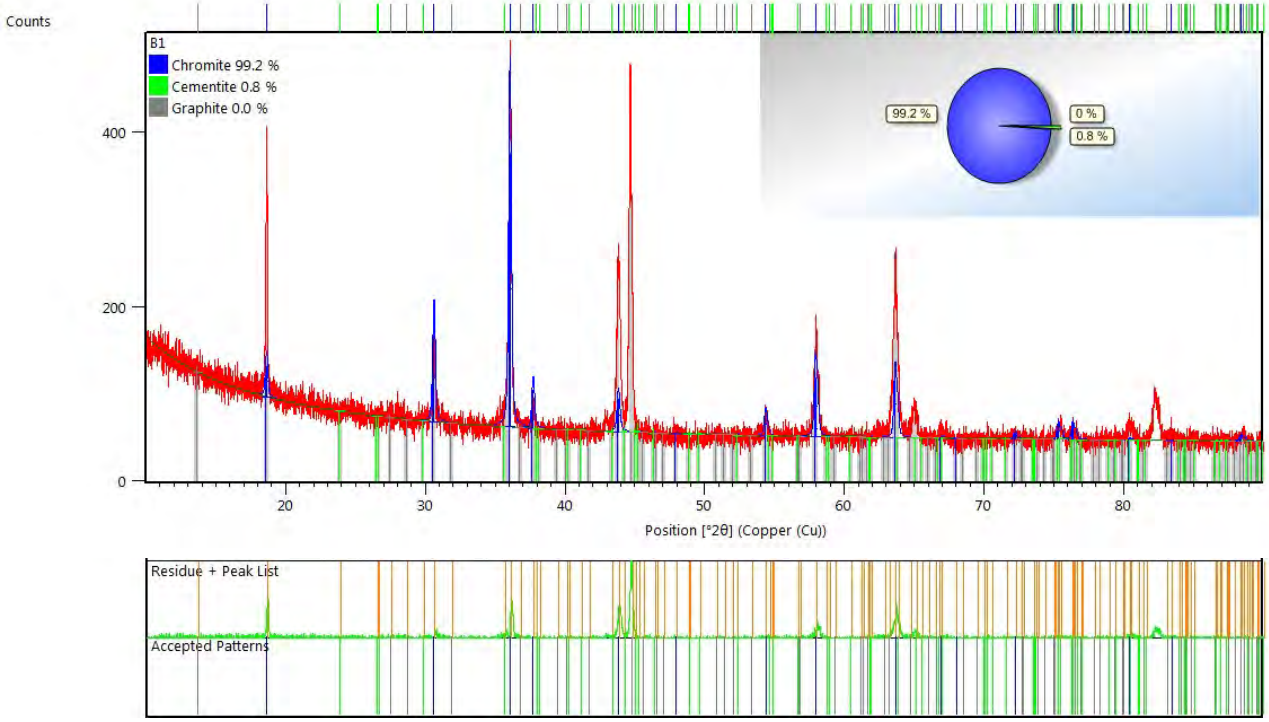

Sample: 1200 ˚C, 10 vol% CH_4, 20 min

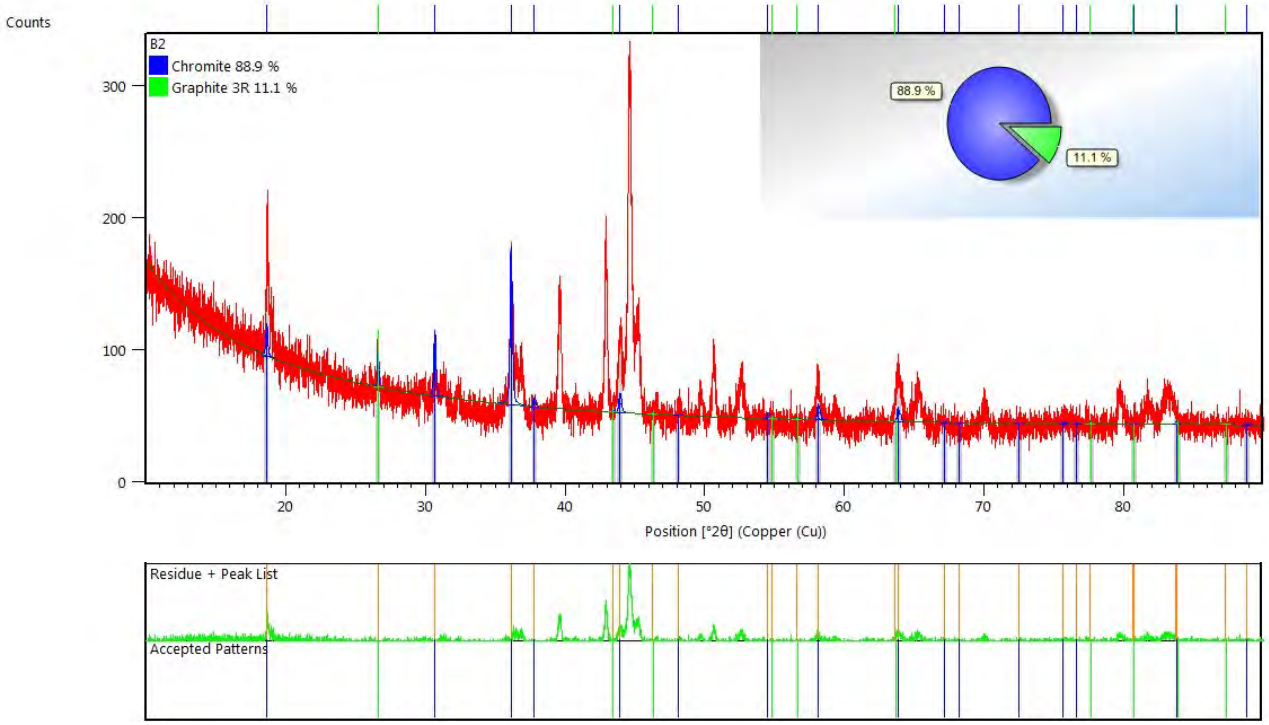

Appendix CXXIII

Sample: 1200 ˚C, 10 vol% CH_4, 30 min

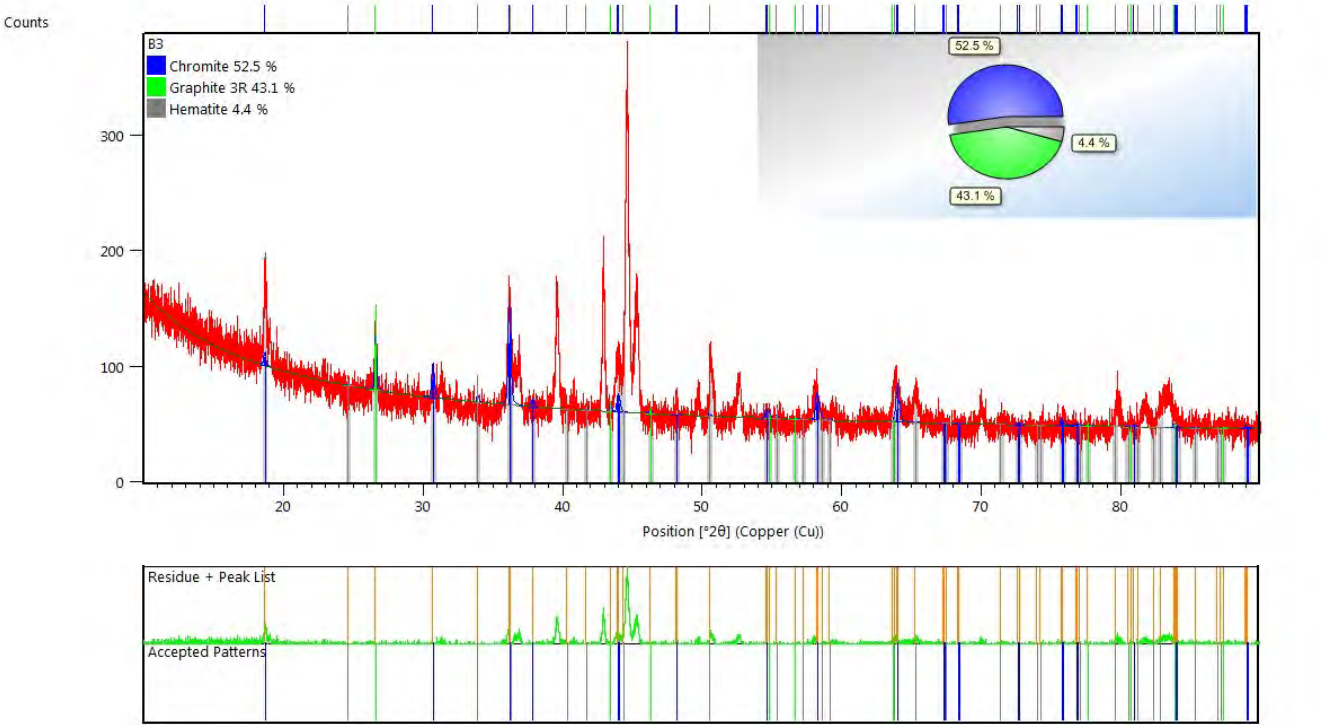

Sample: 1200 ˚C, 10 vol% CH_4, 60 min

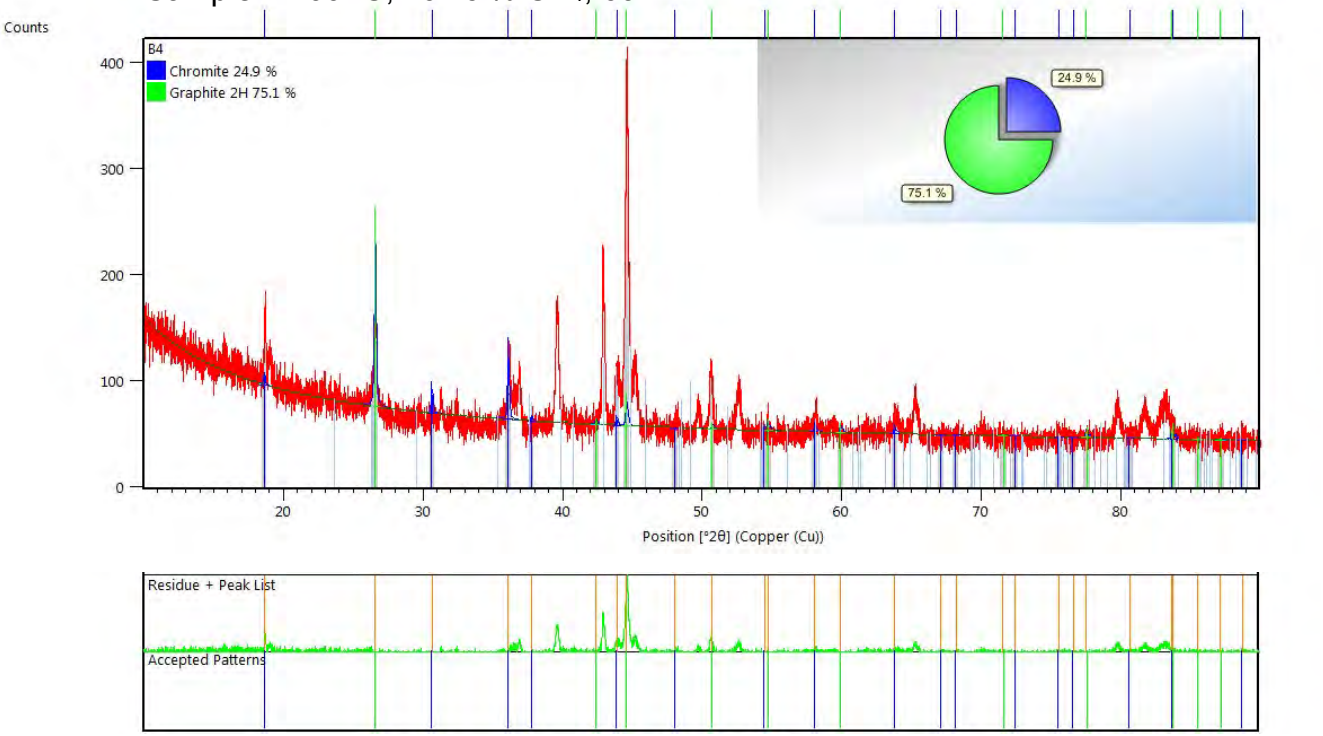

Appendix CXXIV

Sample: 1200 ˚C, 10 vol% CH_4, 90 min

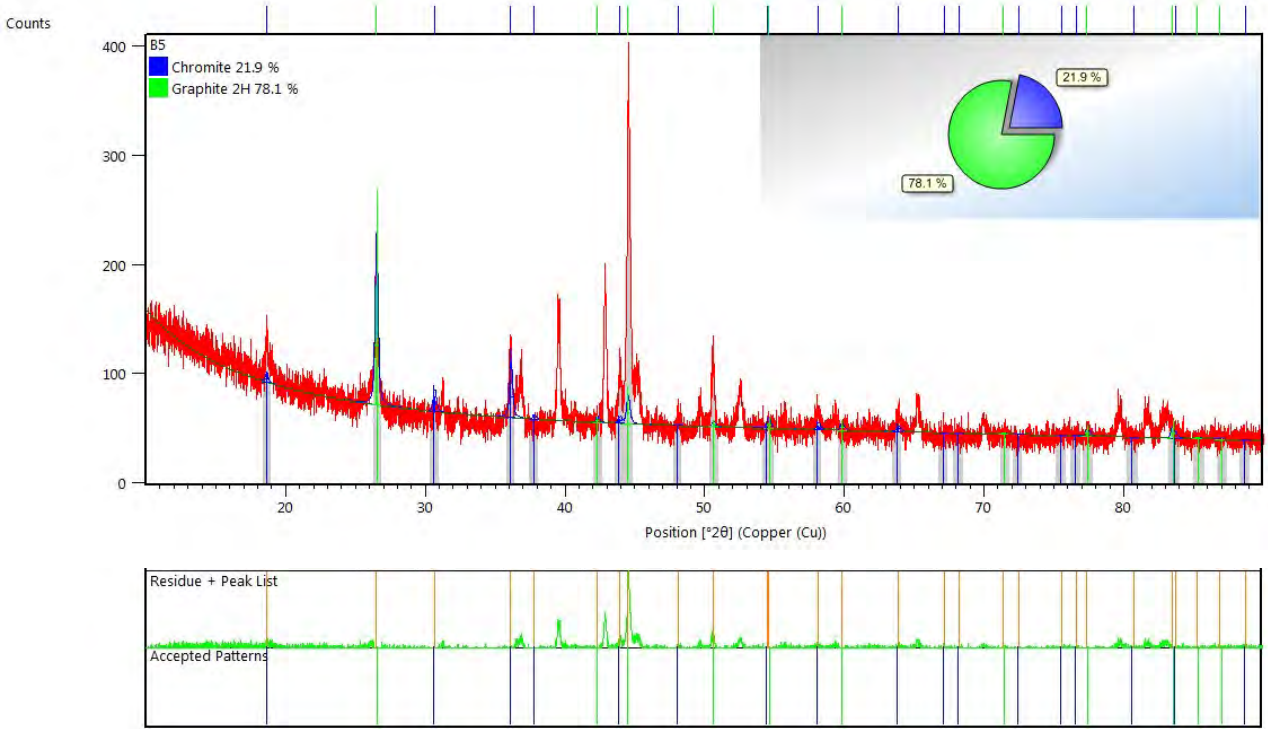

Sample: 1200 ˚C, 10 vol% CH_4, 120 min

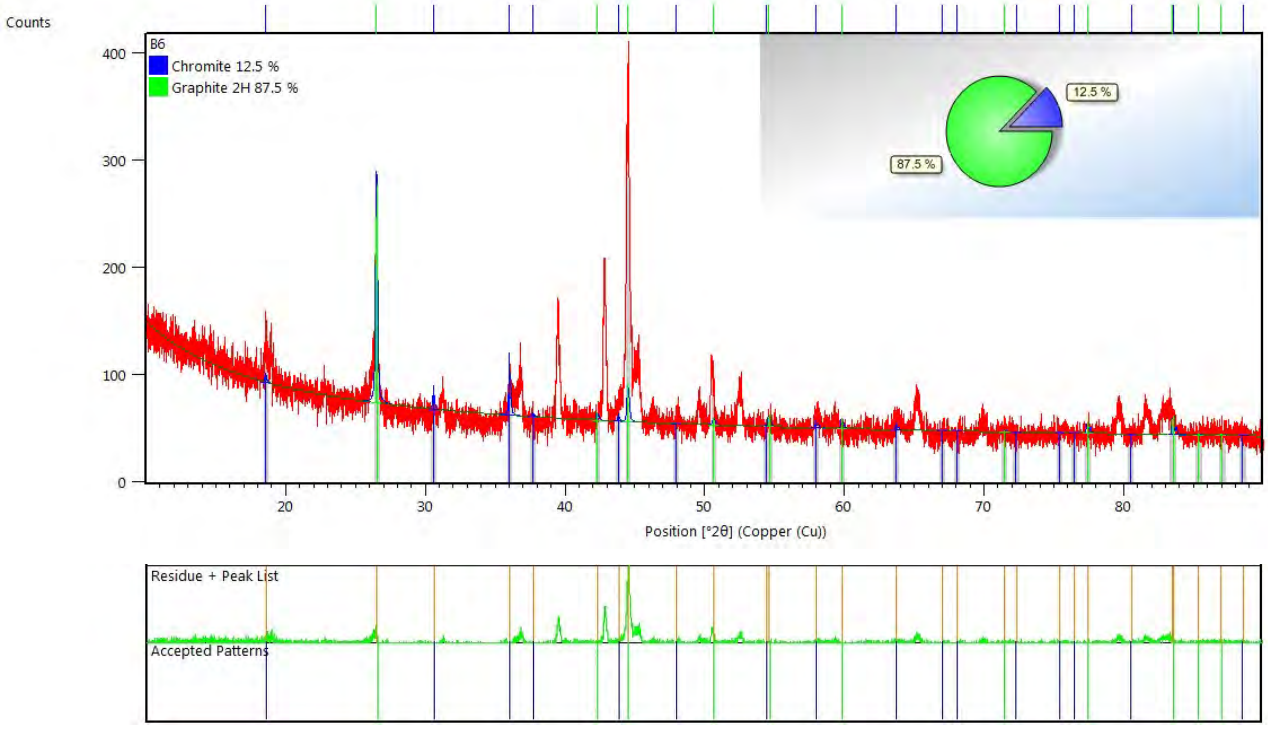

Appendix CXXV

Sample: 1200 ˚C, 20 vol% CH_4, 10 min

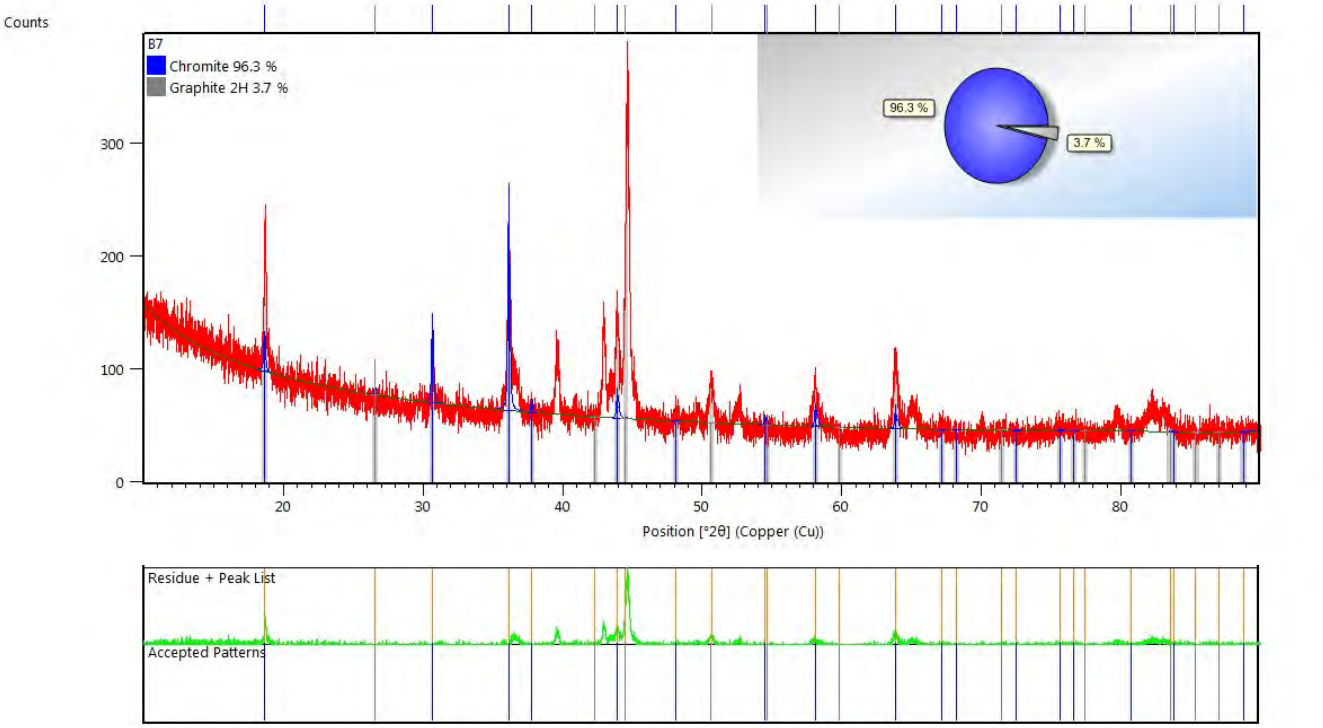

Sample: 1200 ˚C, 20 vol% CH_4, 20 min

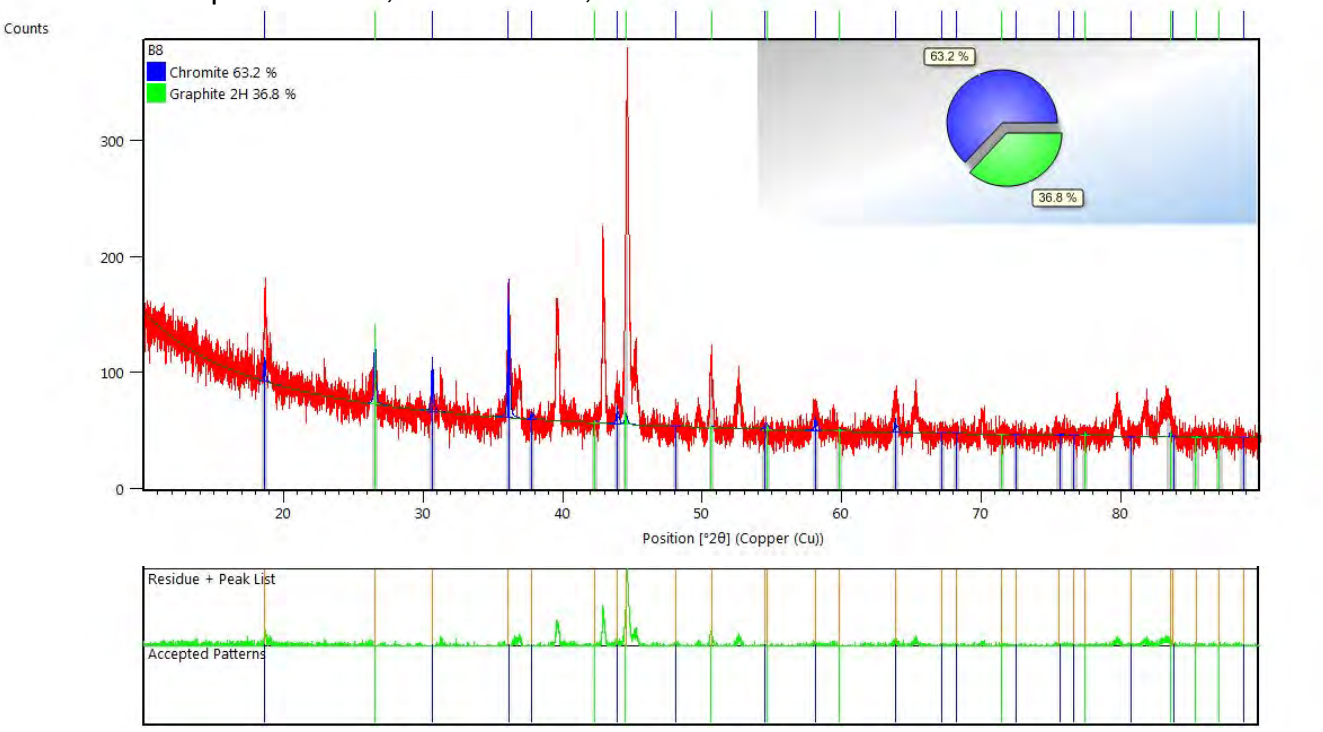

Appendix CXXVI

Sample: 1200 ˚C, 20 vol% CH_4, 30 min

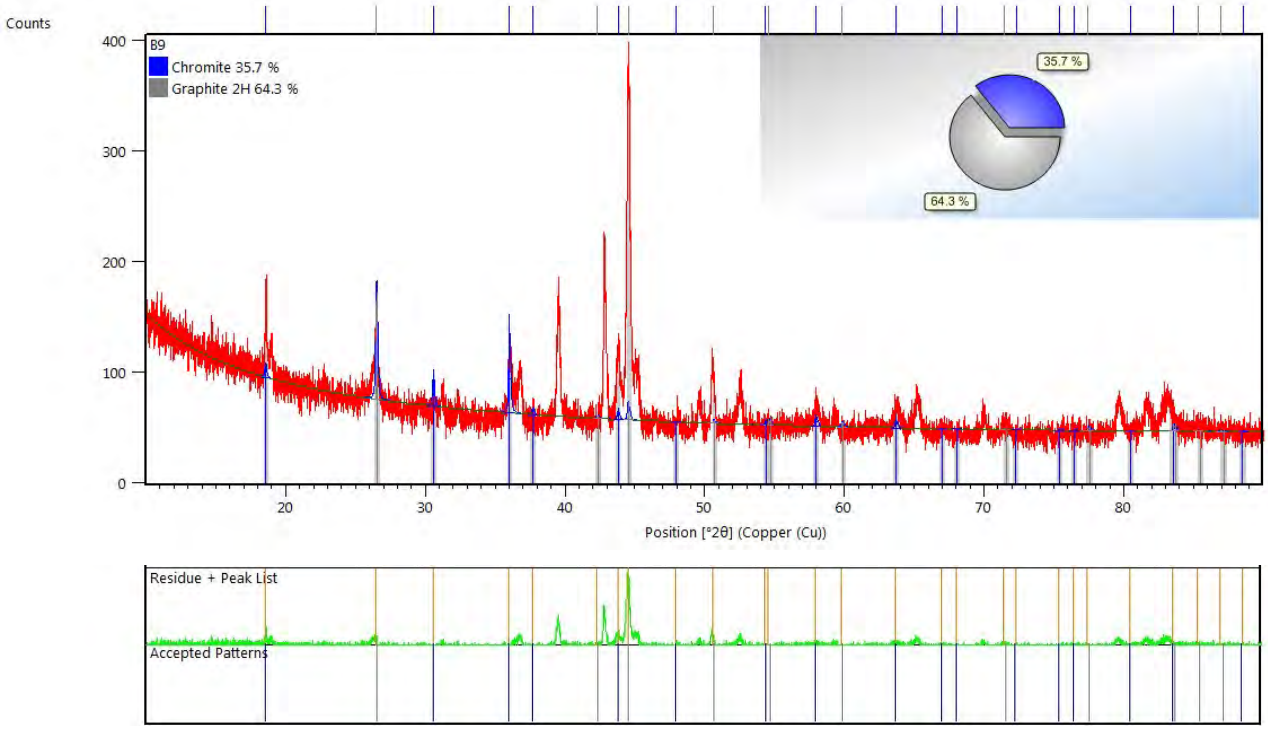

Sample: 1200 ˚C, 20 vol% CH_4, 60 min

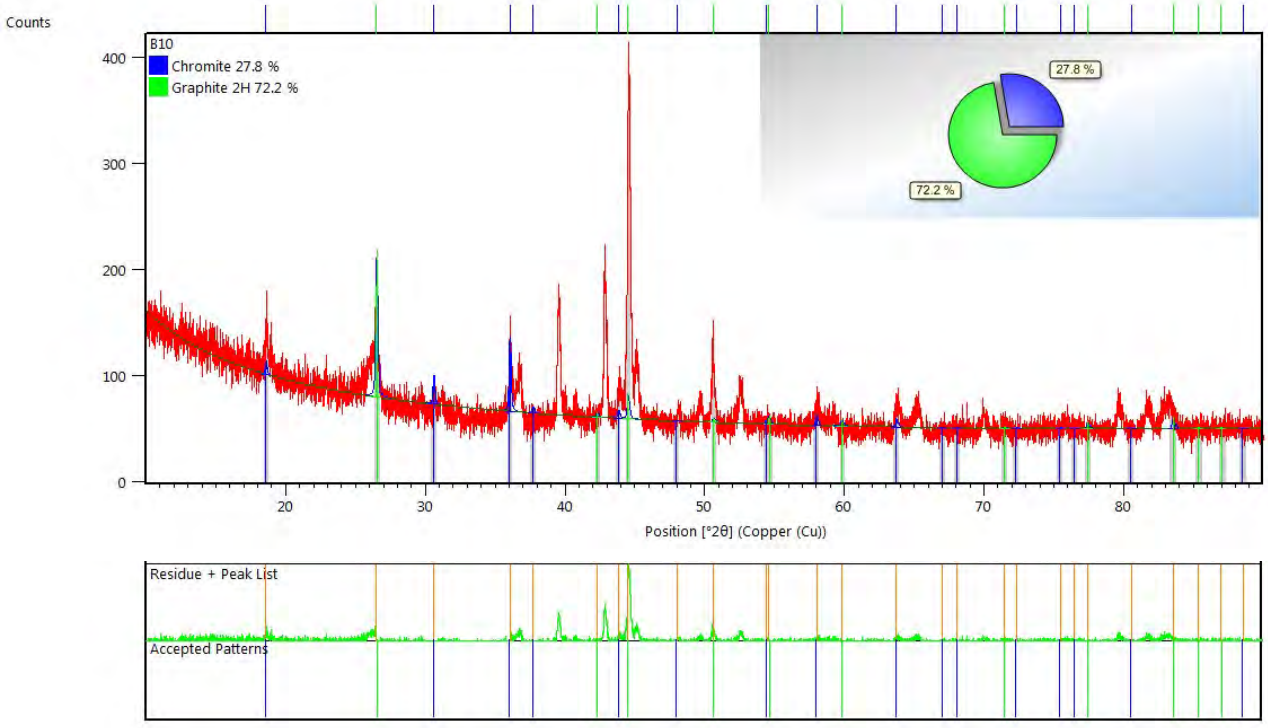

Appendix CXXVII

Sample: 1200 ˚C, 20 vol% CH_4, 90 min

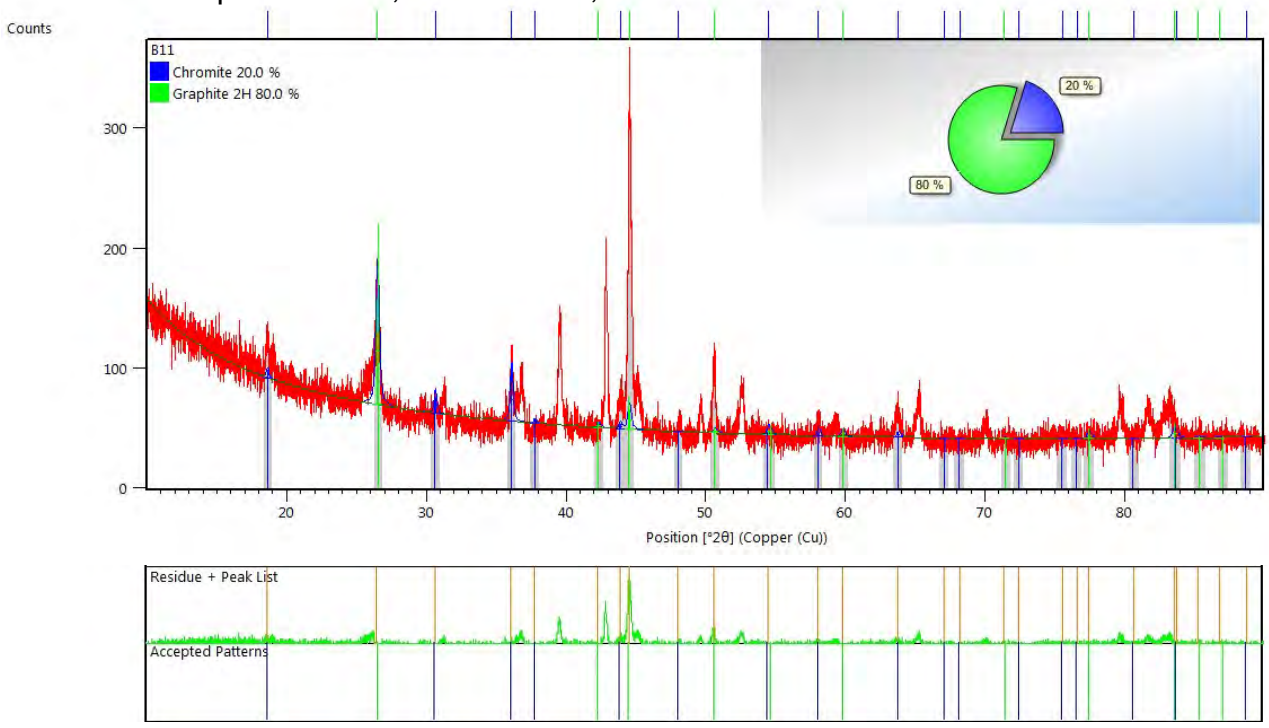

Sample: 1200 ˚C, 20 vol% CH_4, 120 min

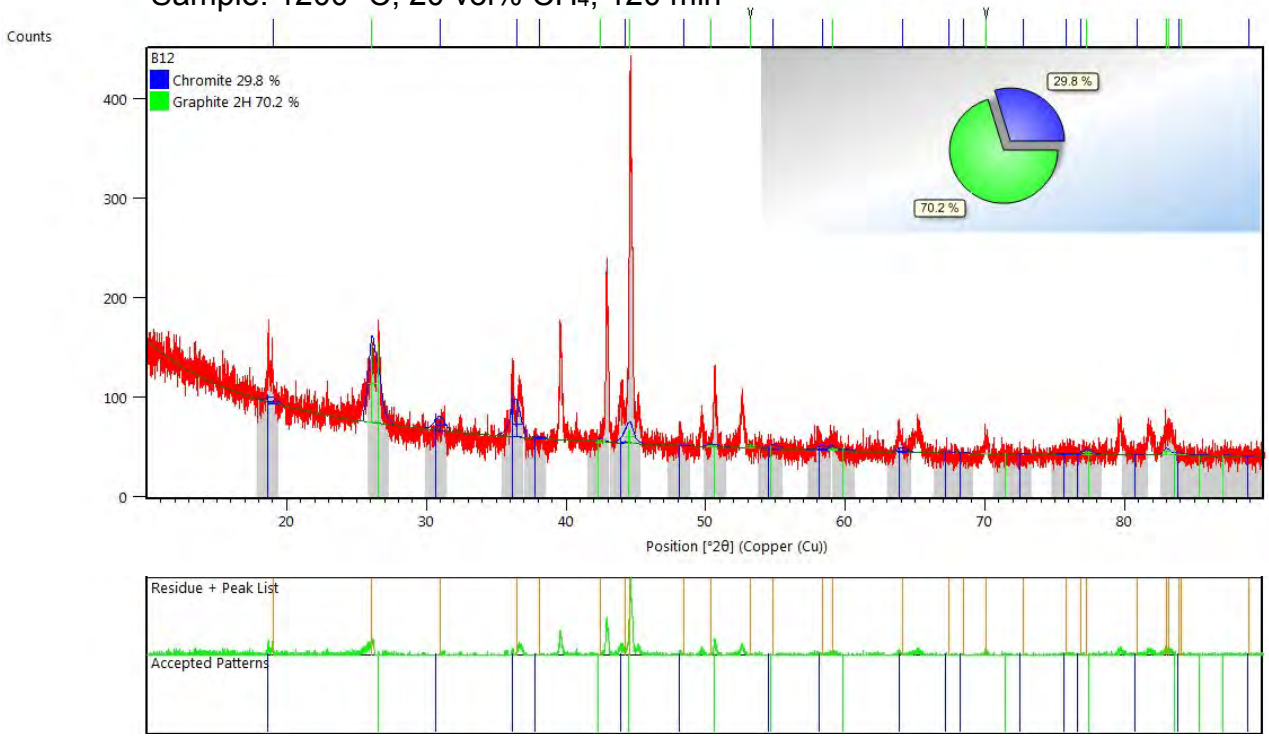

Appendix CXXVIII

Sample: 1200 ˚C, 30 vol% CH_4, 10 min

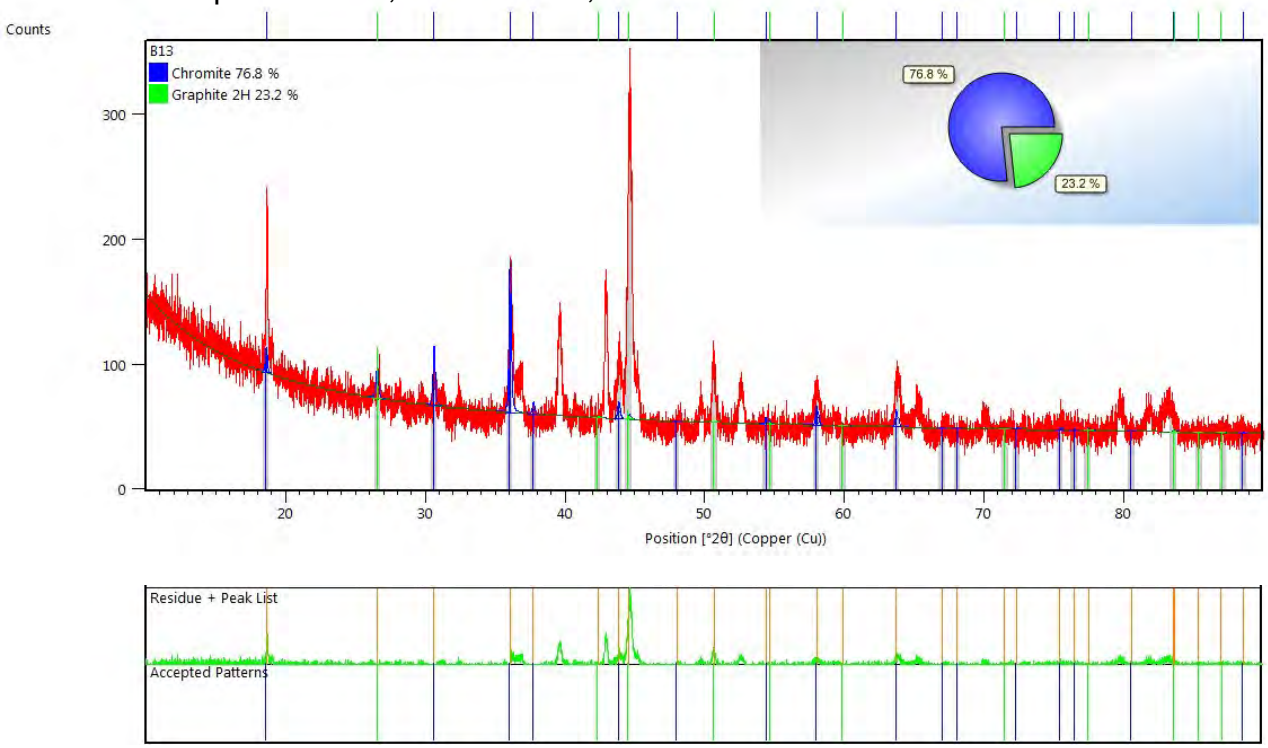

Sample: 1200 ˚C, 30 vol% CH_4, 20 min

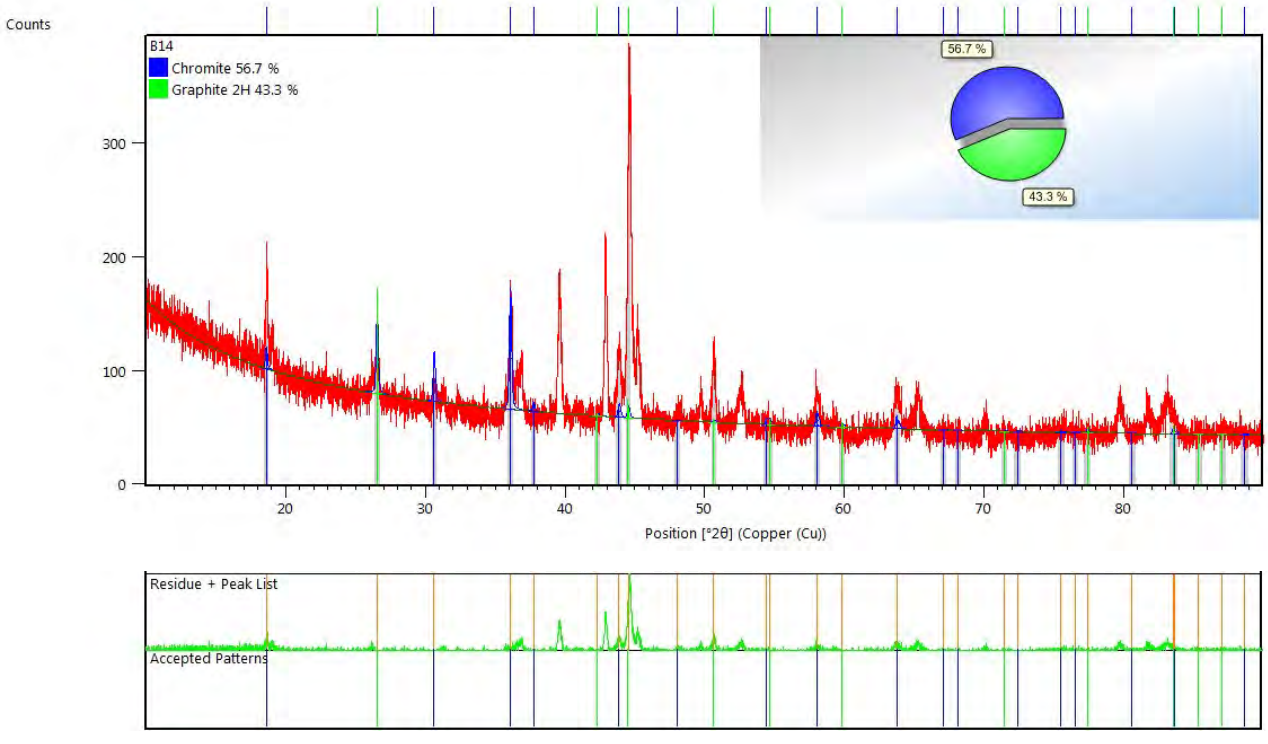

Appendix CXXIX

Sample: 1200 ˚C, 30 vol% CH_4, 30 min

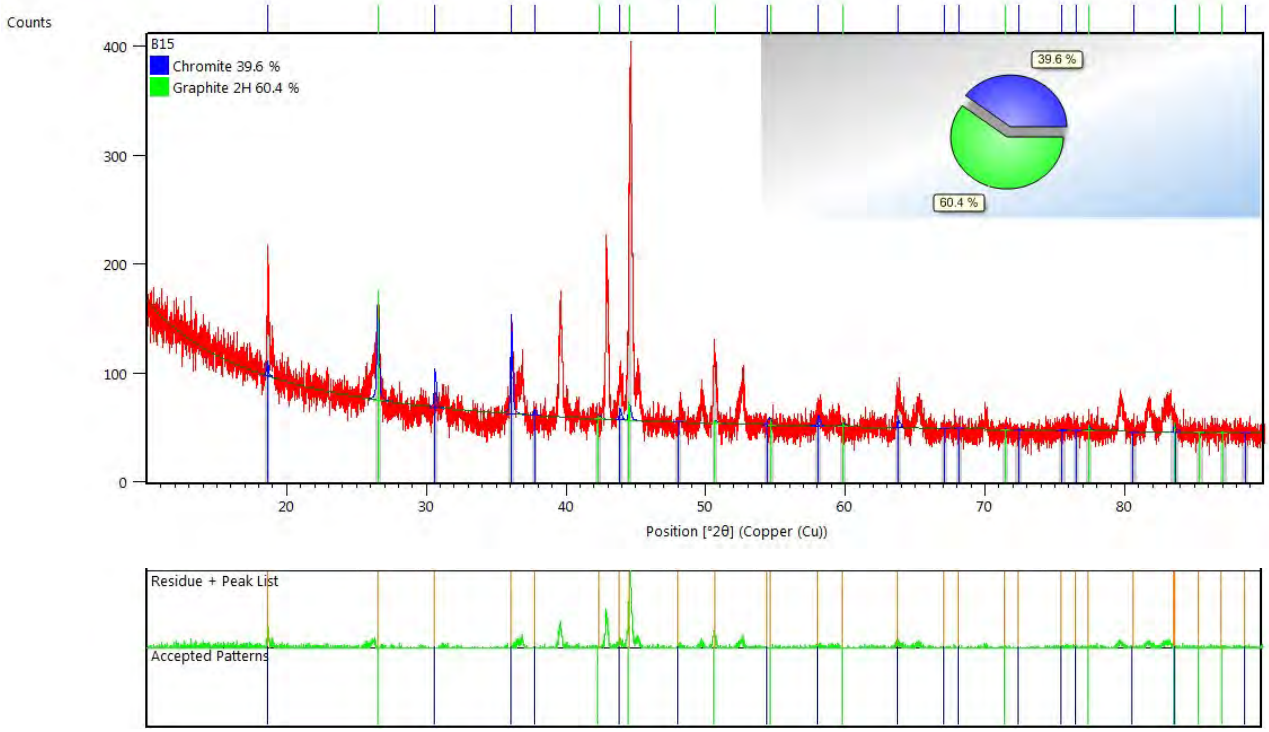

Sample: 1200 ˚C, 30 vol% CH_4, 60 min

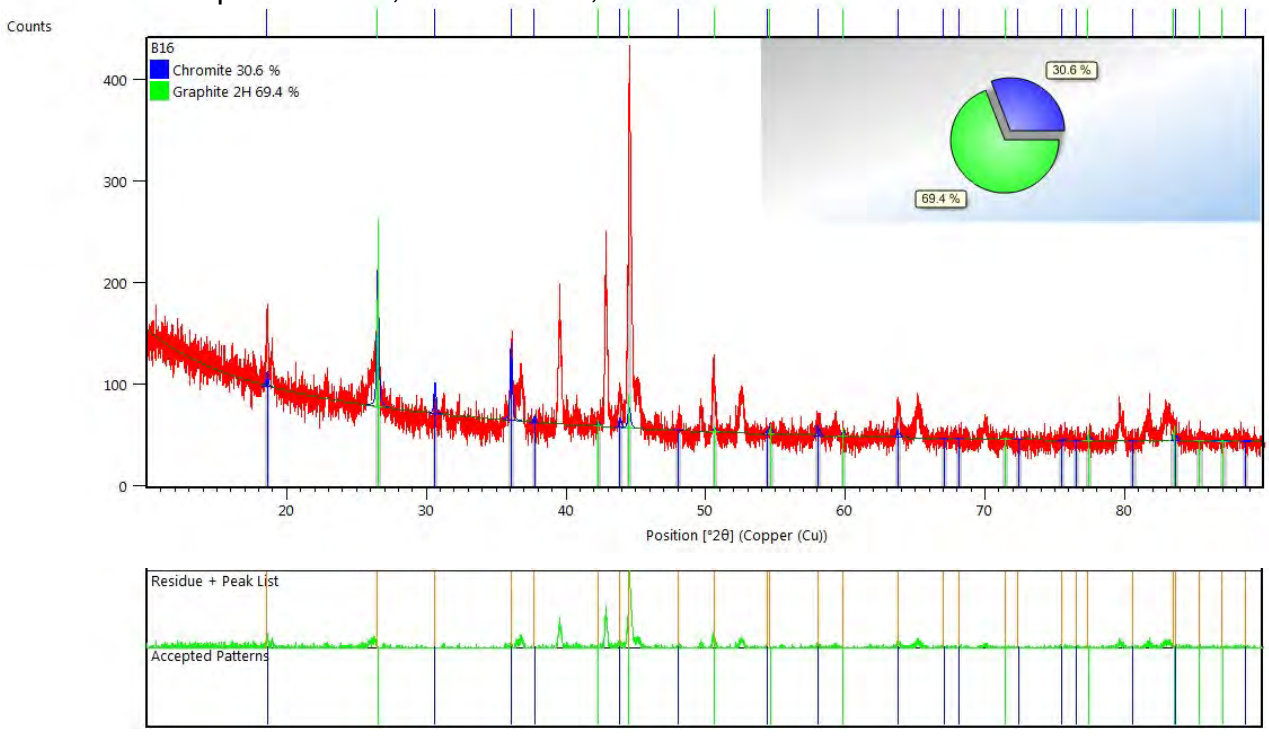

Appendix CXXX

Sample: 1200 ˚C, 30 vol% CH_4, 90 min

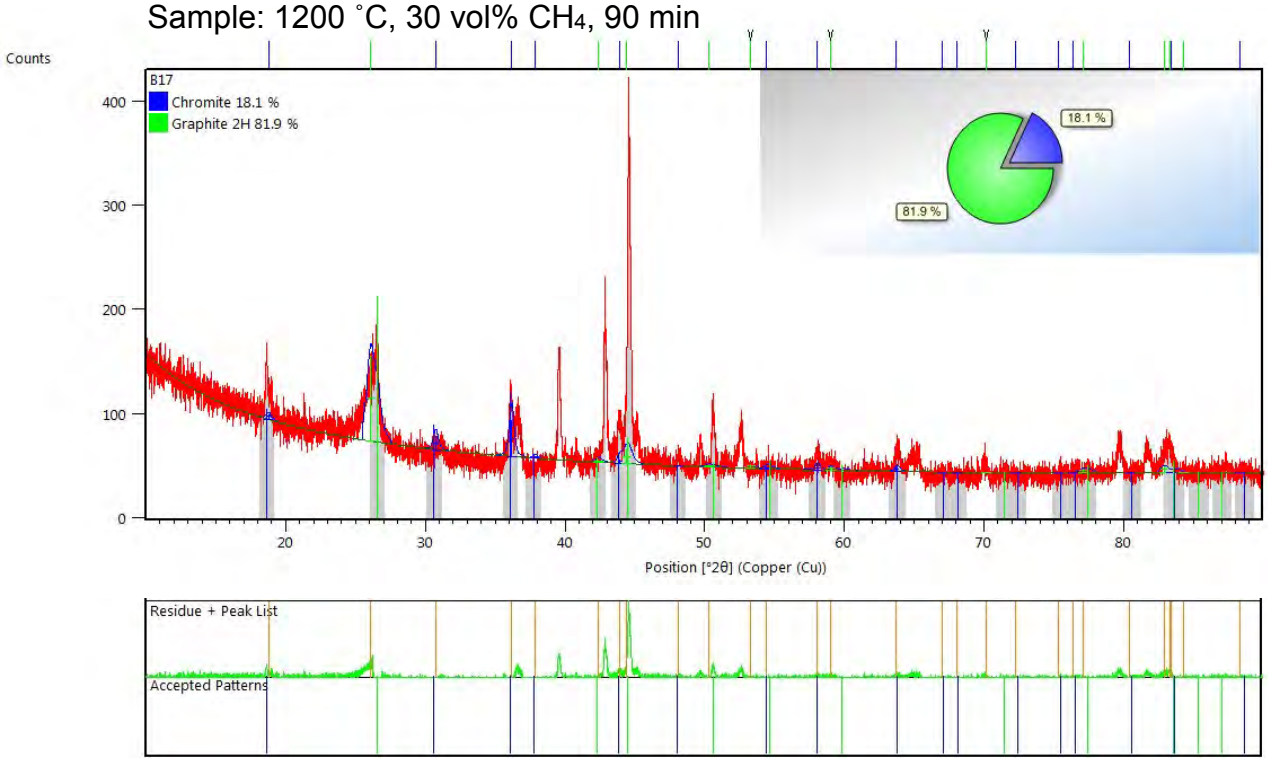

Sample: 1200 ˚C, 30 vol% CH_4, 120 min

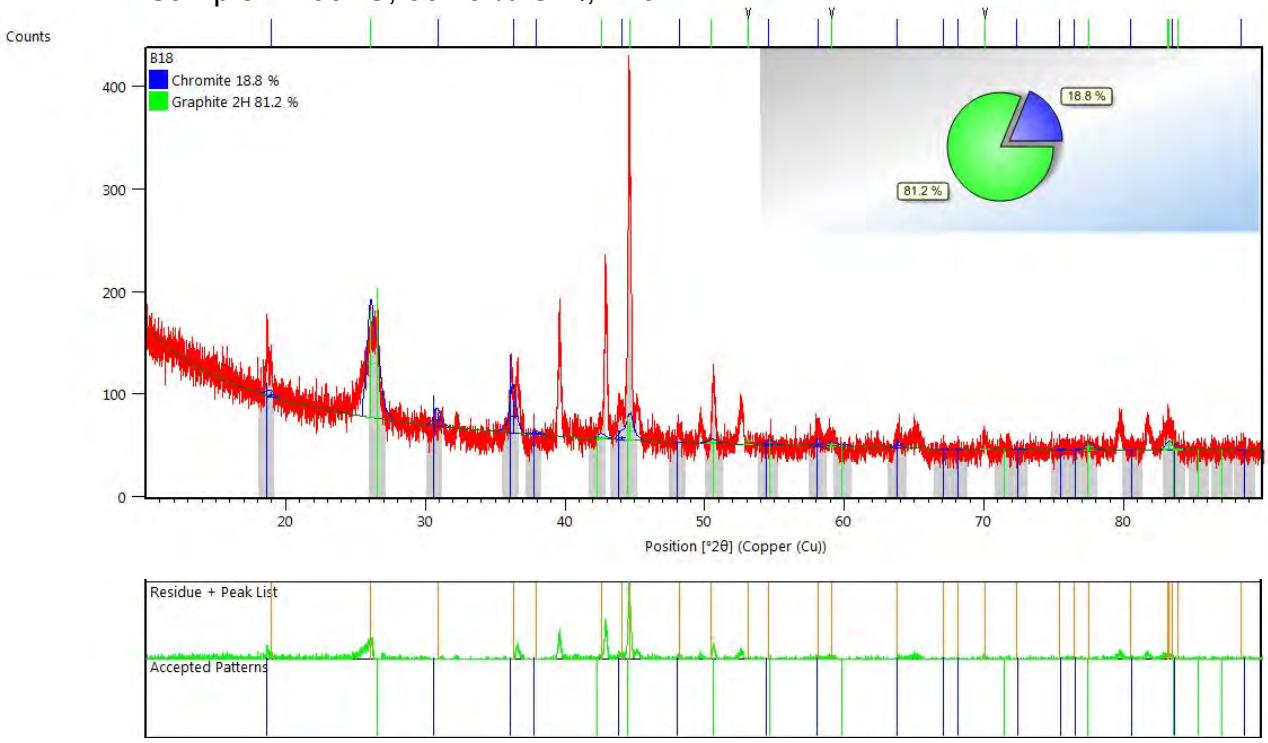

Appendix CXXXI

Sample: 1300 ˚C, 10 vol% CH_4, 10 min

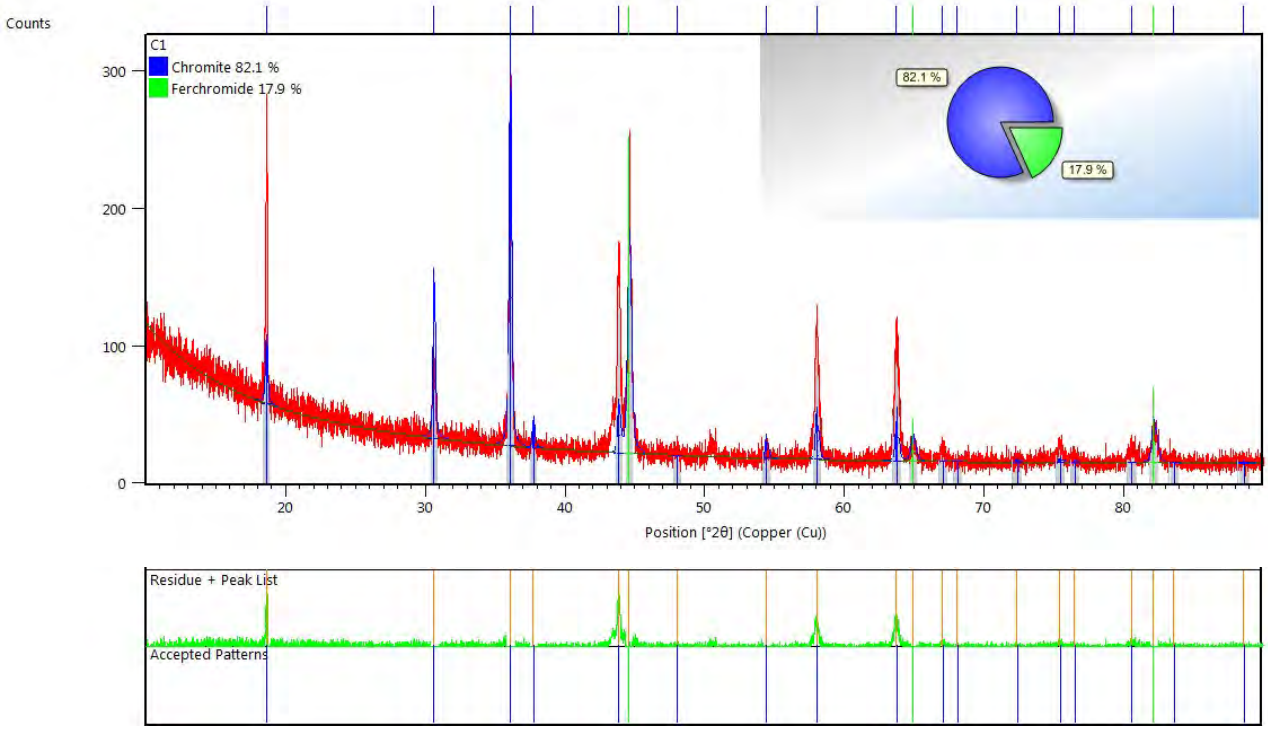

Sample: 1300 ˚C, 10 vol% CH_4, 20 min

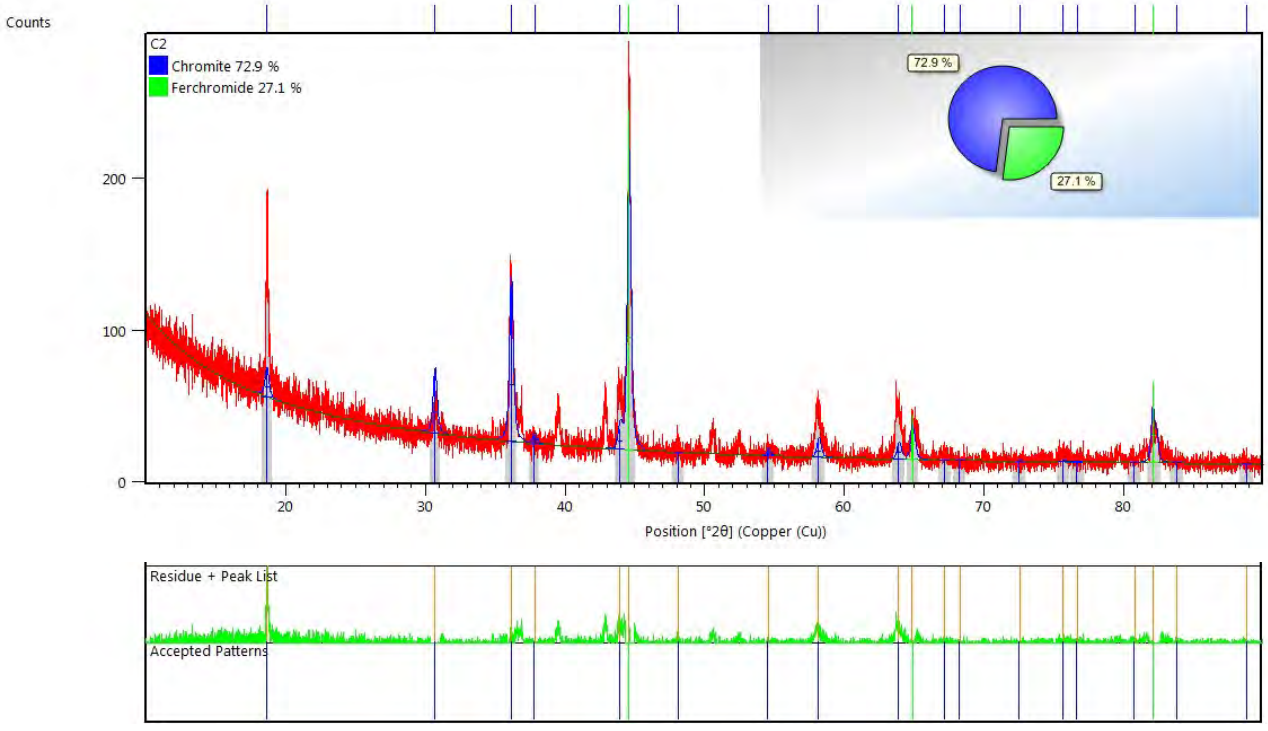

Appendix CXXXII

Sample: 1300 ˚C, 10 vol% CH_4, 30 min

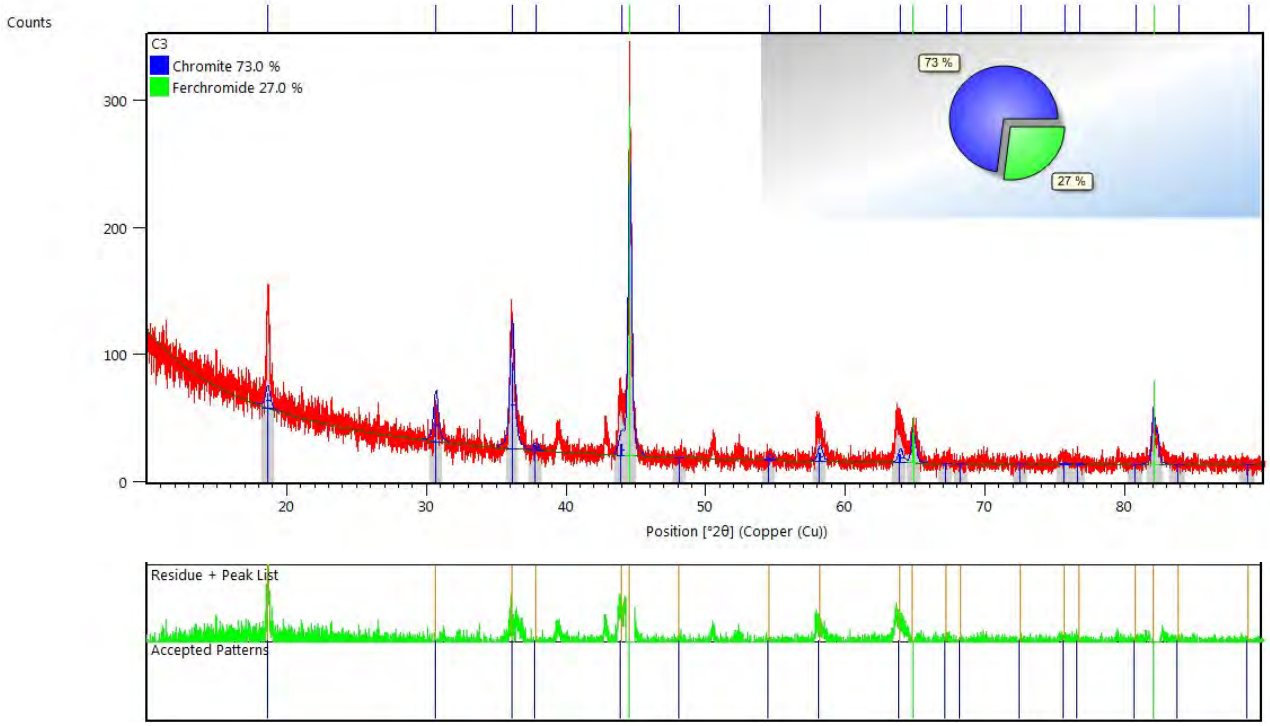

Sample: 1300 ˚C, 10 vol% CH_4, 60 min

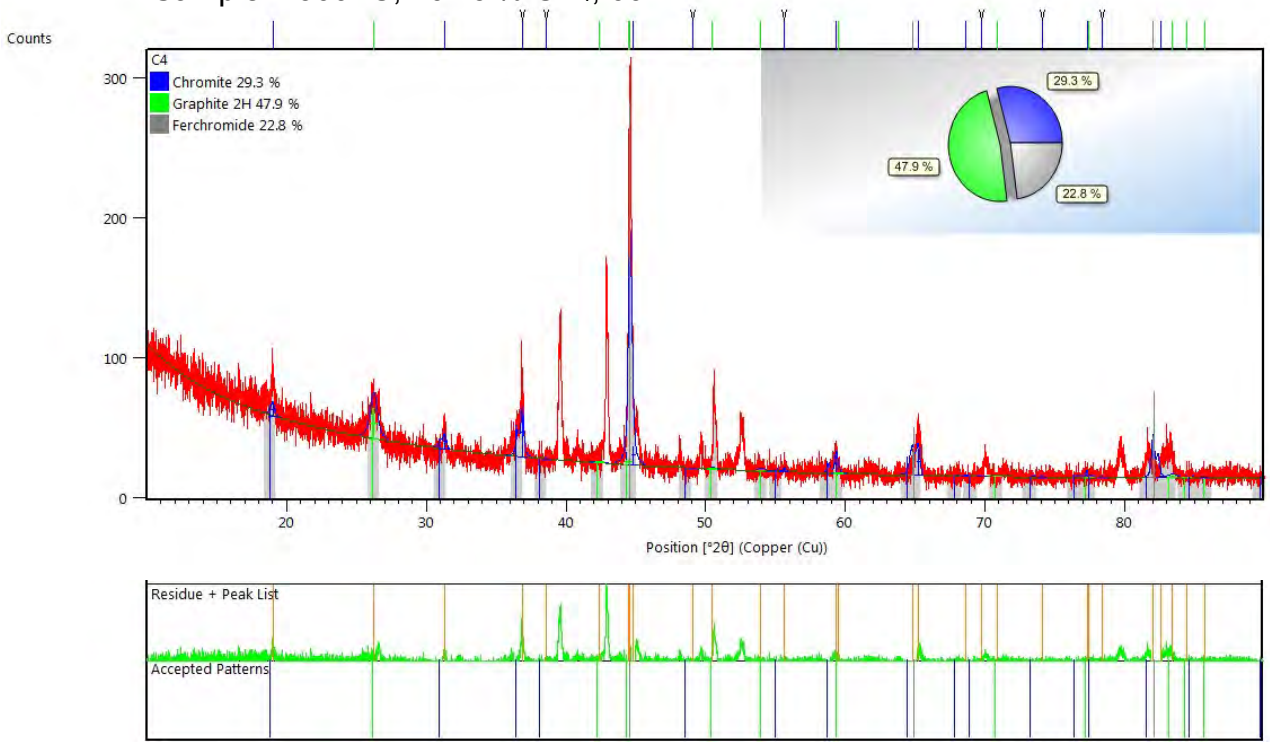

Appendix CXXXIII

Sample: 1300 ˚C, 10 vol% CH_4, 90 min

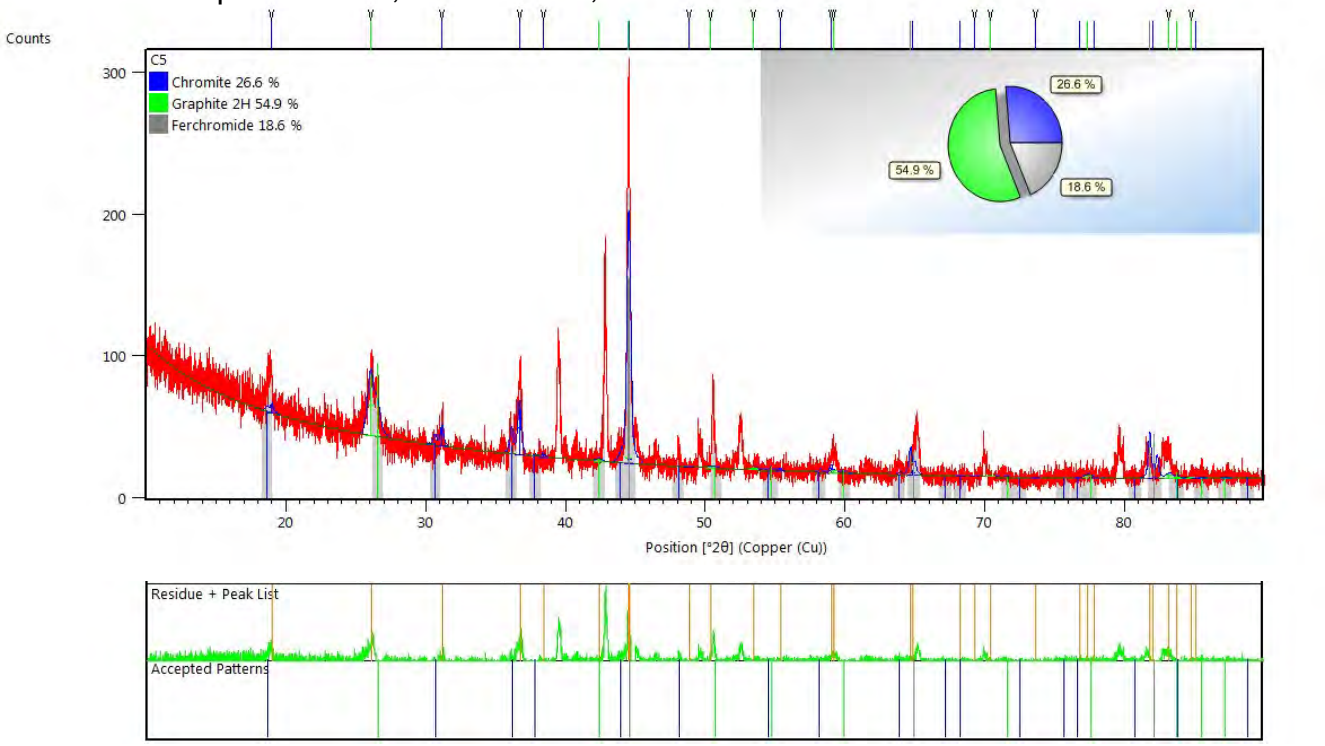

Sample: 1300 ˚C, 10 vol% CH_4, 120 min

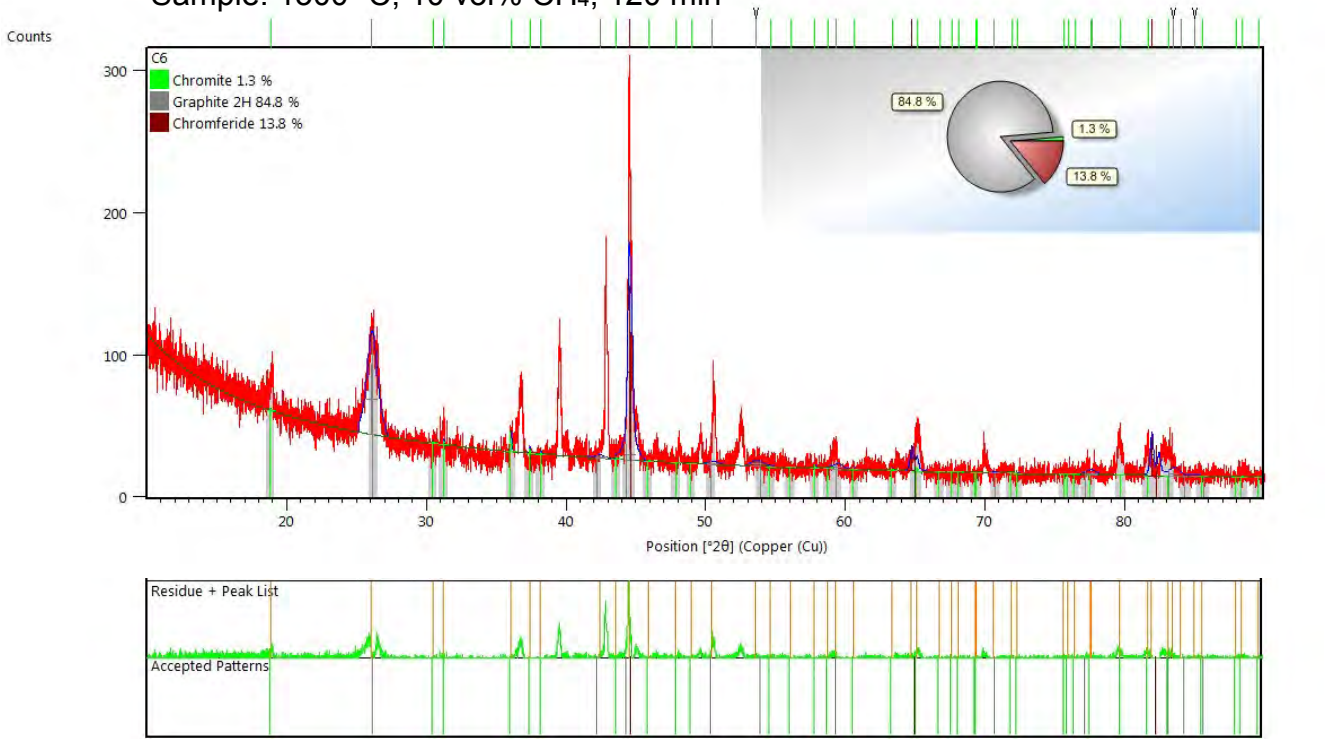

Appendix CXXXIV

Sample: 1300 ˚C, 20 vol% CH_4, 10 min

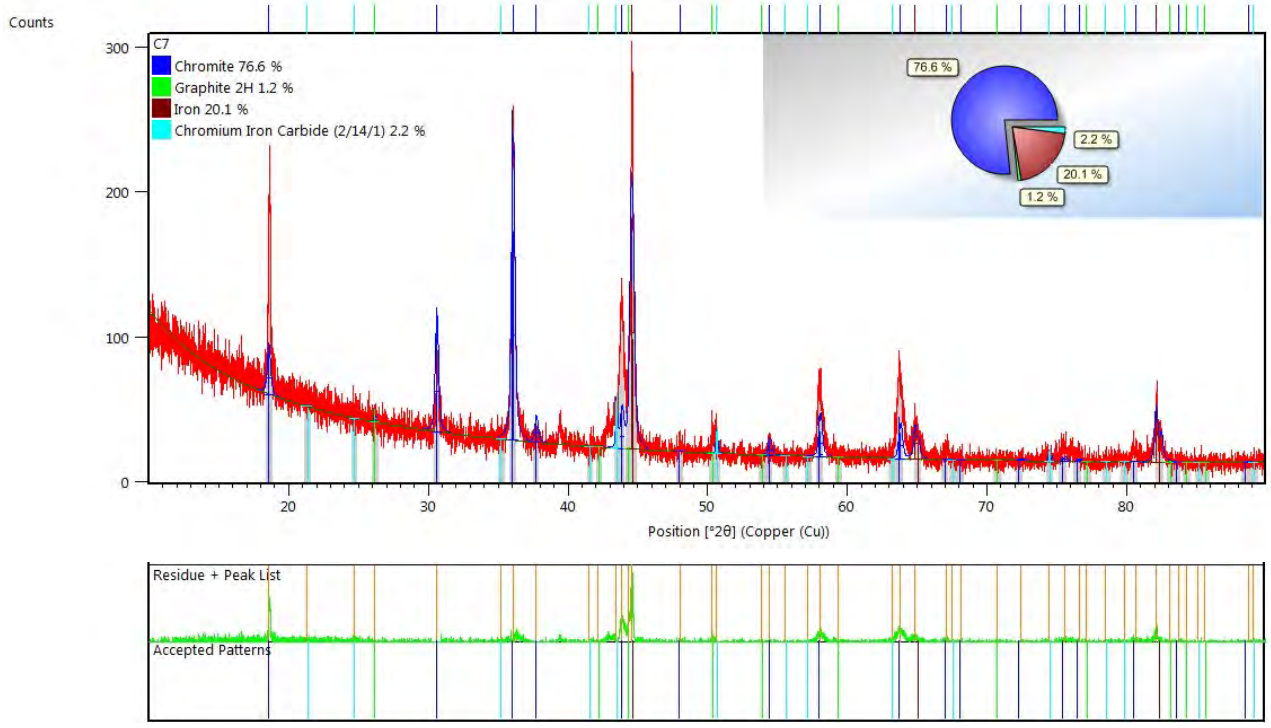

Sample: 1300 ˚C, 20 vol% CH_4, 20 min

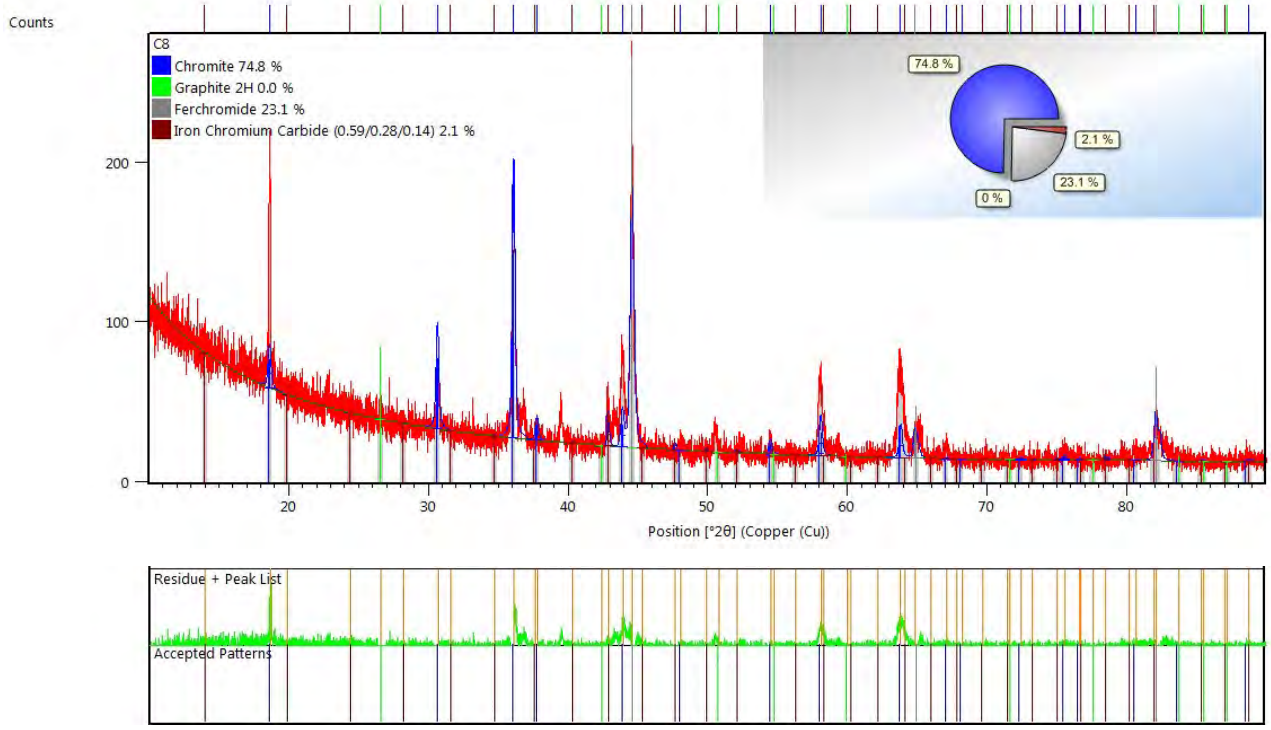

Appendix CXXXV

Sample: 1300 ˚C, 20 vol% CH_4, 30 min

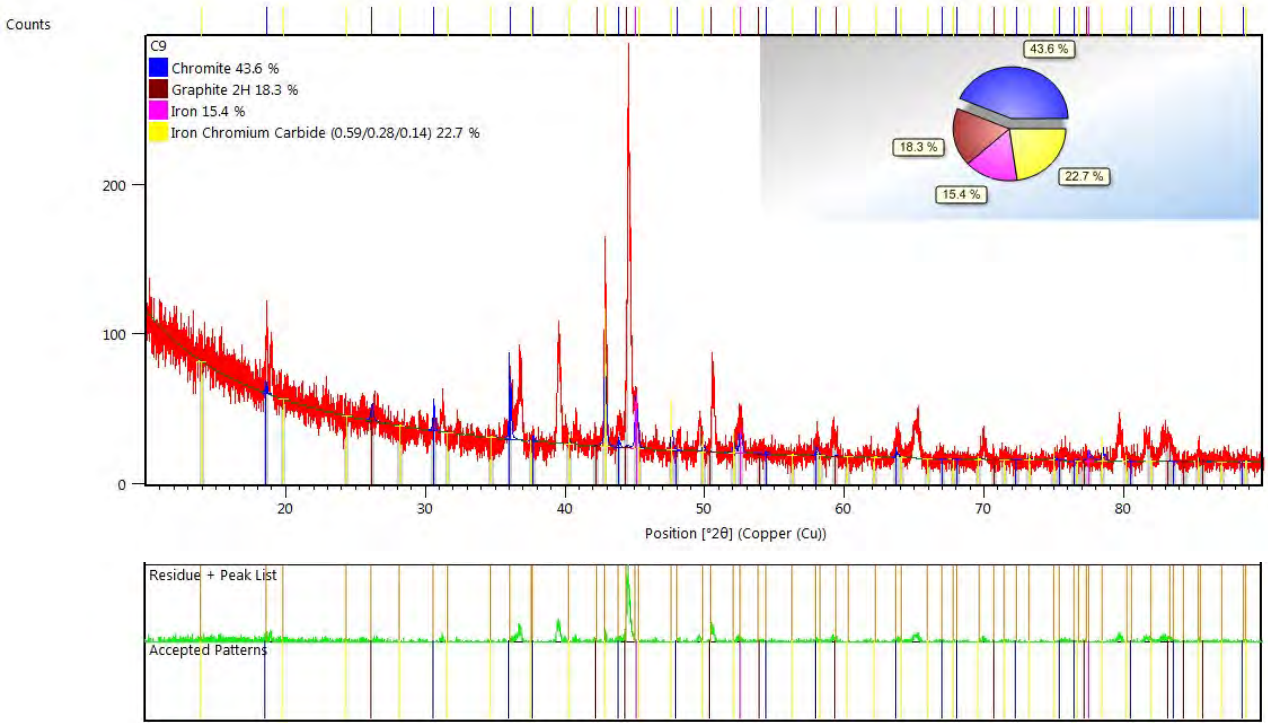

Sample: 1300 ˚C, 20 vol% CH_4, 60 min

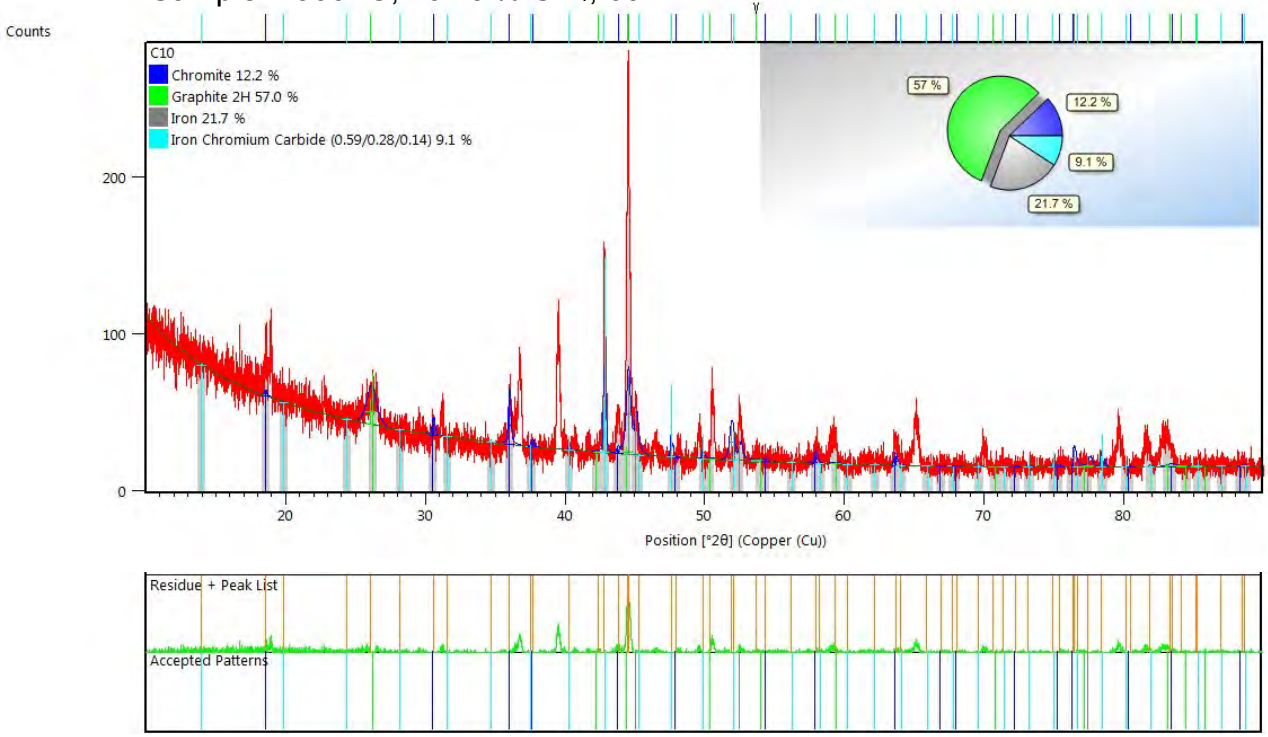

Appendix CXXXVI

Sample: 1300 ˚C, 20 vol% CH_4, 90 min

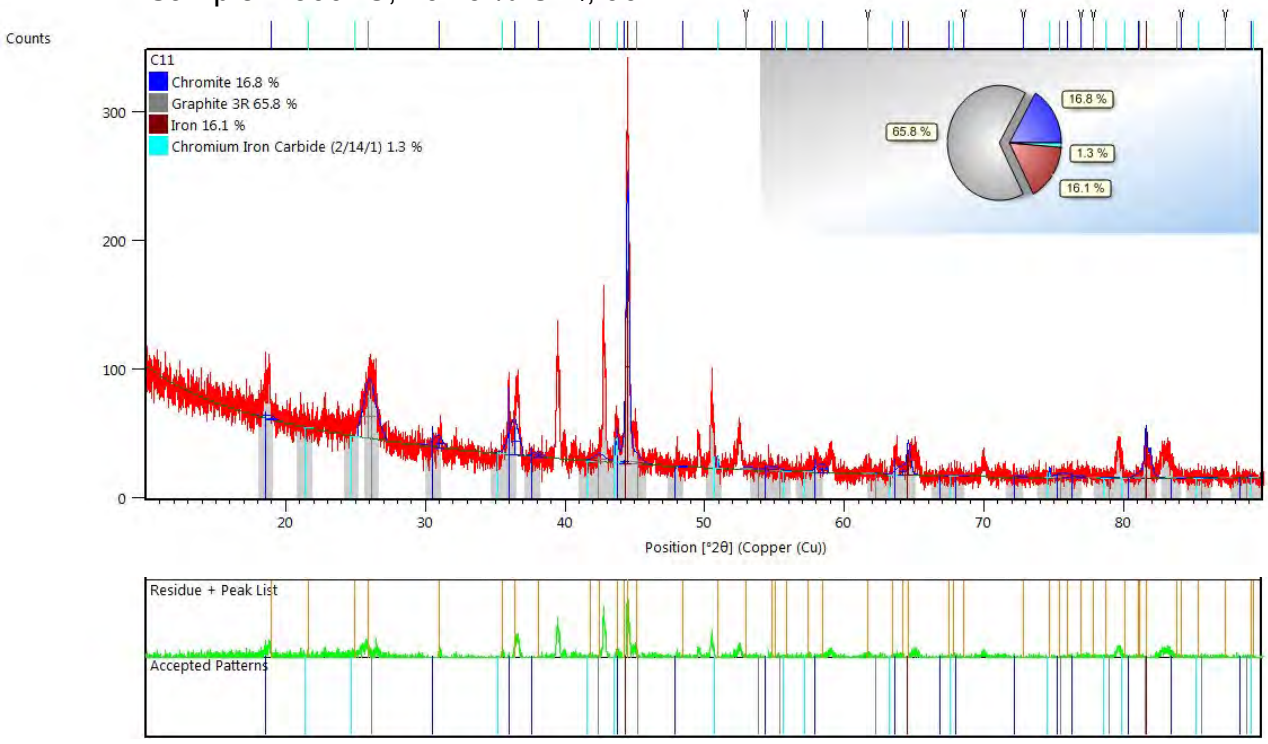

Sample: 1300 ˚C, 20 vol% CH_4, 120 min

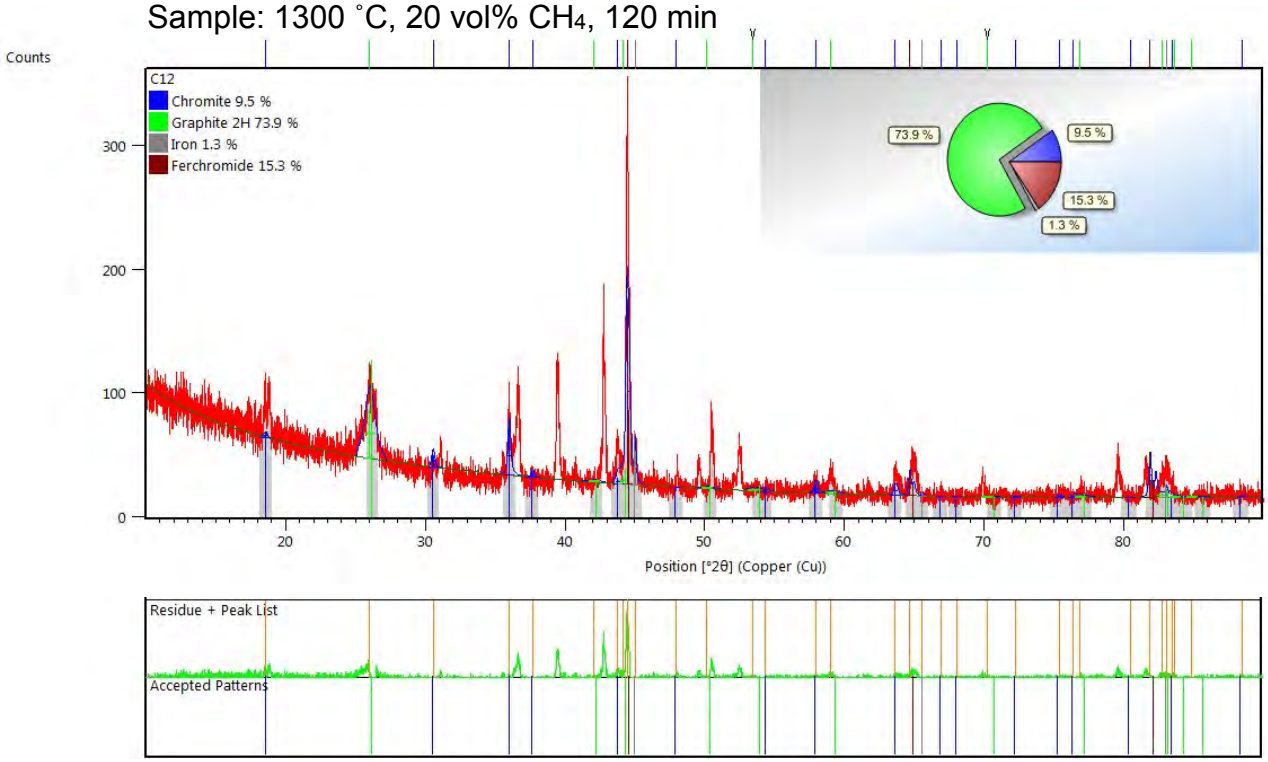

Appendix CXXXVII

Sample: 1300 ˚C, 30 vol% CH_4, 10 min

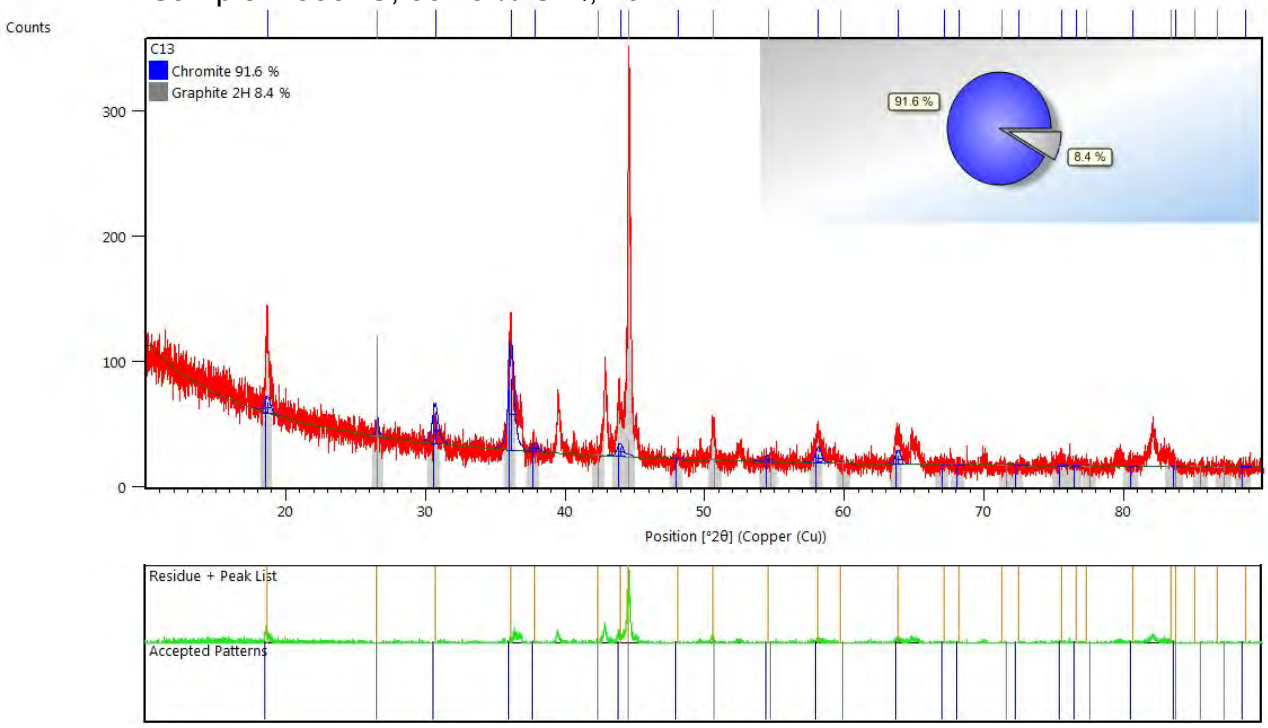

Sample: 1300 ˚C, 30 vol% CH_4, 20 min

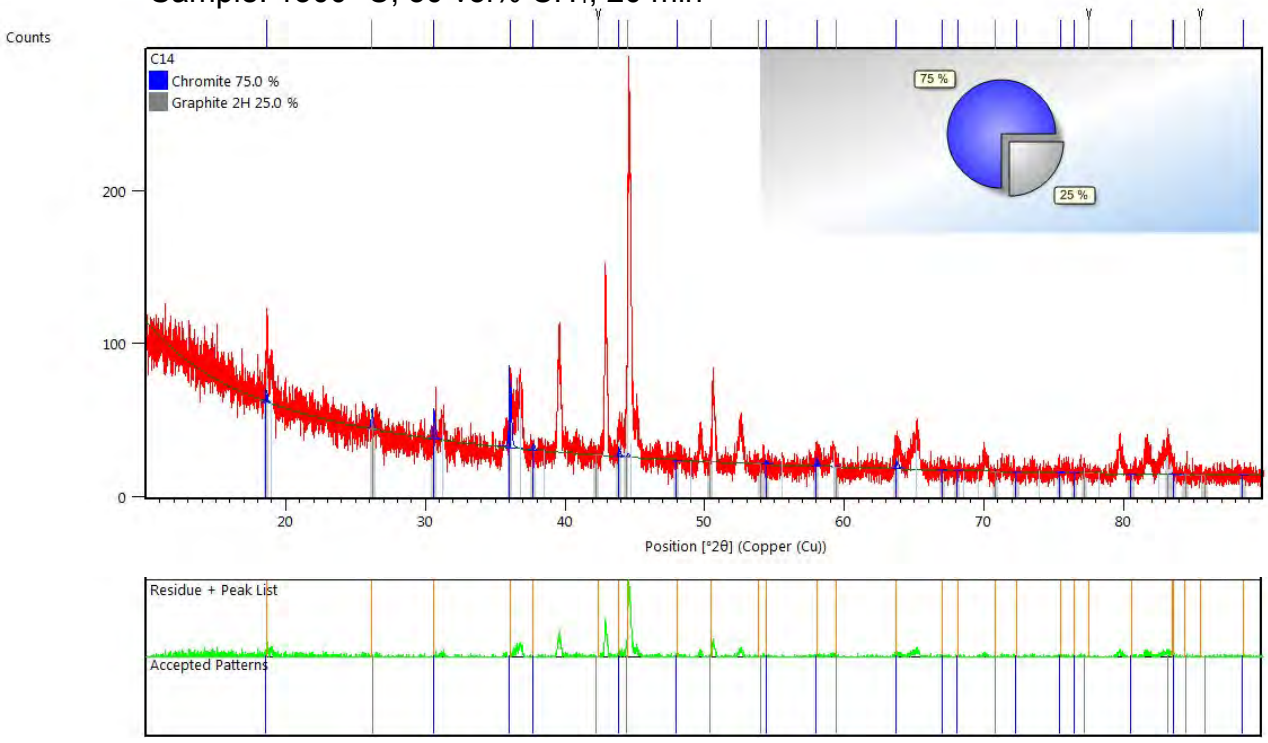

Appendix CXXXVIII

Sample: 1300 ˚C, 30 vol% CH_4, 30 min

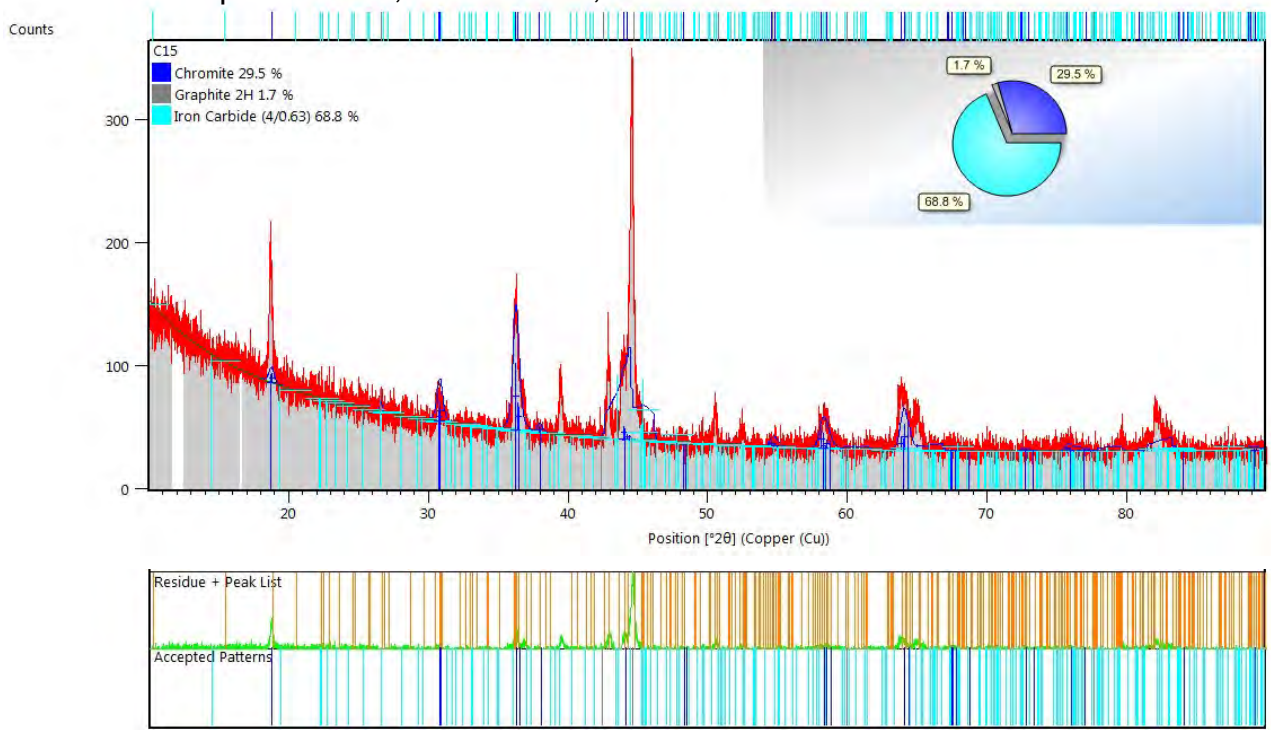

Sample: 1300 ˚C, 30 vol% CH_4, 60 min

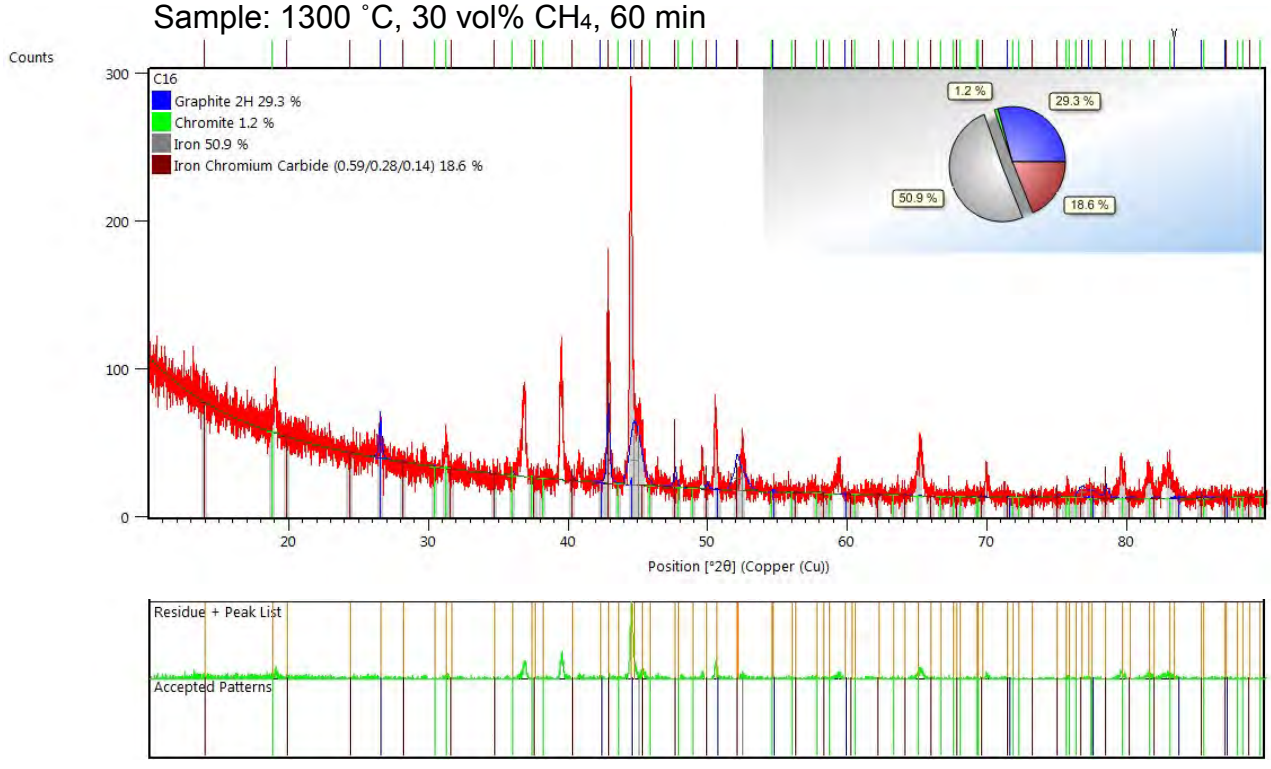

Appendix CXXXIX

Sample: 1300 ˚C, 30 vol% CH_4, 90 min

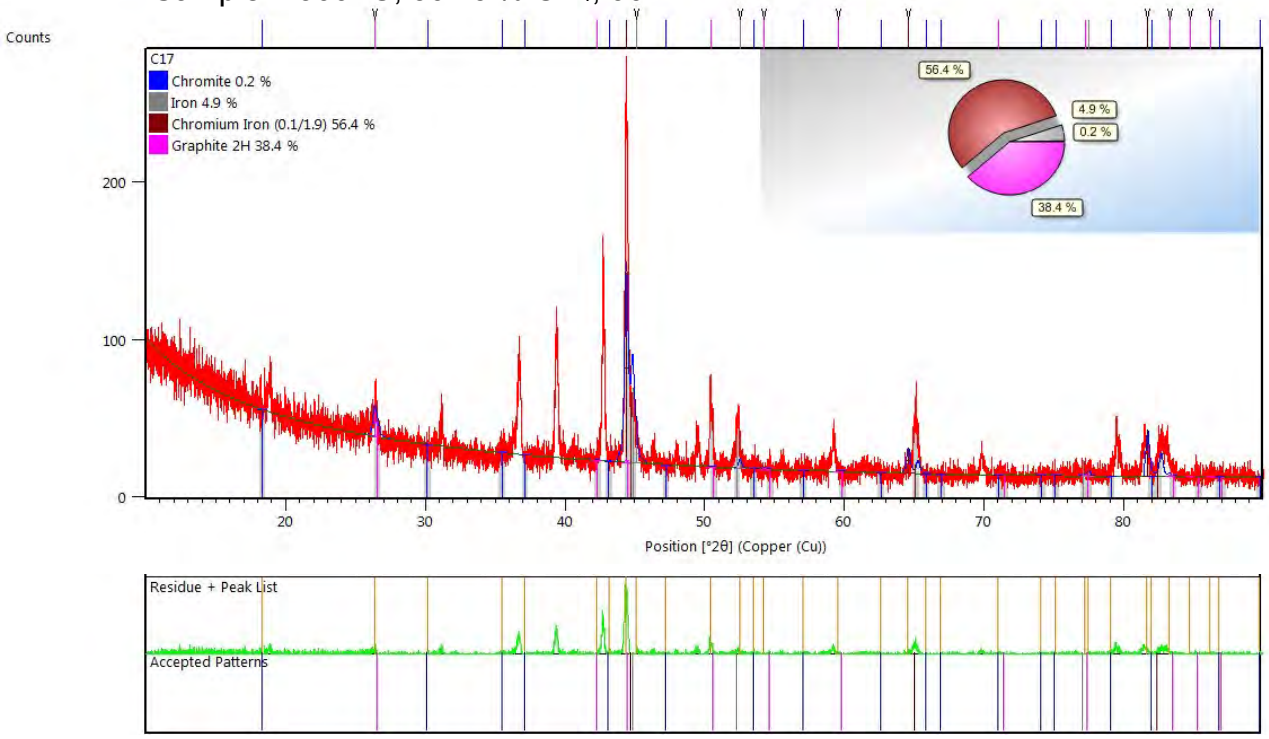

Sample: 1300 ˚C, 30 vol% CH_4, 120 min

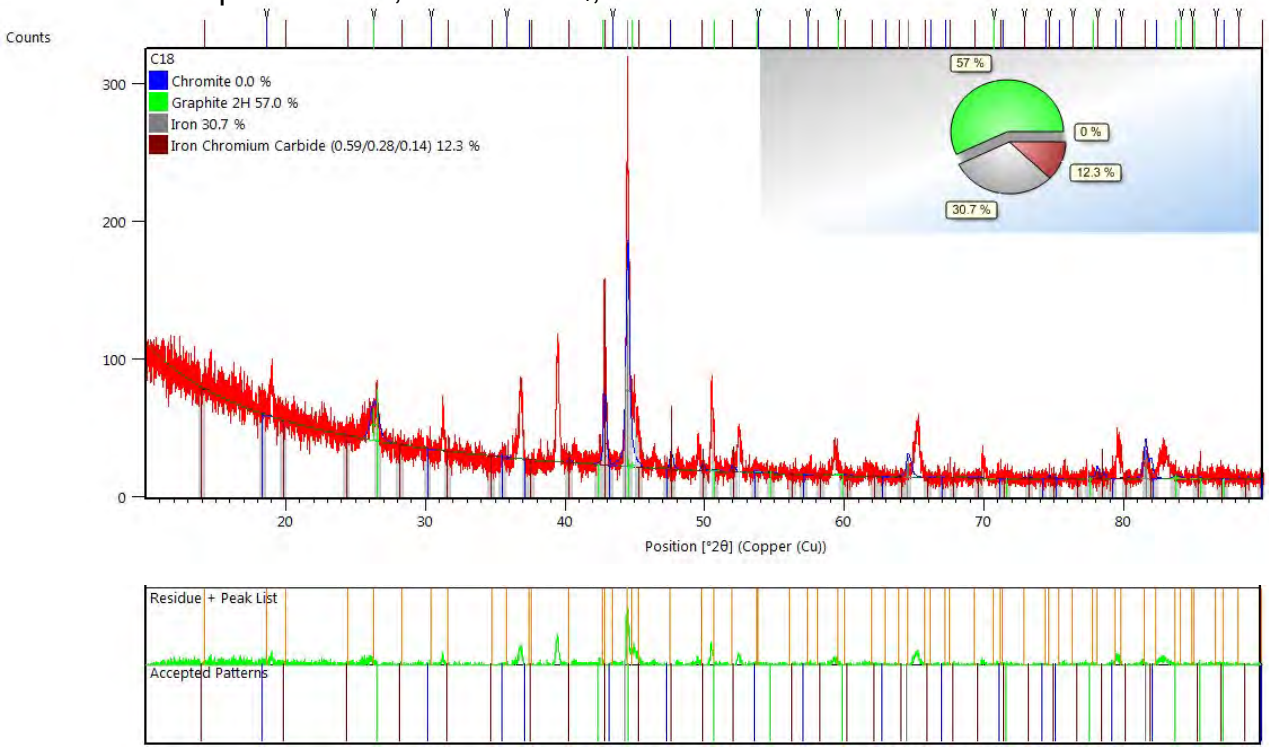

Appendix CXL

Sample: 1350 ˚C, 10 vol% CH_4, 10 min

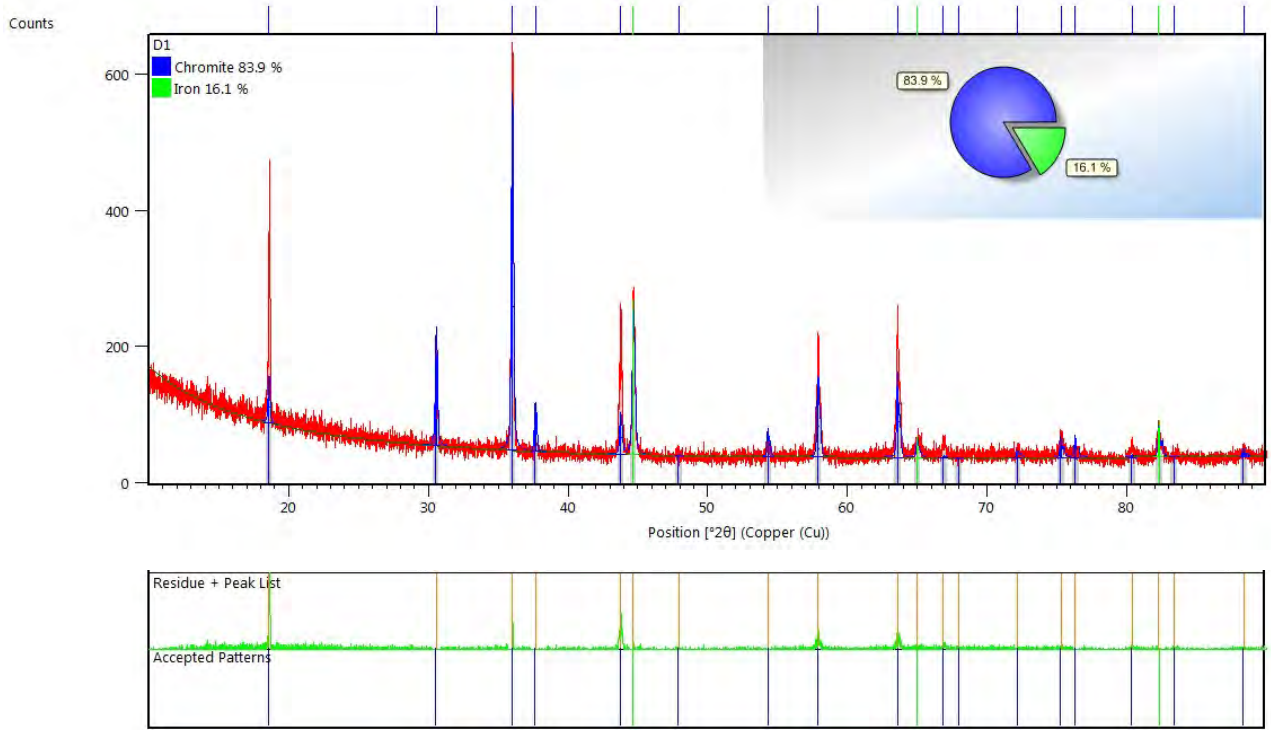

Sample: 1350 ˚C, 10 vol% CH_4, 20 min

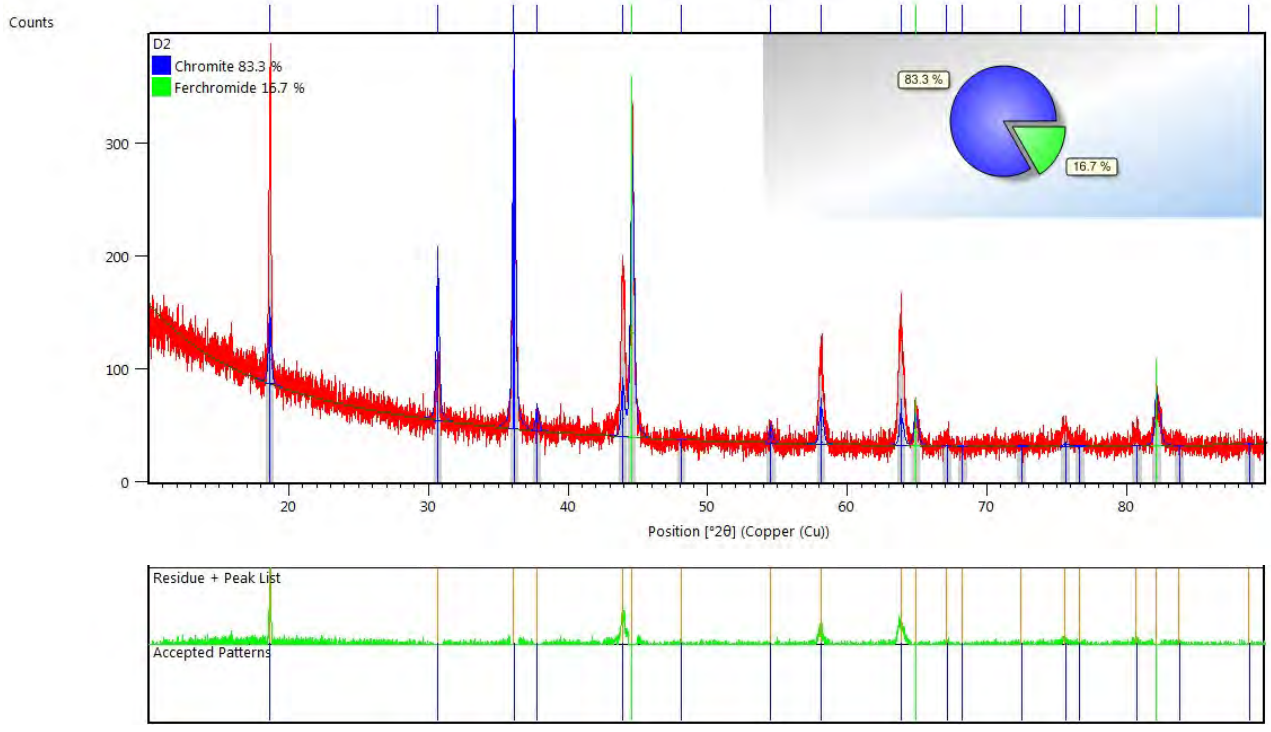

Appendix CXLI

Sample: 1350 ˚C, 10 vol% CH_4, 30 min

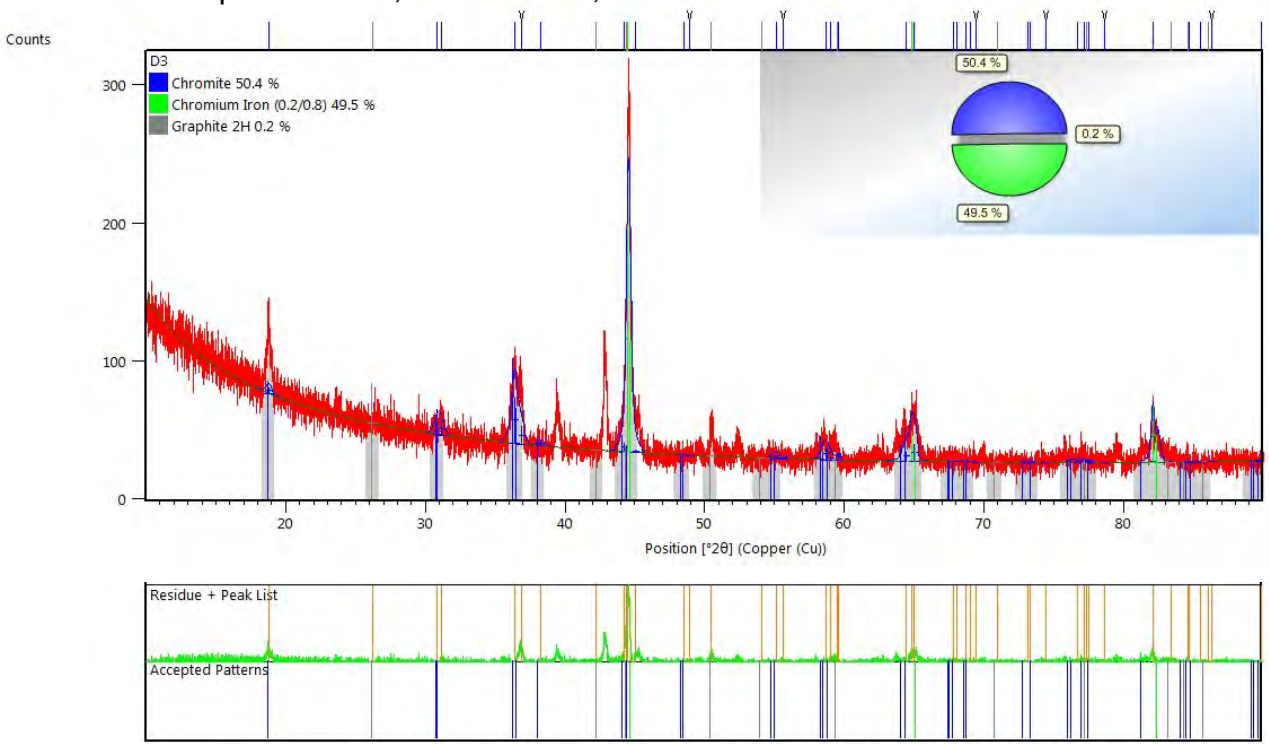

Sample: 1350 ˚C, 10 vol% CH_4, 60 min

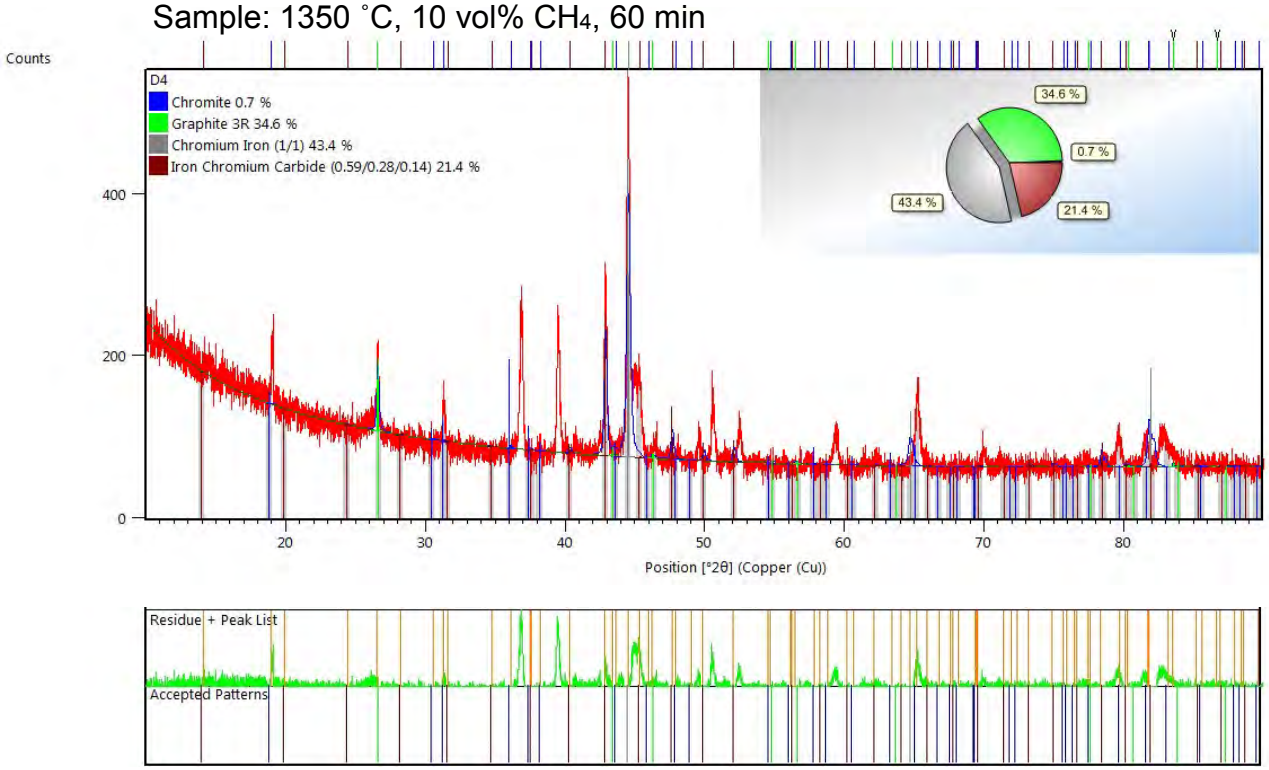

Appendix CXLII

Sample: 1350 ˚C, 10 vol% CH_4, 90 min

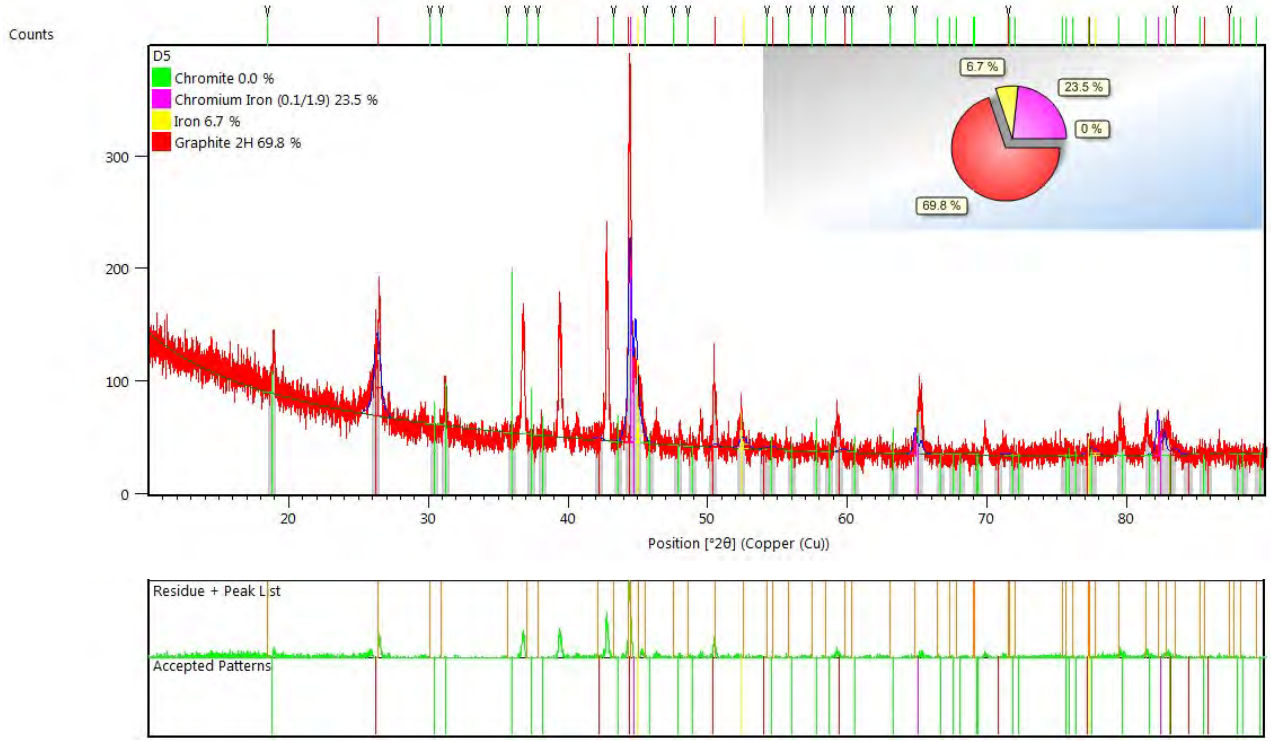

Sample: 1350 ˚C, 10 vol% CH_4, 120 min

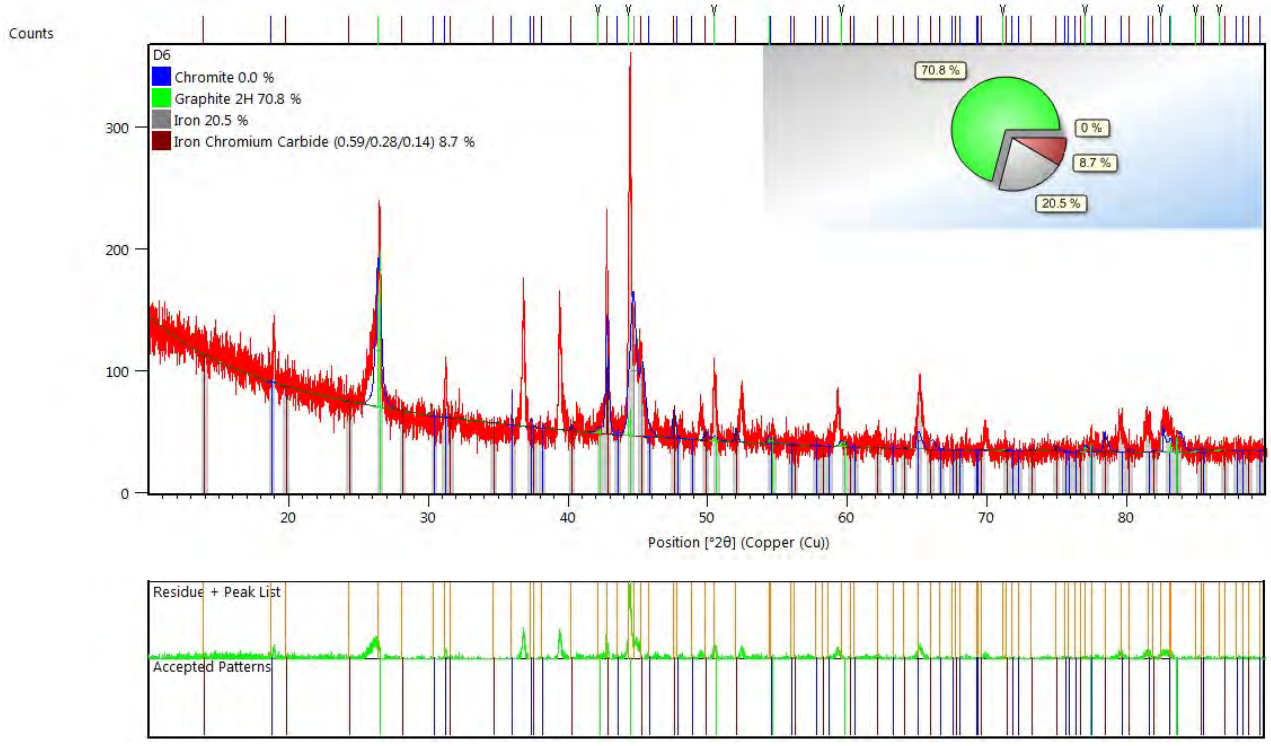

Appendix CXLIII

Sample: 1350 ˚C, 20 vol% CH_4, 10 min

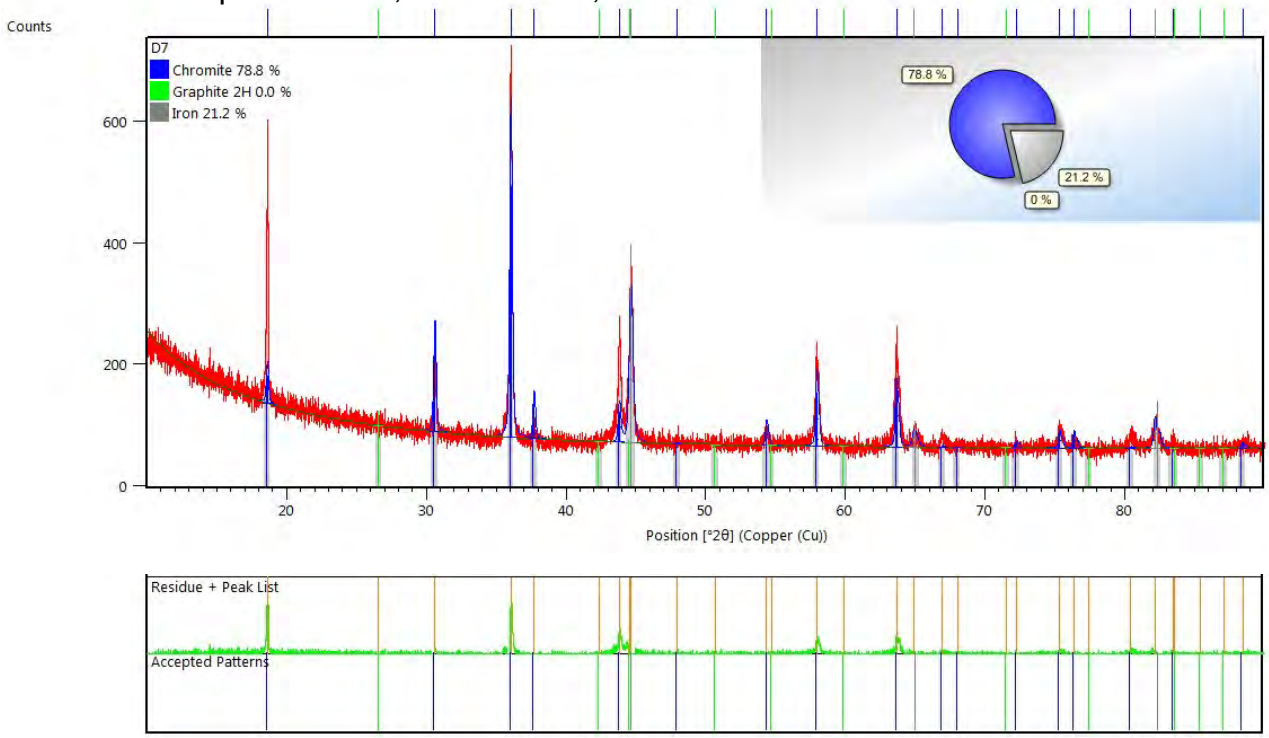

Sample: 1350 ˚C, 20 vol% CH_4, 20 min

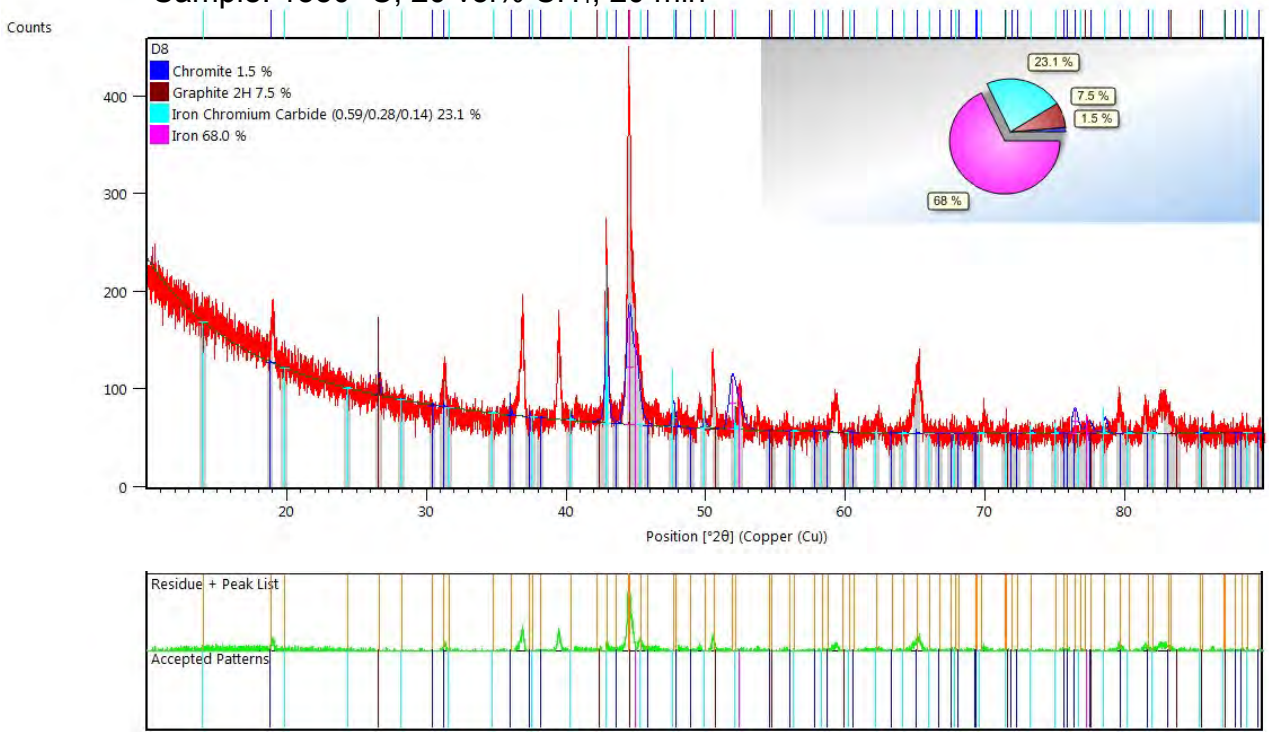

Appendix CXLIV

Sample: 1350 ˚C, 20 vol% CH_4, 30 min

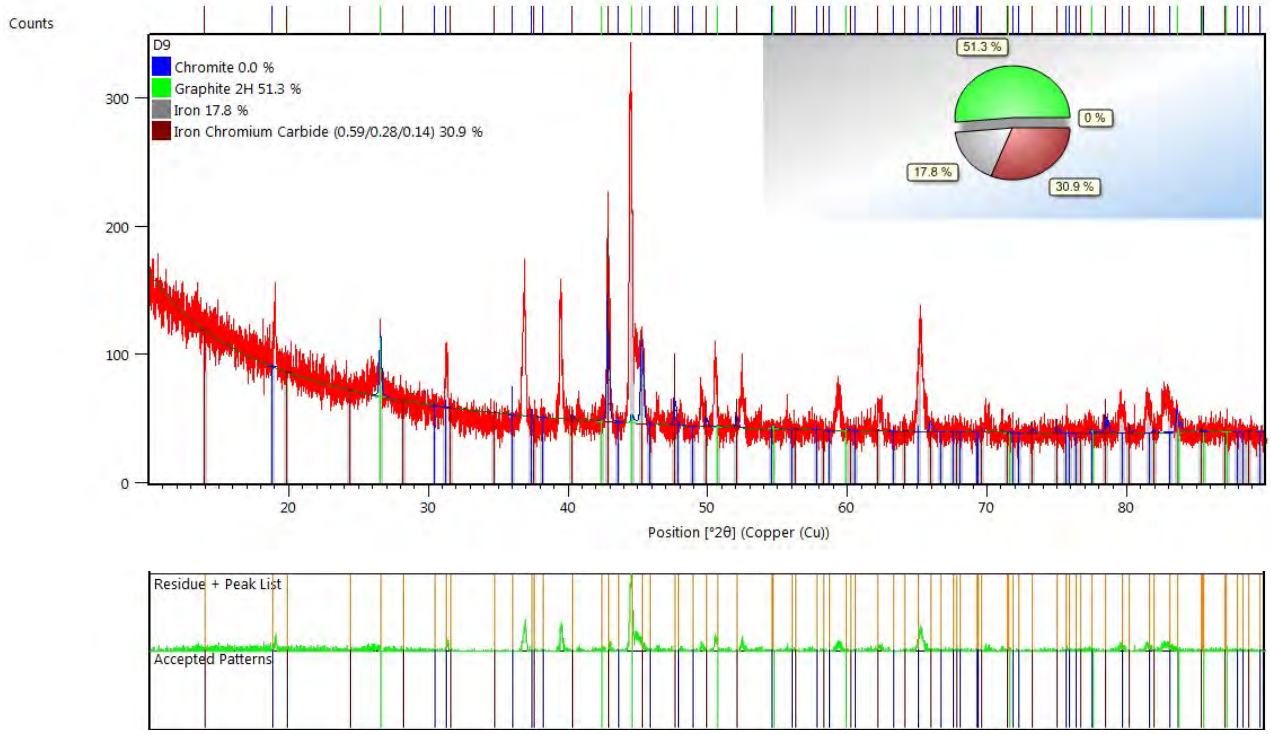

Sample: 1350 ˚C, 20 vol% CH_4, 60 min

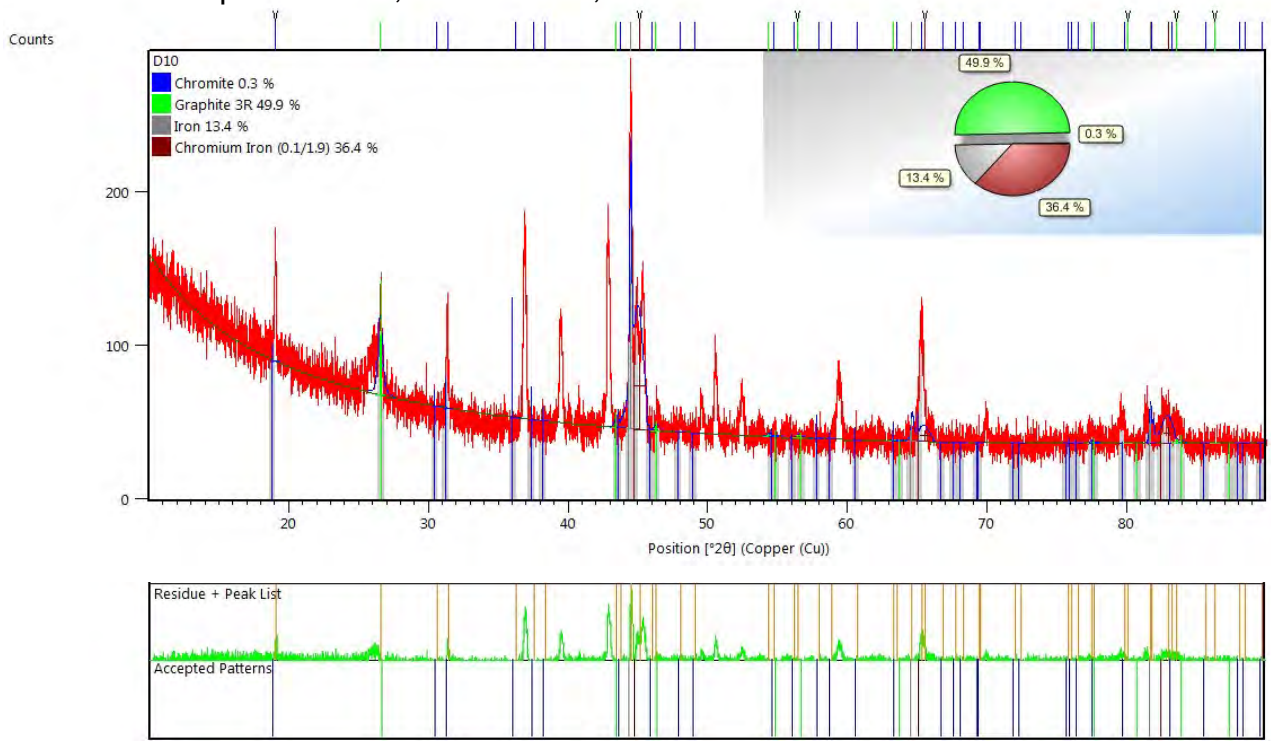

Appendix CXLV

Sample: 1350 ˚C, 20 vol% CH_4, 90 min

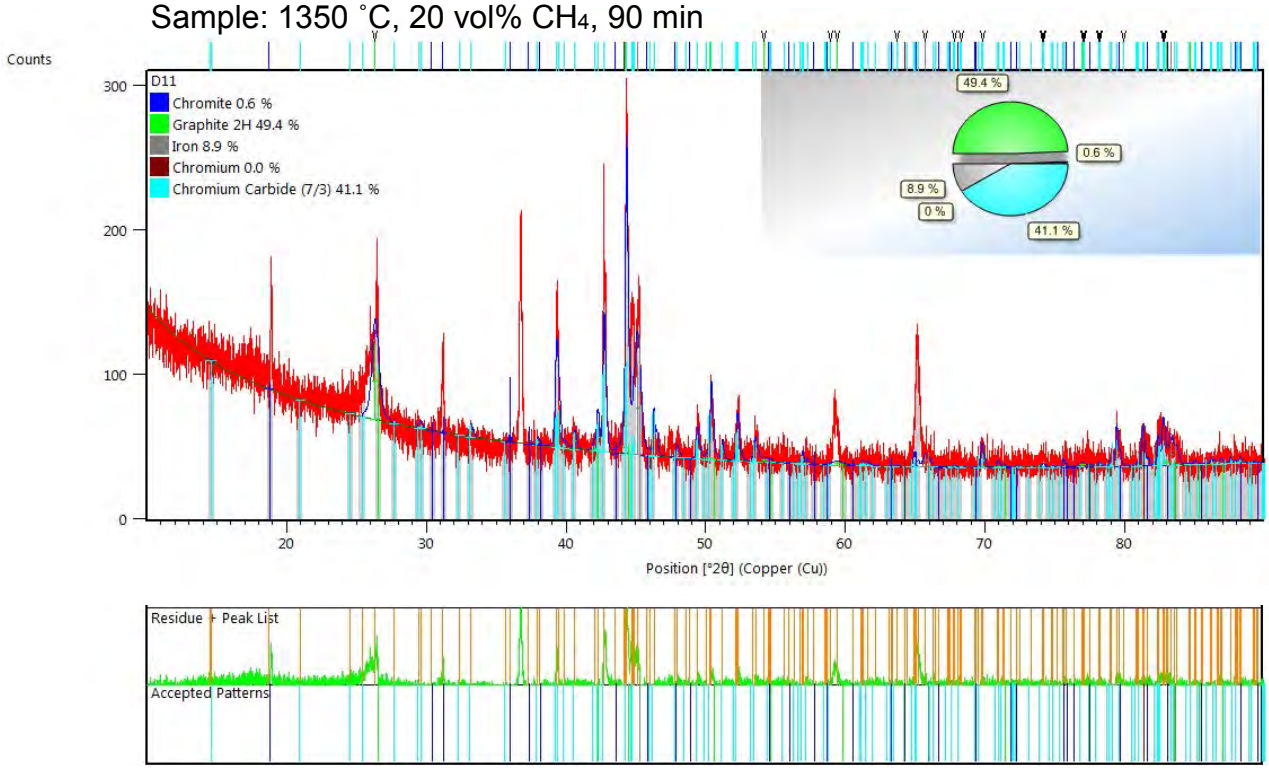

Sample: 1350 ˚C, 20 vol% CH_4, 120 min

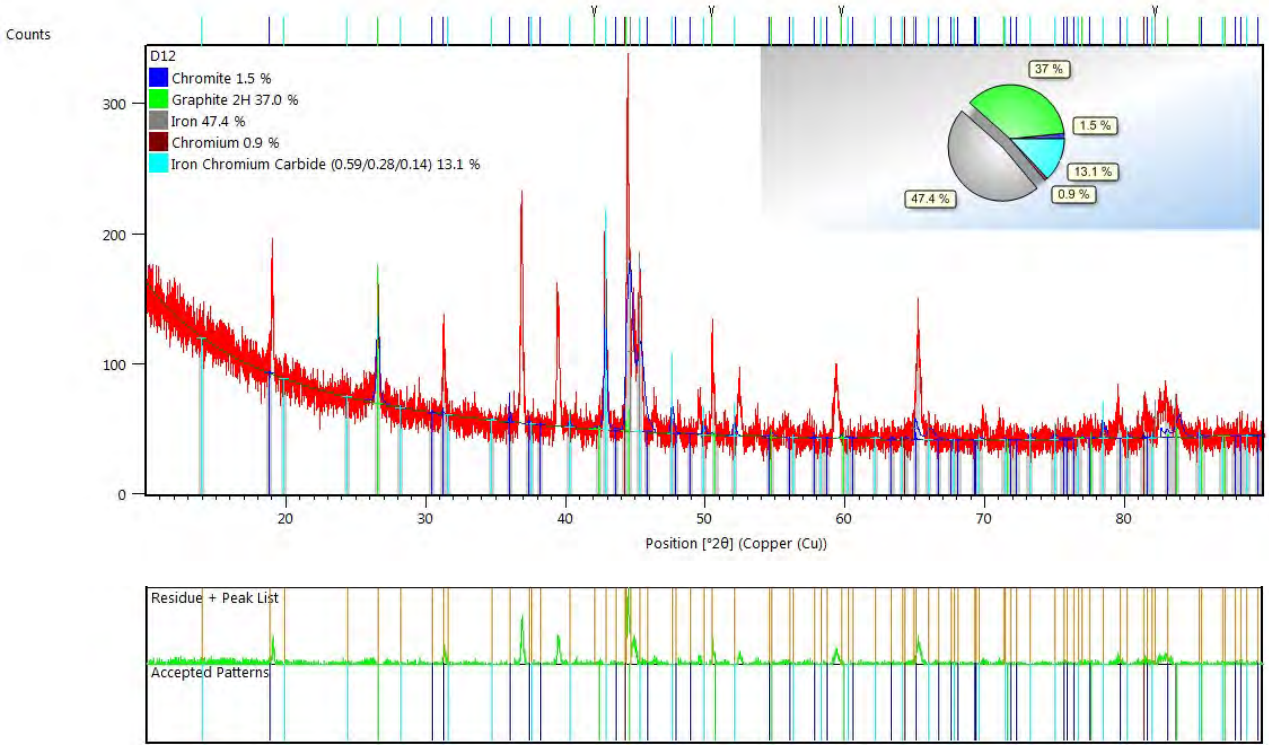

Appendix CXLVI

Sample: 1350 ˚C, 30 vol% CH_4, 10 min

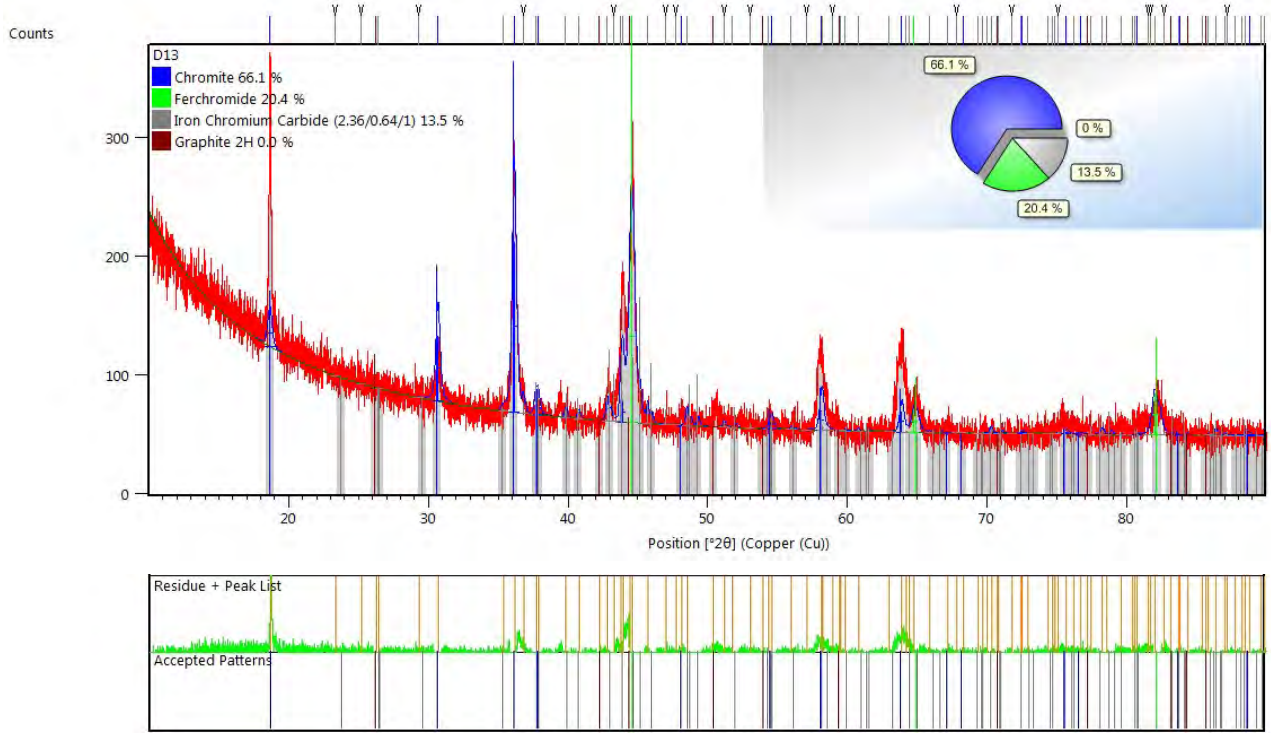

Sample: 1350 ˚C, 30 vol% CH_4, 20 min

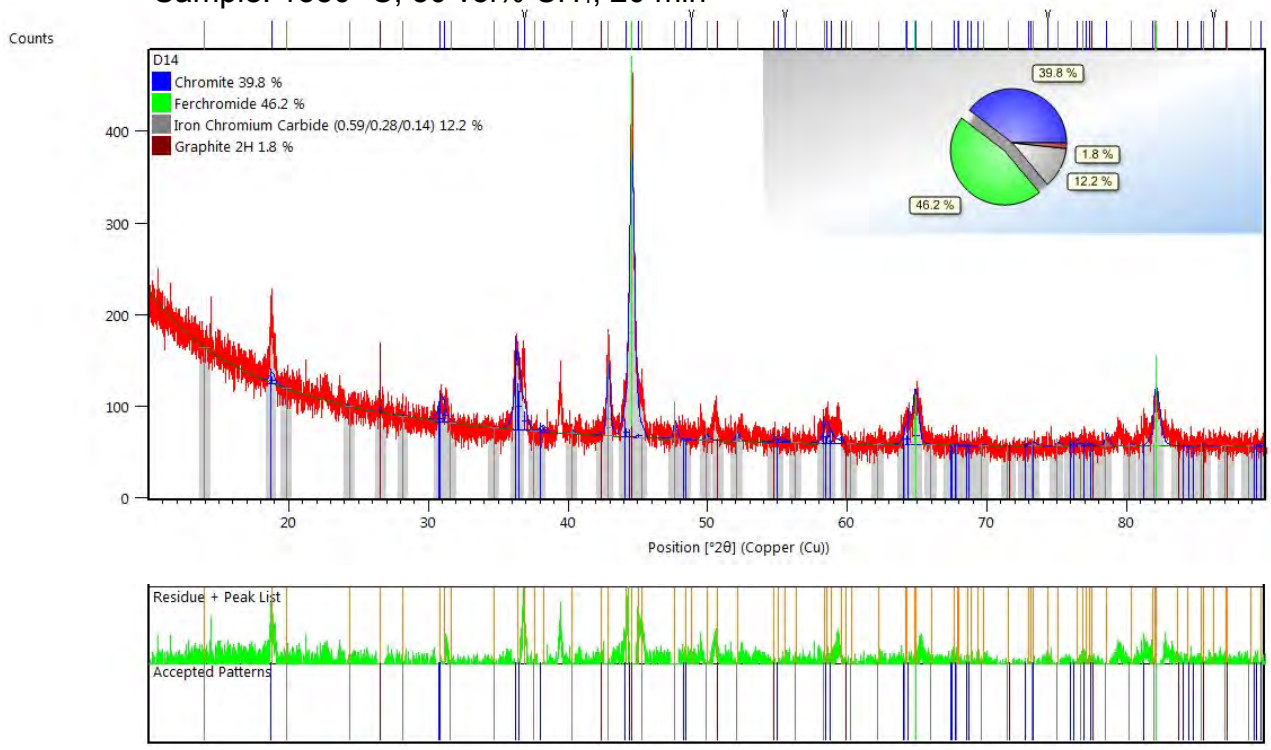

Appendix CXLVII

Sample: 1350 ˚C, 30 vol% CH_4, 30 min

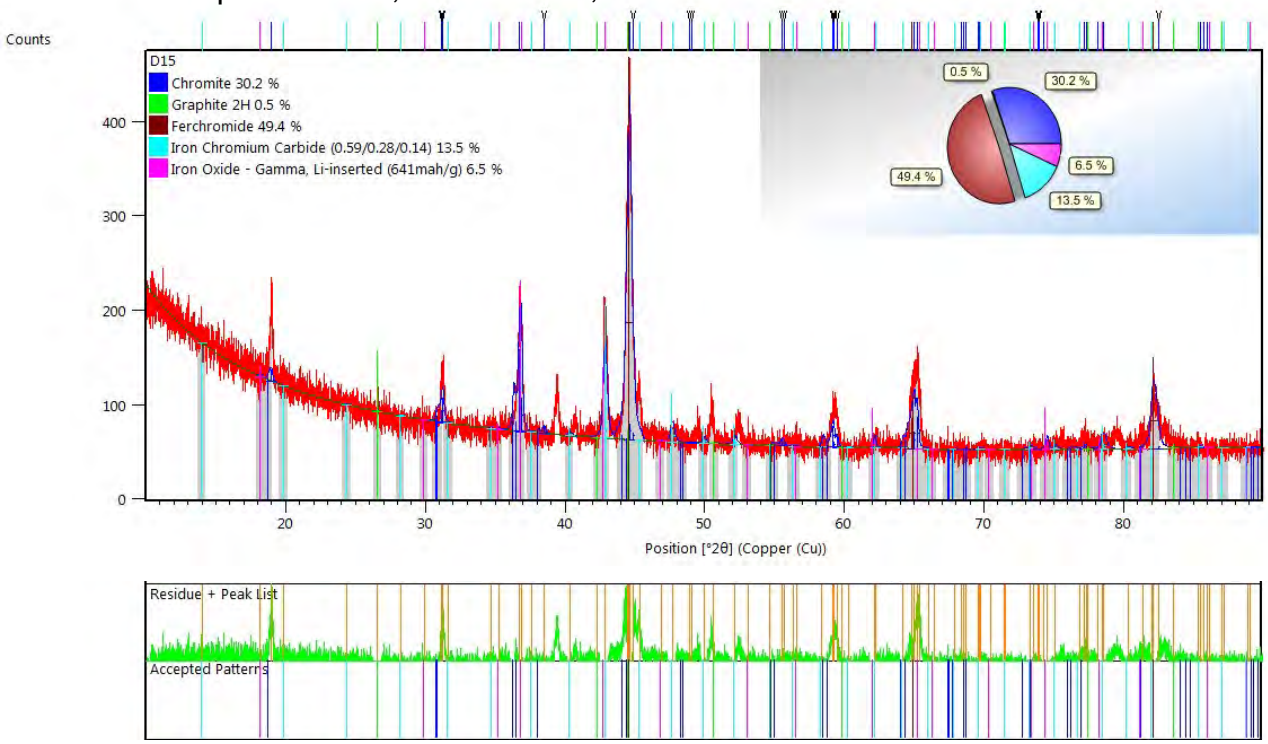

Sample: 1350 ˚C, 30 vol% CH_4, 60 min – categorized as a failed experiment

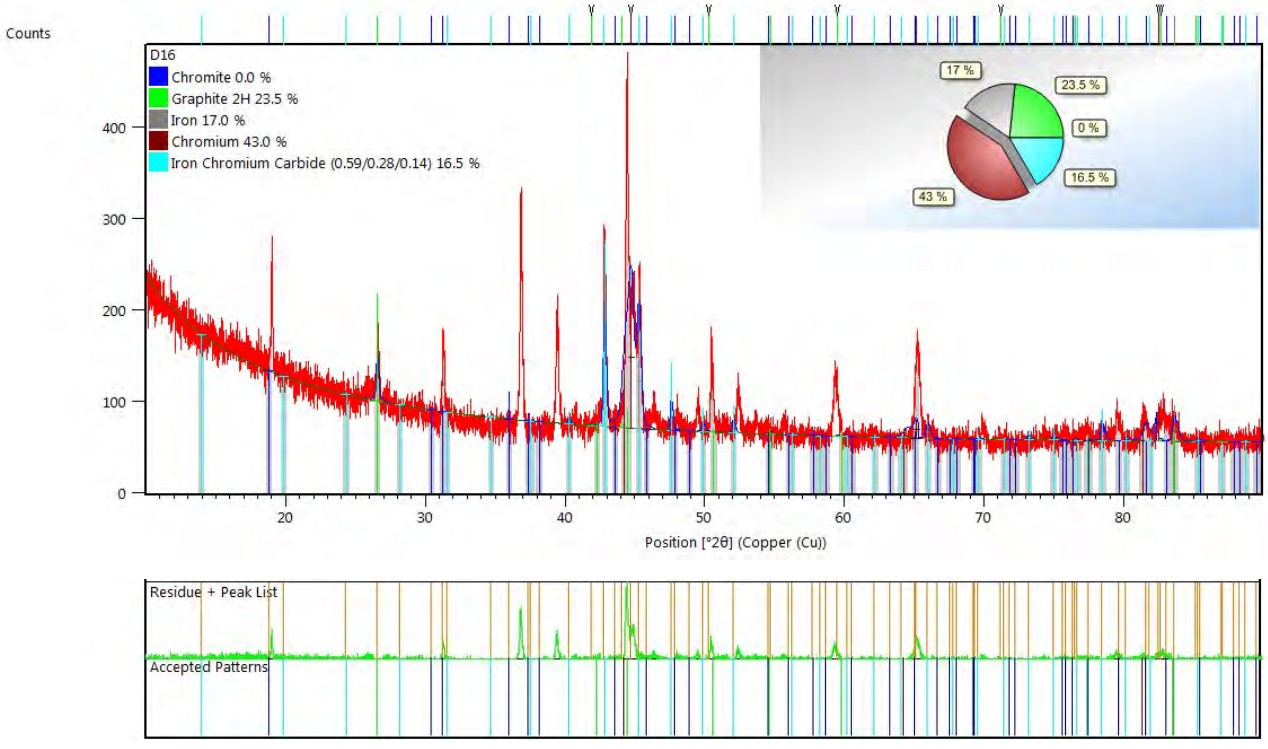

Appendix CXLVIII

Sample: 1350 ˚C, 30 vol% CH_4, 90 min

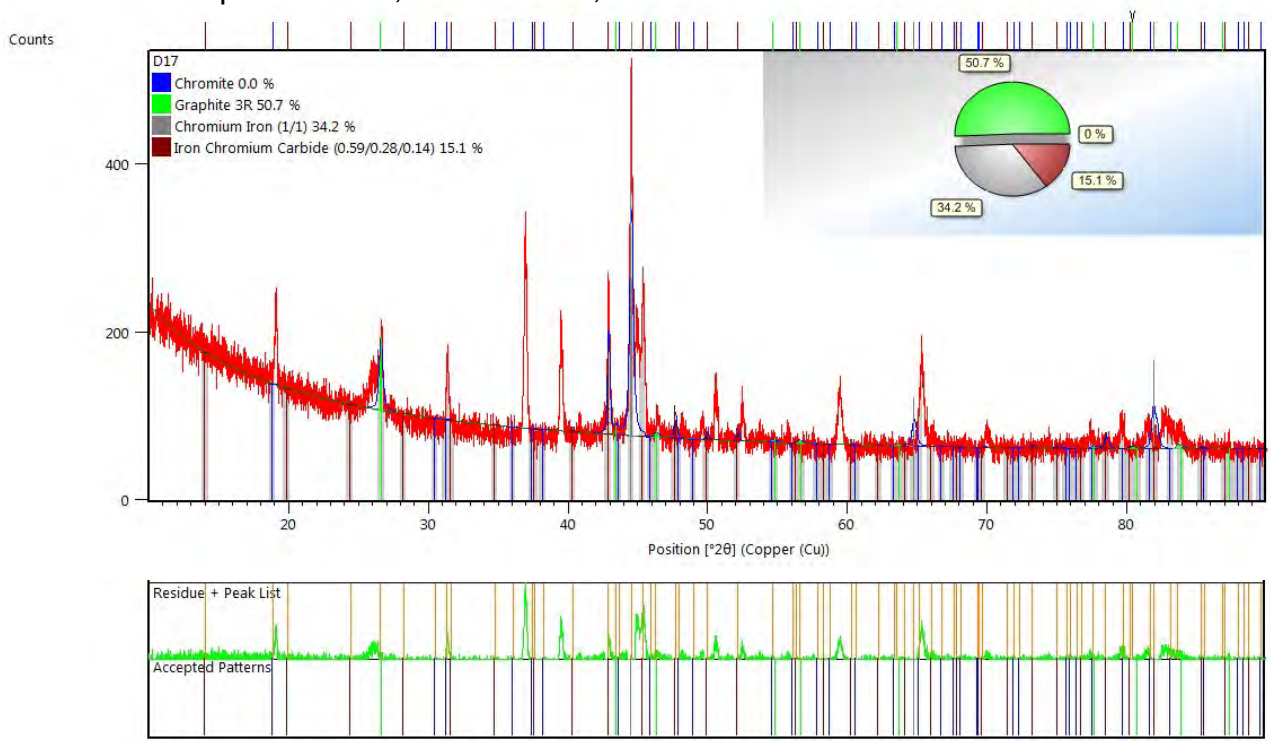

Sample: 1350 ˚C, 30 vol% CH_4, 120 min

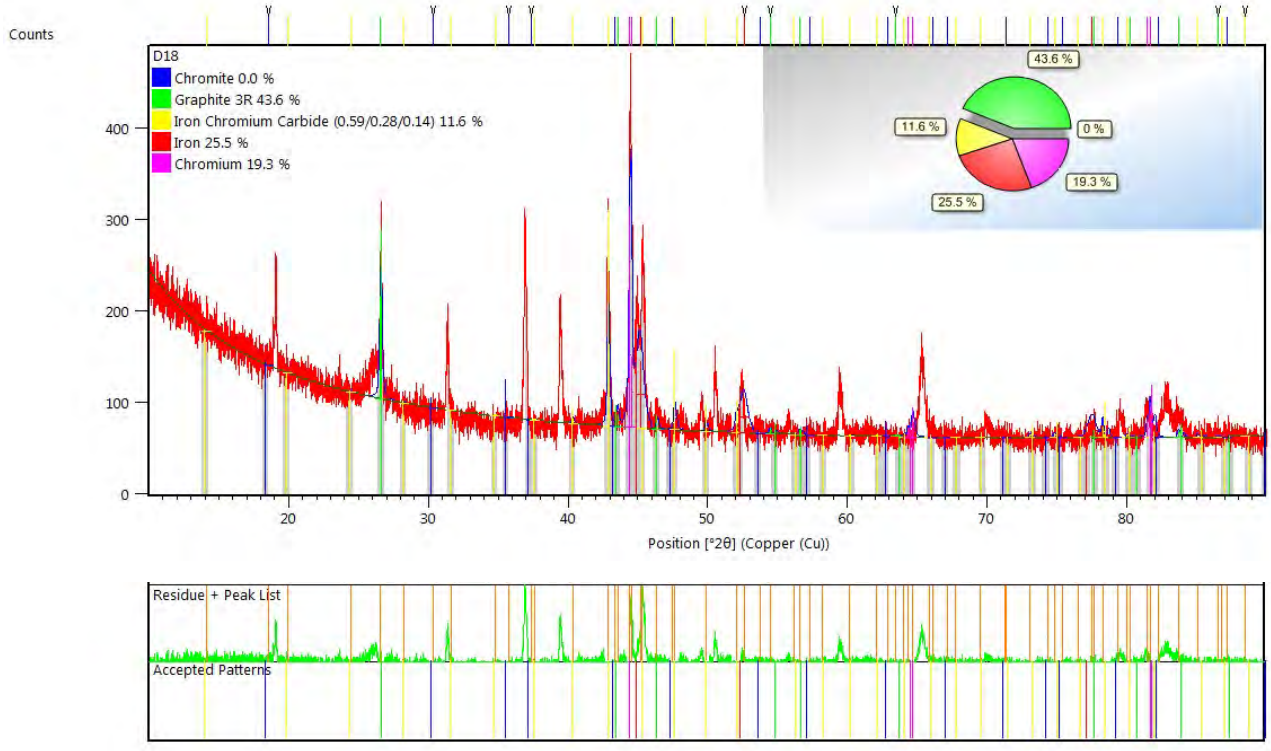

Appendix CXLIX

Sample: 1300 ˚C, 99,9995 vol% C, 120 min

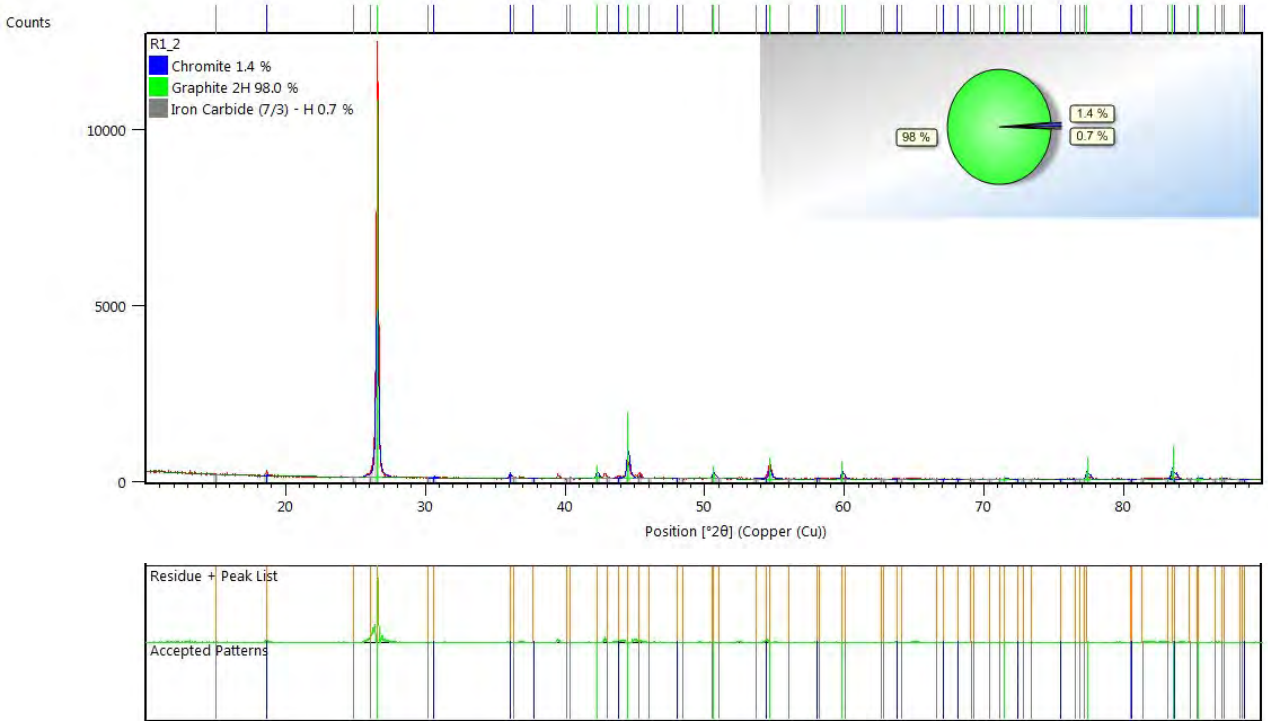

Sample: 1300 ˚C, 99,99 vol% H_2, 120 min

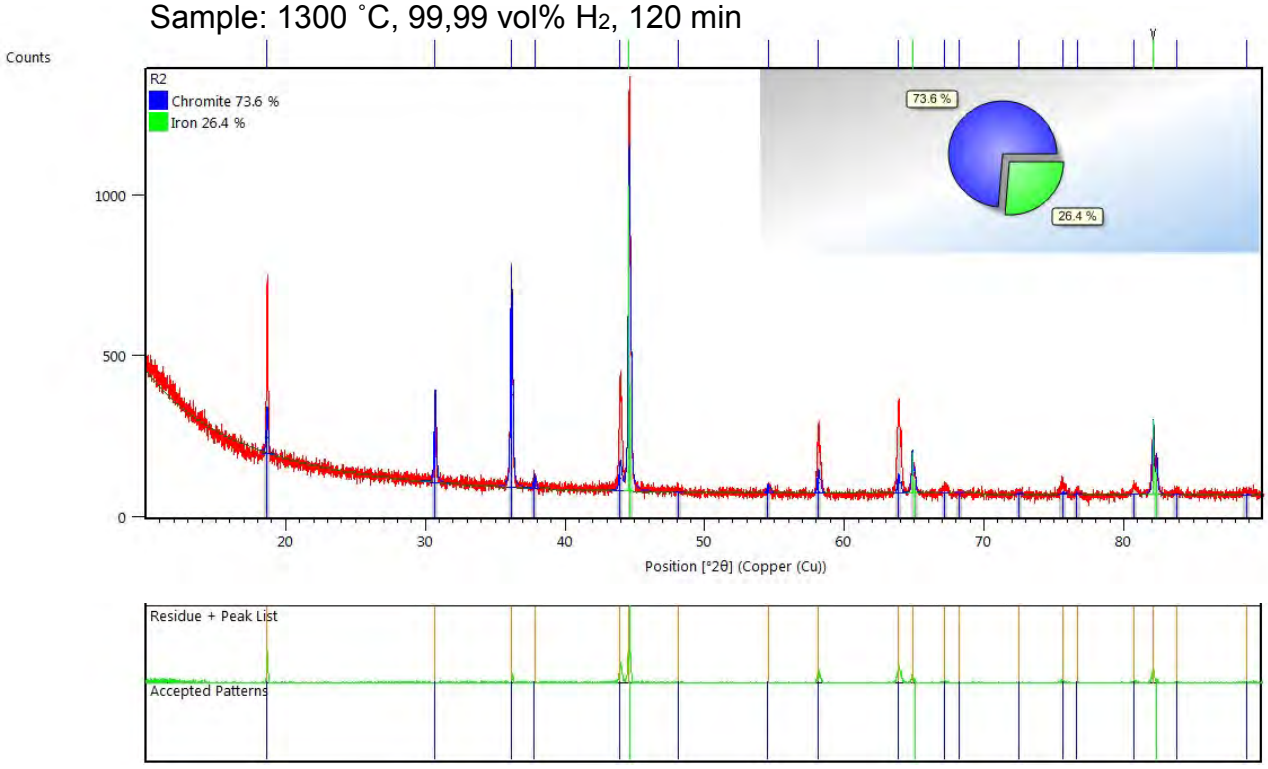

Appendix CL

Sample: Raw material, Kemi chromite

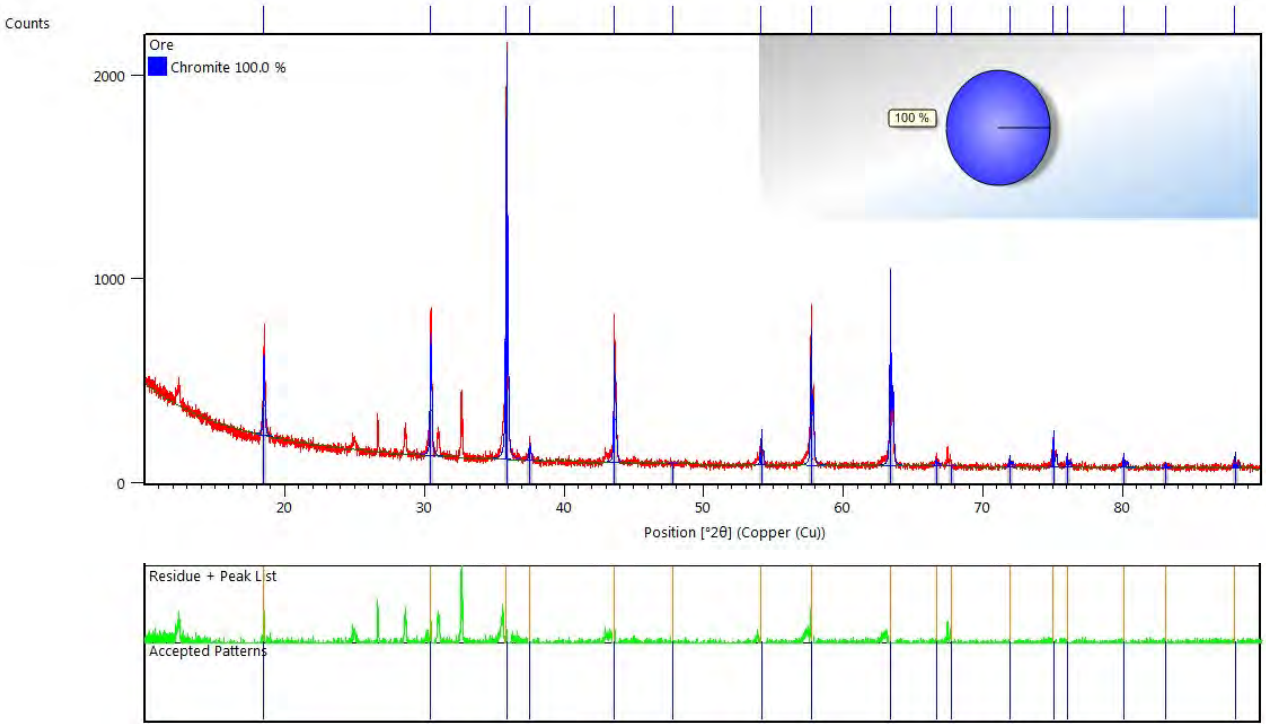

Appendices – S/C analysis results

Appendix CLI

Deposition of carbon at 1100˚C

Sample	T [˚C]	CH_4 [vol%]	Time [min]	C [wt%]
A1	1100	10	10	1.2
A2	1100	10	20	4.6
A3	1100	10	30	11.2
A4	1100	10	60	19.8
A5	1100	10	90	30.6
A6	1100	10	120	38.2
A7	1100	20	10	5.2
A8	1100	20	20	11.7
A9	1100	20	30	15.8
A10	1100	20	60	37.5
A11	1100	20	90	42.7
A12	1100	20	120	44.5
A13	1100	30	10	9.3
A14	1100	30	20	16.9
A15	1100	30	30	24.3
A16	1100	30	60	39.2
A17	1100	30	90	43.6
A18	1100	30	120	48.5

Deposition of carbon at 1200˚C

Sample	T [˚C]	CH4 [vol%]	Time [min]	C [wt%]
B1	1200	10	10	0.27
B2	1200	10	20	6.79
B3	1200	10	30	11
B4	1200	10	60	20.2
B5	1200	10	90	23.6
B6	1200	10	120	22.4
B7	1200	20	10	5.1
B8	1200	20	20	15.8
B9	1200	20	30	20.4
B10	1200	20	60	28
B11	1200	20	90	34
B12	1200	20	120	31.7
B13	1200	30	10	7.88
B14	1200	30	20	13.1
B15	1200	30	30	23.5
B16	1200	30	60	25.8
B17	1200	30	90	38.6
B18	1200	30	120	43.4

Appendix CLII

Deposition of carbon in 1300˚C

Sample	T [˚C]	CH_4 [vol%]	Time [min]	Carbon [wt%]
C1	1300	10	10	0.32
C2	1300	10	20	2.79
C3	1300	10	30	2.82
C4	1300	10	60	19.2
C5	1300	10	90	23.3
C6	1300	10	120	33.6
C7	1300	20	10	1.03
C8	1300	20	20	1.9
C9	1300	20	30	7.66
C10	1300	20	60	18
C11	1300	20	90	27.2
C12	1300	20	120	29.4
C13	1300	30	10	5.16
C14	1300	30	20	10.4
C15	1300	30	30	5.45
C16	1300	30	60	11.6
C17	1300	30	90	14.7
C18	1300	30	120	19.4

Deposition of carbon in 1350˚C

Sample	T [˚C]	CH_4 [vol%]	Time [min]	Carbon [wt%]
D1	1350	10	10	0.1
D2	1350	10	20	0.7
D3	1350	10	30	5.69
D4	1350	10	60	14.2
D5	1350	10	90	21.9
D6	1350	10	120	27.1
D7	1350	20	10	0.3
D8	1350	20	20	7.16
D9	1350	20	30	11.8
D10	1350	20	60	14.7
D11	1350	20	90	21.9
D12	1350	20	120	13.5
D13	1350	30	10	1.61
D14	1350	30	20	3.89
D15	1350	30	30	3.94
D16	1350	30	60	11.8
D17	1350	30	90	16.8
D18	1350	30	120	18.7